Helium: Exploration Methodology for a Strategic Resource

DIVEENA DANABALAN

Helium: Exploration Methodology for a Strategic Resource

Diveena Danabalan

A Thesis presented for the degree of
Doctor of Philosophy

Department of Earth Sciences
Durham University
United Kingdom
June 2017

Contents

Final word count: 69,116

(Word count excluding appendices and references = 55,488)

List of Figures

Chapter One: Introduction

Chapter Two: Methods

Chapter Three: Economic Helium Reservoirs in the Mid-Continent United States

Chapter Four: The Geochemical Characteristics of the ^{4}He-N_2 source in Helium Systems

Chapter Five: High Helium Systems in Tanzania

Chapter Six: The Principles of Helium Exploration

List of Tables

Chapter One: Introduction

Chapter Three: Economic Helium Reservoirs in the Mid-Continent United States

Chapter Four: The Geochemical Characteristics of the ^{4}He-N_2 source in Helium Systems

Chapter Five: High Helium Systems in Tanzania

Chapter Six: The Principles of Helium Exploration

Abstract

Helium: Exploration Methodology for a Strategic Resource

A thesis submitted to Durham University for the degree of Doctor of Philosophy by Diveena Danabalan, June 2017

Helium exploration is still in its infancy. Noble gas and stable isotopic analyses have proven to be effective tools in the past for determining the correlation between ^4He and associated N_2 and the role of groundwater in the transport and focusing of these gases alongside unrelated natural gases such as CH_4 and CO_2 into traps (Ballentine and Sherwood-Lollar, 2002). In this thesis these tracers are used to further understand aspects of the helium system such as source(s), gas migration pathways and trapping mechanisms and from this to ultimately present a framework for a helium exploration method.

Geochemical studies were conducted on CH_4-rich helium gas reservoirs in the Mid-Continent US and, for the first time, on N_2-rich helium gas reservoirs in Utah, Montana and Saskatchewan, Canada. Both types of ^4He-rich system showed consistent ^4He-associated N_2 endmembers with $\delta^{15}N$ values between -3.00‰ and +2.45‰; a range associated with low grade metamorphic crustal sources indicating that the source of the economic ^4He and associated N_2 in shallow reservoirs is likely derived from variable isotopic mixing between the basement and overlying sediments.

From these studies it was also ascertained that in all fields the mechanism for ^4He and associated N_2 degassing into reservoirs appears to be related in some degree to groundwater and to the saturation threshold of ^4He-associated N_2 thereby defining possible secondary migration pathways for the helium system.

New noble gas data from thermal springs in the West and East branches of the Tanzanian section of the EARS show ^4He concentrations of up to 10.5% indicating the active release or primary migration of high helium and high N_2 gases in the region. This coupled with potential traps in the nearby Rukwa Basin could provide a high helium reservoir in the future. First estimates for the basin, derived from ^4He analyses (< 4% ^4He) combined with seismic and soil gas surveys for the basin translate to a P50 estimate of probable reserves of 98 Bcf which would be enough to supply the current global helium demand for ~14 years if current demand remains steady.

Declaration

No portion of the work referred to in this thesis has been submitted in support of an application for another degree or qualification of this or any other university or other institute of learning.

Copyright Statement

About the Author

The author graduated from the University of Bristol in 2012 having obtained an undergraduate masters degree (MSci) with Upper Second Class Honours in Environmental Geoscience. The author commenced the research presented in this thesis in October 2012 under the co-supervision of Professor Jon Gluyas (Durham University), Professor Chris Ballentine (University of Oxford) and Professor Colin Macpherson (Durham University).

The sample collection trip to the USA and Canada was undertaken in June 2014 and the samples from Tanzania were collected by Dr Pete Barry (University of Oxford) and Thomas Abraham-James (Helium One) in November 2015.

The author has been fortunate enough to present the results from this thesis at the Goldschmidt Conference in Prague, Czech Republic, 2015, the 6th Cryogenic Cluster Day, Rutherford Appleton Labs, 2015, the Goldschmidt Conference in Yokohama, Japan, 2016 and the 7th Cryogenic Cluster Day, Rutherford Appleton Labs, 2016.

Funding for this thesis was provided in full by Statoil ASA and in part by Helium One and the Centre for Doctoral Training in Energy (Durham Energy Institute) at Durham University.

Acknowledgements

I would first like to sincerely thank my supervisors Professor Jon Gluyas and Professor Chris Ballentine for their support, feedback, discussions, encouragement and basically superhuman efforts throughout this rollercoaster of a thesis. I would also like to thank Professor Colin Macpherson for his helpful discussions and for setting me off on the right path when I first got to Durham University and Professor Barbara Sherwood-Lollar and her group for processing my nitrogen isotope data.

Huge thanks are given to Dr Pete Barry for his many contributions to this thesis including liaising with Helium One and Dr Tom Darrah, sample collection and analysis and discussions of results. Thanks are also given to Dr Jennifer Mabry, Dr Oliver Warr, Dr Rosie Jones, Dr Michael Broadley, Dr Bastian Joachim and David Byrne of the Noble Group at University of Oxford for teaching me pretty much everything they knew about noble gases, mass spectrometry, the ins and outs of high pressure line maintenance, the importance of helium leak testing (Olly!) and for being great fun both during the long lab days and after work.

I would like to extend my thanks to Statoil ASA for funding my research and to my supervisors at Statoil: Jens Emil Vindstad, Roger Hansen and Kati Tänavsuu-Milkeviciene.

I am grateful for the pro-activity of Bo and Scott Sears of Weil Helium and IACX without whom I wouldn't have my USA and Canada data. Thank you also to Thomas Abraham-James and Josh Bluett of Helium One for your invaluable contributions to Chapter Five of this thesis, for helping with sample collection, and for teaming up with us in your search for helium in Tanzania. I wish you and everyone else at Helium One all the luck in the world- here's hoping for a new helium reserve!

Special thanks go to Dr Mel Murphy for checking in on me during weekend lab sessions, Drs Anke Wohlers and Karen Fontijn for putting up with me gatecrashing their office on a semi-regular basis with random conversations, to my fellow PhD students both past and present at Durham University and University of Oxford, to my housemates over the years, to everyone in the USA and Canada including Clyde Becker and Adam Standiford who helped Chris and I with sampling and provided us with valuable background information, and to Richard Clarke aka 'Mr Helium' for his discussions about the future of helium and for furthering my understanding on an industrial level!

I would like to additionally thank my friends Joseph Hallett, Chelsey Lovell-Smith and Saranja Sivachelvam for their unwavering support and optimism and for keeping me sane through the difficult times.

My final thanks go to my parents and extended family for their love, prayers and support throughout this thesis and always!

I and Pangur Ban, my cat,
'Tis a like task we are at;
Hunting mice is his delight,
Hunting words I sit all night.

Better far than praise of men
'Tis to sit with book and pen;
Pangur bears me no ill will;
He, too, plies his simple skill.

'Tis a merry thing to see
At our task how glad are we,
When at home we sit and find
Entertainment to our mind.

Oftentimes a mouse will stray
Into the hero Pangur's way;
Oftentimes my keen thought set
Takes a meaning in its net.

'Gainst the wall he sets his eye
Full and fierce and sharp and sly;
'Gainst the wall of knowledge I
All my little wisdom try.

When a mouse darts from its den
O how glad is Pangur then!
O what gladness do I prove
When I solve the doubts I love!

So in peace our tasks we ply,
Pangur Ban, my cat and I;
In our arts we find our bliss,
I have mine, and he has his.

Practice every day has made
Pangur perfect in his trade;
I get wisdom day and night,
Turning Darkness into light.

Pangur Bán

(Author unknown. Translated from the original Irish by Robin Flower)

Chapter One: Introduction

1.1 Helium Exploration

1.1.1. Helium in the modern world

The first instance of a significant discovery of inert gases was recorded in 1903 in Dexter, Kansas, USA while exploring for petroleum. Initially dubbed 'wind gas' the gas was analysed and found to contain 1.84% helium, 82.70% N_2 and 14.85% CH_4 by volume and later to contain significant quantities of neon and argon (Cady and McFarland, 1906; Cady and McFarland, 1907a; Cady and McFarland, 1907b).

Past this discovery the helium industry did not boom until after the First World War (circa the end of 1918) when helium, due its inert and lighter than air properties was of interest to the US armed forces for use in zeppelins, dirigibles and balloons (Sears, 2012).

Since this period the demand for helium has grown rapidly as new discoveries were made as to its unique properties such as its extremely low boiling point (4.2K), non-flammability, small molecular size of 0.20 nm, and superfluid properties below 2.2K, makes it an especially valuable element (Smith et al., 2004; Broadhead, 2005). The largest usage of helium currently is by the cryogenic, engineering and medical sectors as a coolant for superconducting magnets in everything from mass spectrometers to MRI machines to particle accelerators such as the Large Hadron Collider at CERN.

As of the end of 2016 the USGS has estimated that 30% of the USA's consumption of helium was used for MRI machines, 17% for lift, 14% for analytical and laboratory applications, 9% for welding, 6% for engineering and scientific

applications, 5% for leak detection, 5% for semiconductor manufacturing and 14% for other minor applications (**Figure 1.1**).

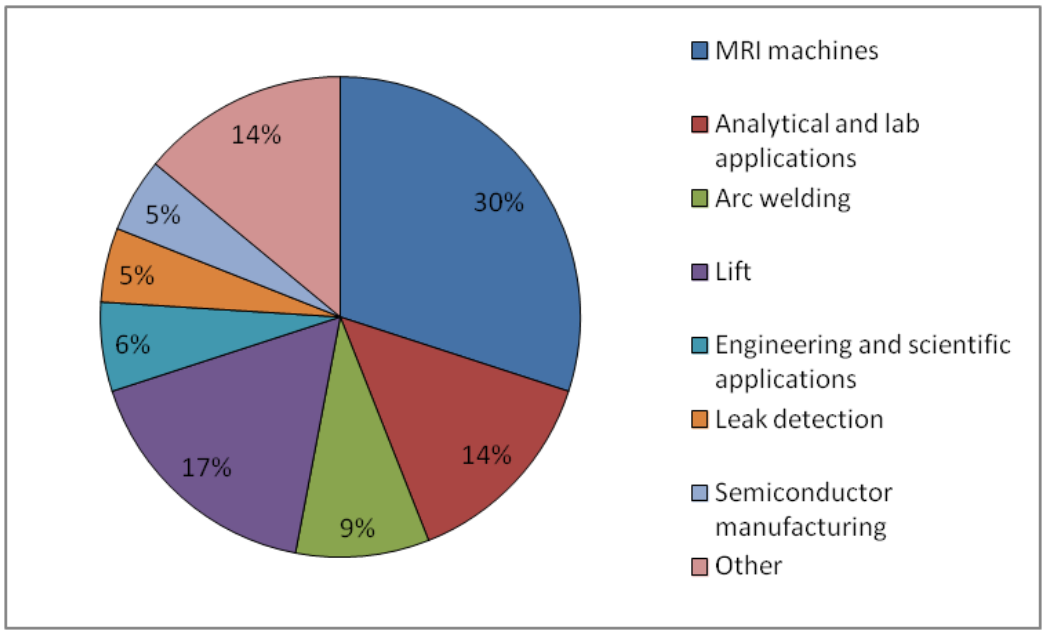

Figure 1.1.: Chart showing the uses of helium in the USA as of 2016 (USGS, 2017).

Since the first discovery of helium-rich gas in Kansas numerous others were made across the USA, in Wyoming, Oklahoma, Texas, Kansas, New Mexico, Utah, Arizona, Montana and Colorado (USGS, 2017). Some of these fields contain up to 10% helium by volume, a significant proportion considering that the economic threshold concentration for helium to be considered extractable is 0.3%; the concentration at which its value equals approximately that of the remaining 99.7% of the discovered CH_4 gas volume.

Other discoveries of helium-rich gas have also been made in Canada, Algeria, Poland, Russia, Germany, Hungary, Romania, Qatar, Kazakhstan, India, Pakistan, China and the Timor Sea. World helium consumption has risen by around 130% over the past 10 years and is set to increase as technology advances (USGS, 2017).

It has been noted that helium is technically a renewable resource due to the continuing decay of U and Th in the Earth's crust however this is over geological timescales. While it is true that the Earth will not run out of helium, current reserves of helium have the potential to become critical over human timescales, thereby making it a non-renewable resource in this respect.

Current helium reserves in the USA are due to be sold off/run out by 2021 which places the onus on the larger fields of Hassi R'mel in Algeria and South Pars in Qatar, which have recently come online, to supply the majority of the world's helium. This however is highly dependent on both the continuing need for Liquified Natural Gas (LNG) which enables large volumes of helium to be produced from near trace concentrations in the fields (0.05% He on average) and also on the political stability of these regions. The issue of political stability with regards to helium supply for the West also extends to potential fields in Russia which are currently under development such as Chayandinskoye, Sobinskoye, Kovyktinskoye and Yurubcheno-Tokhomskoye.

As of 2016 the USGS has estimated world reserves of helium of 51.9 billion m^3. Therefore, despite several new helium fields coming online such as in Algeria, Qatar and Russia there is only enough helium left for approximately 230 years if we assume that current demand remains the same (USGS, 2017).

Current helium reserves are set to decline to critically low levels in a few tens of years making this a significant problem affecting many aspects of industry and society. This has been shown by the need in the past for strategic shutdowns of university hospital equipment around the UK (Connor, 2013; Stokes, 2013).

Recycling is rarely an option except in a laboratory setting, the containment of helium is difficult and leakage from storage inevitably occurs over time due to its

small atomic diameter. Once helium reaches the atmosphere it circulates for approximately 1 Ma before being lost to space due to its escape velocity at Earth temperatures in the exosphere exceeding the planet's gravitational attraction according to Jean's escape (Torgersen, 1989; Pepin and Porcelli, 2002).

Current global helium reserves mosstly originate from serendipitous discoveries and in all cases these were made when exploring for petroleum. This has led to the mistaken general attitude that there is very little need to develop any special geological expertise to target helium-rich gases in order to provide an adequate supply of helium (Maione, 2004). Moreover many gas production companies are unwittingly venting helium because they either do not test their gas or if they do fail to recognise the value of this seemingly minor component (Clarke et al., 2012).

In hydrocarbon fields helium and N_2 are usually vented during the clean up process. For one field this amounts to 300,000 ft^3 per day of helium which is shocking when it is considered that the LaBarge field (Wyoming, USA) initially flowed approximately 270,000 ft^3 per day and is now one of the four main producers of helium in the USA (Gluyas, pers comm., 2012,).

Helium is not only valuable to industry, medicine, physics and engineering but also to geoscientists due to its uses in quantifying groundwater interaction with hydrocarbons, identifying the origin of natural gases and dating the age of groundwater. These applications span not only scientific research but also the petroleum, aviation, medical and nuclear industry to name but a few.

1.1.2. Types of helium reservoir

Economically, a helium-rich gas field is classified as one which has a volume percent of 0.3% or greater. However, in terms of geochemistry, a helium-rich field can be classified as anything above 0.1%, due to helium being present in most fields as trace amounts (<0.05%).

Producing helium-rich fields can be classified according to their primary gas component as one of three main types:

1) N_2-rich: examples - Harley Dome (USA), Pinta Dome (USA)
2) CO_2-rich: examples – LaBarge (USA), Doe Canyon (USA)
3) CH_4-rich: examples - North Dome-South Pars (Qatar/Iran), Hugoton-Panhandle (USA), Hassi R'Mel (Algeria) (**Figure 1.2**)

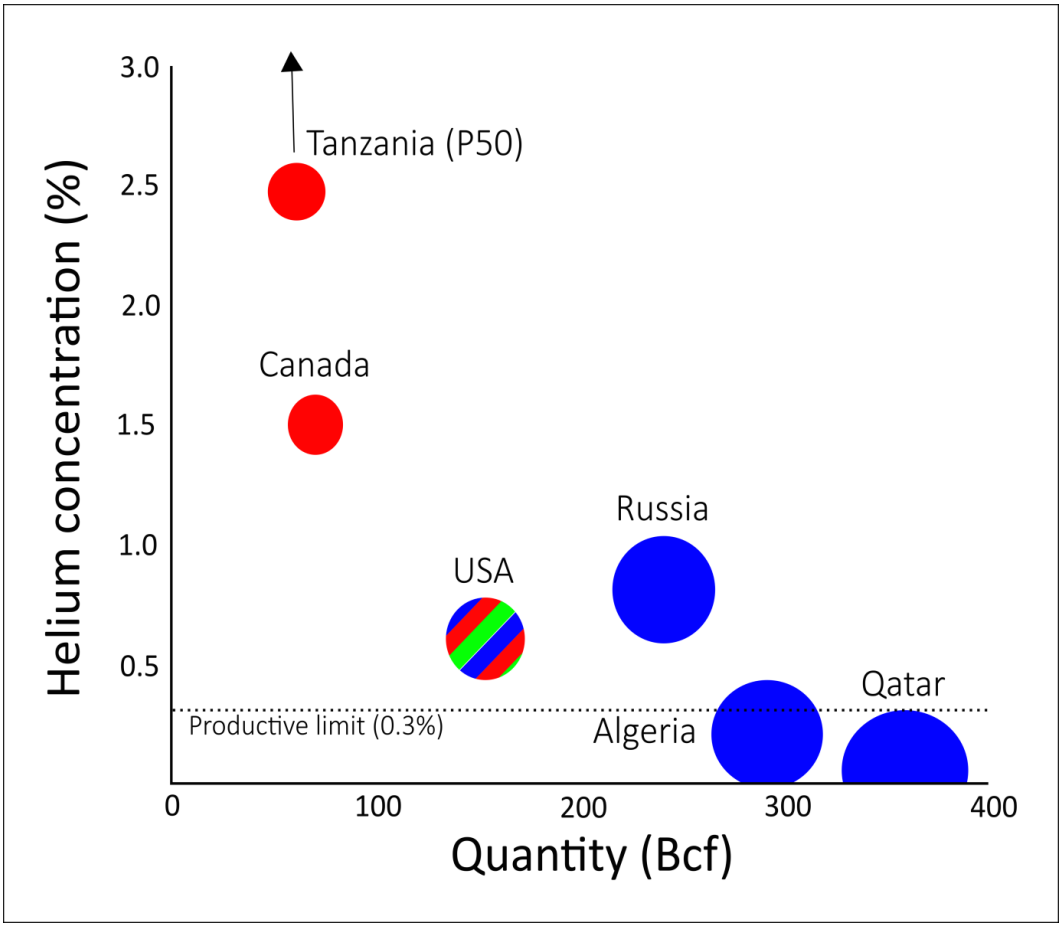

Figure 1.2.: Graph redrawn from Helium One, pers. comms., (2016) showing helium concentration (%) against reserve volume (Bcf). Red circles indicate N_2-rich fields, blue circles indicate CH_4-rich fields and green circles indicate CO_2-rich fields.

1.1.2.1. CO_2-rich fields

These are defined as fields where CO_2 is the primary constituent of the gas volume. Fields like this are often found in close proximity to helium-rich fields where N_2 is the main gas component. Major geochemical studies have been conducted on CO_2-rich gas fields before by both Zhou, (2004) and Gilfillan, (2006).

However, it is in rare cases that gas fields which are CO_2-rich are also classified as helium-rich in the economic sense e.g.: Doe Canyon and LaBarge (Gilfillan, 2006; Merrill et al., 2014). This rarity is most likely due to the bulk of the CO_2 in high CO_2 fields usually originating from a purely magmatic provenance

whereas economic helium reservoirs usually contain a significant input from shallow crustal sources. Therefore, this proportionally large magmatic input into reservoirs has the potential to have a diluting effect on helium and associated crustal gases in reservoirs (Weinlich et al., 1999; Barry et al., 2013; Chapter 5, this thesis).

1.1.2.2. CH_4-rich fields

Methane is the most common gas which is trapped in producing field areas. However, it is generated by a completely different process to helium and usually at shallower depths and lower temperatures which may be factors which influence its dominance in traps relative to helium.

Fields such as the Hugoton-Panhandle field, the North Dome-South Pars field and Hassi R'Mel field are all examples of CH_4-rich fields which are predominantly sourced for natural gas and other petroleum products. However, these three fields fall into two distinct categories.

The Hugoton-Panhandle is classified as a classic example of a helium-rich field under economic terms i.e.: that it has at least 0.3% helium by volume of gas in the reservoir. However, the Hassi R'mel and North Dome-South Pars fields are also classified as helium-rich. Indeed, the South Pars part of this combined field contains one of the largest helium reserves on Earth, dwarfing any currently producing in the USA. Estimates of the helium reserve in this field run to around 10.1 billion m^3; a quarter of the current world helium reserve (USGS, 2017). Despite this, under current economic considerations, the North Dome-South Pars field would not be considered as a viable helium-rich field since this field only contains approximately 0.04% helium. Hassi R'mel also contains subpar concentrations of around 0.05%

helium. However, due to the size of the reservoir, this equates to a diluted concentration but a large overall volume thereby making these giant fields economically viable.

1.1.2.3. N_2-rich fields

Nitrogen-rich fields are a paradox in terms of helium concentrations. In all instances of economic amounts of helium accumulating in natural gas fields, there is always a related amount of nitrogen. Usually this ranges from a 0.02 to 0.20 ratio of $^4He/N_2$. Nitrogen-rich fields like these can contain up to 10% helium by volume in the USA. Outside of the USA however, very few nitrogen-rich fields have been found; whether this is due to lack of knowledge, lack of relevant discoveries or special geological circumstances occurring in the USA remains to be seen.

Despite helium-rich resources occurring in nitrogen-rich fields, in most cases of high nitrogen fields (50%-88%) such as those in NW Germany, there is no economic helium associated with these fields (Barnard and Cooper, 1983; Gerling et al., 1999). Therefore, helium is always related to nitrogen however nitrogen is not always related to helium.

Very few studies have been done on the relationship between helium and nitrogen however there are hypotheses which are linked to the most prominent paper on the topic by Ballentine and Sherwood Lollar (2002). By studying the noble gas isotopes and stable isotopes it was found that radiogenic helium was associated with a nitrogen component that showed a light $\delta^{15}N$ signature (-3.00‰). This indicated that the helium and the nitrogen were sourced from the same rocks and that the source of both the nitrogen and the helium was most likely the low temperature metamorphism of basement rocks both in situ and from the surrounding region.

1.1.3. Introducing helium as a noble gas

Helium is the second most common element in the universe and is believed to be present in all natural gas fields as a trace component (<0.05 ppm). It is classified as a noble gas.

The noble gases, which compose Group 18 of the periodic table, are known for their chemical inertness as a result of their full outer shell electron configuration (IUPAC, 2005). Under standard temperatures and pressures they exist in nature as stable monatomic gases.

Helium has two stable isotopes: rare ^{3}He, 'primordial helium', left over from the formation of the Earth in the mantle, and prolific ^{4}He, 'radiogenic helium', which is a product of the alpha decay of ^{235}U, ^{238}U and ^{232}Th (Mamyrin and Tolstikhin, 1984; Oxburgh et al., 1986). Helium, as with all noble gases, is sourced from three quantifiable sources: the atmosphere, the crust and the mantle. Helium associated with economic reserves is always crust-dominated in source (Ballentine and Sherwood-Lollar, 2002; Gilfillan, et al., 2008; Chapter 3 this thesis; Chapter 4 this thesis).

The ^{3}He isotope is largely associated with areas of tectonic and volcanic activity along with passive degassing of the Earth (O'Nions and Oxburgh, 1988). The most significant terrestrial sources of ^{3}He are mid-ocean ridge and subduction volcanism (Craig et al., 1975; Craig and Lupton, 1976; Torgersen, 1989).

The other major alternative source of ^{3}He is thermal neutron capture by ^{6}Li in predominantly clay-rich areas ($^{6}Li(n,\alpha)^{3}H(\beta^{-}) \rightarrow {}^{3}He$) (Hiyagon and Kennedy, 1992; Ozima and Podosek, 2001; Ballentine and Burnard, 2002). However, this usually only occurs within the upper few metres of the crust.

Large concentrations of radiogenic ^{4}He tend to be confined to areas which contain high amounts of radioactive elements from the U and Th series. These are often granitic bedrocks or sedimentary basins composed of igneous fragments and shales. However, since there is a decreasing trend in terms of U and Th lower in the crust-mantle boundary, there are still potential magmatic sources of ^{4}He.

A small proportion of recorded ^{4}He is derived from mantle sources (due to the continuing decay of U and Th lower in the Earth's asthenosphere), leading it to be called 'magmatic ^{4}He' (Tolstikhin, 1975; Ballentine et al., 1991; Ozima, 1994). Large concentrations of magmatic ^{4}He show a deep crustal input into systems. Approximately 75% of ^{4}He is produced in the upper 10 km of the crust due to preferential partitioning of the incompatible U and Th isotopes into the crust (Ballentine and Burnard, 2002).

1.1.3.1. Sources of helium

Crustal helium (^{4}He) is usually found in natural systems as trace amounts (<0.05 ppm) but concentrations higher than air (5.24×10^{-6} $cm^{3}STP(^{4}He)/cm^{3}$) are most associated with: groundwater, ancient brines, ancient pore water, natural gas fields, Carlin type gold deposits, ore deposits, hydrothermal fluids, volcanic degassing, oil field brines, lakes, ice, sediments and coal measures (Heaton, 1984; Torgersen and Clarke, 1985; Torgersen and Ivey, 1985; Creedy, 1988; Ballentine et al., 1991; Stute et al., 1992; Marty et al., 1993; Pinti and Marty, 1995; Stuart et al., 1995; Ballentine et al., 1996; Pettke et al., 1997; Winckler et al., 1997; Pinti and Marty, 1998; Burnard et al., 1999; Ballentine et al., 2002; Ballentine and Burnard, 2002; Ballentine and Sherwood-Lollar, 2002; Kipfer et al., 2002; Yang et al., 2003;

Poreda et al., 2004; Graupner et al., 2006; Gilfillan et al., 2008; Holzner et al., 2008; Ray et al., 2009; Zhou et al., 2012; Barry et al., 2013; Winckler and Severinghaus, 2013; Caracausi and Paternoster, 2015; Lowenstern et al., 2015; Tomonaga et al., 2017). Out of these possible sources we will be addressing natural gas fields in more detail later in this chapter due to their relevance to the helium exploration narrative.

1.2. The other noble gases

The stable isotopes of helium are often found in association with other stable noble gas isotopes such as: ^{20}Ne, ^{21}Ne, ^{22}Ne, ^{36}Ar, ^{38}Ar and ^{40}Ar; which are either radiogenically or nucleogenically sourced in the crust, mantle or atmosphere. The descriptions below briefly detail the processes which source these other stable isotopes.

1.2.1. Neon

Neon has three stable isotopes: ^{20}Ne, ^{21}Ne and ^{22}Ne. The production of ^{20}Ne is primarily due to carbon-burning during stellar nucleosynthesis ($^{12}C + {}^{12}C \rightarrow {}^{20}Ne + {}^{4}He$) and was trapped by the Earth during accretion (Clayton, 2007). This accounts for the high abundance of ^{20}Ne in our atmosphere. Since the production of ^{20}Ne in the crust is negligible compared to ^{20}Ne sourced from the atmosphere any ^{20}Ne detected in shallow reservoirs is determined to have been introduced into the system by groundwater (Ballentine et al., 1991; Ozima and Podosek, 2001; Ballentine and Burnard, 2002).

The main pathways for the production of ^{21}Ne in the crust are determined by oxygen ($^{17,18}O(\alpha,n)^{20,21}Ne$) and magnesium ($^{24,25}Mg(n,\alpha)^{21,22}Ne$) concentrations (Ballentine and Burnard, 2002). In the crust the magnesium pathway only accounts for <0.13% of total nucleogenic ^{21}Ne production and is considered more important in mantle systems where it can make up 3.37-65.35% (Yatsevich and Honda, 1997; Ballentine and Burnard, 2002).

The main nucleogenic production routes for ^{22}Ne in the crust are determined by fluorine ($^{19}F(\alpha,n)^{22}Na(\beta^{+})^{22}Ne$ and $^{19}F(\alpha,p)^{22}Ne$) and magnesium ($^{24,25}Mg(n,\alpha)^{21,22}Ne$).

1.2.2. Argon

Argon has three stable isotopes: ^{40}Ar, ^{38}Ar and ^{36}Ar. The production of ^{40}Ar is via electron capture during the decay of ^{40}K in the crust. ^{36}Ar production in the crust is negligible (β-decay of ^{36}Cl) compared to atmosphere-derived ^{36}Ar which dominates in systems that contact groundwater. ^{38}Ar excesses in the crust can be produced by the decay of ^{35}Cl ($^{35}Cl(\alpha,p)^{38}Ar$) and of ^{37}Cl ($^{37}Cl(n,\gamma)^{38}Cl(\beta-)^{38}Ar$) (Ballentine and Burnard, 2002). The production of ^{38}Ar also strongly depends on the siting of Cl relative to U and Th in the crust and is therefore sensitive to radioelement heterogeneity. However, the majority of ^{38}Ar concentrations recorded in shallow reservoirs are sourced from the atmosphere due to the low production rates associated with ^{38}Ar in the crust.

1.2.3. Krypton and Xenon

Both krypton and xenon have six stable isotopes each: ^{78}Kr, ^{80}Kr, ^{82}Kr, ^{83}Kr, ^{84}Kr, ^{86}Kr, ^{128}Xe, ^{129}Xe, ^{130}Xe, ^{132}Xe, ^{134}Xe and ^{136}Xe. In the case of krypton, ^{78}Kr and ^{86}Kr are observationally stable (Ozima and Podosek, 2001). The major stable isotopes ^{83}Kr, ^{84}Kr, ^{86}Kr, ^{129}Xe, ^{132}Xe, ^{134}Xe and ^{136}Xe are produced by the fission of ^{238}U.

1.3. The noble gases as geochemical tracers in natural gas systems

The isotopes of the noble gases (He, Ne, Ar, Kr and Xe) act as conservative tracers in natural gas reservoirs. This is due to their properties as inert, unreactive elements. As such, they are unaffected by chemical reactions which affect ratios of other non-hydrocarbon gases within the reservoir fluids. However, once in the crust, the noble gas characteristics of a fluid can be additionally altered by in situ radiogenic production and physical processes such as phase fraction and diffusion.

Noble gas isotopic ratios and concentrations can be used to constrain the origins of fluids, detect subsurface phase interactions and reveal the mechanism of transport responsible for conveying the fluid to the reservoir (Ballentine et al., 1991; Hiyagon and Kennedy, 1992; Pinti and Marty, 1995; Ballentine et al., 1996; Torgersen and Kennedy, 1999; Ballentine et al., 2001; Ballentine et al., 2002; Ballentine and Sherwood-Lollar, 2002; Lippmann et al., 2003; Gilfillan et al., 2008; Zhou et al., 2012; Prinzhofer, 2013).

This is possible because noble gases are introduced into crustal reservoirs from both the mantle and the atmosphere (**Figure 1.3**). In the petroleum industry, four main isotopic ratios are used to quantify oil and gas exploration: $^{3}He/^{4}He$ (R_a), $^{20}Ne/^{22}Ne$, $^{21}Ne/^{22}Ne$ and $^{40}Ar/^{36}Ar$.

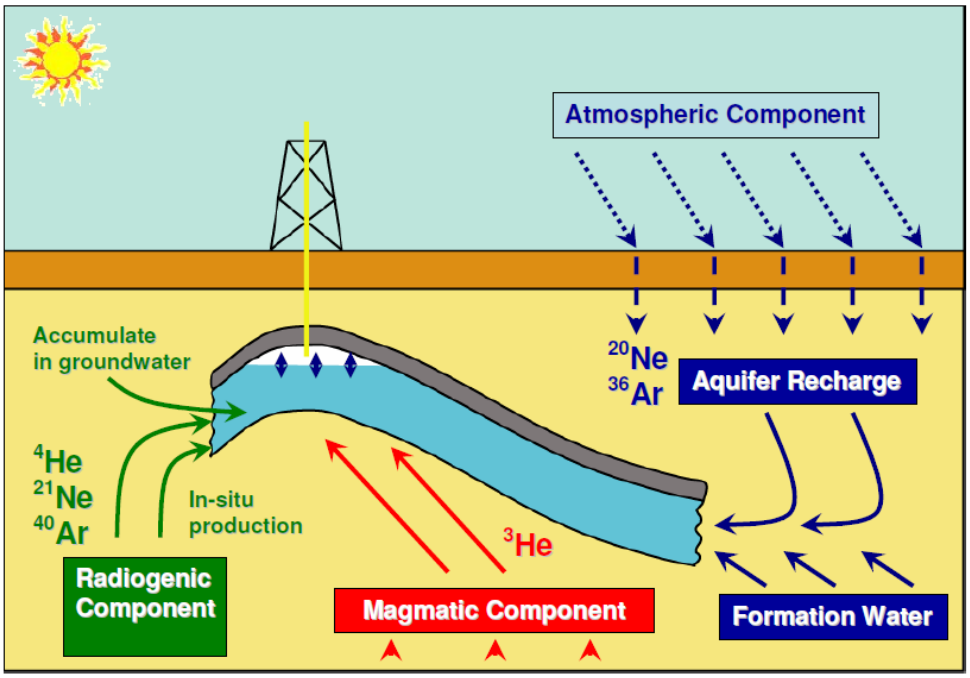

Figure 1.3.: Diagram of a shallow natural gas reservoir showing the three distinct sources of the noble gas isotopes measured in these reservoirs. The atmospherically-sourced noble gases such as ^{20}Ne and ^{36}Ar are input into reservoirs due to air equilibration with groundwater at recharge. The radiogenic noble gases such as ^{4}He, ^{21}Ne and ^{40}Ar are predominantly produced, either directly by or as a by-product of, the radioactive decay of U, Th and K in the crust. In reservoirs near areas of active continental extension or magmatic activity an excess of mantle-sourced noble gas isotopes; predominantly ^{3}He will be present. The distinct isotopic compositions of the noble gas isotopic ratios associated with these three sources enables the contribution from each to be quantitatively resolved (from Gilfillan, 2006).

The ^{3}He/^{4}He ratio is important because it reflects the binary mixing of mantle/crustal helium sources. ^{3}He/^{4}He ratios from samples (designated as R) are normalised to the atmospheric ^{3}He/^{4}He ratio of 1.4 x 10^{-6} (designated as 1 R_a). It is assumed that the endmembers for crust-derived radiogenic helium is 0.020 R_a, for a Mid Ocean Ridge Basalt-derived (MORB) source it is 8.0 R_a and for a Sub-Continental Lithospheric Mantle (SCLM) source it is 6.1 R_a (Craig and Lupton, 1981; Gautheron and Moreira, 2002).

Atmospheric contributions to ^{4}He can be calculated by comparing the ^{4}He/^{20}Ne ratios of samples to the ^{4}He/^{20}Ne ratio of air (0.032) (Kipfer et al., 2002). If

samples are significantly higher than the air value (order of magnitude or more) then it can be safely assumed that there is no significant atmospheric contribution to the R_a value for samples.

1.3.1. Crustal contributions to natural gas systems

Radiogenically and nucleogenically produced noble gases such as ^{4}He,^{21}Ne, ^{40}Ar and ^{136}Xe can be found in excess of atmospheric contributions in natural gas reservoirs. Excesses of noble gas isotopes in natural gas reservoirs can be generated by: 1) addition of gases from a source separate to in situ production within the reservoir or 2) closed system accumulation within the reservoir rock. Ultimately excesses of noble gases in reservoirs are determined by the efficiencies associated with noble gas escape from minerals, migration and trapping. The addition of crustal noble gases to reservoirs results in measurements of low $^{3}He/^{4}He$ ratios and high $^{21}Ne/^{22}Ne$ and $^{40}Ar/^{36}Ar$ ratios in gases.

1.3.2. Mantle contributions to natural gas systems

Mantle contributions to natural gas systems usually occur near areas of volcanism or continental extension. Helium is usually a good tracer of a mantle addition to crustal fluids due to its low abundance in the atmosphere (5.24×10^{-6} cm^3 STP(^{4}He)/cm^3) and isotopically distinct mantle and crust R_a values (8.0 R_a and 0.020 R_a respectively).

However, sometimes it is difficult to identify mantle-derived helium in continental samples with relatively low R_a values because values between the

average crustal radiogenic production ratio of 0.020 R_a and up to 0.10 R_a can be attributed to other sources such as high local Li concentrations or cosmogenic ^{3}He implantation and release from sedimentary materials. In these cases a mantle component is evidenced further when also accompanied by high $^{20}Ne/^{22}Ne$ ratios, $^{21}Ne/^{22}Ne$ ratios and $^{40}Ar/^{36}Ar$ ratios.

1.3.3. Groundwater contributions to natural gas systems

The atmospheric noble gases (^{20}Ne, ^{38}Ar, ^{36}Ar, ^{84}Kr, ^{130}Xe) are introduced into the crust when dissolved in the groundwater during recharge. They are then fractionated according to their relative solubilities in water leading to Xe>Kr>Ar>Ne>He (Crovetto et al., 1982). The concentration of these gases in the groundwater is dependent on several variables including the partial pressure of the noble gases in the atmosphere (dictated by the equilibration altitude), the temperature at which equilibration occurs (generally only relevant when calculating palaeo-temperatures) and the volume of air trapped in groundwater by periodic fluctuations in the vadose zone referred to as 'excess air' (Kipfer et al., 2002).

The salinity of the groundwater also has an effect on the amount of noble gases dissolved within it. There is still an on-going debate as to whether this is due to the salinity itself or simply the advanced age of the water. Once the fluids enter the crust, the increase in hydrostatic and/or lithostatic pressure prevents the loss of noble gases from the fluid, regardless of the temperature or salinity of the groundwater (Ballentine et al., 2002).

From these fundamental principles it can be seen that with careful measurement these distinct sources can be distinguished isotopically from each other to show the extent of crustal, mantle and atmospheric contributions to the reservoir fluid.

1.4. Literature review of the helium system

Since most economically viable helium deposits are found in natural gas reservoirs which are already tapped for their petroleum potential we shall be splitting the stages of the helium system along the lines of petroleum exploration: from source to entrapment for ease of discussion.

1.4.1. Generation and accumulation

As outlined in Section 1.1.3. ^{4}He, the dominant isotope of economically viable helium gas in reservoirs, is radiogenically sourced from the decay of U and Th isotopes over the entire crust whereas hydrocarbon products are biogenically sourced from the decay of organic matter. Overlap of this source material occurs in shales which can produce both hydrocarbons and ^{4}He over geological time however this will inevitably lead to the dilution of ^{4}He concentrations produced from these source rocks with increasing CH_4 generation from maturation.

Crustal/cratonic rocks of Proterozoic to Archean age (< 3.8 Ga) are predominantly metamorphic-granitic in character and rich in U and Th, thereby enabling the production of ^{4}He. Concentrations of ^{4}He increase in the subsurface over time as these cratons act as closed systems with helium either remaining within producing minerals or either diffusing or being ejected into the fluid within the

porosity of the rocks (Reimer, 1976; Bottomley et al., 1984; Zadnik and Jeffrey, 1985; Lippmann-Pipke et al., 2011; Holland et al., 2013).

The fraction of ^{4}He lost by recoil is a strong function of the effective grain size (sur-face to volume ratio of the grain). Low surface area/volume ratios of <0.03 μm^{-1} result in >90% retention of ^{4}He in all but the most planar or acicular crystal morphologies (Ballentine and Burnard, 2002). Therefore, as metamorphic grade and crustal depth increase, the rate of recoil loss will decrease due to the average grain size increasing.

Rates of ^{4}He accumulation from crustal sources are controlled locally by porosity, local advection/diffusion, compressive stresses and tectonics (Torgersen and Ivey, 1985).

Over short time scales, helium accumulation is controlled by the radioactive decay rate of U and Th. However on longer time scales it is controlled by the vertical flux from ^{4}He degassing plus the in situ rates (Torgersen and Clarke, 1987).

Over time, high volumes of ^{4}He accumulate in the basement rock. However, due to a combination of low concentration (ppm) and the ability of some minerals such as apatite, zircon and titanite to retain helium below their closure temperatures; the atoms need a mechanism for mass release (**Table 1.1**).

Mineral	**Closure temperature range** (°C)	**References**
Apatite	55-100	Lippolt et al., 1994; Wolf et al., 1996; Farley, 2000; Farley, 2002; Shuster et al., 2006
Hematite	90-250	Bähr et al., 1994; Farley, 2002
Zircon	180-200	Farley, 2002; Reiners, 2005; Reich et al., 2007;

		Cherniak et al., 2009
Garnet	590-630	Dunai and Roselieb, 1996; Farley, 2002
Monazite	182-299	Boyce et al., 2005
Titanite	150-200	Reiners and Farley, 1999; Farley, 2002
Uraninite	~200	Martel et al., 1990; Stuart et al., 1994

Table 1.1.: Helium closure temperatures for helium retentive minerals. Variations in closure temperature for individual minerals are due to combinations of differing grain sizes and cooling rates.

1.4.2. Primary migration

There are two possible routes for helium to be released from basement rocks in the concentrations found in the shallow crust: 1) mass diffusion of accumulated helium produced from the decay of U and Th in the crust or 2) advection of accumulated helium produced from the decay of U and Th in the crust.

Following calculations by Ballentine and Burnard (2002) diffusion as a major mass transport mechanism is insignificant and transport to the shallow systems is single phase. Walther and Orville (1982), using a theory of single pass flow mechanics, calculated that during progressive metamorphism, dehydration and carbonation reactions produce fluid which flows upwards due to its lower density than the surrounding country rock. This can occur one of two ways: either through convection or through what is known as ‘single pass flow’ where the fluid travels vertically one way.

In order for fluids to convect, the rock must be able to maintain a hydrostatic gradient within its fracture and pore networks. This involves balancing the difference between the hydrostatic pressure and the higher lithostatic pressure of the overlying rocks. However, if the rock strength is insufficient to hold open the pores and

fractures then they will anneal until the fluid equilibrates to lithostatic pressures. This mechanism results in ‘single pass flow’ as the fluids reach lithostatic pressure.

A possible reason that helium is released from source rocks and into overlying strata is the impact of a geological event causing significant fracturing and heating of the basement rock (Salah and Alsharhan, 1998). Events on a tectonic scale which could cause intense fracturing and heating of the surrounding country rock could either be an orogenic event, an extensional event (rifting) or deep burial (diagenesis).

The vertical movement of fluids by deep faults most likely helps this method of migration until it is further channelled into fractures or pore networks in the shallow crust (Bebout and Carlson, 1986).

Diffusion alone is not enough to transport the volumes of helium found concentrated in some shallow crustal areas, therefore helium gas must be subject to advection in order to be distributed in the quantities found in the shallow crust.

1.4.3. Helium and associated carrier gases

The presence of nitrogen and carbon dioxide in large amounts in hydrocarbon systems is now regarded with significantly more importance due to their proportions determining the commercial value of the reservoir. However in the interest of helium exploration, it is noted that producing fields consistently show high nitrogen coupled with significant amounts of helium (Anderson and Hinson, 1950; Dobbin, 1968; Dunlap, 1969; Stewart and Street, 1992; Ballentine and Sherwood Lollar, 2002; Gilfillan et al., 2008; Chapter 3, this thesis; Chapter 4, this thesis).

In recent sediments the main source of nitrogen is mainly the trapping of air however nitrogen can also be released from organic matter during high temperature thermal decay, from sediments and the basement during metamorphism, from air being dissolved in groundwater and from localised mantle inputs (Stahl et al., 1977; Kreulen et al., 1982; Haendel, et al., 1986; Coveney et al., 1987; Gold and Held, 1987; Jenden et al., 1988a; Bebout and Fogel, 1992; Boyd et al., 1993; Krooss et al., 1993; Littke et al., 1995; Gerling et al., 1998; Bebout et al., 1999; Hutcheon, 1999; Weinlich et al., 1999; Zhu et al., 2000; Boyd, 2001; Ballentine and Sherwood-Lollar, 2002).

There is evidence for separate systems for noble gas transport and hydrocarbon transport in the subsurface and of admixtures of ^{4}He and N_2 which are sourced from the same region of the crust giving credence to the concept of carrier gases aiding the bulk advection of volumes of helium from depth to the shallow crust (Gold and Held, 1987; Jenden et al., 1988a; Giggenbach and Poreda, 1993; Ballentine and Sherwood-Lollar, 2002; Gilfillan et al., 2008; Chapter 3, this thesis; Chapter 4, this thesis).

1.4.4. Secondary migration

For the purposes of the helium system this is defined as migration past the limit for lithostatic pressure where there is interaction between circulating groundwater and fluids from depth produced by primary migration. Due to the change in pressure, there will be the potential for convection and not just single pass flow. The migration of helium is assumed to be similarly governed to migration of

petroleum, in that the balance between hydrostatic and lithostatic pressure are the main causes followed by porosity, permeability and capillary pressure.

Due to the scale of the events which potentially release the volumes of helium and associated gases, an equally large scale must also be applied to secondary shallow migration via groundwater. During orogeny tectonic compression and thrusting produce large overpressures, forcing fluids out towards the thrust front. Although the flow rates in this scenario are not yet known, maximum velocities are suggested to be around 0.5 m/yr for aquifers. This will dissipate quickly following the relaxation of the stress (Garven et al., 1993). It thought that the compaction-driven events which stimulated continental groundwater migration dissipated after a few hundred years in the case of the Appalachian Orogeny, driving fluids from SE to NW in periodic pulses.

The generation of basin-and-range formations on the west side of the USA were most probably responsible for continental scale groundwater flow (west to east) during the Late Cretaceous-Tertiary. The Sevier-Laramide Orogeny created the Rocky Mountains and simultaneously uplifted the foreland platform to the east of the deformation front (Garven, 1995). Evidence of this is prevalent on both sides of the United States, both from the Sevier-Laramide Orogeny and the Appalachian Orogeny on the east coast of the continent. Brines from the Colorado Front Range (an offshoot of the Rocky Mountains) have been found in aquifers in Missouri (Banner et al., 1989).

Lateral migration from different basins is also possible if there are carrier beds within the underlying stratigraphy which contain good to excellent porosity (Jenden et al., 1988b). Included within lateral migration is the effect of long distance groundwater focusing on noble gas accumulation (Ballentine and Sherwood Lollar,

2002). There is greater potential for this where fracture networks and faults intersect groundwater flow (Ciotoli et al., 2005).

Torgersen and Clarke (1985), suggest that the accumulation of ^{4}He in some basins is governed by a combination of three distinct processes: 1) in situ release of the products of the radioactive decay of U and Th (recoil), 2) the in situ weathering of the basement rock releasing ^{4}He which had accumulated along grain boundaries and 3) another input from a different system i.e.: an outside input of ^{4}He to the basin. By this principle, outside input > recoil > weathering which is supported by the helium mass balance conducted in Chapter 3 for helium-rich reservoirs in Kansas and for the Hugoton-Panhandle gas field.

The focusing of noble gases is sometimes attributed to the gas phase composed of CO_2 stripping old groundwater containing accumulated ^{4}He and nitrogen (Ballentine et al., 2000; Gilfillan et al., 2008). CO_2 flushing of magmatic systems can also lead to a strong crustal overprint of ^{4}He and ^{3}He which have been carried by the gas from depth. CO_2 is released from the basement and clay layers by heat like N_2, however it is prone to being used up in other reactions and lost perhaps attributing to its almost negative correlation to helium.

1.4.5. Entrapment and escape

In order for a trap to hold petroleum products in place, it must either be sealed by an impermeable caprock or faulted against an impermeable rock type. It is far more probable for gases which would normally remain in solution to exsolve in the presence of another gas already filling the gas cap.

The proportion of helium in pore spaces which is in solution is dependent on the partial pressure of the helium. The total pressure in the pores is generally fixed by the overburden pressure, which would mean that the partial pressure of helium is reliant on the quantities of other gases present. This could explain why CO_2 and N_2 have often been cited as carriers (Newton and Round, 1961).

Alternatively helium gas atoms have a diameter of approximately 0.20 nm, and the associated nitrogen gas molecules are larger at around 0.34 nm (Hunt, 1996). Seals which contain other gases may not a good representation of a seal for helium since seals which may seal CO_2, might not hold helium according to its smaller atomic diameter. Due to the small size, helium could very well diffuse through a seal therefore seals with smaller pores will have a lower rate of diffusive loss (Broadhead, 2005).

In a review of the world's 176 giant gas fields, almost all of them were dependent on shale or evaporite seals (62% and 38% respectively) (Grunau, 1981). Seal thickness is also an issue, however it doesn't linearly influence the amount of hydrocarbon column to be held by a top seal.

The timing of trap formation is key for helium systems, especially for fields which contain high levels of N_2. Most traps which hold significant amounts of helium gas were formed in the latter part of the Cenozoic which coincides with several key orogenic events in the Earth's history and seal sandstone or carbonate reservoirs.

Rates of trap destruction through geological processes such as weathering, erosion and tectonic events vary over time. Free gas can migrate upwards due to differences in the specific weight between the gas and the surrounding fluids. It can then escape through the caprock due to either natural fractures in the caprock,

manmade fractures or the destruction of porosity which enables the smaller molecular elements to escape (Robertson et al., 2012).

Complex fold belts and overthrust belts are commonly subject to seal destruction. Of the world's 25 largest gas fields, 21 are in cratonic settings and 4 are in fold belts (Grunau, 1981). It is suggested in Ungerer et al., (1990) that gas escape from some caprocks display a cycle of escape and replenishment and that others show characteristic seismic 'gas chimneys' which indicate gas is escaping from the caprock due to fractures (Løseth et al., 2003).

1.5. Objectives and thesis outline

Both scientific and industrial research into a unified helium exploration method is either still in its infancy or not available for public consumption. Currently there is only one study available which specifically records the geochemistry of a high CH_4-high ^4He system and identifies a source and migration pathway into reservoirs; and even this study was an examination of the N_2 characteristics of the system (Ballentine and Sherwood-Lollar, 2002).

To date this will be the first systematic study undertaken using noble gas isotopes and stable isotope analyses to identify the source(s) of economic helium reserves, the potential migration pathways which lead to its focusing into reservoirs and its interaction with other gases which are found in the same reservoirs with the aim of providing the first stage of a helium exploration method.

This thesis will accomplish this by: 1) providing a comprehensive noble gas and stable isotope study focusing on ^4He sourcing and migration pathways using 21 samples taken from helium-rich fields within 2 geological provinces (the Central

Kansas Uplift and the Kansas Basin in the USA) which are compared to and with measurements taken from the neighbouring Hugoton-Panhandle giant gas field (Chapter 3), 2) identifying the isotopic character of the nitrogen endmember associated with ^{4}He by conducting a noble gas and stable isotope study on 3 samples taken from high N_2-high ^{4}He wells from Utah, Montana and Saskatchewan, Canada (Chapter 4) and 3) synthesising what we have learned from these regions of North America into a helium exploration methodology which can then be used to identify economic helium areas on another continent (Tanzania, Central Africa) (Chapter 5 and Chapter 6).

In addition to the introduction and objectives of this thesis outlined above and the four data chapters this thesis also includes: the field sampling techniques and experimental procedures used in all studies (Chapter 2) and a summary of the results, overall conclusions and the potential for future work (Chapter 7).

Chapter Two: Methods

2.1 Introduction

The collection and analysis of noble gases in natural gas samples has been documented by other authors (Zhou, 2004; Gilfillan, 2006) however there are five main requirements for successful analyses: 1) the collection of the sample into a sealed vessel which is either free from or minimally air contaminated and which will not leak both gas out and air in over a significant timescale (years) 2) a purification line with an ultra-high vacuum (UHV) of ~10^{-8} mbar and the maintenance of low blank levels (ideally 1% of the sample/standard concentration or lower), 3) efficient methods of removing reactive gases from the sample e.g.: nitrogen, carbon dioxide, water, hydrogen, 4) a way to separate the noble gases so they can be analysed individually and 5) specialised mass spectrometer(s) to analyse the stable isotopes of the noble gases.

This chapter gives an overview of the design and commissioning of the Oxford Purification Line and the methodology involved in line development, sample analysis and sample collection in the field at the time of sample analyses (2015 to 2016).

2.2 Sampling in the field

The greatest challenge during the sampling of gases, oil or water is avoiding or minimising air contamination. So as to minimise this the vessel containing the gas sample must be considered helium leak-tight and to this end internally polished refrigeration grade copper tubes were used (Beyerle et al., 2000; Hilton et al., 2002; Zheng, 2004; Gilfillan, 2006). These copper tubes were approximately 70 cm in

length and 10 mm outer diameter. Alongside these tubes was a portable stainless steel rack and stainless steel clamps used for holding sample tubes in place and then cold welding them shut after gas flushing.

When sampling from helium-rich natural gas reservoirs gases are taken directly from the wellhead. The sampling setup commences when a single (or double stage) regulator which is appropriate for the wellhead pressures (the maximum inlet pressure for our regulator was 310 bar) is attached to a valve on the wellhead using a suitable NPT fitting. The regulator is then attached to the end of the copper tube by a length of heavy duty PVC pressure hose capable of withstanding pressures of at least 2 bar. Sample tubes can be attached in series when collecting more than one sample from a wellsite. At the end of the series of copper tubes, another piece of the same heavy duty hose is attached to act as an exhaust port (**Figure 2.1**).

Gas is then flushed through the copper tubes at around 1 bar or below (this is the maximum pressure the copper tubes can withstand) for 5 mins. After flushing the tubes, the tubes are clamped starting with the end of the tube furthest from the wellhead and working backwards towards the wellhead. After this the tubes are marked with the location, date and position in series with permanent marker on the copper body and in pencil on strips of masking tape attached to either end of the tube.

Individual copper tubes were wrapped in layers of bubble wrap to prevent damage in transit before being packaged and shipped back to the United Kingdom for gas analyses. Before samples could be shipped from locations appropriate MSDS (Material Safety Data Sheets) were required for the contents of the samples and due to the contents of samples being classified as Dangerous Goods I had to take a

Dangerous Goods course in order to become IATA certified so that samples could be flown back to the United Kingdom from the USA and Canada.

Figure 2.1.: Collection of natural gas samples from the Bonnie Carson #1 well using the field sampling setup outlined above, Ford County, Kansas in 2014.

2.3. Analytical equipment

2.3.1. The Oxford Purification Line

The first stage of the Oxford Purification Line is the Proc Line. It is based on the construction of the MAP Extraction Line originally created in-house at University of Manchester described in Gilfillan (2006). It acts as the primary area for the removal of reactive gases such as N_2, CH_4, CO_2 and the heavier hydrocarbons and hydrogen from samples (**Figure 2.2**). The line is constructed of stainless steel tubing (18 mm diameter) and bakeable all-metal valves.

The Proc Line is kept at approximately 10^{-8} mbar during the purification process by a diaphragm backed turbomolecular pump which can also pump any part of the line depending on the combination of open and closed valves thereby achieving line maintenance.

The Proc Line also contains a Baratron® gauge which measures pressure up to 1000 torr. This is located adjacent to the part of the line into which the pipette volume is expanded and is used to calibrate the pressure of the sample admitted into this section of the line relative to the background air pressure (760 torr).

A Pirani™ gauge is also attached to the line which measures the vacuum pressure of the roughing line which is kept at around 10^{-3} mbar by a rotary pump while pumping down a closed sample. A Magnetron™ gauge is attached to the line adjacent to the turbomolecular pump and measures the vacuum pressure of the rest of the line which is usually around 10^{-8} mbar.

The line also contains a lower sensitivity Hiden™ quadrupole mass spectrometer (QUAD) described in Warr, (2013) which is exposed to a 1 cm^3 aliquot

of the sample before any of the cleaned sample is let into the prep section of the line so as to gauge preliminary concentrations of the noble gases. The QUAD is kept isolated from the rest of the line at UHV. This is achieved by a separate ion pump which keeps the pressure around 10^{-9} mbar.

Gas samples are cleaned by being first equilibrated with a Ti-sponge furnace operating at 950°C which removes reactive gases. The temperature of the Ti-sponge furnace is then lowered to room temperature to remove hydrogen from the sample. From here the sample is then expanded to two getters; one of which is a SAES GP50 Zr-alloy getter that operates at 523K thus removing any leftover active gases. The other is a SAES NP10 getter which operates at near room temperature (295K) and removes hydrogen from the gas sample.

The second part of the gas purification process is the Cryo Line (**Figure 2.2**). To separate the inert noble gases, the sample is equilibrated with a stainless steel water trap (operating at a temperature gradient set at 250K and 180K) to adsorb water, and two refrigerated cryotraps to adsorb the noble gases. These three traps are enclosed within a vacuum shroud to maintain thermal stability. The first trap (a Janis 24K Closed Cycle Refrigerator) uses a stainless steel sorb and operates at a temperature of 31K so as to adsorb Ar, Kr and Xe. The second trap (a Janis 10K Cycle Refrigerator) operates at 15K and adsorbs Ne onto a charcoal finger. Such low temperatures are achieved by cooling the refrigerated via a two stage helium expansion process. Temperatures on these traps are set by computer control and are stable to ± 0.2K or better.

The last stage of the process, the Prep Line, contains both manual and automatically controlled valves whereas both the Cryo Line and Proc Line contain only manual valves. Individual noble gases are run through this part of the line and

are sometimes split into smaller volumes depending on readings from the QUAD. Helium is redirected through this line to the Helix SFT™ mass spectrometer or, if concentrations are low, is adsorbed onto an activated charcoal cryotrap and then heated up again and released into the mass spectrometer. Run times for Helix analyses were approximately 15 minutes. Ne, Ar, Kr and Xe are equilibrated with and measured by the Argus VI™ mass spectrometer. Run times for Ne were approximately 10 minutes, for Ar approximately 10 mins and for Kr and Xe approximately 20 minutes.

The Prep Line contains four getters, two of which are run similarly to the getters on the Proc Line (one hot and one cold). The other two getters are held at a constant temperature and are adjacent to the inlet valves of each mass spectrometer. These extra getters are a precaution against any stray reactive gases entering the mass spectrometers. The prep line is kept at UHV by a Varian ion pump at around 10^{-9} mbar.

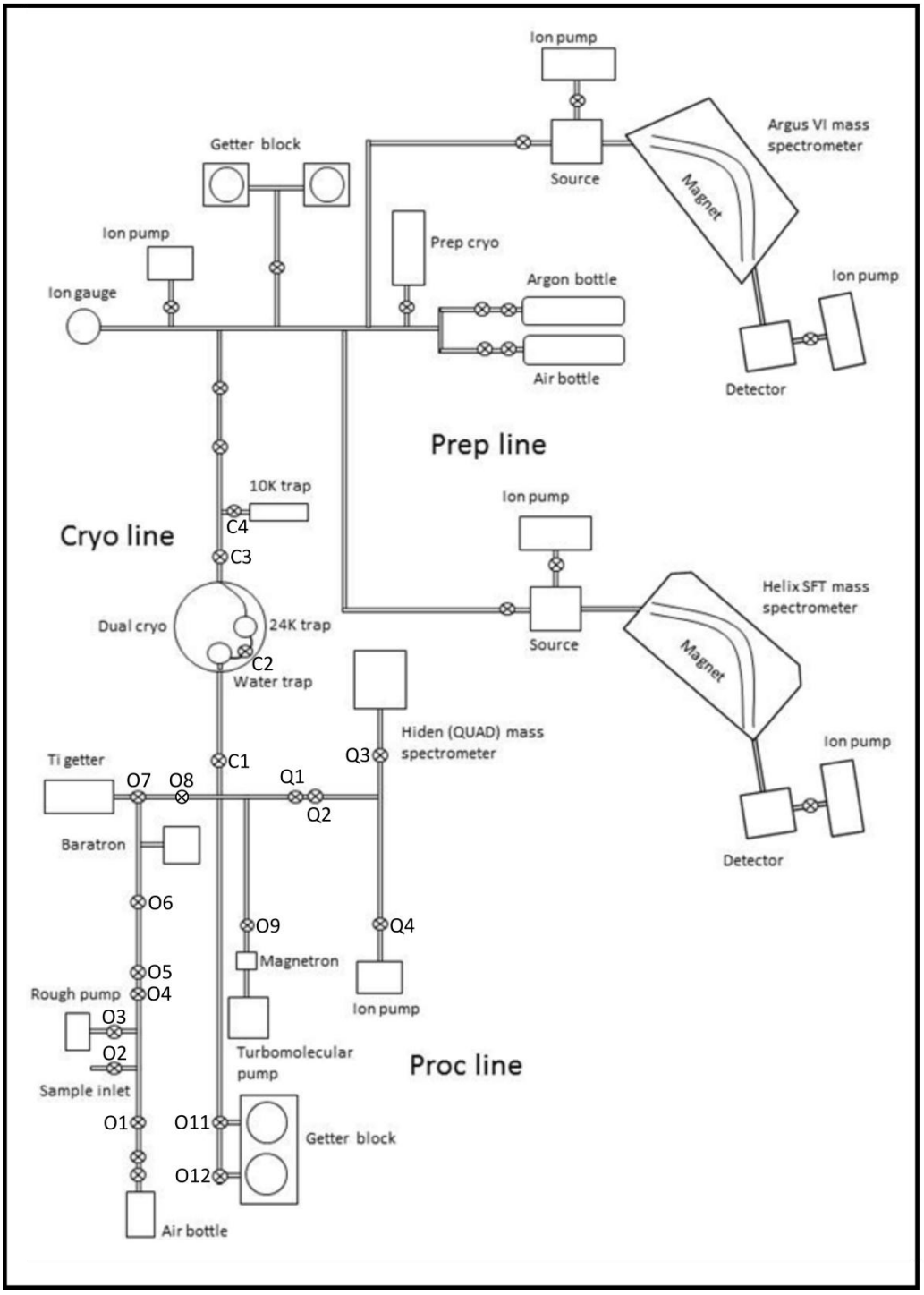

Figure 2.2: Schematic of the Oxford Purification Line.

2.4. Mass spectrometers

2.4.1 Helix SFT™

Helium isotope measurements were conducted by the Helix SFT™ static vacuum mass spectrometer (Thermo Scientific™). The Helix SFT™ contains a magnetic sector analyser with a 35cm radius of curvature and 120º sector extended geometry ion optics. The split flight tube is suited to the simultaneous collection and analysis of both ^{3}He and ^{4}He. The spectrometer uses a Nier-type ion impact source giving sensitivities of >2.0 x 10^{-4} Amp/Torr at <1.2 mA trap current for helium (Nier, 1940). The Helix has an internal volume of approximately 1400cm^{3}.

The Helix is fitted with a detector assembly comprising of a high mass voltage depressed deep Faraday bucket and a low mass Balzers SEM ion counting multiplier with an electrostatic analyser (ESA). The Faraday is fitted with a software switchable 1 x 10^{11} and 1 x 10^{12} Ω gain amplifier. During analysis, the Faraday is used to determine ^{4}He and the electron multiplier is set to measure ^{3}He. The electron multiplier has a maximum resolution of >700 which is necessary for the separation of the ^{3}He-HD^{+} doublet and $^{3}He^{+}$ peaks. The Faraday has a lower resolution with a maximum of >400. The low mass detector is also fitted with a 90°, 50mm energy filter (ESA) which enables the system to measure extremely large ratios without peak tailing.

A Varian VacIon Plus 40 StarCell™ ion pump maintains an ultra-high vacuum in the spectrometer. Its pumping speed is 40L/sec. During sample analysis, the mass spectrometer is isolated from the ion pump while a SAES Zr-Al alloy NP10 getter pump operating at room temperature removes any hydrogen still remaining in the sample.

2.4.2 Argus VI™

The Argus VI™ static vacuum mass spectrometer (Thermo Scientific™) is used to measure the other noble gas isotopes: ^{20}Ne, ^{21}Ne, ^{22}Ne, ^{36}Ar, ^{38}Ar, ^{40}Ar, ^{78}Kr, ^{80}Kr, ^{82}Kr, ^{83}Kr, ^{84}Kr, ^{86}Kr, ^{124}Xe, ^{126}Xe, ^{128}Xe, ^{129}Xe, ^{130}Xe, ^{132}Xe, ^{134}Xe and ^{136}Xe. It is a stainless steel, single focus, extended geometry mass spectrometer with a 90° sector and 13cm radius flight tube. The Argus contains a tapered flight tube and has an internal volume of approximately 700cm^3. The spectrometer uses a Nier-type bright source giving sensitivities in excess of 1 x 10^{-3} Amp/Torr at 200 μA trap current for argon (Nier, 1940).

The collector array contains 5 Faraday cups and a low mass CDD (compact discrete dynode) ion counting multiplier. The Faraday cups are denoted as H1, H2, AX, L1 and L2. H values denote high mass cups, AX denotes the axial cup and L values denote low mass cups. Ion beams are measured relative to the axial cup. The resolution of the system is defined by the collection apertures and is in the range of 225-250. The resolving slits and 1mm entry apertures are designed to give a simultaneous collection of the Ar isotopes 36 to 40.

The ultra-high vacuum in the Argus is maintained by a Varian VacIon Plus 20 StarCell™ ion pump. This pumps at 20L/sec. During sample analysis the spectrometer is isolated from the ion pump but sample gas is still exposed to a Sorb-AC Zr-Al alloy SAES NP10 getter pump at room temperature to trap residual hydrogen.

2.5. Blanks

Full line background blanks were measured prior to running each set of samples through the purification system. This was done so as to check that there

were no leaks in the line and also to check that there was no residual contamination in either the line or the mass spectrometers from the previous samples. The procedure for running both full line blanks and samples will be outlined below (2.8 Sample loading and preparation).

For all samples it was ensured that background blank levels were below 1% of typical sample concentrations before proceeding with running samples. In the event of high blank backgrounds (mostly from either helium or argon) the line was left to bake overnight with another blank taken the following morning to recheck blank levels.

Blank measurements over the course of the thesis were as follows; for the USA and Canada samples: $^{4}He = 1.63 \times 10^{-8}$ to 3.08×10^{-6} cm^3STP/cm^3, $^{20}Ne = 3.69 \times 10^{-9}$ to 2.11×10^{-8} cm^3STP/cm^3, $^{40}Ar = 7.30 \times 10^{-6}$ to 8.01×10^{-5} cm^3STP/cm^3. For the Tanzania samples: $^{4}He = 2.06 \times 10^{-9}$ to 4.63×10^{-8} cm^3STP/cm^3, $^{20}Ne = 2.49 \times 10^{-9}$ to 3.73×10^{-9} cm^3STP/cm^3, $^{40}Ar = 1.66 \times 10^{-5}$ to 6.45×10^{-5} cm^3STP/cm^3. These concentrations are negligible compared to the sample concentrations for all isotopes.

2.6. Air standards

Full line air standards were run on a weekly basis and calibrated against internal standards which were run every night following sample analyses from the Prep Line. He, Ne, Kr and Xe overnight standards were purified from a stock air cylinder on the Prep Line, whereas Ar running standards were run from a reduced pressure, pre-cleaned Ar-cylinder also situated on the Prep Line.

The overnight standards for all noble gas isotopes were determined over a concentration range which spanned two orders of magnitude, to ensure that samples

could be normalised to similar abundance magnitude standards. These standards primarily show whether there are any changes in mass spectrometer sensitivity but can also show variations from normal background leftover by samples and over time can show mass spectrometer drift. Due to the consistency of these internal standards they are used to ascertain the noble gas isotopic ratios of samples (**Figure 2.3**).

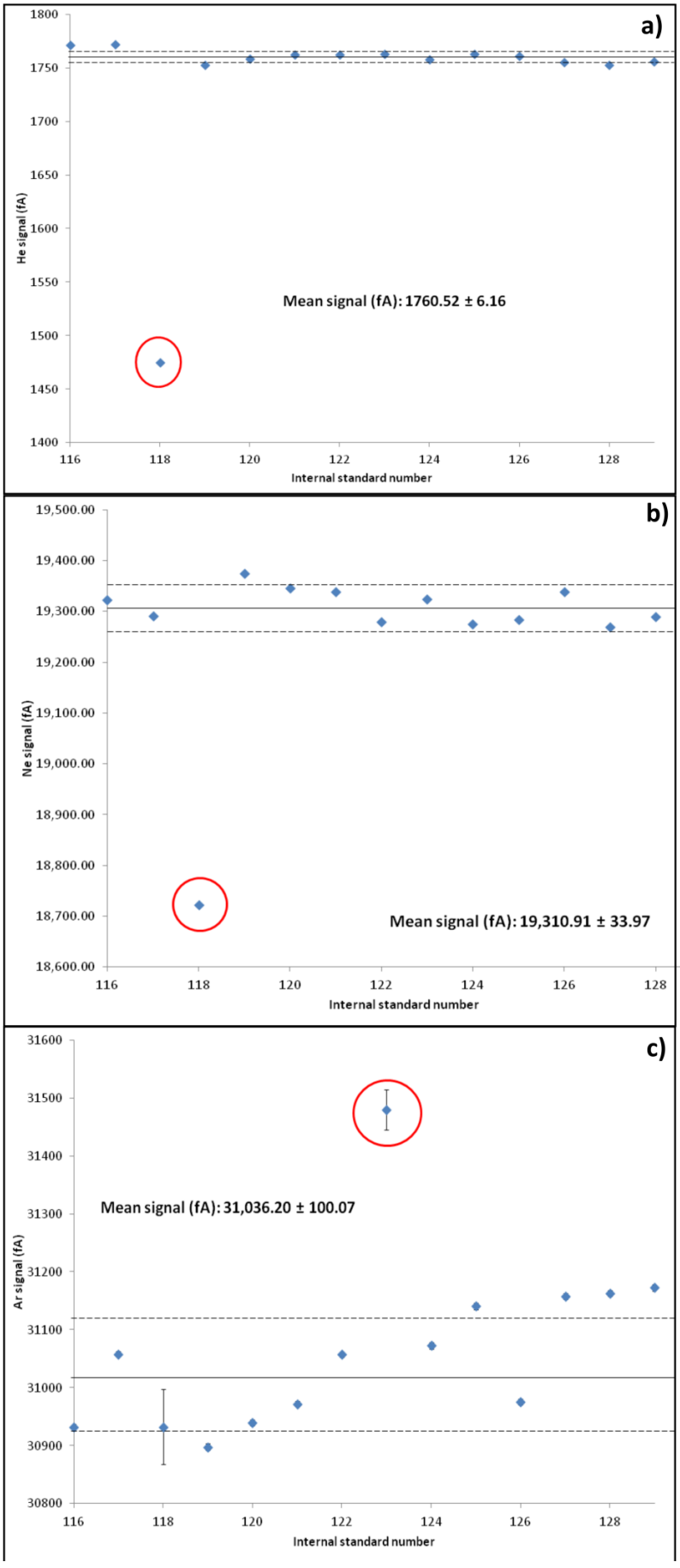
a)
He signal (fA)
Mean signal (fA): 1760.52 ± 6.16
Internal standard number
b)
Ne signal (fA)
Mean signal (fA): 19,310.91 ± 33.97
Internal standard number
c)
Ar signal (fA)
Mean signal (fA): 31,036.20 ± 100.07
Internal standard number

Figure 2.3. Plots of the variance in signal measured for the internal overnight standards for a) He, b) Ne and c) Ar against the standard number illustrating the stability of both the Helix SFT™ and Argus VI™ mass spectrometers over a 2 week period. Solid lines represent the mean for each element and dashed lines denote the 1σ error bounds. Samples normalised to the internal standards propagate the error through to the final uncertainty despite errors falling below 0.3%. Red circles denote anomalous readings which were not taken into account for the mean and error. The red circles for helium and neon were caused by a heater error on the cryotrap and the red circle on the argon was potentially caused by a high argon background after a long sample run.

Full line air standards are standards which are run in exactly the same way as a sample and originate from the air standard bottle on the Proc Line which was collected in University Parks, Oxford, UK on November 24, 2014. The standard cylinder contains air at a known temperature, humidity and pressure of 4°C, 95% and 1027 mbar respectively. The concentrations of the noble gas isotopes in the air standard were calculated from typical atmospheric partial pressures (Ozima and Podosek, 2001; Ballentine and Burnard, 2002).

2.7. Sample loading and preparation

The first part of the process involves attaching the clamped copper tube containing the sample gas to the inlet port (O2) of the Proc Line (**Figure 2.2**). Before this, valves O1, O2, O3, O4 and O5 should be closed. Once the sample is successfully attached O2 can be opened and also O3 (to the rotary pump) which will start roughing the line. The line should reach around 1 x 10^{-3} mbar once vacuum is achieved. Once vacuum is reached, close O3, O7 (to the Ti-furnace), O11 and O12 to the getter valves and the C1 valve to the cryoline. Valves O4 and O5 are then opened to the turbomolecular pump and the system is left to pump down to background pressure overnight (10^{-8} mbar). Before the system is left for the night, the sample inlet and roughing line are helium leak tested using the Hiden™ software.

The next morning, once it has been ascertained that the pressure is at normal background levels (10^{-8} mbar), the line is again helium leak tested before sample release.

Once valves O1, O3, O4 and O5 are closed, the sample can be released into the line by opening and removing the clamp and then clamping a v-notched copper tube opener (collar) around the previously clamped section of tube. When the collar is tightened it squeezes the clamped section open enabling gas to flow into the sample inlet manifold.

Once in the sample inlet manifold the sample can then be isolated between three calibrated sections of the Proc Line: 1) Section O1 to O4 designated the 'manifold volume' (78.5 cm^3 ± 0.12%), 2) Section O4 to O5 designated the 'pipette volume' (1.4 cm^3 ± 2.06%) and 3) Section O5 to O8 designated the 'calibrated volume' (previously calibrated by CJ Balletine and Z Zhang as 69.7 cm^3 ± 0.5%). Between the introduction of gas to each part of the line the sample is given 30 seconds to equilibrate.

For known high helium samples (8.0 x 10^{-3} $cm^3STP(^4He)/cm^3$ ≤) the pipette volume was isolated from the manifold volume and then introduced into the calibrated volume. Once the correct volumes for samples are established the gas sample can either be reduced to a lower pressure using the O6 and O8 valves or more pressure can be generated by adding pipette amounts of gas from the manifold volume. The safest course of action for an unknown sample, however, is to start off with a pipette volume of the sample.

Once the sample is isolated between valves O4 and O7 and its final pressure has been recorded it can then be introduced to the first stage of the cleanup process; a Ti-sponge furnace (by opening valve O7) heated to 950°C for 15 mins. The furnace

is then removed and the Ti-sponge cooled to room temperature for 20 mins to remove excess hydrogen from the sample which could interfere with the ^{3}He peak. While the sample is being cleaned by the Ti-sponge valves O11 and O12 to the getter block are reopened to prepare for the next stage of cleanup. Valve Q1, the inlet to the QUAD pipette, is also opened during this time.

The line is then isolated from the turbomolecular pump by closing valve O9 before the sample is exposed to the getter block for 15 mins. The two Proc Line getters outlined in Section 2.3.1 operate in the same manner as the Ti-sponge furnace to remove any leftover reactive gases from the sample.

After this stage the sample is then introduced to the first trap in the Cryo Line by opening valve C1 for 15 mins. After 15 mins, valve Q1 is closed, isolating the QUAD pipette of the cleaned sample to be equilibrated with the Hiden™ QUAD mass spectrometer as a first look at the isotopic abundances. This ensures the separated noble gases can be reduced to levels safe for the mass spectrometers to measure.

By opening valve C2 the rest of the gas sample is equilibrated with the second cryogenic trap which adsorbs Ar, Kr and Xe over 15 mins. After this time the sample is manually introduced to the final trap which adsorbs Ne leaving only He as a free gas phase in the line. From this point onwards the system is mostly automated.

2.7.1 Helium measurements

Helium measurements are conducted on the Helix SFT™ mass spectrometer. Dependent on the results of the Hiden™ isotopic scan, it can be established whether helium is within safe limits for the machine by directly comparing a sample as it

appears in the mass spectrometer (fA) to as it appears in the Hiden™. By using this method as a first approximation it becomes apparent when helium levels are too high for the Helix SFT™ to measure safely (over 50,000 fA). For most high helium samples (8.0×10^{-3} $cm^3STP(^4He)/cm^3 \leq$) another split is required before the sample can enter the mass spectrometer.

There are three ways to further reduce sample volume if it becomes apparent that certain isotopes (either ^4He or ^{40}Ar in high helium samples) are too high for either mass spectrometer to run safely. In the Prep Line these are known as: 1) an aux split: splitting the gas by expanding and isolating a portion in the auxillary volume on the prep line before re-expanding the gas to the manifold from the auxillary volume multiple times, 2) manifold split: expanding the gas into the manifold volume before isolating the gas in just the manifold volume, or 3) pipette split: expanding the gas into the pipette volume before isolating it, pumping out the main manifold, and then re-expanding the pipette volume into the manifold volume. The method used for all high helium samples was the more extreme pipette split which was determined to be the equivalent of 2161±13 times less than the Prep Line manifold volume and is taken into account when propagating the uncertainty on sample concentrations.

Once the correct split has been conducted, helium is introduced into the Helix SFT where ^4He and ^3He are measured simultaneously on the Faraday cup and CDD respectively. Simultaneously, the system up to C3 (which is closed) is pumped out by another turbomolecular pump, clearing the line of excess helium in preparation for the release of Ne from the 31K charcoal trap. After the sample has finished running the Helix SFT is manually pumped out.

2.7.2 Neon measurements

The automated prep bench system can control both mass spectrometers simultaneously, enabling Ne to be released while the Helix SFT™ is still measuring helium isotopes. The charcoal finger behind valve C4 is heated to 90K and is left to equilibrate for 15 mins. This releases all neon into a free gas phase in the line. The gas is then split accordingly and released into the Argus VI™ mass spectrometer. After 30 seconds to equilibrate the mass spectrometer is isolated during the measurement. The Argus VI™ measures ^{20}Ne and ^{22}Ne on two Faraday cups (H2 and AX) and ^{21}Ne on the CDD. The peaks for $^{40}Ar^{++}$ and $^{44}CO_2^{++}$ are also measured to determine interference to ^{20}Ne and ^{22}Ne respectively. During the measurement of neon isotopes the line is pumped back to the C3 valve to clear the line of excess gases and after the measurement the mass spectrometer is automatically pumped out.

2.7.3 Argon, krypton and xenon measurements

The heavy noble gases are released by a stepwise process of heating and cooling on the 24K stainless steel trap. Argon is the first to be released by setting the temperature of the trap to 60K for 15 mins before splitting the free gas phase and inletting into the Argus VI™. The Argus measures ^{40}Ar on the H1 Faraday cup and ^{38}Ar and ^{36}Ar on the CDD by peak jumping. During this time the stainless steel trap (second stage trap) is then subjected to three cycles of heating, cooling and then pumping. The trap is heated to a maximum of 375K and then back down to 60K for each temperature cycle. This trap temperature cycling releases most of the residual

Ar in the Cryo Line so that there is minimal interference/suppression to the krypton and xenon results.

The last stage of the process is the simultaneous release of krypton and xenon. This is achieved by heating the stainless steel trap to 200K for 15 mins which releases both elements into a free gas phase. The Argus VI™ has the capacity to simultaneously analyse both krypton and xenon by peak jumping between the two elements. Following the measurement the traps are raised to their maximum temperature of 375K to release any residual sample and then both the Prep Line and Proc Line systems are pumped out to their respective turbomolecular pumps. A complete analysis of all noble gases including preparing the system takes approximately 6 hours meaning that a maximum of 3 sample measurements could be

2.8. Data reduction and error propagation

2.8.1. Data reduction

Both the Helix SFT™ and Argus VI™ have the ability to automatically peak centre once an isotopic peak has been identified within a set scan region. The Helix SFT™ in the Oxford Noble lab is set to manually peak centre. This is achieved by manually setting a scan range before inletting the sample or standard. The peak centre can then be read off the graph and manually input into the system.

Once the peak centre has been identified the mass spectrometer determines the signal intensity of the same point in the scan 30 times (Argus VI™) or 100 times (Helix SFT™) to generate an exponential decay curve as a function of time for each

isotope. A regression algorithm to the data gives both the initial signal intensity and the uncertainty on that measurement.

Two types of error must be taken into account during the data reduction phase: 1) internal error such as the precision to which the signal regression to t = 0 can be measured by the mass spectrometers and 2) external error or reproducibility such as the variance in the isotope signals during the overnight internal standards (**Figure 2.3**).

Due to the stability of both systems the errors for machine measurement are consistently below 0.3% across all Faraday cups however errors on the CDDs tend to be higher due to dependence on the counting statistic. Procedural blanks run after a sample in the same way indicate that blank levels are below 1% of total major isotope concentrations. This indicates that despite the high levels of ^{4}He and ^{40}Ar in high helium samples the system pump down time is sufficient if running 2 samples a day.

Corrections for doubly-charged $^{40}Ar^{++}$ were applied to ^{20}Ne data following the methods of Niedermann et al., (1993) however it was not necessary to apply CO_2^{++} corrections to ^{22}Ne concentrations because CO_2 backgrounds were observed to be at the detection limit therefore rendering them insignificant.

2.8.1.1. Concentration calculations

Noble gas measurements are compared against a procedural air standard run in exactly the same way as the sample in order to ascertain the isotope concentrations. The partial pressures of noble gases are potentially subject to changes in instrument sensitivity over time. The sensitivity of the system is checked

daily by running internal standards over night. Procedural standards are run with procedural blanks before each set of sample runs. These give a view of overall changes to the full system.

In order to construct an equation which will enable us to discern the concentration of a sample we need three primary assumptions: 1) the intensity of the extrapolated measurement (fA) registered on the mass spectrometer is directly proportional to the number of moles of an isotope in a sample i.e.: the linearity of the system which was most likely determined at the beginning of system setup, 2) that all noble gases conform to the laws governing an ideal gas and 3) that machine stability is high thereby making any sensitivity correction by the internal standards minimal (**Figure 2.3**).

From these assumptions we can derive a sensitivity correction (*k*) for concentrations:

$$k = \frac{I_{pp}}{I_{sp}} \quad (1)$$

where I_{pp} is the intensity (fA) of an internal standard run on the same day as the procedural standard and I_{sp} is the intensity (fA) of an internal standard run on the same day as the sample. Due to the stability of the system, internal standards are less than 1% different from each other, showing that machine sensitivity is in this case negligible as a source of error.

From this we can derive:

$$I = kn \quad (2)$$

where I is the intensity of the mass spectrometer measurement (fA), k is the correction for the sensitivity of the machine and n is the number of moles of a specific isotope.

Using the third assumption of an ideal gas:

$$pVC_i = nRT \tag{3}$$

where p is pressure (Pa), V is volume (cm^3), C_i is concentration of isotope, R is the Universal Gas Constant (8.31 $JK^{-1}mol^{-1}$) and T is temperature (K). In order to compare a proc standard to a sample:

$$\frac{n_1 \cancel{RT}}{n_2 \cancel{RT}} = \frac{p_1 V_1 C_1}{p_2 V_2 C_2} \tag{4}$$

where terms (1) relate to the sample and terms (2) relate to the procedural standard. Terms R and T cancel each other out since similar isotopes are being compared (R) and the Noble Lab is held at a constant temperature of 18°C.

By expanding equation (2) and assuming that variation in k is negligible:

$$\frac{I_1}{I_2} = \frac{\cancel{k} n_1}{\cancel{k} n_2} \tag{5}$$

From Equation (5), C_1 can be derived and applied to raw data to determine sample concentrations:

$$C_1 = \frac{p_2 V_2 C_2 I_1}{p_1 V_1 I_2} \quad [\text{cm}^3 \text{ STP}] \quad (6)$$

2.8.2 Error propagation

All experimentally derived values are subject to a degree of uncertainty. In order to calculate the error on a measurement all uncertainties must be accounted for and either discarded as negligible or propagated accordingly for both noble gas concentrations and ratios. This is achieved by determining the error on each part of the process and then either applying the rules for the addition/subtraction of measured quantities or the rules for multiplication/division of measured quantities.

An example of the rules behind addition/subtraction can be given by blank correcting a sample.

In the simplest terms:

$$I_1 - I_B = I_C \quad (7)$$

where I_B is the intensity (fA) of the background blank and I_C is the intensity (fA) of the corrected sample.

In order to propagate the error:

$$I_{Cerr} = \sqrt{(I_{Berr})^2 + (I_{1err})^2} \quad (8)$$

Where I_{Cerr} is the error on I_C, I_{Berr} is the error associated with the background blank and I_{1err} is the error associated with the raw measurement for the sample.

This is used along with the rules for multiplying/dividing which can be illustrated by the last stage of data reduction: normalising the sample to an air standard to ascertain concentration. For this we use equation 6 to form the error propagation equation:

$$C_{1err} = C_1 \times \sqrt{\left(\frac{p_{1err}}{p_1}\right)^2 + \left(\frac{V_{1err}}{V_1}\right)^2 + \left(\frac{I_{1err}}{I_1}\right)^2 + \left(\frac{p_{2err}}{p_2}\right)^2 + \left(\frac{V_{2err}}{V_2}\right)^2 + \left(\frac{I_{2err}}{I_2}\right)^2 + \left(\frac{C_{2err}}{C_2}\right)^2}$$

(9)

where all terms using x_{err} are the propagated errors associated with the particular components. Both equation 8 and equation 9 are used to propagate errors from the raw dataset to isotopic concentrations and ratios.

2.8.2.1. Worked error example for isotopic ratios

This section outlines how to propagate errors for the $^3He/^4He$ ratio (R_a) of the Poverty Hill #1 sample from the Kansas Basin dataset in Chapter 3 (**Figure 2.4**).

Standard ID	Date	4He	3He	SE 4He	SE 3He
Proc Blank #18	15-02-15 11:26	13.81096	N/A	0.002671	N/A
Proc Air #29	15-02-15 16:59	601.7589	0.014102	0.041232	0.000192
Poverty Hill #1	19-02-15 12:26	38,406.99	0.075381	5.835369	0.00042

Figure 2.4.: Table displaying raw signal data (fA) for the Poverty Hill #1 sample and the blank and procedural standard associated with it.

1) Blank correct both the raw standard and sample data (if needed). For all data in this thesis blank concentrations were less than 1% of sample concentrations. Errors from this step can be calculated by summing in quadrature:

$\sqrt{(5.84)^2 + (0.0027)^2} = 5.84$

From the above equation it can be calculated that the blank error contribution is only 0.02% of the total sample intensity and for the procedural air standard the blank is 0.01% of the total intensity.

2) To calculate the error on the $^3He/^4He$ ratio once again sum the errors in quadrature:

$(\sqrt{(5.84/38407)^2+(0.00042/0.075)^2}) \times 1.9627 \times 10^{-6} = 1.094 \times 10^{-8}$

The error is now 0.56% of the total sample intensity and 1.36% of the total air standard intensity which is due to the counting error on ^3He.

3) The final step is calculating the error on the sample R_a ratio which incorporates errors associated with the ^4He internal standards and utilises Equation 9:

$(\sqrt{(1.09 \times 10^{-8}/1.96 \times 10^{-6})^2+(1.42 \times 10^{-7}/2.17 \times 10^{-5})^2+(1.45 \times 10^{-7}/2.44 \times 10^{-5})^2}) \times 0.085 = 8.92 \times 10^{-4}$

At this stage the propagated error makes up 1.05% of the total sample ratio.

2.8.2.2. Propagating errors for isotopic abundance

This section outlines how to propagate the errors for the ^{4}He concentration of the Poverty Hill #1 gas sample. Error propagation for ^{4}He concentration follows directly on from the error propagation carried out for blank correction. The errors associated with the blank corrected sample and the standard are summed in quadrature in a similar fashion to step 3 of the previous section along with errors for: volume, pressure, correcting for the prep pipette split relative to the prep manifold volume, the average of the internal standards and the concentration of ^{4}He in the atmosphere at standard pressures and temperatures. Ultimately the propagated error makes up 1.36% of the total sample concentration.

Chapter Three: Economic Helium Reservoirs in the Mid-Continent United States

3.1. Introduction

Most of the helium-rich natural gas reservoirs discovered to date are in the United States. From the first discovery of helium-rich natural gas in Dexter, Kansas in 1903 (1.84% of total gas composition) to the finding of the highest concentrations of commercial helium in 1950 at Pinta Dome, Arizona (<10% of total gas composition) the USA has been the world's largest producer, consumer and exporter of helium gas. Commercial helium reservoirs are usually classified as those containing over 0.3% helium by volume of gas. The USA contains over 100 identified high helium fields however 97% of its helium output is produced by two fields: Riley Ridge (Wyoming) and the Hugoton-Panhandle giant gas field (Oklahoma, Kansas and Texas) (**Figure 3.1.**). Enriched helium gas from the Hugoton-Panhandle is also stored in the Cliffside Federal Reserve located in Bush Dome. Together these fields constitute an estimated reserve of 20.6×10^9 m^3 (USGS, 2017).

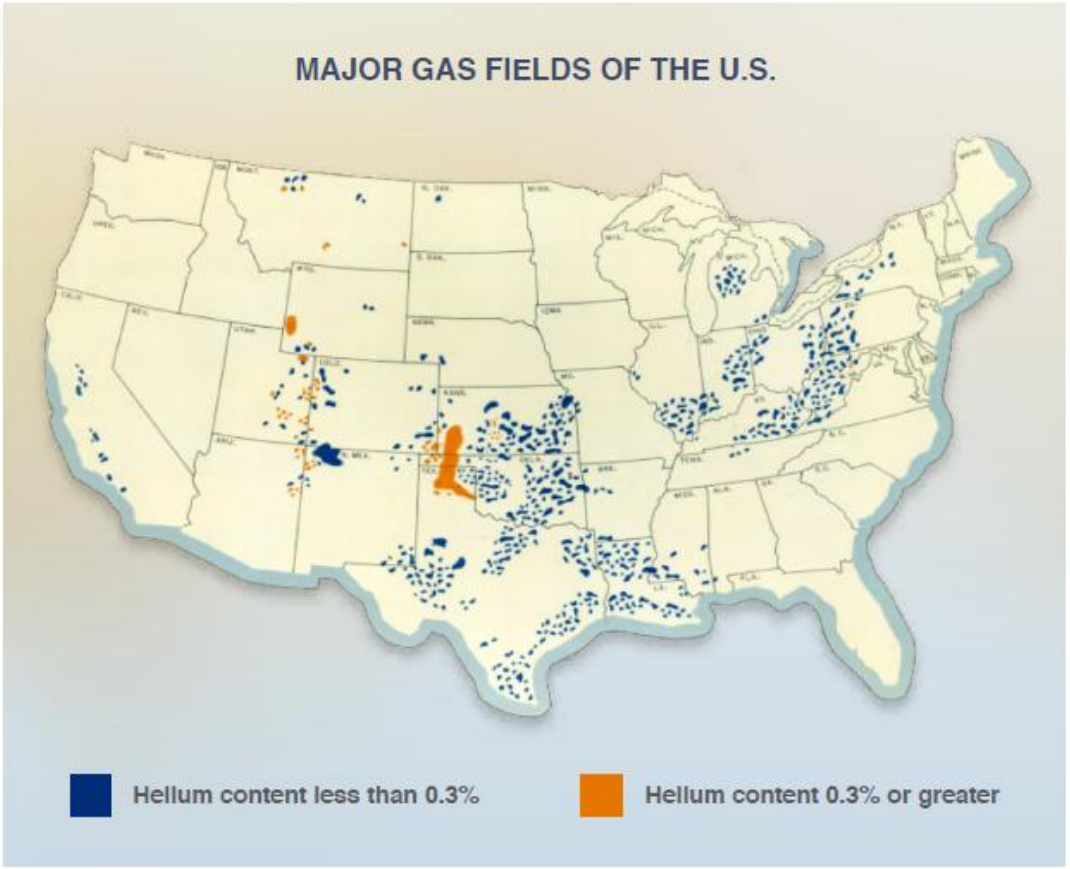

Figure 3.1.: Map of the United States showing identified helium-rich wells since 1970 (from American Physical Society et al., 2016).

With the now large scale production of liquified natural gas (LNG) in Qatar and Algeria, and the large gas volumes involved, the economic concentration threshold for helium in natural gas has been lowered in these locations. The helium reserve associated with Qatar's South Pars Field (the world's largest gas field) is estimated to be 10.1×10^9 m^3 despite helium concentrations in the field of around 0.04% (USGS, 2017).

The helium in these natural gas reservoirs consists of the more ubiquitous ^{4}He isotope which is generated by the alpha decay of uranium and thorium in the Earth's crust. Both stable isotopes of helium (^{4}He and ^{3}He) can also be sourced from the mantle and, in the case of seeps and contaminated samples, from the atmosphere (Ozima and Podosek, 2001; Ballentine and Burnard, 2002).

The determination of where economic quantities of helium has originated and how it has migrated into gas traps can be determined by using other noble gases as tracers (Ne, Ar, Kr and Xe) alongside major stable isotope systems such as those associated with N_2, CO_2 and C.

Producing helium fields fall into three categories: N_2-rich, CH_4-rich or CO_2-rich. N_2-rich fields often contain negligible amounts of CH_4 and CO_2 however significant concentrations of N_2 are always found in CH_4 and CO_2-rich systems. This is hypothetically due to N_2 acting as a carrier gas for helium to enable advection from the deep crust into shallow regions (Etiope and Lombardi, 1996; Etiope and Martinelli, 2002; Ballentine and Burnard, 2002; Fu et al., 2005; Fu et al., 2008; Walia et al., 2009; Hong et al., 2010).

The most detailed geochemical study on a CH_4-rich helium system was conducted on the Hugoton-Panhandle giant gas field. This is particularly significant since the Hugoton-Panhandle is a major producer of the USA's helium. From this previous study a correlation was found between N_2 (concentrations and isotopes) derived from the crystalline basement and crustal ^4He with atmospherically sourced ^{20}Ne derived from groundwater. Since both N_2 and ^4He came from the same source and isotopic ratios indicated mixing of the gases before interaction with groundwater it was determined that they were released together during low grade metamorphism. Once in the shallow crust the two gases dissolved and were accumulated into overlying laterally flowing west-east groundwater. Later this groundwater may have contacted a discrete gas phase, in this case CH_4, in pre-existing traps, at which point the dissolved ^4He and N_2 were released and partitioned into the methane (Ballentine and Sherwood-Lollar, 2002).

Results from the previous study allow us to ask new questions: what tectonic processes are responsible for the release of helium? Do high helium fields show local or regional trends? What are the directions and length scales associated with regional groundwater flow? What role does stratigraphy play in the occurrence of helium-rich fields? When and from where were hydrocarbons introduced into reservoirs and what degree of control does this timing have over helium accumulations? Is there evidence for the interaction of multiple sources of helium into the system? This chapter endeavours to address at least a few of these questions.

3.2. The geology of South-West Kansas and the Hugoton-Panhandle system

The Kansas Basin lies to the east of the Hugoton-Panhandle giant gas field in the region known as the Hugoton Embayment of the Anadarko Basin. Individual fields within the basin range from single wells to the 47.9 km^2 Hanston-Oppy Field which has over 100 wells.

The Kansas Basin can be divided into the Hugoton Embayment and the Dodge City Embayment (McClellan, 1930; Maher and Collins, 1949; Jewett, 1951; Huffman, 1959). Both are considered to be the northward extension of the Anadarko Basin into western Kansas (Merriam, 1963). The basin is approximately 74,074 km^2 and plunges south into the 150,219 km^2 Anadarko Basin where sediments thicken to around 9500 ft. The Anadarko Basin is of Palaeozoic origin with initial formation in the Cambrian as an extension of the southern Oklahoma aulacogen (Ballentine and Sherwood-Lollar, 2002; Bowen and Weimer, 2003).

The Central Kansas Uplift, the north-eastern confining structure of the Kansas Basin, is thought to be south-eastward trending offshoot of the Precambrian-

age Transcontinental Arch (Koester, 1935; Rascoe Jr, 1962; Merriam, 1963; Rascoe Jr and Adler, 1983; Lam and Yarger, 1989).

The Kansas Basin is structurally confined on three sides: to the west by the Sierra Grande Uplift and Las Animas arch of Colorado, to the east by the Central Kansas Uplift (~14,763 km^2), Pratt Anticline and Cambridge Arch and to the south by the Amarillo-Wichita Uplift in Texas and Oklahoma (Merriam, 1963; Adler et al., 1971; Rascoe Jr and Adler, 1983). To the north the basin pinches out against the Central Kansas Uplift and Las Animas Arch (**Figure 3.1**).

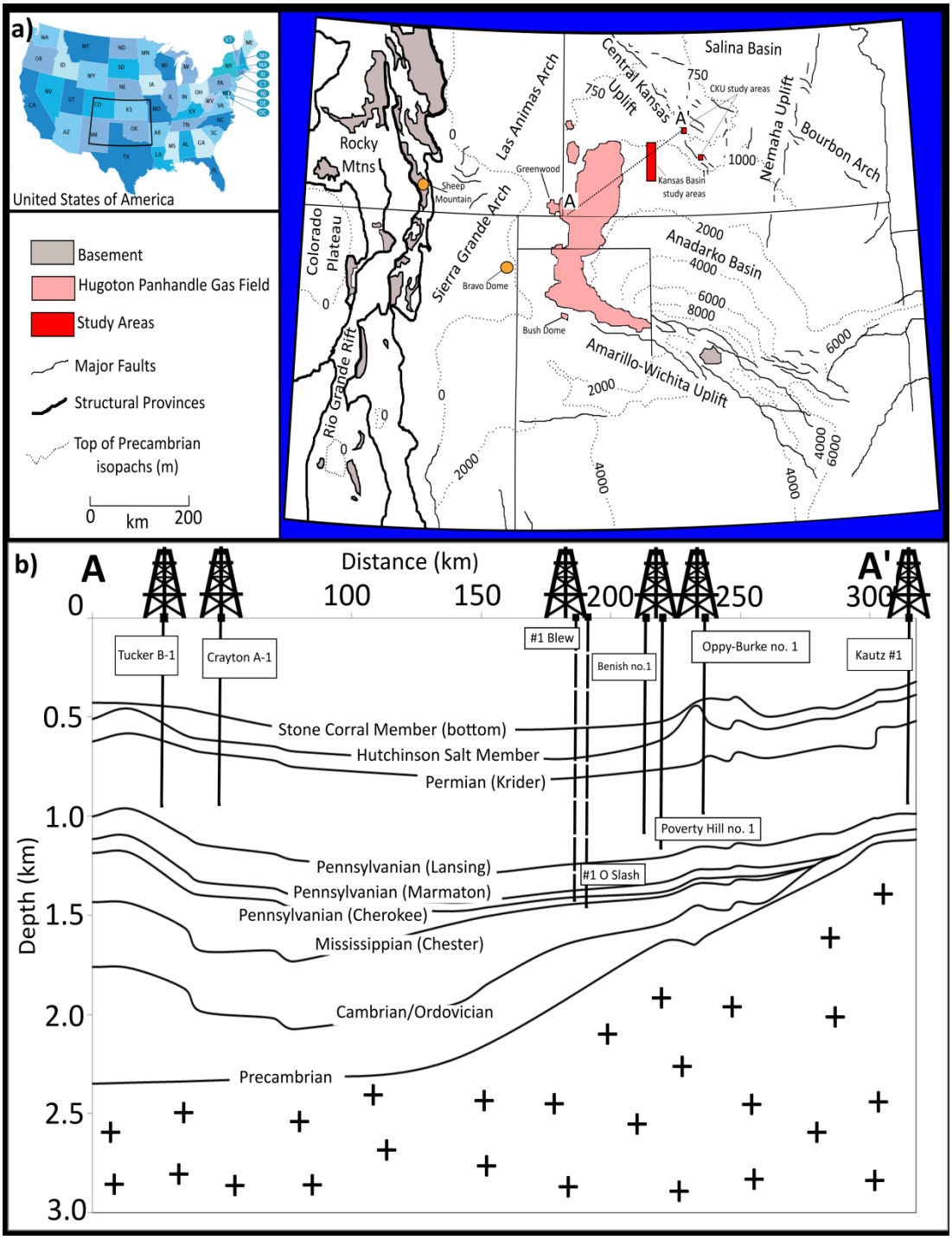

Figure 3.2.: a) Locations of the Kansas Basin study area, Hugoton-Panhandle and Central Kansas Uplift (CKU) in relation to other geological features. Contains features from Ballentine and Sherwood-Lollar, (2002) and Merriam (1963). b) The cross section of A-A' from the Keyes Dome in the Hugoton field to the Kautz #1 well on the Central Kansas Uplift including the positioning of several sample wells along the cross section. Wells #1 Blew and #1 O Slash which have dashed lines are projected from their positioning further south of the cross section line. Strata displayed show formation tops for all except the Stone Corral member.

The Kansas Basin lies on the southern-most part of the stable North American cratonic complex (Merriam, 1963). The 1.8-1.1 Ga Yavapai-Mazatzal Precambrian basement complex beneath Kansas is an extension of the Archean-aged stable continental craton formed from younger accretionary terranes (Hamilton and Kroner, 1981; Condie, 1982; Bowring and Karlstrom, 1990; Shaw and Karlstrom, 1999; Magnani et al., 2004). Subduction of arc terranes during this period led to the younger Precambrian basement beneath Kansas becoming a mixture of rhyolite, metasediments and granite (Landes, 1927). These basement blocks are highly fractured and faulted (Gerhard, 2004; Merriam, 2010).

The basement beneath Kansas can be split into a roughly north-south divide. The north consists of a ~1.63 Ga terrane of sheared igneous and metamorphic rocks whereas the south consists of a younger (1.48-1.34 Ga) terrane which is mainly unmetamorphosed rhyolitic to dacitic volcanics, and associated epizonal plutons which is similar to the basement underlying Oklahoma and the Texas Panhandle.

The northern terrane is similar in rock type and age to exposed Precambrian rocks from the Front Range in Colorado. The sheared granites within the terrane record chlorite and epidote and no medium or high metamorphic indicators. Alongside these are younger, unmetamorphosed granites similar to those encountered in the south of the region which have been dated to 1.48-1.34 Ga.

Metamorphic rocks within the terrane are mainly quartzite or schist indicating a metasedimentary origin. Within the Stevens and Scott counties, which are part of the Kansas Hugoton gas field, zircon U–Pb ages vary between 1.37-1.38 Ga from basement granites. In the southern terrane no rocks older than 1.2 Ga are present (Bickford et al., 1981).

The south-west of Kansas was subject to two major episodes of cratonic epeirogeny the first occurring at the end of the Devonian which uplifted an existing active Precambrian structure to create the Central Kansas Arch; the precursor to the Central Kansas Uplift. The arch separated the North Kansas Basin from the Southwest Kansas Basin (ancestral Hugoton Embayment). This marked the start of an extended period of uplift for the Central Kansas Arch and downwarping for the Southwest Kansas Basin (**Figure 3.3a**).

The Amarillo-Wichita uplift in Texas began around the Mid-Devonian and ended in the late Morrowan (early Pennsylvanian) by which time the uplift had been block faulted into a mountain chain. The Anadarko and Palo Duro Basins in Oklahoma and Texas were separated in the Mississippian during the uplift of the Amarillo-Wichita mountains (Eddleman, 1961). After the Amarillo-Wichita uplift the Anadarko Basin continued to subside and take on an asymmetric look as it was infilled by sediments.

During the Pennsylvanian many of the geological structures still present in the modern day developed due to a second stage of epeirogeny such as the Hugoton Embayment, the Central Kansas Uplift and the Pratt Anticline (Koester, 1935; Merriam, 1963) (**Figure 3.3b**). At this time the Central Kansas Uplift was elevated and folded along a northeast-southwest trend. The Keyes Dome in the extreme south-west of the Hugoton field actively uplifted from the end of the Mississippian to the end of the Pennsylvanian restricting input into the Hugoton from the southwest (Merriam, 1963).

In the Permian uplift on the Central Kansas Uplift ceased around the Hutchinson and it tilted to the SE. Downwarping of the Hugoton Embayment also

stopped around the same time. At the end of the Wolfcampian the Anadarko Basin became landlocked thereby ending significant sedimentation.

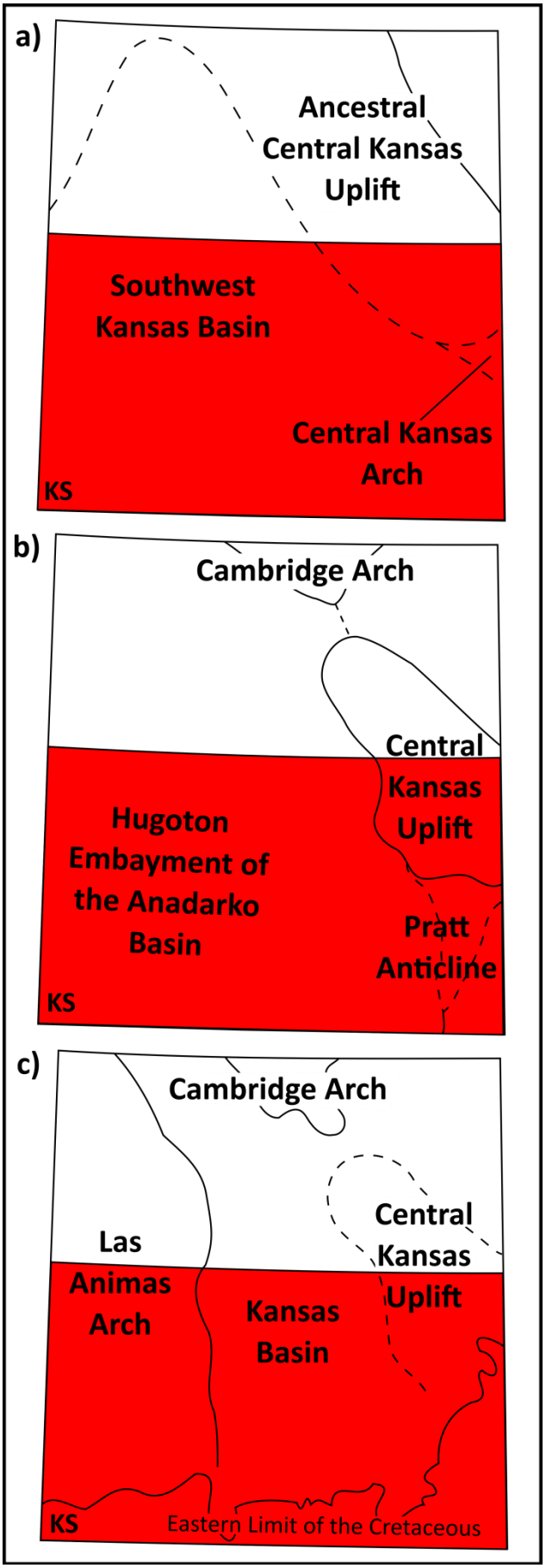
a)
Ancestral
Central Kansas
Uplift
Southwest
Kansas Basin
Central Kansas
Arch
KS
b)
Cambridge Arch
Central
Kansas
Uplift
Hugoton
Embayment of
the Anadarko
Basin
Pratt
Anticline
KS
c)
Cambridge Arch
Central
Kansas
Uplift
Las
Animas
Arch
Kansas
Basin
KS
Eastern Limit of the Cretaceous

Figure 3.3.: The structural development of the geological features of Kansas over time (modified from Merriam, 1963): a) pre-Mississippian post-Devonian; b) pre-Desmoinesian post-Mississippian and; c) Mesozoic. The red box denotes the area of interest for the study.

During the Tertiary, the area between eastern Colorado and western Kansas tilted eastwards forming a homocline which affected only the post-Palaeozoic layers. This is thought to have been influenced by the uplift of the Las Animas Arch on the Colorado-Kansas border during the late Cretaceous to Eocene (Jewett and Merriam, 1959; Merriam, 1963; Rascoe Jr, 1978; Bowen and Weimer, 2003; Merriam, 2010).

Economic helium deposits in the Kansas region have been found in Palaeozoic strata (in dolomite, limestone and sandstone) from the Permian Chase Group down to the Ordovician Arbuckle Group (**Figure 3.4**). In the sampled fields from the south-west, gas production zones come from two geological layers: the Permian and the Carboniferous (Pennsylvanian/Mississippian) (**Appendix A**).

Helium-rich gas appears to be concentrated in specific layers in the subsurface. Layers inbetween these may also contain helium except at sub-economic concentrations.

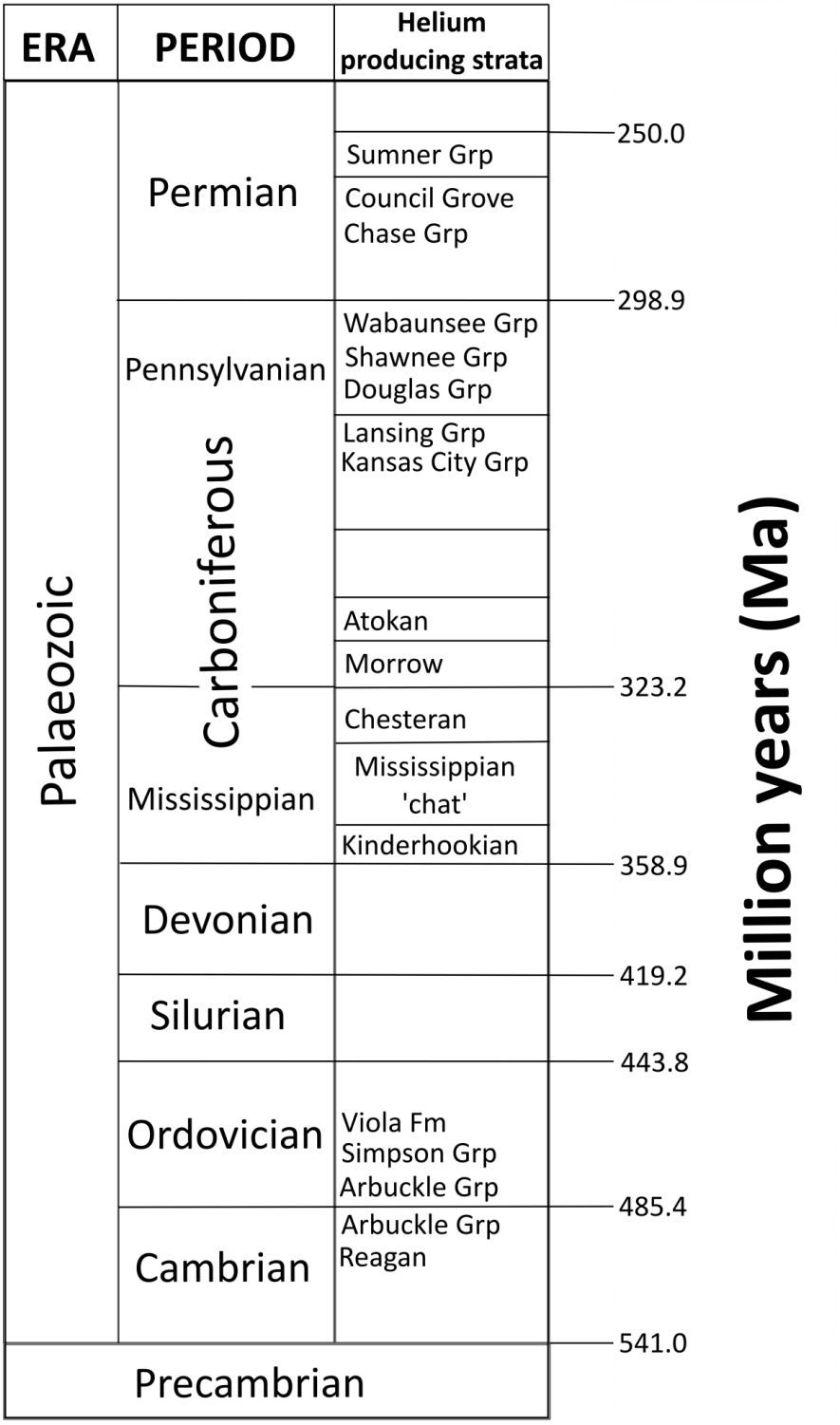

Figure 3.4.: General stratigraphy of Kansas in relation to known helium reservoirs (modified from Newell et al., 1987).

Throughout the Hugoton Embayment, helium accumulations are associated with high concentrations of N_2. As with the Hugoton-Panhandle, the hydrocarbons associated with these localised fields are thought to have been generated in the Anadarko Basin to the south as early as 350 Ma; with maximum temperatures reached in the Pennsylvanian (Schmoker, 1989).

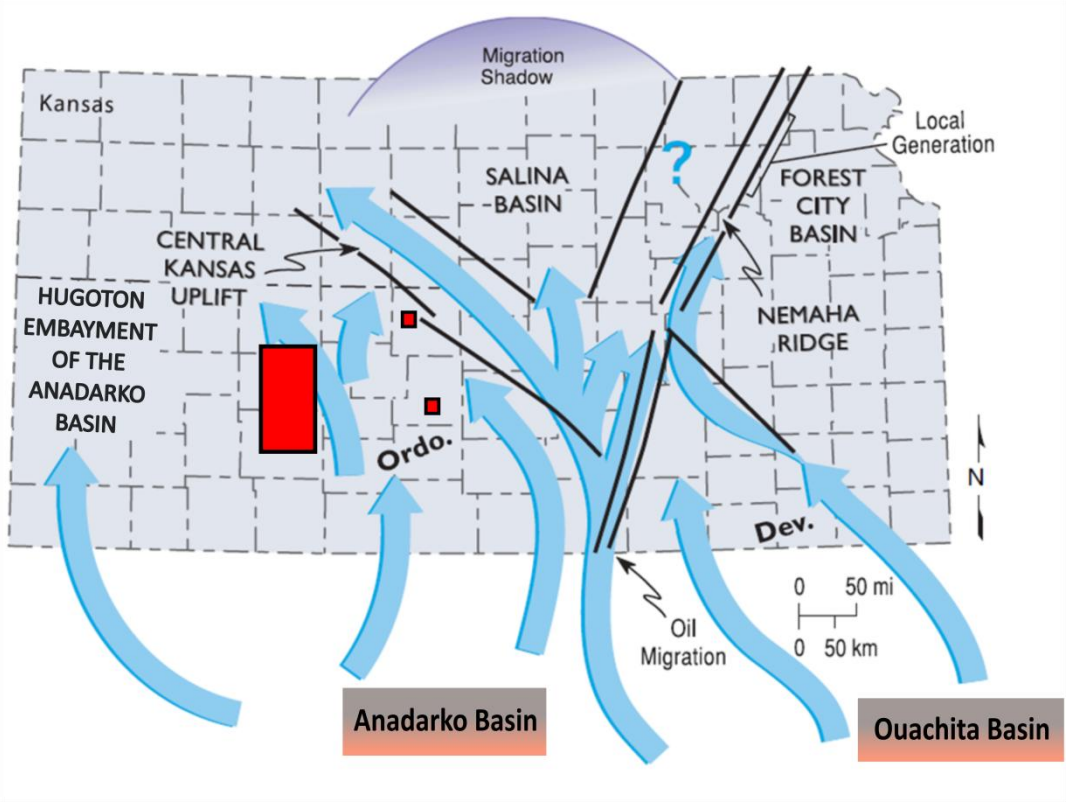

Figure 3.5: Map of Kansas showing approximate migration pathways for oils generated in the Ouachita and Anadarko basins, and local generation in the Forest City basin (modified from Gerhard, 2004). There is a migration shadow in the Salina basin where faults defining the Central Kansas Uplift and Nemaha Ridge acted as barriers to flow into the basin and instead channelled oils north-westward and north-eastward. 'Ordo' (Ordovician) and 'Dev' (Devonian) denote the primary contributing migratory oil source. Red boxes denote study areas from this study (Kansas Basin and Central Kansas Uplift).

The idea of the long distance migration of hydrocarbons in this region was postulated by Rich (1931) and Walters (1958) for the origin of oils in the Central Kansas Uplift and Burruss and Hatch (1989) for the source of oils in the Cambridge Arch due to the similarities between the chemistry of the oils found in these regions

and those sourced from the Anadarko Basin (**Figure 3.5**). This combined with evidence of the thermal immaturity of Permian and Pennsylvanian rocks in the province is indicative of the gas being emplaced by migration and differential entrapment (Higley, 1995; Gerhard, 2004).

Nitrogen is always associated with economic concentrations of helium but helium is not always associated with high nitrogen concentrations. This is due to the multiple sources of N_2 compared with helium such as atmospheric nitrogen, nitrogen released from rocks during metamorphism and nitrogen generated by the high temperature thermal maturation of hydrocarbons (Pierce et al., 1964; Poreda et al., 1986; Gold and Held, 1987; Jenden et al., 1988a; Jenden and Kaplan, 1989; Stilwell, 1989; Hiyagon and Kennedy, 1992; Krooss et al., 1995; Littke et al., 1995; Hutcheon, 1999; Ballentine and Burnard, 2002; Ballentine and Sherwood-Lollar, 2002).

In the Hugoton-Panhandle two types of N_2 were found: N_2 which was associated with ^4He was of metamorphosed metasedimentary origin and N_2 which was not associated with ^4He was generated by the thermal cracking of hydrocarbons in the Anadarko Basin (Ballentine and Sherwood-Lollar, 2002). It is postulated that the N_2 associated with ^4He acts as a carrier gas enabling the advection of helium to shallow layers via fault and fracture systems (Etiope and Lombardi, 1996; Etiope and Martinelli, 2002; Ballentine and Burnard, 2002; Fu et al., 2005; Fu et al., 2008; Walia et al., 2009; Hong et al., 2010).

Typically $^4He/N_2$ ratios for a producing helium field fall into a narrow range between 0.02 to 0.20 which the Hugoton-Panhandle exemplifies (0.020-0.049 across the field and at most 0.077 in the Bush Dome; Pierce et al., 1964; Gold and Held, 1987; Jenden et al., 1988b; Ballentine and Sherwood-Lollar, 2002).

Fields sampled in this study were from a modest area within the Kansas Basin and Central Kansas Uplift and are compared with the larger Hugoton-Panhandle system (~200 km^2 compared to ~20,000 km^2) (**Figure 3.6**). Specifically 21 fields were sampled in three counties: Ford, Hodgeman and Ness. Samples from the Central Kansas Uplift were taken from the Stafford and Barton counties (**Table 3.1**). Samples from this study are then combined with data taken from Ballentine and Sherwood-Lollar, 2002 for the Kansas section of the Hugoton-Panhandle to complete the dataset.

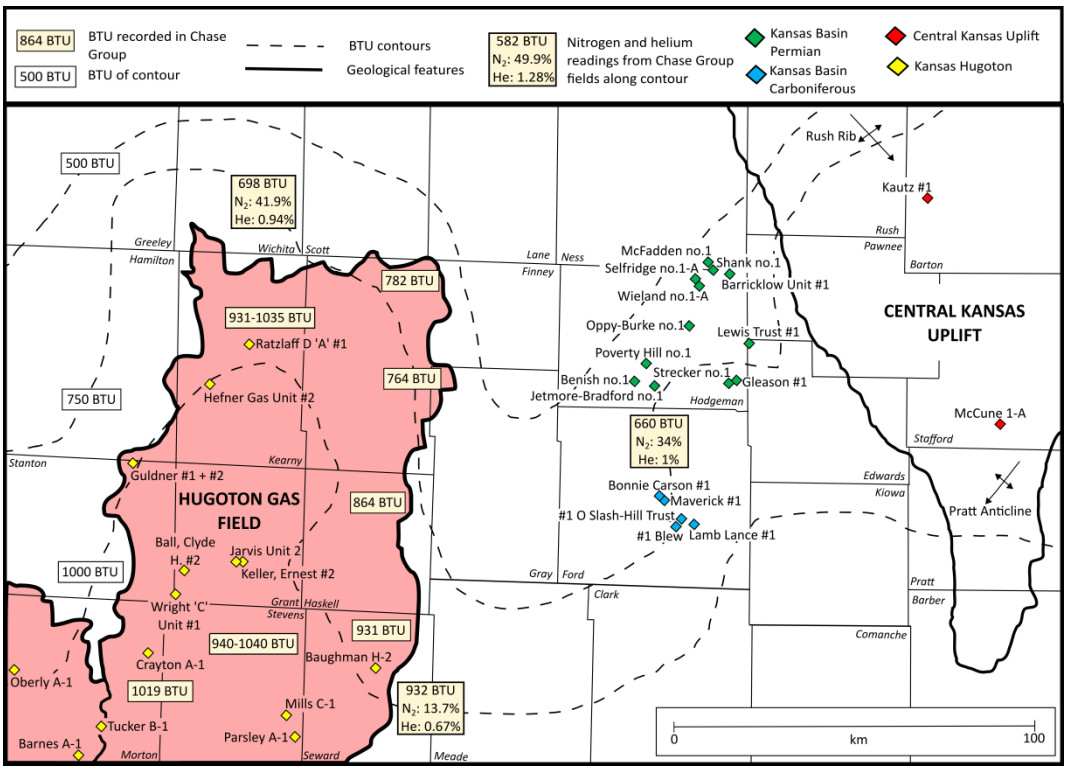

Figure 3.6.: BTU map of the Kansas Basin, Central Kansas Uplift and Hugoton field showing sample positioning in relation to contours (Clyde Becker, pers comms, 2014). Kansas Hugoton data (yellow diamonds) was taken from Ballentine and Sherwood-Lollar, (2002).

We collected a total of 19 samples from the Kansas Basin and Central Kansas Uplift to add to the suite of 30 samples from the Hugoton-Panhandle (split into Kansas Hugoton, Guymon Hugoton and Texas Panhandle). Seventeen samples are

from the Kansas Basin and these are split into two groups designated Kansas Basin Permian (KBP) and Kansas Basin Cretaceous (KBC). Two samples are from the Central Kansas Uplift (CKU) however since they show significant differences in isotopic character will be referred to separately where appropriate (**Table 3.2 and 3.3**).

Field name	Associated sample well	County	Producing reservoir	Field area (km^2)	Cumulative gas production (m^3)
Carson	Bonnie Carson #1	Ford	Morrow Sands	4.7	2.26×10^6
Maverick	Maverick #1	Ford	Morrow Sands	0.6	6.89×10^4
Blew (wildcat)	#1 Blew	Ford	Morrow Sands	N/A	1.49×10^6
Lamb	Lamb-Lance #1	Ford	Mississippian	0.6	2.33×10^7
Steel	#1 O Slash-Hill Trust	Ford	Mississippian	3.8	2.97×10^7
Barrick	Barricklow Unit #1	Hodgeman	Chase Group	3.0	7.57×10^6
Wieland North	Selfridge no.1-A	Hodgeman	Chase Group	24.4	4.95×10^6
Wieland	Wieland no.1-A	Hodgeman	Chase Group	0.6	7.52×10^6
Hanston-Oppy	Oppy-Burke no.1	Hodgeman	Chase Group	64.6	7.34×10^6
Groner	Lewis Trust #1	Hodgeman	Chase Group	24.4	2.18×10^7
Saw Log Creek Southeast	Strecker no.1	Hodgeman	Chase Group	20.9	5.21×10^6
Saw Log Creek	Gleason #1	Hodgeman	Chase Group	31.4	4.71×10^6
Jetport	Jetmore-Bradford no.1	Hodgeman	Chase Group	0.6	5.91×10^6
Stella B	Benish no.1	Hodgeman	Chase Group	0.6	8.62×10^6
Don	Poverty Hill no.1	Hodgeman	Chase Group	31.4	2.51×10^6
Neho	Shank #1	Ness	Chase Group	0.6	8.22×10^6
Barricklow East	McFadden no.1	Ness	Chase Group	0.6	4.67×10^6
Leesburgh	McCune 1-A	Stafford	Chase Group	7.7	1.09×10^7
Bahr	Kautz #1	Barton	Chase Group	1.2	2.19×10^7

Table 3.1.: Data regarding the fields sampled from in the Kansas Basin and Central Kansas Uplift (this study). Field names, areas and cumulative gas production were taken from the Kansas Geological Society Oil and Gas database.

3.3. Sample collection and analytical techniques

Samples were collected in the field directly from the wellhead by connecting a high pressure regulator with a 3/4" NPT adaptor to the wellhead. The regulator was then attached to a 70 cm length of internally polished, refrigeration grade copper tubing with a diameter of 3/8" via a length of high pressure hose. Well gas was then flushed through the collection apparatus at pressures around 1 bar (atmospheric) for approximately 10 minutes so as to decrease the possibility of air contamination before the copper tube was cold welded at both ends by closing a pair of stainless steel clamps. This follows the same procedures as Ballentine and Sherwood-Lollar, (2002), Zhou, (2004) and Gilfillan, (2006).

Splits of each sample were taken in the lab not only for the purpose of determining noble gas isotopic composition and concentration but also for the analysis of nitrogen concentration and isotopes by University of Toronto. Noble gas analyses were carried out at the Noble Lab at University of Oxford.

Stable helium isotopes ^{3}He and ^{4}He were specifically measured on the Helix SFT mass spectrometer which has a split flight tube. This gives it the ability to simultaneously measure both isotopes thereby decreasing the error on the measurement.

All stable isotopes of the other noble gases (Ne, Ar, Kr, Xe) were measured on the Argus VI mass spectrometer. Ne and Ar were analysed individually by stepwise heating of the cryotrap purification system while Kr and Xe were analysed together by peak jumping (see Methods Chapter).

Before each sample run a blank and standard were run a day in advance using the same procedure as a sample to check standard reproducibility and background

levels of residual gas. These are used in conjunction with automated standards run nightly which check system stability, mass spectrometer drift and daily changes in system conditions to calculate sample concentrations. Due to the consistency of these overnight standards they are used to ascertain the ratio of samples from the same day.

All data errors are quoted at the 1σ level of confidence and include the analytical, blank and standard errors. In the case of concentration errors the expansion volume, pressure and relative prep volume errors are also included. All error corrections on noble gas analyses were made during data reduction.

Due to the radiogenic nature of the majority of the samples, errors were 1.0% to 4.3% for helium ratios however this does not affect sample reproducibility. Ratios were the most affected in this respect due to the statistical counting error on the very low ^{3}He signal which at that early a stage in the laboratory setup was not yet optimally adjusted.

During analyses mass peaks $^{40}Ar^{++}$ and $^{44}CO_2^{++}$ which could cause major interference to ^{20}Ne and ^{22}Ne signals respectively were monitored. Across all samples it was determined that the ^{22}Ne signal of the sample was high enough that the $^{44}CO_2^{++}$ contribution was below 1% and therefore negligible. Corrections were made accordingly to the ^{20}Ne signal of samples for $^{40}Ar^{++}$ interference during data reduction which varied between 10.6% to 11.7% $^{40}Ar^{++}$ contribution following the methods of Niedermann et al. (1993). Uncertainities in $^{40}Ar^{++}$ contribution were propagated through to the final calculated error.

Nitrogen isotope analysis for CKU, KBP and KBC samples was undertaken at University of Toronto using procedures detailed in Ballentine and Sherwood-Lollar (2002) and Sherwood-Lollar et al., (1997). Individual errors on the $\delta^{15}N$ (‰)

results range between ±0.01 to 0.90‰. For Ballentine and Sherwood-Lollar samples $\delta^{15}N$ (‰) errors are all ±0.20‰.

3.4. Results

In all samples the $^{4}He/^{20}Ne$ ratio, which is an indicator of air contamination, is >18,000 compared with 0.032 for air (Kipfer et al., 2002). This shows there is negligible air-helium contribution to these samples indicating that any differences between the predominantly crustal $^{3}He/^{4}He$ ratios are due to discrete mantle contributions.

Sample well and geological province	Location Lat/Long	Producing formation	$^{3}He/^{4}He$ (R_a)	$^{20}Ne/^{22}Ne$	$^{21}Ne/^{22}Ne$	$^{40}Ar/^{36}Ar$	$^{38}Ar/^{36}Ar$
Central Kansas Uplift							
Kautz #1	38°27'4.92"N, 98°57'17.45"W	Chase Group	0.11 (0.008)	9.32 (0.029)	0.053 (0.0006)	1410 (3)	0.189 (0.0005)
			0.12 (0.003)	9.30 (0.029)	0.053 (0.0006)	1409 (3)	0.189 (0.0005)
McCune 1-A	37°53'27.09"N, 98°41'59.37"W	Chase Group	0.08 (0.002)	9.49 (0.033)	0.045 (0.0005)	592 (1)	0.187 (0.0005)
Kansas Basin Carboniferous							
Bonnie Carson #1	37°41'47.10"N, 99°51'36.38"W	Morrow Sands	0.09 (0.003)	9.18 (0.028)	0.058 (0.0006)	1718 (3)	0.183 (0.0006)
Maverick #1	37°41'16.43"N, 99°50'58.85"W	Morrow Sands	0.10 (0.001)	8.95 (0.028)	0.063 (0.0007)	2142 (5)	0.187 (0.0008)
#1 Blew	37°37'35.27"N, 99°48'38.53"W	Morrow Sands	0.09 (0.002)	9.13 (0.028)	0.055 (0.0006)	1642 (3)	0.185 (0.0006)
#1 O Slash-Hill Trust	37°38'31.47"N, 99°47'46.52"W	Mississippian	0.10 (0.001)	9.16 (0.028)	0.056 (0.0006)	1494 (4)	0.184 (0.0009)
Lamb Lance #1	37°37'44.59"N, 99°44'52.86"W	Mississippian	0.09 (0.003)	9.14 (0.028)	0.060 (0.0006)	1635 (4)	0.185 (0.0008)
Kansas Basin Permian							
Barricklow Unit #1	38°15'13.98"N, 99°38'17.73"W	Chase Group	0.10 (0.001)	9.74 (0.030)	0.042 (0.0004)	588 (1)	0.189 (0.0005)
Shank no. 1	38°15'45.71"N, 99°41'48.81"W	Chase Group	0.09 (0.001)	9.71 (0.030)	0.040 (0.0004)	584 (1)	0.189 (0.0005)
McFadden no. 1	38°16'52.86"N, 99°42'56.11"W	Chase Group	0.13 (0.002)	9.74 (0.030)	0.041 (0.0004)	604 (1)	0.189 (0.0005)

Selfridge no. 1-A	38°14'7.62"N, 99°45'21.74"W	Chase Group	0.13 (0.002)	9.75 (0.030)	0.042 (0.0004)	583 (1)	0.189 (0.0005)
Wieland no. 1-A	38°13'19.77"N, 99°44'39.21"W	Chase Group	0.11 (0.001)	9.74 (0.030)	0.042 (0.0004)	591 (2)	0.190 (0.001)
Oppy-Burke no. 1	38° 7'26.40"N, 99°46'37.57"W	Chase Group	0.07 (0.001)	9.73 (0.030)	0.044 (0.0005)	554 (2)	0.189 (0.001)
Lewis Trust #1	38° 5'2.84"N, 99°34'14.74"W	Chase Group	0.10 (0.002)	9.68 (0.030)	0.043 (0.0005)	555 (1)	0.186 (0.0007)
Strecker no. 1	37°59'4.10"N, 99°38'13.99"W	Chase Group	0.06 (0.002)	9.57 (0.030)	0.044 (0.0005)	555 (3)	0.195 (0.004)
			0.06 (0.003)	9.56 (0.032)	0.045 (0.0005)		
Gleason #1	37°59'14.11"N, 99°36'31.71"W	Chase Group	0.06 (0.001)	9.72 (0.030)	0.044 (0.0005)	537 (1)	0.189 (0.0006)
Jetmore-Bradford no. 1	37°58'15.58"N, 99°53'37.79"W	Chase Group	0.06 (0.002)	9.62 (0.030)	0.044 (0.0005)	525 (1)	0.187 (0.0007)
Benish no. 1	37°58'59.37"N, 99°57'47.65"W	Chase Group	0.06 (0.001)	9.75 (0.030)	0.044 (0.0005)	547 (2)	0.191 (0.001)
Poverty Hill no. 1	38°1'30.37"N, 99°55'13.08"W	Chase Group	0.08 (0.001)	9.81 (0.031)	0.043 (0.0004)	569 (1)	0.191 (0.0006)
***Kansas Hugoton**							
Ratzlaff D ‘A’ #1	38°2'12.2"N, 101°16'43.7"W	Chase Group	0.16 (0.005)	9.70 (0.050)	0.039 (0.0004)	818 (10)	nr
Hefner Gas Unit #1	37°56'5.8"N, 101°23'18.9"W	Chase Group	0.16 (0.005)	9.74 (0.053)	0.039 (0.0005)	851 (11)	nr
Guldner Unit #1	37°43'43.0"N, 101°39'46.9"W	Chase Group	0.14 (0.004)	9.73 (0.041)	0.040 (0.0005)	835 (16)	nr
Guldner Unit #2	37°43'43.0"N, 101°39'46.9"W	Panoma	0.15 (0.004)	9.66 (0.025)	0.044 (0.0009)	889 (5)	nr
Campbell, R.W. #2	37°35'0.8"N, 101°37'35.7"W	Chase Group					nr

Keller, Ernest #2	37°29'47.5"N, 101°16'49.3"W	Chase Group	0.20 (0.006)	9.66 (0.059)	0.041 (0.0005)	1066 (11)	nr
Jarvis Unit #2	37°29'47.5"N, 101°17'54.9"W	Panoma	0.20 (0.006)	9.68 (0.061)	0.041 (0.0006)	1038 (20)	nr
Ball, Clyde H. #2	37°28'3.1"N, 101°27'45.3"W	Panoma		9.61 (0.027)	0.051 (0.0011)	974 (47)	nr
Wright “C” Unit #1	37°24'34.2"N, 101°31'2.1"W	Chase Group	0.18 (0.005)	9.69 (0.018)	0.039 (0.0008)	948 (6)	nr
Baughman H-2	37°14'2.7"N, 100°50'22.7"W	Chase Group		9.69 (0.018)	0.040 (0.0008)	977 (10)	nr
Crayton A-1	37°15'47.6"N, 101°36'3.5"W	Chase Group	0.19 (0.006)	9.70 (0.039)	0.040 (0.0006)	969 (25)	nr
Mills C-1	37°6'10.6"N, 101°9'57.4"W	Chase Group	0.21 (0.006)	9.71 (0.030)	0.045 (0.0009)	1155 (29)	nr
Parsley A-1	37°2'40.7"N, 101°6'41.6"W	Chase Group	0.21 (0.006)	9.80 (0.034)	0.040 (0.0005)	925 (12)	nr
Oberly A-1	37°13'10.2"N, 102°1'4.4"W	Greenwood	0.19 (0.006)	9.73 (0.035)	0.039 (0.0005)	830 (13)	nr
Tucker B-1	37°4'25.7"N, 101°44'45.6"W	Chase Group	0.19 (0.006)	9.80 (0.043)	0.041 (0.0007)	967 (18)	nr
Barnes A-1	37°0'3.4"N, 101°49'6.6"W	Greenwood		9.68 (0.015)	0.041 (0.0008)	913 (18)	nr
***Guymon Hugoton**							nr
Hill A-1	36°52'15.9"N, 101°42'44.0"W	Chase Group					nr
Buzzard D-1	36°47'56.8"N, 101°44'7.9"W	Chase Group	0.19 (0.006)	9.81 (0.038)	0.039 (0.0006)	938 (26)	nr
Stonebraker A-69	36°38'21.0"N, 101°45'12.5"W	Chase Group	0.21 (0.006)	9.91 (0.023)	0.038 (0.0003)	1113 (7)	nr
***Texas Panhandle**							nr
Coffee Estate #1	36°3.365'N, 101°43.052'W	Brown Dolomite	0.24 (0.007)	9.63 (0.025)	0.042 (0.0009)	1156 (7)	nr

Blake Trust Estate #2	36° 4.230'N, 101° 40.905'W	Brown Dolomite	0.25 (0.007)	9.77 (0.029)	0.040 (0.0004)	1105 (25)	nr
Mary A Long #1	36° 18.131'N, 101° 45.307'W	Brown Dolomite	0.20 (0.006)	9.67 (0.039)	0.040 (0.0005)	1039 (17)	nr
Donelson et al #1	36° 20.790'N, 101° 59.721'W	Brown Dolomite	0.21 (0.006)	9.83 (0.027)	0.037 (0.0003)	1076 (7)	nr
Sarah Claybaugh #1	36° 22.496'N, 101° 59.681'W	Brown Dolomite	0.18 (0.005)	9.80 (0.046)	0.037 (0.0004)	865 (33)	nr
Cameron Walls #1	36° 16.436'N, 101° 58.614'W	Brown Dolomite		9.66 (0.040)	0.040 (0.0005)	1112 (15)	nr
Horner #1	36° 4.847'N, 102° 6.201'W	Brown Dolomite		9.65 (0.025)	0.043 (0.0009)	1058 (14)	nr
Whitherbee #2	36° 6.224'N, 101° 49.193'W	Brown Dolomite	0.21 (0.006)	9.69 (0.036)	0.040 (0.0005)	983 (11)	nr
Flores 23	36° 2.738'N, 101° 48.120'W	Brown Dolomite		9.59 (0.025)	0.040 (0.0008)	1118 (12)	nr
Nisbett #1	36° 0.146'N, 101° 52.410'W	Brown Dolomite	0.19 (0.006)	9.62 (0.032)	0.041 (0.0005)	1045 (9)	nr
McDade #2 + #5	35° 54.124'N, 102° 2.606'W	Brown Dolomite	0.18 (0.005)				nr
Brumley A #1	35° 57.554'N, 101° 55.098'W	Brown Dolomite					nr

Table 3.2.: Noble gas ratios from this study and from Ballentine and Sherwood-Lollar, 2002 for the Hugoton-Panhandle (starred sections). 1σ errors for samples are shown in brackets. Nr in the table denotes the $^{38}Ar/^{36}Ar$ values were not recorded in Ballentine and Sherwood-Lollar, 2002.

Sample well and geological province	^{4}He concentration (x 10^{-2}) (cm^3 STP)	^{20}Ne concentration (x 10^{-7}) (cm^3 STP)	^{40}Ar concentration (x 10^{-4}) (cm^3 STP)	^{84}Kr concentration (x 10^{-8}) (cm^3 STP)	^{130}Xe concentration (x 10^{-10}) (cm^3 STP)	N_2 concentration (±5%) (cm^3 STP)	$\delta^{15}N(N_2)$ (±0.2‰)
Central Kansas Uplift							
Kautz #1	2.12 (0.025)	1.78 (0.011)	56.6 (0.57)	1.21 (0.02)	0.31 (0.01)	0.373	2.45 (0.07)
	2.13 (0.025)	1.77 (0.011)	57.0 (0.57)				
McCune 1-A	0.86 (0.011)	1.71 (0.017)	2.16 (0.22)	1.25 (0.02)	0.99 (0.01)	0.237	3.45 (0.07)
Kansas Basin Carboniferous							
Bonnie Carson #1	1.22 (0.013)	2.75 (0.030)	9.67 (0.083)	1.49 (0.05)	3.10 (0.05)	0.198	3.80 (0.14)
Maverick #1	2.47 (0.025)	4.78 (0.051)	19.6 (0.16)	2.43 (0.07)	12.84 (0.12)	0.508	6.50 (0.42)
#1 Blew	1.31 (0.013)	4.31 (0.046)	14.0 (0.12)	2.32 (0.07)	4.42 (0.07)	0.339	1.85 (0.21)
#1 O Slash-Hill Trust	0.48 (0.007)	1.56 (0.017)	4.88 (0.042)	0.63 (0.19)	1.91 (0.03)	0.102	
Lamb Lance #1	0.58 (0.006)	1.43 (0.015)	4.72 (0.041)	0.32 (0.10)	1.52 (0.01)	0.092	2.90 (0.07)
Kansas Basin Permian							
Barricklow Unit #1	1.22 (0.020)	2.93 (0.044)	4.66 (0.071)	1.84 (0.04)	1.27 (0.02)	0.369	4.03 (0.90)
Shank no. 1	1.15 (0.019)	3.04 (0.046)	3.49 (0.053)	1.86 (0.04)	1.28 (0.02)	0.387	4.70 (0.28)
McFadden no. 1	1.16 (0.019)	3.07 (0.047)	5.01 (0.076)	1.92 (0.04)	1.27 (0.02)	0.416	1.45 (0.07)
Selfridge no. 1-A	1.08 (0.018)	2.56 (0.039)	4.17 (0.063)	1.65 (0.03)	1.21 (0.02)	0.338	2.20 (0.35)
Wieland no. 1-A	1.15 (0.019)	2.63 (0.040)	4.00 (0.061)	1.70 (0.03)	1.19 (0.02)	0.341	3.10 (0.14)
Oppy-Burke no. 1	0.96 (0.016)	2.03 (0.031)	3.03 (0.046)	1.45 (0.03)	1.15 (0.02)	0.330	4.00 (0.14)
Lewis Trust #1	1.00 (0.010)	2.03 (0.028)	3.82 (0.034)	1.29 (0.01)	0.96 (0.02)	0.280	
Strecker no. 1	0.87 (0.014)	1.82 (0.028)	2.75 (0.042)	1.35 (0.03)	1.08 (0.02)	0.220	3.45 (0.21)
	0.87 (0.012)	1.77 (0.030)					
Gleason #1	0.86 (0.014)	1.80 (0.027)	2.87 (0.044)	1.40 (0.03)	1.17 (0.02)	0.264	3.70 (0.14)

Jetmore-Bradford no. 1	1.05 (0.011)	2.13 (0.028)	4.03 (0.035)	1.39 (0.01)	1.52 (0.03)	0.280	2.45 (0.21)
Benish no. 1	0.95 (0.016)	2.02 (0.031)	3.03 (0.046)	1.46 (0.03)	1.15 (0.02)	0.275	2.99 (0.01)
Poverty Hill no. 1	0.89 (0.015)	1.83 (0.028)	3.30 (0.050)	1.53 (0.03)	1.18 (0.02)	0.311	4.00 (0.14)
***Kansas Hugoton**							
Ratzlaff D 'A' #1	0.48 (0.024)		5.53 (0.28)	Nm	Nm	0.189	8.7
Hefner Gas Unit #1	0.40 (0.020)	1.08 (0.075)	5.12 (0.26)	Nm	Nm	0.181	7.8
Guldner Unit #1	0.50 (0.025)	1.56 (0.11)	5.75 (0.29)	Nm	Nm	0.207	9.4
Guldner Unit #2	0.43 (0.004)	1.41 (0.012)	5.10 (0.050)	Nm	Nm	0.203	9.0
Campbell, R.W. #2	0.40 (0.020)		4.42 (0.22)	Nm	Nm	0.154	8.0
Keller, Ernest #2	0.38 (0.019)	0.86 (0.060)	4.68 (0.23)	Nm	Nm	0.145	6.4
Jarvis Unit #2	0.39 (0.020)	1.07 (0.075)	4.27 (0.21)	Nm	Nm	0.148	6.5
Ball, Clyde H. #2	0.35 (0.004)	1.11 (0.011)	4.58 (0.26)	Nm	Nm	0.151	
Wright "C" Unit #1	0.37 (0.004)	1.19 (0.012)	4.44 (0.050)	Nm	Nm	0.156	7.8
Baughman H-2	0.58 (0.006)	1.80 (0.018)	5.92 (0.090)	Nm	Nm	0.178	6.5
Crayton A-1	0.43 (0.021)	1.19 (0.083)	4.62 (0.23)	Nm	Nm	0.166	7.5
Mills C-1	0.38 (0.004)	1.03 (0.010)	4.46 (0.16)	Nm	Nm	0.127	5.3
Parsley A-1	0.57 (0.028)	1.23 (0.086)	4.19 (0.21)	Nm	Nm	0.152	6.7
Oberly A-1	0.49 (0.025)	1.61 (0.013)	4.46 (0.22)	Nm	Nm	0.208	7.1
Tucker B-1	0.39 (0.020)	0.99 (0.079)	5.38 (0.27)	Nm	Nm	0.147	7.1
Barnes A-1	0.41 (0.004)	1.57 (0.016)	4.21 (0.16)	Nm	Nm	0.203	8.5
***Guymon Hugoton**							
Hill A-1	0.40 (0.020)		5.23 (0.26)	Nm	Nm	0.146	5.7
Buzzard D-1	0.45 (0.023)	1.58 (0.11)	7.10 (0.36)	Nm	Nm	0.184	6.9
Stonebraker A-69	0.65 (0.032)	2.35 (0.16)	9.30 (0.47)	Nm	Nm	0.214	6.1
***Texas Panhandle**							
Coffee Estate #1	0.63 (0.006)	1.93 (0.019)	7.21 (0.080)	Nm	Nm	0.136	4.5
Blake Trust Estate #2	1.05 (0.052)	2.92 (0.21)	10.73 (0.54)	Nm	Nm	0.214	5.3
Mary A Long #1	0.76 (0.038)	1.98 (0.14)	7.66 (0.38)	Nm	Nm	0.165	4.9

Donelson et al #1	0.98 (0.049)	5.03 (0.35)		Nm	Nm	0.258	4.9
Sarah Claybaugh #1	0.92 (0.046)	4.96 (0.35)		Nm	Nm	0.253	4.4
Cameron Walls #1	0.66 (0.033)	1.75 (0.12)	7.97 (0.49)	Nm	Nm	0.180	5.3
Horner #1	0.92 (0.009)	3.69 (0.031)	10.99 (0.24)	Nm	Nm	0.220	5.0
Whitherbee #2	0.35 (0.018)	0.82 (0.057)	7.10 (0.35)	Nm	Nm	0.080	3.6
Flores 23	0.61 (0.006)	1.75 (0.018)	6.97 (0.12)	Nm	Nm	0.135	4.0
Nisbett #1	0.55 (0.027)	1.52 (0.11)	5.86 (0.29)	Nm	Nm	0.141	3.4
McDade #2 + #5	0.29 (0.015)		2.73 (0.14)	Nm	Nm	0.066	2.7
Brumley A #1	0.33 (0.017)			Nm	Nm	0.089	2.7

Table 3.3.: Noble gas concentrations from this study and the Ballentine and Sherwood-Lollar, 2002 study on the Hugoton-Panhandle (starred sections). Nitrogen concentrations for CKU, KBP and KBC samples are taken from the KGS database and are deemed to be within acceptable limits due to ^{4}He concentrations from this study being within 1σ error of previously recorded helium concentrations from wells. 1σ errors for samples appear in column headers as % or in brackets if variable.

3.4.1. Noble Gases

3.4.1.1. Helium

The $^{3}He/^{4}He$ ratio (R_a) varies noticeably between the Kansas Hugoton and the Kansas Basin and CKU regions. Across the Hugoton-Panhandle $^{3}He/^{4}He$ ratios vary between 0.14 to 0.25 R_a. Across both the Kansas Basin and CKU, $^{3}He/^{4}He$ ratios range from 0.06 to 0.13 R_a. Within the Kansas Basin subgroups the KBC has a very narrow range of ratios from 0.09 to 0.10 R_a whereas the KBP has a wider range from 0.06 to 0.13 R_a.

There also appear to be opposing spatial trends to the KBP and Hugoton-Panhandle samples. The Hugoton-Panhandle samples have the highest $^{3}He/^{4}He$ ratios to the south whereas the highest KBP $^{3}He/^{4}He$ ratios are towards the north.

Concentrations of ^{4}He are high throughout the Kansas Basin and CKU sample set and range from 4.8×10^{-3} to 2.47×10^{-2} $cm^3STP(^{4}He)/cm^3$ whereas the Hugoton-Panhandle concentrations lie within a narrower range of 3.5×10^{-3} to 1.05×10^{-2} $cm^3STP(^{4}He)/cm^3$ indicating that helium gas across the field is relatively well mixed.

Within the Kansas Basin region it can be seen that the subsets KBC and KBP have overlapping concentrations and ratios with KBC having a greater range of concentrations to KBP (4.8×10^{-3} to 2.47×10^{-2} $cm^3STP(^{4}He)/cm^3$ compared to 8.6×10^{-3} to 1.22×10^{-2} $cm^3STP(^{4}He)/cm^3$). Across all samples there is no obvious spatial trend to the helium concentrations or any relationship to depth.

Due to the high concentrations of ^{4}He in all well gases, magmatic ^{3}He concentrations across the Kansas Basin (KBC and KBP) and CKU range between

5.81 x 10^{-10} and 3.13 x 10^{-9} $cm^3STP(^3He)/cm^3$ which directly compare to values calculated for the complete Hugoton-Panhandle dataset of 6.8 x 10^{-10} to 3.3 x 10^{-9} $cm^3STP(^3He)/cm^3$ (Ballentine and Sherwood-Lollar, 2002). Magmatic contributions to the ^4He in the Kansas Basin and CKU samples are between 0.5-1.4% assuming a crustal end member of 0.02 R_a and a mantle end member of 8.0 R_a (Ballentine and Sherwood-Lollar, 2002). This again compares to the Hugoton-Panhandle which shows magmatic ^4He contributions of between 1.5-2.8%.

3.4.1.2. Neon

Concentrations of ^{20}Ne across the Kansas Basin and CKU range from 1.43 x 10^{-7} to 4.78 x 10^{-7} $cm^3STP(^{20}Ne)/cm^3$ which falls within the range for the Hugoton-Panhandle (0.86 x 10^{-7} to 5.0 x 10^{-7} $cm^3STP(^{20}Ne)/cm^3$). $^{20}Ne/^{22}Ne$ in the Kansas Basin-CKU system varies between 8.95 to 9.81 (compared with the air value of 9.8). Within this the Kansas Basin shows a split in $^{20}Ne/^{22}Ne$ between the subsets. The KBC displays lower $^{20}Ne/^{22}Ne$ values (8.95 to 9.18) than the KBP (9.61 to 9.81) which falls within the range of the Hugoton-Panhandle (9.59 to 9.91).

The $^{21}Ne/^{22}Ne$ ratio in the Kansas Basin and CKU has a range of 0.040 to 0.063 (compared with the air value of 0.029). All samples show ratios which are distinct from air indicating a resolvable excess of ^{21}Ne (referred to as $^{21}Ne^*$). Once again there is a split in the Kansas Basin subsets with the KBC showing higher ratios than the KBP (0.055-0.063 compared with 0.040-0.044). Ratios for the KBP again fall within range of the Hugoton-Panhandle (0.037-0.051).

The endmembers for $^{20}Ne/^{22}Ne$ and $^{21}Ne/^{22}Ne$ are well defined for air, crust and mantle contributions and can be affected by both mass fractionation and mixing

between groups (**Table 3.4**). From the three neon isotopic graph it can be seen that all systems are spread along two mixing lines between air and the crust (**Figure 3.7**). Both CKU and KBC samples fall along the mixing line for modern crust which is younger than the Archean. Samples from the KBP and Hugoton-Panhandle regions show potential mixing between mantle, Archean crust and Precambrian crust however this is difficult to determine given the relatively narrow sample range. Mixing between the two crustal lines is either caused by mass fractionation or a small mantle addition.

$^{21}Ne^*$ contributions to ^{21}Ne concentrations in the CKU vary from 34.8%-45.5%. In the KBC they are between 47.2-53.5% and in the KBP they are from 28.2-34.5%. The KBP samples fall within the range of the Hugoton-Panhandle (21.0-42.7%).

The mantle and crustal contributions to the ^{21}Ne concentration can be calculated from $^{20}Ne/^{21}Ne/^{22}Ne$ using methods outlined in Ballentine and O'Nions, 1992 and Ballentine, 1997. In all systems crustal $^{21}Ne^*$ dominates however in the CKU and KBC systems $^{21}Ne^*$ is almost entirely sourced from the crust (assuming that the air, crust and mantle endmembers are distinct and well defined). The CKU samples contain mantle $^{21}Ne^*$ ($^{21}Ne^*_{mntl}$) components which constitutes 1.3-1.5% of the total ^{21}Ne concentration of the gases. The KBC contains $^{21}Ne^*_{mntl}$ components of up to 2.0% of the ^{21}Ne concentration. In the KBP and Hugoton-Panhandle there are resolvable mantle components with a maximum of 13.9% $^{21}Ne^*_{mntl}$ in the KBP and up to 15.0% $^{21}Ne^*_{mntl}$ in the Hugoton-Panhandle field.

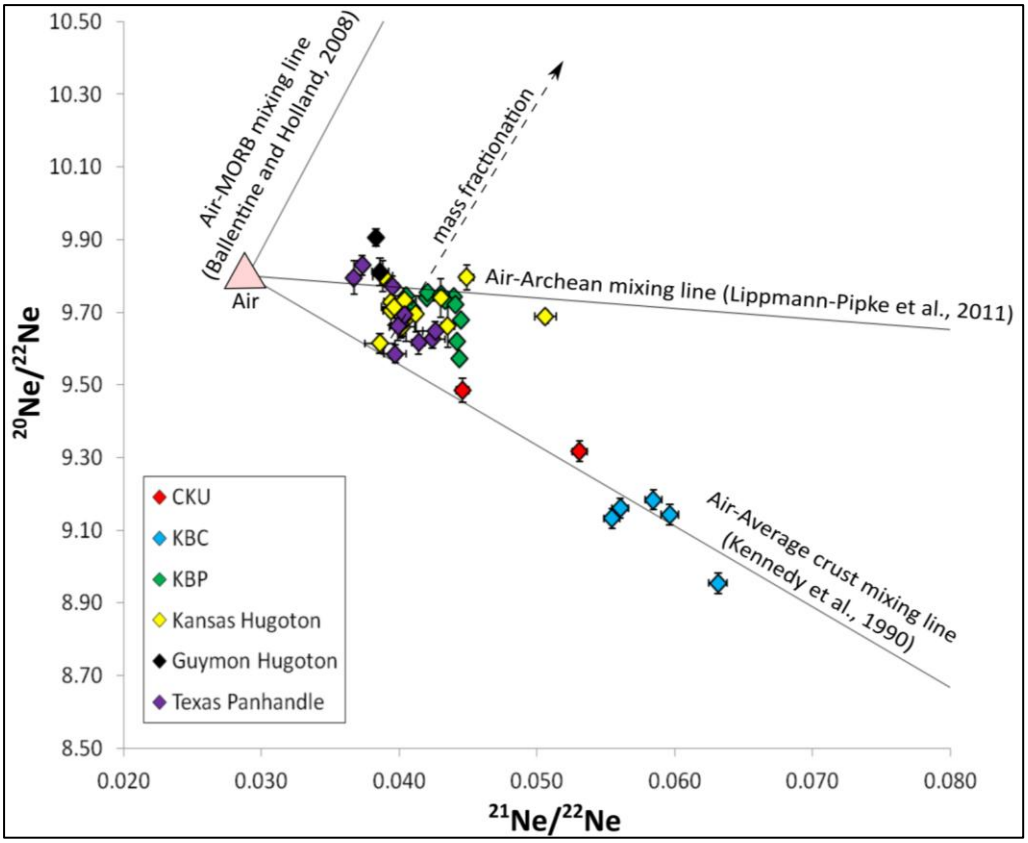

Figure 3.7.: Three neon isotope graph showing isotopic ratios in samples relative to predefined mixing lines for air-crust and air-mantle mixtures (Table 3.4.). All samples show significant excesses of $^{21}Ne/^{22}Ne$. For the air-average crust mixing line the lower $^{21}Ne/^{22}Ne$ endmember value of 0.47 is used for the data due to the goodness of fit with regard to the majority of samples.

End member	$^{20}Ne/^{22}Ne$	$^{21}Ne/^{22}Ne$	Reference
Air	9.80	0.029	Ballentine and Burnard, 2002
Archean crust	0	3.30±0.2	Lippmann-Pipke et al., 2011
Precambrian crust	0	0.47±	Kennedy, 1990
MORB mantle	12.5	0.0677	Ballentine and Holland, 2008

Table 3.4.: Endmembers for three neon graph mixing lines.

3.4.1.3 Argon

The $^{40}Ar/^{36}Ar$ ratios in the Kansas Basin-CKU systems vary from 525 to 2142 which is split again between the KBC and KBP. On average the KBC has a ratio of 1726 ± 246 and the KBP has a ratio of 566 ± 24 compared to the air ratio of 295.5. All samples have a resolvable ^{40}Ar excess (denoted as $^{40}Ar^*$). In these samples it is not possible to separate out crust from mantle contributions with regard to $^{40}Ar^*$, however, given the geological context, it can be assumed that the dominant contribution is from the crust. $^{40}Ar^*$ constitutes 43.7-86.2% of the Kansas Basin and CKU ^{40}Ar concentrations. This can be further differentiated into the KBC (80.2-86.2%) and the KBP (43.7-51.1%). Neither subset falls into the 63.9-74.4% range for the Hugoton-Panhandle.

The ratios of $^{38}Ar/^{36}Ar$ for samples, which determine atmospheric contributions, differ depending on the geological system. For KBP samples the range is narrow and falls between 0.186 to 0.191 compared with the air value of 0.188. All KBP samples except the Wieland no.1-A, Strecker no.1, Benish no.1, Poverty Hill no.1 and Lewis Trust #1 wells fall within 1σ of the air value. KBC samples have a range from 0.183 to 0.187. The Maverick #1 well is the only well from this sample subset within 1σ of the air value; all others are significantly below the air value but within 1σ error of each other. Both CKU samples fall just outside the 1σ error of the air ratio. McCune 1-A falls below the air value and Kautz #1 is above the air ratio. Hugoton-Panhandle ratios are not available however they are assumed to be within 1σ error of the air ratio since they are undocumented.

3.4.1.4 Krypton and Xenon

In the CKU samples ^{84}Kr concentrations vary between 1.20 x 10^{-8} and 1.25 x 10^{-8} $cm^3STP(^{84}Kr)/cm^3$. In the KBC concentrations range from 3.19 x 10^{-9} and 2.43 x 10^{-8} $cm^3STP(^{84}Kr)/cm^3$. There is a marked differentiation within the KBC between samples from the Mississippian and the Morrow of up to ~7.6 times more ^{84}Kr in the Morrow compared with the Mississippian. In the KBP concentrations fall within a narrow range of 1.29 x 10^{-8} to 1.92 x 10^{-8} $cm^3STP(^{84}Kr)/cm^3$. In general the wells to the north of the study area are higher in ^{84}Kr concentration than those in the south however there is no obvious spatial trend.

In the CKU ^{130}Xe concentrations are between 3.20 x 10^{-11} and 9.87 x 10^{-11} $cm^3STP(^{130}Xe)/cm^3$. In the KBC concentrations range between 1.51 x 10^{-10} and 1.28 x 10^{-9} $cm^3STP(^{130}Xe)/cm^3$ and exhibit the same differentiation between the Mississippian and Morrow strata as for ^{84}Kr except the difference is greater at up to ~8.5 times more ^{130}Xe in the Morrow than in the Mississippian. The KBP shows concentrations of 9.57 x 10^{-11} to 1.52 x 10^{-10} $cm^3STP(^{130}Xe)/cm^3$.

3.4.1.5 Crust-derived noble gases

The average $^4He/^{21}Ne^*$ ratios for the KBC, KBP and Hugoton-Panhandle are: 1.2 x 10^7, 3.2 x 10^7 and 2.8 x 10^7 (**Table 3.5**). All ratios except for the KBC are significantly higher than the average $^4He/^{21}Ne^*$ value of 1.71 x 10^7 (Ballentine and Burnard, 2002). Correction of both the ^4He and $^{21}Ne^*$ isotopes for magmatic contributions does not affect this discrepancy.

The average $^4He/^{40}Ar^*$ ratio for the KBC (13.7) is within range of the average ratio for the Hugoton-Panhandle (12.5). The KBP has a far higher average of 59.8. Wells in the CKU show two distinct $^4He/^{40}Ar^*$ ratios of 4.7 in the Kautz #1

well and 7.9 in the McCune 1-A well both of which are close to the average crustal $^{4}He/^{40}Ar^{*}$ ratio of 5.0 (Taylor and McLennan, 1985; Ballentine and Burnard, 2002).

In all cases both the $^{4}He/^{40}Ar^{*}$ ratio and $^{4}He/^{21}Ne^{*}$ are significantly higher than average observed and predicted crustal ratios except in the case of the KBC. The $^{40}Ar^{*}/^{21}Ne^{*}$ ratio for the Hugoton-Panhandle comes close to values predicted for the crust (2.4×10^{6} compared with 3.05×10^{6}). Across the Kansas Basin subsets $^{40}Ar^{*}/^{21}Ne^{*}$ ratios are significantly lower than those for the average crust (5.4×10^{5} for the KBP and 8.8×10^{5} for the KBC) (**Table 3.5**). Ratios corrected for $^{21}Ne^{*}$ magmatic contributions increase this discrepancy.

Well name/geological province	**$^{4}He/^{40}Ar^{*}$**	**$^{4}He/^{21}Ne^{*}$**	**$^{40}Ar^{*}/^{21}Ne^{*}$**
Hugoton-Panhandle (average)	12.46 ± 2.48	2.85 ± (0.62) x 10^{7}	2.43 ± (0.81) x 10^{6}
Kansas Hugoton	13.26 ± 2.46	2.85 ± (0.70) x 10^{7}	2.19 ± (0.59) x 10^{6}
Guymon Hugoton	9.40 ± 0.09	2.93 ± (0.001) x 10^{7}	3.12 ± (0.03) x 10^{6}
Texas Panhandle	11.73 ± 2.10	2.83 ± (0.61) x 10^{7}	2.66 ± (1.09) x 10^{6}
Kansas Basin Carboniferous	13.72 ± 1.75	1.21 ± (0.16) x 10^{7}	8.83 ± (0.53) x 10^{5}
Kansas Basin Permian	59.81 ± 7.63	3.16 ± (0.14) x 10^{7}	5.38 ± (0.83) x 10^{5}
Kautz #1 (CKU)	4.73 ± 0.17	4.59 ± (0.29) x 10^{7}	9.70 ± (1.58) x 10^{6}
McCune 1-A (CKU)	7.94 ± 0.54	3.05 ± (0.33) x 10^{7}	3.84 ± (0.82) x 10^{6}
Average upper crust (theoretical) (Ballentine and Burnard, 2002)	6.0	2.33 ± (0.44) x 10^{7}	3.88 ± (0.73) x 10^{6}
Average upper crust (observed) (Ballentine and Burnard, 2002)	5.0±1.0	1.71 ± (0.09) x 10^{7}	3.60 ± (1.27) x 10^{6}

Table 3.5.: Average radiogenic ratios of samples.

3.4.1.6 Groundwater-derived noble gases

The isotopes ^{20}Ne, ^{36}Ar, ^{84}Kr and ^{130}Xe are predominantly introduced into shallow crustal systems by being dissolved into groundwater (ASW). As such, when they are then partitioned into gas or oil, they can be used as indicators of groundwater interaction with the reservoir (Ballentine, 1991; Ballentine and Burnard, 2002; Gilfillan et al., 2008; Zhou et al., 2012).

In the CKU $^{20}Ne/^{36}Ar$ ratios are similar for the McCune 1-A and Kautz #1 wells (0.04-0.05). These ratios are up to 3.3 times lower than the ASW ratio (with ASW being 0.154 assuming an equilibration temperature of 10°C, pressure of 1 atm, an excess air component of 10% Ne and freshwater) (Kipfer et al., 2002). KBC samples range between 0.477-0.521 with all samples being below the air ratio (0.524) and significantly higher than the ASW ratio. KBP samples range between 0.277 and 0.509 which are significantly higher than the ASW ratio but also lower than the air ratio.

$^{84}Kr/^{36}Ar$ ratios for both CKU samples are uniform at 0.003 which is approximately 11 times lower than the ASW ratio of 0.040 at 10°C and 7 times lower than the air ratio of 0.021. $^{130}Xe/^{36}Ar$ ratios for the same samples are different at 0.00001 for Kautz #1 and 0.00003 for McCune 1-A. Both ratios are 14.5 to 51.3 times lower than the ASW ratio of 0.00041 at 10°C and 4.2 to 14.7 times lower than the air ratio of 0.00011.

In the KBC samples there is a marked difference between the $^{84}Kr/^{36}Ar$ ratios in the Mississippian and Morrow samples. Mississippian samples range from significantly below the air ratio at 0.011 to 0.019 which is within error of the air ratio (0.021). In the Morrow samples $^{84}Kr/^{36}Ar$ ratios are remarkably uniform and range between 0.026 and 0.027. All three samples are significantly above the air ratio but

below the ASW ratio (0.040). $^{130}Xe/^{36}Ar$ ratios lie within a narrow range for most samples in the KBC suite at 0.00052 to 0.00058 with a local maximum at the Maverick #1 well of 0.0014. All samples are significantly above the ASW ratio (0.00041).

$^{84}Kr/^{36}Ar$ ratios for KBP samples range between 0.018 to 0.031 indicating that all samples lie between the air ratio (0.021) and the ASW ratio (0.040). $^{130}Xe/^{36}Ar$ ratios for these samples are between 0.00014 and 0.00022. All samples are significantly above the air ratio (0.00011) and below the ASW ratio (0.00041).

The characteristics of the groundwater-derived noble gas ratios vary dependent on the subset. Noble gas solubility in water increases with elemental mass where Ne<Ar<Kr<Xe. When looking at the fractionation patterns in the subsets and at their relationships to crustal isotopic ratios ($^{4}He/^{21}Ne^{*}$ and $^{4}He/^{40}Ar^{*}$) there are no clear relationships. This could indicate either that the process responsible for the fractionation of the groundwater-derived noble gases does not significantly affect the crustal noble gases or that the fractionation of the groundwater derived component occurred prior to mixing with the crustal gases in the reservoir.

The KBC subset shows $^{20}Ne/^{36}Ar$ and $^{84}Kr/^{36}Ar$ ratios which are between ASW and air but $^{130}Xe/^{36}Ar$ ratios which are above ASW indicating an excess of xenon. This trend is similarly seen in $^{136}Xe/^{36}Ar$ ratios from this sample set. This trend in the groundwater-sourced isotopes could potentially be caused by the introduction of xenon isotopes from another source mixed with isotopes sourced from partially fractionated groundwater. The alternative source for the xenon isotopes could potentially be either from the underlying sediments or from an associated oil phase (Zhou et al., 2005).

In the CKU, the lower than ASW characteristics of all groundwater isotopic ratios potentially points to (along with having the highest $^{4}He/^{20}Ne$ ratios of 5.01 x 10^{4} to 1.19 x 10^{5}) minimal to potentially no significant groundwater interaction.

In the KBP samples the pattern of $^{20}Ne/^{36}Ar$, $^{84}Kr/^{36}Ar$ and $^{130}Xe/^{36}Ar$ ratios which all fall between air and ASW ratios points to varying degrees of degassing of groundwater since none of the samples are fully at equilibrium with the groundwater ratio of 0.154. The higher than groundwater ASW ratios, especially for $^{20}Ne/^{36}Ar$, could be an indicator of multiple stage solubility fractionation where the original gas has undergone several dissolution-exsolution events which would preferentially enrich ^{20}Ne relative to ^{36}Ar.

3.4.1.7 The interaction between ^{20}Ne and crust-derived isotopes

The correlation between atmosphere-derived ^{20}Ne and radiogenically-produced ^{4}He was first noted in the Ballentine and Sherwood-Lollar (2002) study on the Hugoton-Panhandle. The strong positive correlation indicates that these two differently sourced isotopes were potentially mixed prior to the degassing of groundwater into reservoirs. Since the primary source of ^{20}Ne in the subsurface is air-saturated groundwater this shows that groundwater plays a major role in the transport of ^{4}He to these reservoirs.

Similarly to the Hugoton-Panhandle there is a positive correlation between ^{4}He and ^{20}Ne across all subsets from this study. Alongside this we also see positive correlations between the other radiogenic noble gas isotopes ($^{21}Ne^{*}$ and $^{40}Ar^{*}$) and ^{20}Ne (**Figure 3.8**).

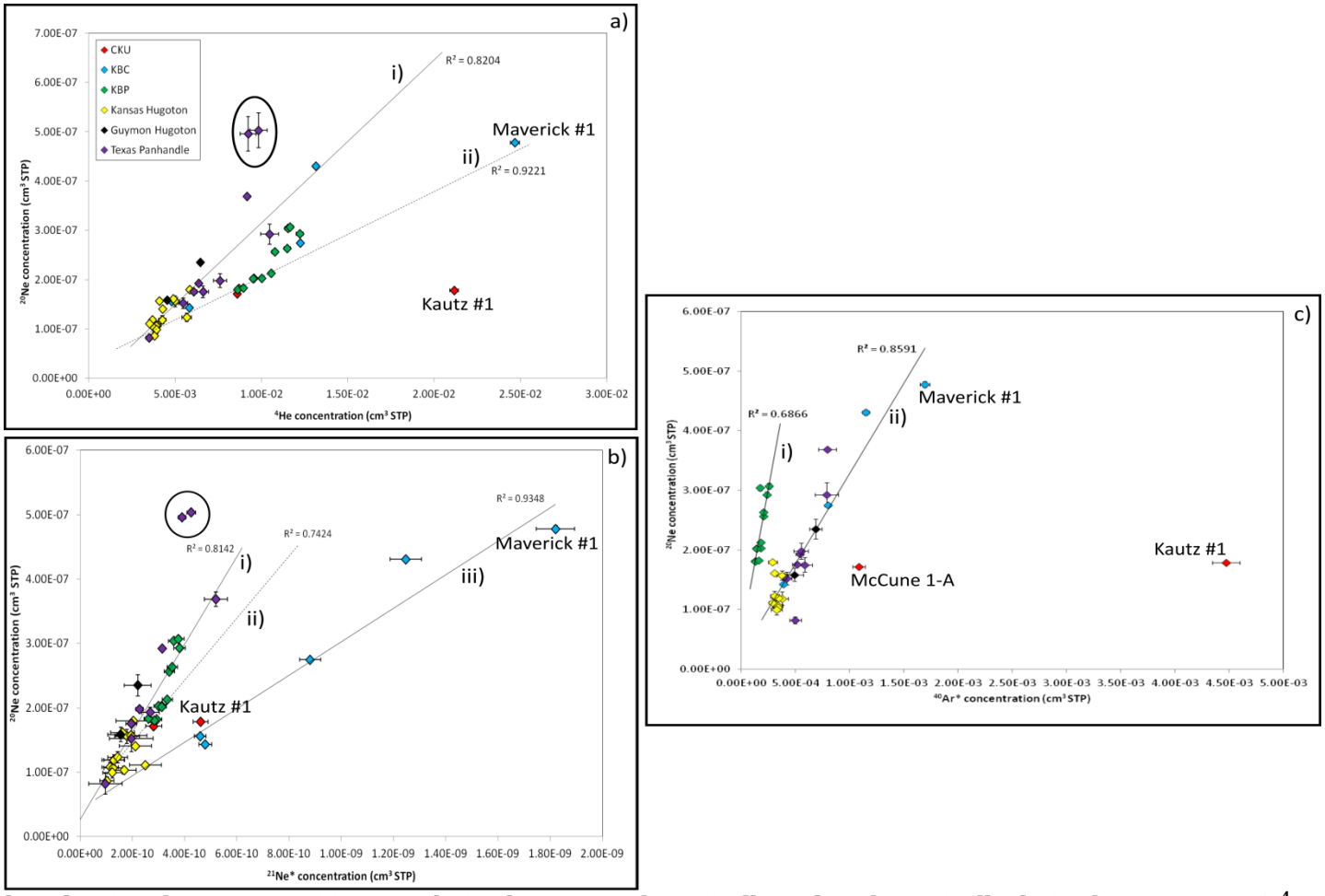

Figure 3.8.: Plots showing the strong positive correlation between radiogenically and nucleogenically derived components a) ^{4}He, b) ^{21}Ne*, c) ^{40}Ar* and groundwater-derived ^{20}Ne. All lines fall within error of the origin. There appear to be several potential trends associated with each isotope as outlined here: a) i) the original trend from Ballentine and Sherwood-Lollar which discounts the outlying Donelson et al., and Sarah Claybaugh wells, ii) the southern wells of the KBP dataset (Oppy-Burke no.1, Benish no. 1, Poverty Hill no. 1, Strecker no. 1, Jetmore-Bradford no. 1, Gleason 1 and Lewis Trust 1). b) i) the Hugoton-Panhandle dataset excluding the Donelson et al., and Sarah Claybaugh wells, and ii) the KBC dataset. c) i) the KBP dataset and ii) the combined Hugoton-Panhandle and KBC datasets.

The upper and lower boundary trends for each radiogenic isotope vary depending on subset. Only the subsets of the Hugoton-Panhandle fall along the same trend each time. Mixing can be seen between each of the upper and lower trends indicating that strata and depth is, for the most part, irrelevant in these systems especially in the case of ^{4}He.

3.4.2. Other Major Gases

3.4.2.1. Methane

Across the KBP samples, the gas composition includes methane at concentrations between 56.0-73.6%. When compared with the Hugoton-Panhandle (56.1-71.5%) these concentrations fall within the same range. Data for the KBC is more limited and ranges between 42.2-59.1%. CKU well gases contain between 60.6% CH_4 (Kautz #1) and 72.4% CH_4 (McCune 1-A). Isotopic analyses of CH_4 were conducted on the Hugoton Panhandle gases by Ballentine and Sherwood-Lollar (2002) and $\delta^{13}C_{CH4}$ values range between -41.80‰ and -45.10‰. Isotopic analysis of the CH_4 component for the CKU, KBC and KBP wells was not conducted.

3.4.2.2. Nitrogen

Nitrogen concentrations vary across the Kansas Basin dependent on subset. In the KBC N_2 concentrations range from 9-51% and in the KBP from 22-42%. In the CKU samples N_2 concentrations vary between 31-37%. Isotopic $\delta^{15}N$ values vary widely in the KBC from between +1.85‰ to +6.50‰ and similarly in the KBP

samples which are between +1.45‰ to +4.70‰. Isotopic $\delta^{15}N$ values in the CKU samples fall within range of both the KBP and KBC with the McCune 1-A well at +3.45‰ and the Kautz #1 well at +2.45‰.

Nitrogen concentrations from the Hugoton-Panhandle can be split between the Kansas Hugoton-Guymon Hugoton system (12.7-21.4%) and the Texas Panhandle (6.6-25.8%). Isotopic $\delta^{15}N$ values show a transition between these two systems with the Hugoton system showing values of +5.30‰ to +9.40‰ and of between +2.70‰ to +5.30‰ for the Texas Panhandle.

In general there is a trend in the Permian (Chase Group) samples in the Kansas Hugoton field from west to east of a decrease in $\delta^{15}N$ values coinciding with a well-recognised low BTU rim which sits on the northern and eastern edges of the Hugoton-Panhandle field (**Figure 3.9a**). This also shows the updip filling of the Kansas Hugoton by high BTU gases after eastward tilting caused by the Laramide Orogeny (Sorenson, 2005). In general there is a decrease in $\delta^{15}N$ values from SW to NE across the Kansas study regions (**Figure 3.9b**).

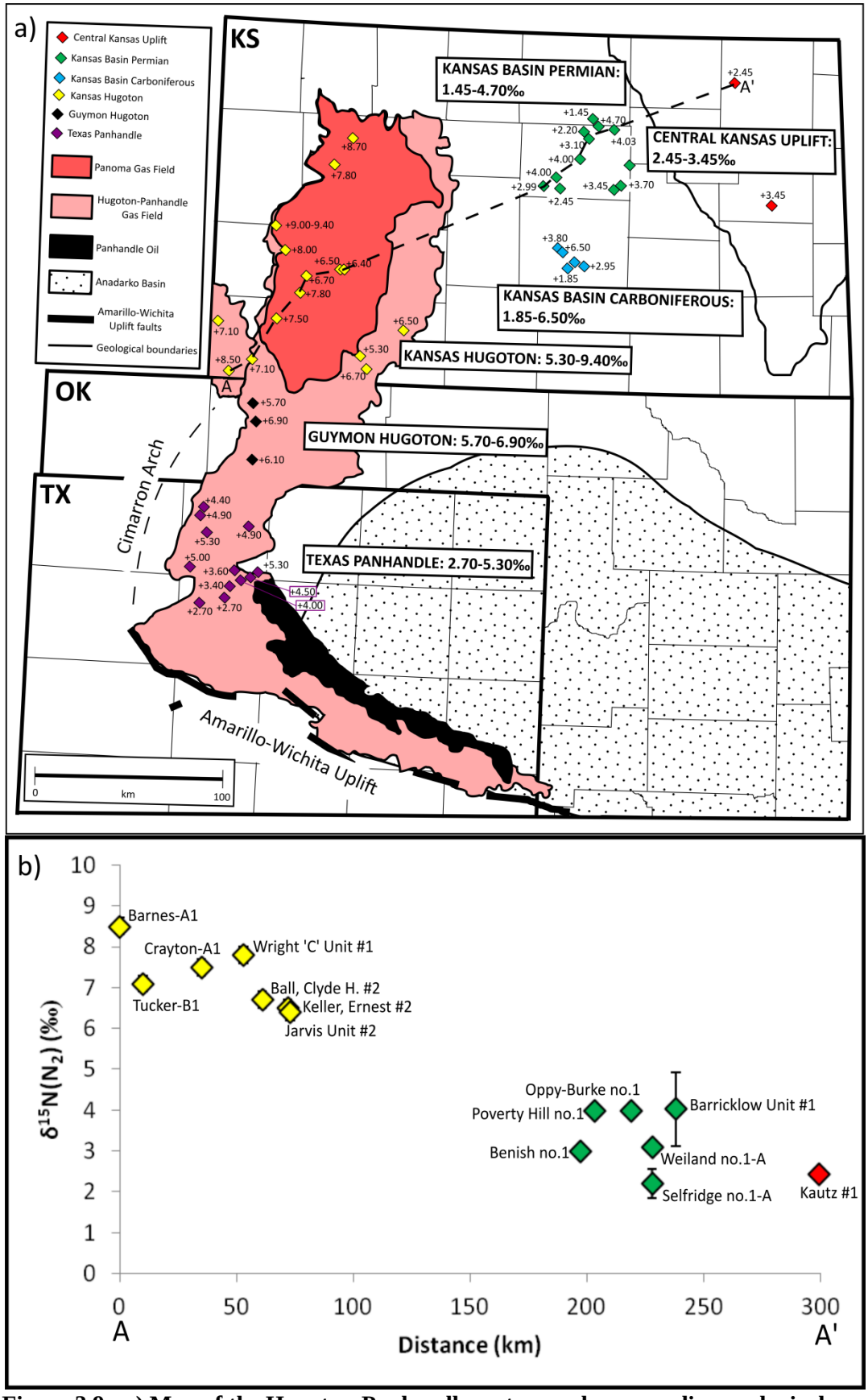

Figure 3.9.: a) Map of the Hugoton-Panhandle system and surrounding geological features including study areas with $\delta^{15}N_{N2}$ (‰) values displayed, b) The change in δ^{15}

values from SW to NE across the study areas from A-A' in a). The distance between wells is measured relative to distance from Barnes A-1.

Although the lowest value of $N_2/^{40}Ar$ for the Texas samples and both CKU samples are in the same range as the atmospheric and groundwater values it is clear that the variation across the sample sets are not caused by significant mixing with these components (**Figure 3.10**). This indicates that there is negligible addition of air-derived N_2 to the N_2 concentrations found across all datasets alongside air saturated groundwater which at most may only be affecting one well (Kautz #1).

Since air-derived N_2 can be ruled out, this leaves three other potential sources: mantle sourced, crust sourced and hydrocarbon sourced. It is possible to estimate the percentage of mantle contribution across the dataset. The derived $N_2/^3He$ ratio for a MORB-like mantle is 6×10^6 (Ballentine and Sherwood-Lollar, 2002). When this is applied to the previously calculated mantle ^3He concentration in samples, this gives a mantle N_2 contribution to total concentrations of between 1.7-5.7% for the Kansas Basin-CKU system. Mantle N_2 contributions to the Hugoton-Panhandle N_2 concentrations range between 2.6-10.1% and on average are higher in the Texas Panhandle than in the Kansas Hugoton-Guymon Hugoton region ($7.3 \pm 1.5\%$ compared with $4.1 \pm 1.1\%$).

From the above calculation it can be determined that overall less than 10% of N_2 concentrations can be attributed to mantle contributions and therefore the majority of N_2 present must be attributed to a combination of either the thermal cracking of hydrocarbons or thermal release from the crust.

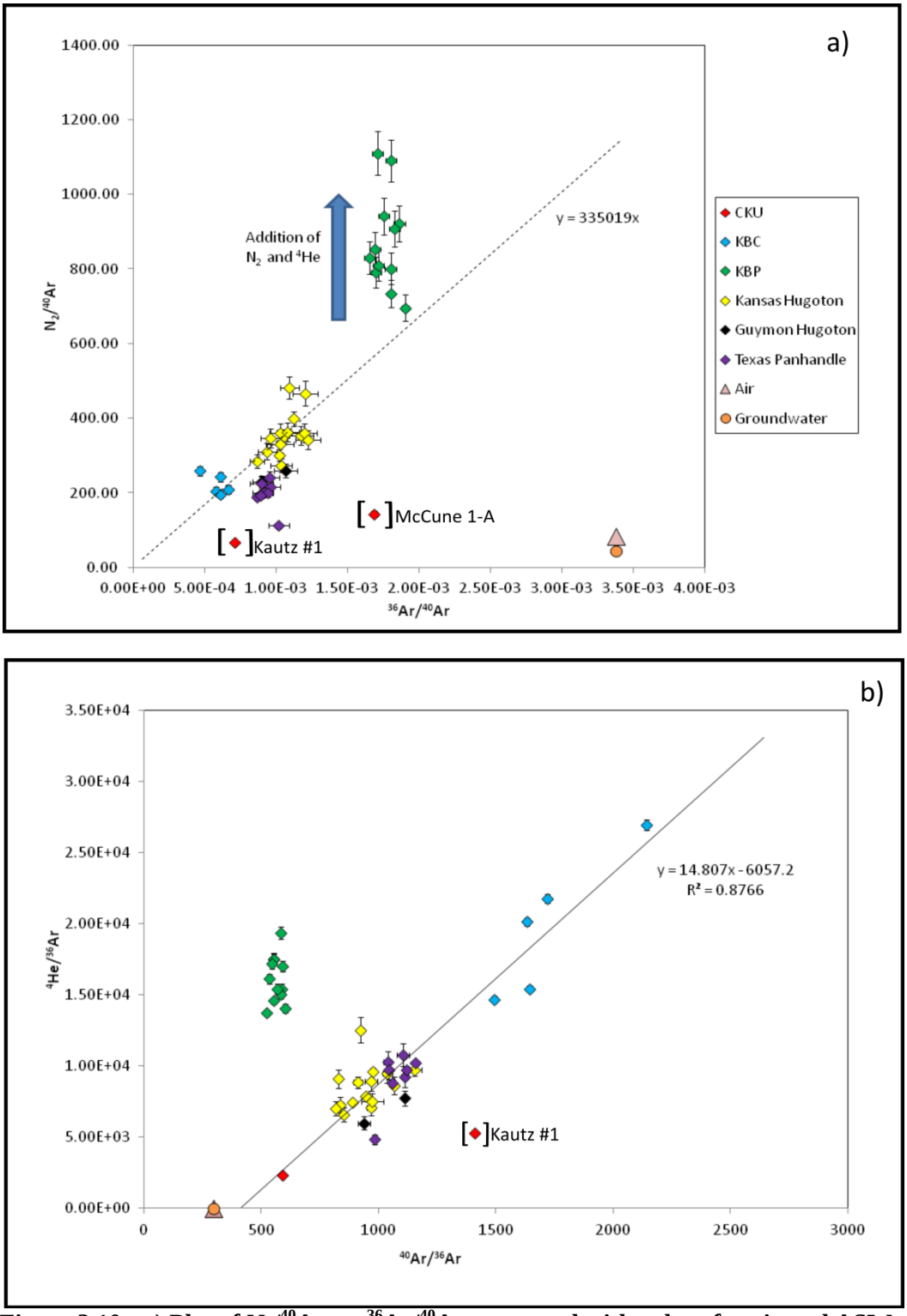

Figure 3.10.: a) Plot of $N_2/^{40}Ar$ vs. $^{36}Ar/^{40}Ar$ compared with values for air and ASW. This diagram shows that nitrogen for all samples cannot be explained by mixing with a dissolved air component and there is instead a separate mixing line which encompasses the Hugoton-Panhandle, KBC and McCune 1-A samples. b) Plot of $^4He/^{36}Ar$ vs. $^{40}Ar/^{36}Ar$ compared with values for air and ASW. Like the N_2 component the ^4He component cannot be explained by either air or ASW and therefore most likely migrated with the N_2 indicating either a similar source, migration mechanism or both.

3.4.3. Nitrogen and the noble gases

Across all samples ^4He concentrations are strongly positively correlated with N_2 concentrations (**Figure 3.11**). $^4He/N_2$ ratios in the Texas Panhandle and Kansas Hugoton-Guymon Hugoton gases show a split in ratio (0.020-0.037 in Kansas/Guymon Hugoton and 0.036-0.049 for the Texas Panhandle) from north to south as evidenced in both Gold and Held, (1987) and Ballentine and Sherwood-Lollar, (2002).

There also appears to be significant overlap between the KBP, KBC, CKU and the Texas Panhandle subset which breaks with this spatial trend. There are no readily resolvable spatial trends within individual subsets.

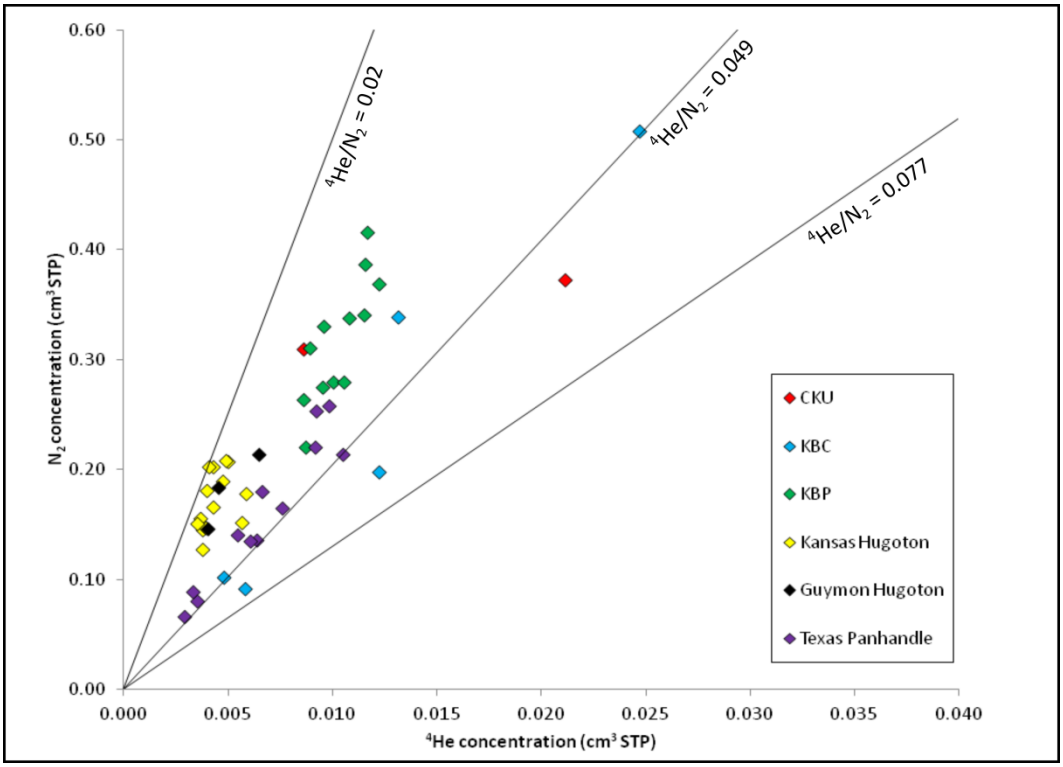

Figure 3.11.: Plot of N_2 concentration versus ^4He concentration showing a split in ratio between the KBP and Kansas Hugoton samples and the Texas Panhandle and KBC samples. Values in the Kansas Hugoton are as low as 0.020 and values in the KBC are as high as 0.063. The $^4He/N_2$ ratio of 0.077 comes from the average of samples taken from the Bush Dome which lies at the southern end of the Hugoton-Panhandle field

(Gold and Held, 1987). It is taken to be the pure ^{4}He endmember in associated N_2 calculations for the region following on from Ballentine and Sherwood-Lollar, (2002) due to it being the upper limit of $^4He/N_2$ ratios taken from the Texas Panhandle region.

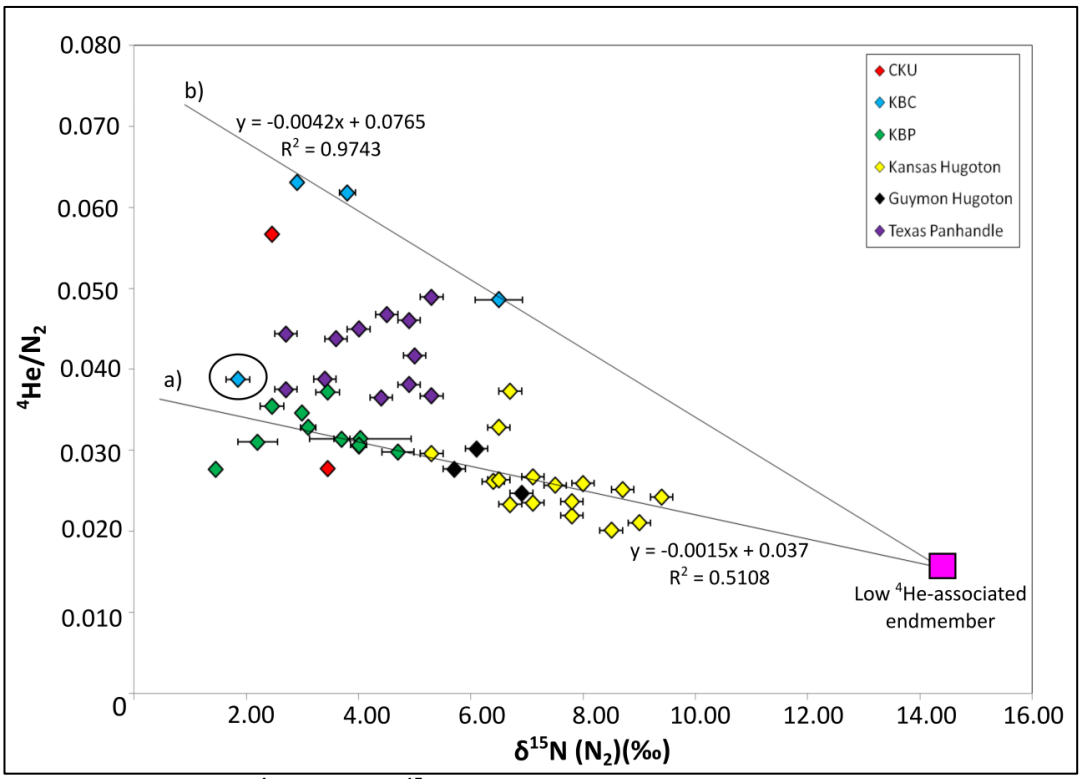

Figure 3.12.: Plot of $^4He/N_2$ vs. $\delta^{15}N(N_2)$. Mixing lines shown a) for the KBP and Kansas Hugoton samples, and b) the KBC samples excluding the anomalously low #1 Blew well (circled).

Similar to the previous study there appears to be a correlation between ^{4}He and N_2 for the new samples indicating a link between two potentially differently sourced components (Ballentine and Sherwood-Lollar, 2002) (**Figure 3.12**). Following on from this we propose two new mixing lines (a and b) which utilise three nitrogen endmembers; two of which are associated with high concentrations of ^{4}He and low $\delta^{15}N$ values and one which is shared by both mixing lines and is characterised by low concentrations of ^{4}He and high $\delta^{15}N$ values. Since the Hugoton-Panhandle samples show mixing between all nitrogen endmembers we can assume that they are applicable to all datasets to varying degrees.

The lower and upper boundaries which encompass the bulk of the datasets intersect at a point determined as the $\delta^{15}N$ value of +14.60‰ which corresponds to a

lowered $^4He/N_2$ ratio of 0.015. This low-^4He associated nitrogen endmember directly compares to the 'non-^4He associated' endmember calculated in Ballentine and Sherwood-Lollar, (2002) of +13.00‰. The narrow range of these endmember values indicates a common source of low ^4He-associated nitrogen for most of the Hugoton-Panhandle, Kansas Basin and CKU system. The $\delta^{15}N$ values for this endmember fit into the range quoted by Zhu et al., (2000) for gases derived from the late stage denitrification of post-mature sedimentary organic matter ($\delta^{15}N$ = +4.00‰ to +18.00‰).

Extrapolating the original mixing line from Ballentine and Sherwood-Lollar (2002) to determine the high ^4He-associated nitrogen endmember produces a significantly less enriched $\delta^{15}N$ value of -5.00±0.30‰ when considering an endmember with the $^4He/N_2$ ratio of 0.077 (Gold and Held, 1987; Ballentine and Sherwood-Lollar, 2002). This directly compares to the value of -3.00‰ calculated for the same ^4He-associated nitrogen endmember calculated in Ballentine and Sherwood-Lollar, (2002).

Despite the observation that both new ^4He-associated nitrogen endmembers have $^4He/N_2$ ratios which are significantly different to the $^4He/N_2$ ratio of 0.077 used by Ballentine and Sherwood-Lollar, (2002), if it is assumed that their $\delta^{15}N$ isotopic endmembers fall within the same narrow range of $\delta^{15}N$ values (-5.00‰ to -3.00‰) it could indicate that they most likely share a source from the low temperature metamorphism of the crust (-5‰ to +4‰) (Haendel et al., 1986; Kreulen et al., 1982; Bebout and Fogel, 1992; Bebout et al., 1999; Zhu et al., 2000; Ballentine and Sherwood-Lollar, 2002).

Alternatively, if it is assumed that the lowest $\delta^{15}N$ values from each boundary (+1.85‰ for the upper boundary and +1.45‰ for the lower boundary) are

representative of being close to the original $\delta^{15}N$ endmember in the area then the metamorphism of ammonium clay minerals in sediments could also be a sourcing option (+1‰ to +4‰). Both modern sediments and metamorphosed rocks up to greenschist facies show indistinguishable $\delta^{15}N$ value ranges (Zhu et al., 2000; Boyd, 2001).

Ammonium (NH_4^+) bound in clays makes up < 60% of sedimentary nitrogen (Ader et al., 2016). In this form it is highly thermally stable and therefore cannot be released by temperature alone under geological conditions in study areas since temperatures must exceed 500°C (Whelan et al., 1988; Zhu et al., 2000). There is only evidence of low temperature regional metamorphism to, at most, greenschist facies near the Amarillo-Wichita Uplift making this an unlikely scenario (Nicholas and Rozendal, 1975; Cardott, 1988).

The limited number of studies on the thermal maturation of organic matter during burial diagenesis shows that it does not significantly modify the nitrogen isotopic composition of either bulk sediments or kerogens relative to clay minerals within a closed system (Williams et al., 1995; Mingram et al., 2005; Adler et al., 2016).

Another method of releasing ammonium from clays is fluid-rock interactions with highly saline brines (Mingram et al., 2005). Ammonium is known to be highly soluble in groundwater and past literature has shown that migrating hydrocarbon phases tend to become enriched in ^{15}N as they move through authigenic illite (Williams et al., 1995). However, without $\delta^{15}N$ and N_2 whole rock analyses for the study areas it is difficult to determine exactly which rocks N_2 has been sourced from or whether the gases measured in fields have either experienced $\delta^{15}N$ enrichment during migration or from mixing with a more $\delta^{15}N$ enriched gas component.

If we assume that the high ^{4}He-associated nitrogen endmember has a δ^{15}N value of approximately -3.00‰ then the $^4He/N_2$ ratio for mixing line (a) has a value of 0.043 whereas mixing line (b) has a ratio of 0.089. Alternatively if we assume that the high ^{4}He-associated endmember δ^{15}N value for produced gas had a value of +1.00‰ which encompasses both metamorphosed crust and ammonium release from clays then the $^4He/N_2$ ratio for mixing line (a) has a value of 0.036 and mixing line (b) has a ratio of 0.072.

The differences in $^4He/N_2$ ratios between the mixing line endmembers could be caused by a variety of factors including: differing accumulation times before release, variations in the N_2 content of the source rock(s), differences in U content relative to N_2 in the various source rocks or variable dilution of the $^4He/N_2$ ratio by CH_4.

In summary the bulk of the dataset can be explained by mixing between three nitrogen endmembers, one of which is associated with low concentrations of ^{4}He and two which are associated with high ^{4}He concentrations. These endmembers may share similar ^{4}He and N_2 release mechanisms but potentially not the same combination of source rocks.

3.5 Discussion

3.5.1 Helium mass balance

Calculating the total ^{4}He produced by U and Th decay over specific time periods can help to estimate the volume of rock needed to generate the volume of ^{4}He occurring in study area reservoirs.

As there are no estimates for the reserve volumes associated with sample fields we calculated minimum reserve estimates for the ^4He produced from each field by first estimating the original gas in place (OGIP) using a basic volumetric equation **(Equation 1**):

$$OGIP(SCM) = Ah\phi(1-S_w)/B_{gi} \quad (\mathbf{1})$$

where A = area of reservoir (m^2) in our case assumed to be the same area as the field; h = thickness of pay zone (m) estimated from log data; ϕ = porosity (decimal) from log data; S_w = connate water saturation (decimal) estimated from drill stem tests and B_{gi} = formation volume factor for the gas at initial conditions (m^3/SCM) (**Table 3.6**).

For fields where there was insufficient information provided to determine a plausible estimate (Bahr, Blew, Lamb and Stella B) it was assumed that the cumulative production to date represented 50% of the OGIP replicating recovery estimates (**see Table 3.1**).

Field name	Producing reservoir	Estimated OGIP (m^3)	Estimated helium reserves (m^3)
Bahr	Chase Group	4.39×10^7	9.28×10^5
Leesburgh	Chase Group	1.72×10^8	1.48×10^6
Carson	Morrow Sands	6.85×10^6	8.38×10^4
Maverick	Morrow Sands	8.51×10^5	2.10×10^4
Blew (single well)	Morrow Sands	2.98×10^6	3.92×10^4
Steel	Mississippian	1.05×10^8	5.02×10^5
Lamb	Mississippian	4.66×10^7	2.71×10^5
Barrick	Chase Group	6.30×10^7	7.70×10^5
Neho	Chase Group	2.51×10^7	2.89×10^5
Barricklow East	Chase Group	5.20×10^7	6.06×10^5
Wieland North	Chase Group	1.11×10^9	1.20×10^7
Wieland	Chase Group	4.93×10^7	5.67×10^5
Hanston-Oppy	Chase Group	1.64×10^9	1.57×10^7
Groner	Chase Group	8.82×10^8	8.84×10^6
Saw Log Creek	Chase Group	1.84×10^9	1.60×10^7

Southeast Saw Log Creek	Chase Group	4.07×10^7	3.50×10^5
Jetport	Chase Group	2.92×10^7	3.08×10^5
Stella B	Chase Group	1.72×10^7	8.21×10^4
Don	Chase Group	2.12×10^9	1.89×10^7
Hugoton-Panhandle	Chase Group	1.85×10^{12}	1.11×10^{10}

Table 3.6.: Estimated gas and helium reserves for all fields studied. Information regarding all fields in the table can be found on the KGS Oil and Gas Lease Database. The estimate for the Hugoton-Panhandle OGIP is from Dubois, (2007). ^{4}He estimates for the Hugoton-Panhandle are based off an average concentration of 0.6% (Ballentine and Sherwood-Lollar, 2002).

The total estimated OGIP from sampled fields in the study regions is 8.25 x 10^9 m^3. With the individual ^{4}He content from all wells (0.48-2.12%) this gives an in place ^{4}He estimate total of 7.78×10^7 m^3 which is approximately 0.7% of the Hugoton-Panhandle ^{4}He volume.

3.5.1.1. In situ ^{4}He production

To determine where ^{4}He in the Hugoton-Panhandle and Kansas System has been sourced from we need to determine whether the ^{4}He volumes in reservoirs have been generated in situ or externally. Below we present three scenarios for the time period following 250 Ma (after the deposition of the evaporite caprock across the region):

1. Volume of ^{4}He produced by the reservoir over 250 Ma within field areas.
2. Area required to source the in place volume of ^{4}He in reservoirs.
3. Volume of ^{4}He produced by an enriched reservoir (20.5 ppm U); which only applies to the Hugoton-Panhandle and KBP subsets (Luczaj and Goldstein, 2000).

We have given all producing reservoirs within the study areas (Chase Group, Council Grove Group, Brown Dolomite, Morrow Sands and Mississippian) an average crust composition of 2.8 ppm U and 10.7 ppm Th, an average crust density of 2.7 cm^3/g, an average porosity of 13% and an average thickness of 100 m for the Chase Group reservoirs in the KBP, 170 m for Hugoton-Panhandle areas, 15 m for the Morrow sands and 36 m for the CKU area (Halverson, 1988; Luczaj and Goldstein, 2000; Dubois et al., 2006; KGS, 2017).

We assume 100% release, transport and trapping efficiency which, while unrealistic, represents a minimum value for areal extent required and for gas volumes produced (**Table 3.7**).

Region and in place helium (m^3)	**Scenario**	**Helium volume produced (m^3)**	**Source area needed (km^2)**	**Percentage of in place ^{4}He (%)**
Hugoton-Panhandle (1.11×10^{10})	1	1.85×10^9	2.5×10^4	17
	2	1.11×10^{10}	1.1×10^5	100
	3	7.84×10^9	2.5×10^4	71
KBP (7.45×10^7)	1	3.21×10^6	203.0	4
	2	7.45×10^7	1.50×10^3	100
	3	1.39×10^7	203.0	19
KBC (9.17×10^5)	1	6.25×10^4	9.8	7
	2	9.17×10^5	124.6	100
CKU (2.40×10^6)	1	1.37×10^5	8.9	6
	2	2.40×10^6	135.9	100

Table 3.7.: Scenarios for the in situ production of ^{4}He. Scenario 3 does not apply to either the KBC or CKU due to there being no evidence for enrichment in these regions.

All of the above scenarios show that in situ production alone is not a viable explanation for the total ^{4}He volume in reservoirs. At most in situ production makes up 17% of the ^{4}He volume within reservoirs meaning that the other 83% must be sourced externally; either from sediments or the basement. Given the depths of these reservoirs and the palaeothermal gradient associated with the neighbouring Anadarko Basin (24°C/km) it is unlikely that a significant proportion of ^{4}He atoms

were released from producing minerals such as apatite and zircon (**see Table 1.1**) (Lee and Deming, 1999; Lee and Deming, 2002).

Enrichment by U in reservoirs (Scenario 3) can potentially make up to 71% of the volume however this assumes homogeneity when in reality it would most likely be highly heterogeneous throughout the reservoir making it unlikely to be a prolific source of ^{4}He enrichment except on a local scale.

In terms of areal extent (Scenario 2), the Hugoton-Panhandle would require in situ production from an area approximately 4 times bigger than the field itself, the KBP requires an area 7 times larger, the KBC 12 times bigger and the CKU 15 times its area in order to source ^{4}He volumes purely from continuous reservoir strata.

Since these scenarios all require 100% efficiency of release, migration, focusing and trapping the area required would in reality be even larger than these estimates therefore ruling out significant input from in situ production.

3.5.1.2. External sources of ^{4}He production

When considering alternative sources of ^{4}He the next step is to examine the viability of the associated underlying sediments and the basement rock down to 10 km beneath the fields due to ~ 90% of the Earth's ^{4}He being produced in the upper 10 km of the crust (Ballentine and Burnard, 2002).

Sediments below the evaporite seal in the deepest part of the Hugoton-Panhandle to the top of the Precambrian basement are approximately 1.7 km thick, shallowing to around 0.90 km thick in the KBP study area and then to approximately 0.60 km thick in the CKU (**Figure 3.2b**). In the KBC study area the sedimentary

package below the Morrow (Pennsylvanian) is approximately 0.50 km thick (KGS, 2017).

For the following scenarios we consider three time periods after events which may have affected the study areas and caused the reset of ^{4}He production: 1) 530 Ma (the time period since the last perturbation of the Precambrian basement), 2) 300 Ma (the time period following the inception of the Anadarko Basin) and 3) 250 Ma (the time period after the emplacement of the evaporite seal on the region). For the periods of 530 Ma and 300 Ma we assume that there is no significant ^{4}He loss during the emplacement of sedimentary layers.

Due to the variable composition of the underlying sediments and the variable but unknown composition of the basement we have given them an average crust composition of 2.8 ppm U and 10.7 ppm Th, an average crust density of 2.7 cm^3/g and we have assigned an average porosity of 13% to the sediments and 5% porosity to the basement assuming granite is the primary component (Flawn, 1956; Bickford et al., 1981).

When we consider the external sources of ^{4}He we can estimate an upper limit for the bulk release of ^{4}He from minerals according to temperature at depth. ^{4}He is released from apatite at temperatures between 55-100°C (on average 70°C), zircon between 170-200°C and titanite around 200°C (Ballentine et al., 1994; Wolf et al., 1996; Ballentine and Sherwood-Lollar, 2002; Shuster et al., 2006; Reich et al., 2007; Hunt et al., 2012). For the purposes of our calculations we will use the lowest recorded ^{4}He closure temperature in apatites of 55°C as the limit of the ^{4}He release window throughout the crust. It is assumed that above this temperature 100% of ^{4}He atoms will be released from minerals and below this temperature 100% of ^{4}He atoms are preferentially retained by minerals. The above scenarios are presented for the

estimated average palaeothermal gradient of the Anadarko Basin (24°C/km) at a surface temperature of 15°C (**Table 3.8**).

Region and in place ^4He (m^3)	Producing layer	Time period (Ma)	Depth range from top to bottom of producing area (km)	^4He volume produced (m^3) at 100% release	% of ^4He generation from source needed for volume in reservoir	Thickness of strata within ^4He release window with thermal gradient of 24°C/km (km)	^4He volume produced (m^3) within release window with thermal gradient of 24°C/km	% of ^4He generation from source needed for volume in reservoir
Hugoton-Panhandle (1.11×10^{10})	Sediments	530	0.6-2.3	3.47×10^{10}	32	0.6	1.22×10^{10}	91
		300		1.93×10^{10}	57		6.83×10^{9}	100
		250		1.61×10^{10}	69		5.67×10^{9}	100
	Basement	530	2.3-10.0	1.72×10^{11}	6	7.7	1.72×10^{11}	6
		300		9.57×10^{10}	12		9.57×10^{10}	12
		250		7.95×10^{10}	14		7.95×10^{10}	14
KBP (7.45×10^{7})	Sediments	530	0.7-1.6	1.52×10^{8}	49	0	No significant input	100
		300		8.46×10^{7}	88			
		250		7.02×10^{7}	100			
	Basement	530	1.6-10.0	1.55×10^{9}	5	8.4	1.55×10^{9}	5
		300		8.62×10^{8}	9		8.62×10^{8}	9
		250		7.16×10^{8}	10		7.16×10^{8}	10
KBC (9.17×10^{5})	Sediments	530	1.5-2.0	4.05×10^{6}	23	0.3	2.43×10^{6}	38
		300		2.26×10^{6}	41		1.35×10^{6}	68
		250		1.87×10^{6}	49		1.12×10^{6}	82
	Basement	530	2.0-10.0	7.07×10^{7}	1	8.0	7.07×10^{7}	1
		300		3.94×10^{7}	2		3.94×10^{7}	2
		250		3.28×10^{7}	3		3.28×10^{7}	3
CKU (2.40×10^{6})	Sediments	530	0.5-1.1	4.43×10^{6}	54	0	No significant input	100
		300		2.47×10^{6}	97			
		250		2.05×10^{6}	100			
	Basement	530	1.1-10.0	7.17×10^{7}	3	8.3	6.69×10^{7}	4
		300		4.00×10^{7}	6		3.73×10^{7}	6
		250		3.32×10^{7}	7		3.10×10^{7}	8

Table 3.8.: ^4He production scenarios for external sources to fields.

The respective ^{4}He volumes associated with the Hugoton-Panhandle, KBP, KBC and CKU could have conceivably been generated by either the underlying sediments (sandstone, limestone, dolomite and shale) or the basement rocks or a combination of the two.

However, if it is then assumed that near 100% ^{4}He release occurs above mineral closure temperatures over the geological timescales considered, 82-100% ^{4}He generation would have had to occur in the Hugoton-Panhandle and KBC fields and remain in fields for over 250 Ma in order to source ^{4}He volumes. Conversely, the KBP and CKU areas sediments are currently below the closure temperature of producing minerals, implying that the contribution of the sediments to ^{4}He reservoir volumes in these areas is negligible.

An alternative source of ^{4}He which also needs to be considered is black shale such as the Mississippian-Devonian aged Woodford Shale primarily located in the Anadarko Basin. The Anadarko Basin contains on average 0.07% ^{4}He which amounts to approximately 5.0×10^{10} m^3 of in place ^{4}He (Dong et al., 2012; Ellis, 2014). The shale, which contains on average 38.5 ppm U and 6.3 ppm Th and is ~100 m thick, could have produced the ^{4}He volumes observed in the Anadarko Basin over the course of 300 Ma; however it would require near 100% release and trapping of ^{4}He atoms (Krystyniak, 2003; Paxton et al., 2006). The < 11 km thick package of sediments in the basin of average U and Th content and 13% porosity could also have generated the volumes of ^{4}He in all study areas over 250 Ma.

An added complication is that present day depths within the study areas do not represent maximum depths within individual study regions. However, it is not known what the maximum depths for the KBC and KBP regions would have been or when these were reached; the CKU has been an area of near-continual uplift.

Maximum depths in the Hugoton-Panhandle, reached in the early Tertiary (~ 65 Ma), were 1.37-1.62 km for the Wolfcampian (Sorenson, 2005). This would have increased the thickness of sediments within the ^{4}He release window to an average of ~1.1 km thick over the course of the Late Permian (250 Ma) to the present. Even with this increased release window it would require 100% of all ^{4}He atoms within the Hugoton-Panhandle to be released and retained within the field to generate helium volumes which is unlikely.

With several options for the source of ^{4}He it is difficult to determine with certainty the true source of the helium simply from a mass balance due to the large uncertainties in release efficiency, helium loss during erosional periods and lateral migration in and out of fields over geological time. The area needed for sourcing the helium could be orders of magnitude larger than is calculated here. At the very least our first order calculations indicate that there is either: 1) a variable basement input into fields, or 2) focusing/migration of ^{4}He from a larger sedimentary area.

Despite these uncertainties it is clear that the source of the helium is predominantly from the shallow crust; most likely from differing combinations of sediments and basement rocks, however, it has also been observed in this study that a discrete deep crustal component is also involved which has delivered mantle-derived ^{3}He, ^{4}He, $^{21}Ne^{*}$ and N_2 into these shallow reservoirs as well. These components could not have been generated in situ from the sediments or from a hypothetical purely granitic basement complex therefore we need to examine the mechanisms involved in not only sourcing the mantle component but ultimately also the mixing and focusing of all gas components into reservoirs.

3.5.2 Thermal controls on the release of radiogenic isotopes

The ratios and concentrations of the radiogenically produced isotopes in the well gases across the dataset vary considerably dependent on the study area (**Table 3.9**). In this section we expand on the observations presented in Section 3.4.1.5.

Well name/geological province	$^{4}He/^{40}Ar^{*}$	$^{4}He/^{21}Ne^{*}$	$^{40}Ar^{*}/^{21}Ne^{*}$	$^{21}Ne^{*}$ (%)	$^{40}Ar^{*}$ (%)
Hugoton-Panhandle (average)	12.46 ± 2.48	2.85 ± (0.62) x 10^{7}	2.43 ± (0.81) x 10^{6}	28.6 ± 4.3	69.9 ± 3.2
Kansas Hugoton	13.26 ± 2.46	2.85 ± (0.70) x 10^{7}	2.19 ± (0.59) x 10^{6}	30.1 ± 4.6	68.4 ± 3.1
Guymon Hugoton	9.40 ± 0.09	2.93 ± (0.001) x 10^{7}	3.12 ± (0.03) x 10^{6}	24.6 ± 0.4	71.0 ± 3.5
Texas Panhandle	11.73 ± 2.10	2.83 ± (0.61) x 10^{7}	2.66 ± (1.09) x 10^{6}	27.3 ± 3.6	72.5 ± 1.4
Kansas Basin Carboniferous	13.72 ± 1.75	1.21 ± (0.16) x 10^{7}	8.83 ± (0.53) x 10^{5}	49.8 ± 2.5	82.6 ± 2.2
Kansas Basin Permian	59.81 ± 7.63	3.16 ± (0.14) x 10^{7}	5.38 ± (0.83) x 10^{5}	32.0 ± 2.2	47.7 ± 2.3
Kautz #1 (CKU)	4.73 ± 0.14	4.59 ± (0.29) x 10^{7}	9.70 ± (0.66) x 10^{6}	45.5 ± 7.3	79.0 ± 2.8
McCune 1-A (CKU)	7.94 ± 0.43	3.05 ± (0.33) x 10^{7}	3.84 ± (0.46) x 10^{6}	34.8 ± 7.0	50.1 ± 3.4
Average upper crust (theoretical) (Ozima and Podosek, 2001; Ballentine and Burnard, 2002)	6.0	2.33 ± (0.44) x 10^{7}	3.88 ± (0.73) x 10^{6}		
Average upper crust (observed) (Ballentine and Burnard, 2002)	5.0±1.0	1.71 ± (0.09) x 10^{7}	3.60 ± (1.27) x 10^{6}		

Table 3.9: **Concentrations and ratios of the radiogenically produced isotopes in samples. Errors are to 1σ.**

The main trend to the bulk of the data can be explained by three component mixing between the Hugoton-Panhandle , KBC samples and McCune 1-A from the CKU sample set (**Figure 3.13**). From this we observe that all samples except for the KBC subset are preferentially enriched in ^{4}He relative to both $^{21}Ne^{*}$ and $^{40}Ar^{*}$. The KBC samples are lower in both radiogenic ratios compared to the bulk of the dataset and the KBP dataset is depleted in $^{40}Ar^{*}$ relative to both ^{4}He and $^{21}Ne^{*}$.

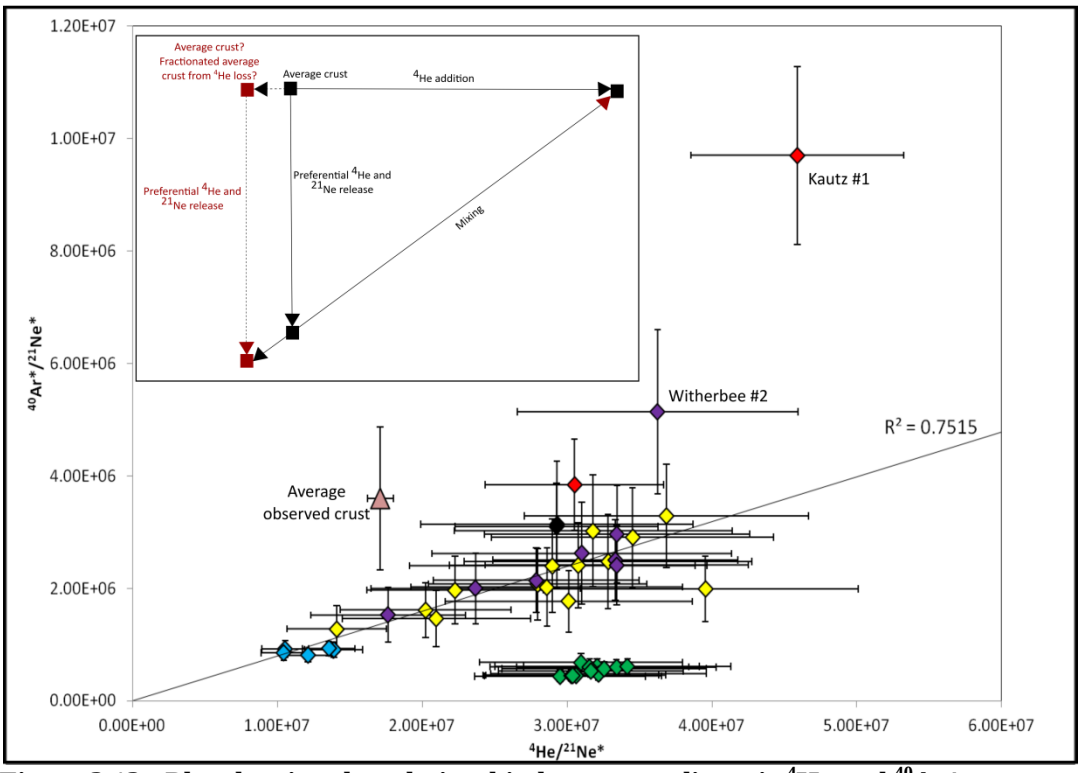

Figure 3.13.: Plot showing the relationship between radiogenic ^{4}He and $^{40}Ar^{*}$ normalised to nucleogenic $^{21}Ne^{*}$. The graph shows three component mixing; one aspect of which is controlled by the $^{21}Ne^{*}$ component since the $^{4}He/^{40}Ar^{*}$ ratio for the mixing line is constant. The Whitherbee #2 well, CKU and KBP samples are excluded from the mixing line data points. The inset shows how the main trend can be created by 1) the addition of excess ^{4}He to the system, 2) mixing with an endmember which has been created by the release of either a) a different type of average crust or b) an average crust which has lost ^{4}He but retained ^{21}Ne.

Due to the constant $^{4}He/^{40}Ar^{*}$ ratio associated with the main mixing line this indicates that the governing influence on the trend is the varying input of $^{21}Ne^{*}$ into the system relative to both ^{4}He and $^{40}Ar^{*}$. This makes it difficult to explain the low

$^{4}He/^{21}Ne^{*}$-low $^{40}Ar^{*}/^{21}Ne^{*}$ endmember since there is no source which could produce $^{21}Ne^{*}$ without ^{4}He increasing proportionally with it due to the main mechanism for ^{21}Ne production being the $^{18}O(\alpha,n)^{21}Ne$ route where the α particles are produced by U and Th decay and eventually stabilise to form ^{4}He.

Solubility fractionation between gas, oil and water phases has also been known to fractionate $^{40}Ar^{*}/^{21}Ne^{*}$ more than $^{4}He/^{21}Ne^{*}$ due to the similarity between He and Ne solubility (Ballentine et al., 1991; Ballentine and O'Nions, 1994; Ballentine and Burnard, 2002; Ballentine and Sherwood-Lollar, 2002; Gilfillan, 2006). However, this would also fractionate $^{20}Ne/^{36}Ar$ accordingly and there is no clear relationships seen between $^{20}Ne/^{36}Ar$ and any of the crust-derived noble gas ratios. While there may be an argument for the single stage degassing of groundwater for the KBC samples and a potential multi-stage solubility fractionation process affecting the KBP samples these are beyond the scope of this work and require further investigation therefore we need an alternative mechanism.

Lower than average $^{4}He/^{21}Ne^{*}$ crustal ratios have been recorded before in Kyser and Rison, 1982 and have been factored into average crustal estimates (1.08×10^{7} from Ballentine and O'Nions, 1991). The KBC samples are also within range of the lowest of the Kansas Hugoton samples; Clyde H. Ball #2 which also shows enrichment in $^{21}Ne^{*}$ compared to the other wells in the locality ($^{21}Ne^{*}$= 42.7% when the local average is 28.6% for the Kansas Hugoton). The low value for the Kyser and Rison paper, however, refers to mafic lavas generated from fractionated melts which have preferentially lost their ^{4}He and retained ^{21}Ne and ^{40}Ar during metasomatism leaving them with a lower than average $^{4}He/^{21}Ne^{*}$ ratio.

This mechanism could explain the higher $^{21}Ne^{*}$ excesses in certain samples if either: 1) the underlying basement, while being predominantly granitic, also

consisted of rapidly cooled, fractionated solidified melts which had retained most of their nucleogenic $^{21}Ne^*$ or more reasonably, 2) the ^{4}He endmember associated with the KBC region experienced metasomatism early in its geological history leading to the preferential loss of ^{4}He and resulting in a lowered $^{4}He/^{21}Ne^*$ ratio before release and mixing with the enriched $^{4}He/^{21}Ne^*$ endmember associated with the Hugoton-Panhandle samples or, 3) the ^{4}He endmember associated with the KBC is sourced from a different type of average crust which has below normal average crustal $^{4}He/^{21}Ne^*$ ratios as a result of being affected by magmatism (Kyser and Rison, 1982; Ballentine, 1991; Ballentine et al., 2001; Ballentine and Burnard, 2002).

Mafic and felsic terranes ranging from gabbro to rhyolite to granite have been identified in the Precambrian and Cambrian in Kansas, Oklahoma and Texas (Flawn, 1954; Merriam et al., 1961; Bickford et al., 1981; Yarger, 1981; Adams and Keller, 1994) however the entire basement complex beneath southwestern Kansas has not been fully mapped to the extent of the southeast of Kansas therefore there is no way to truly determine if the cause of the lowered radiogenic ratios is local or due to sourcing from a different region of the crust.

The study areas all show evidence of a shallow crustal thermal regime where ^{4}He and ^{21}Ne is preferentially released over ^{40}Ar. The decoupling of ^{4}He and $^{21}Ne^*$ from $^{40}Ar^*$ typically occurs at depths above 6 km under regular geothermal conditions (30°C/km with a surface temperature of 15°C) based on the argon closure temperature in quartz (~200°C) and the average helium closure temperature in apatite (~70°C) (Ballentine et al., 1994; Ballentine and Sherwood-Lollar, 2002; Hunt et al., 2012). These closure temperatures are highly dependent on both the grainsize and the retentivity of the minerals housing the radioelements.

Another possible source of $^{40}Ar^*$ contributions to reservoirs could be the production and release of the isotope from K-rich clays associated with shales. However, for smectite-illite clays closure temperatures for ^{40}Ar fall within the range of 190°C-350°C which would be achieved at depths > 7 km (given a 24°C/km thermal gradient for the Anadarko Basin) (Daniels et al., 1994; Lee and Deming, 2002; Duvall et al., 2011).

This is supported by the K/Ar and Rb/Sr dating of NH_4-bearing illites in Appalachian anthracites which demonstrate the ability of illite to retain ^{40}Ar over significant geological time periods (≤ 253±8 Ma) after temperatures exceeded 200°C during the Alleghanian Orogeny (Daniels et al., 1994). This makes it highly unlikely that K-rich clay minerals at the shallow reservoir depths within all study areas contributed significant ^{40}Ar concentrations to reservoirs since there is no evidence of sedimentary temperatures exceeding 190°C.

Alkhammali, (2015) also records that Woodford Shale samples in Oklahoma at depths shallower than 2.3 km show good correlations between K and ^{40}Ar concentrations enabling the dating of the authigenic illite clays to specific Mississippian stages; indicating low losses of ^{40}Ar from the shale.

The recrystallisation of clays has also been thought to release ^{40}Ar generated within its structure however in oceanic illite-smectite clays it was found that smectite samples from the Pacific preferentially acted as traps for the heavy noble gases (Ar, Kr and Xe) (Clauer, 2006). The Woodford Shale within the Anadarko Basin depocenter, thought to be a potential source for the low ^{4}He associated endmember, could hypothetically also be associated with a portion of the $^{40}Ar^*$ concentrations observed in fields. Phase changes related to a change in ordering from R=0 to R≥1 illite within shales occurs around 100°C. During this phase change K^+ is released

into solution (Whittington II, 2009). No doubt $^{40}Ar^*$, produced from the decay of ^{40}K would also be released into solution, however, how much of this free K and ^{40}Ar is recaptured by the newly formed illite is unknown. The Woodford Shale currently lies at depths between 0.5 to 4.0 km deep; indicating that under a geothermal gradient of 24°C/km this would place parts of the basin > 3.5 km within this illite phase change window.

In summary there appears to be at least two sources of ^{4}He associated with the study areas. One of these sources is from the shallow crust and characterised by the preferential addition of ^{4}He; the other source is associated with enrichment in $^{21}Ne^*$ and $^{40}Ar^*$ relative to ^{4}He and indicates potential fractionation but also increasing temperature which corresponds to depths > 7 km in the crust. This deeper source most likely also corresponds to the area(s) sourcing the magmatic gases associated with samples.

3.5.3. Groundwater, N_2, CH_4 and the noble gases

Crust-derived ^{4}He, $^{21}Ne^*$ and $^{40}Ar^*$ concentrations are positively correlated with groundwater-derived ^{20}Ne concentrations in the KBC, KBP and Hugoton-Panhandle (**Figure 3.8**). This indicates that these disparate components are closely linked but with systematic differences which may relate to the three component mixing shown between ^{4}He, N_2 and the isotopes of N_2 in **Figure 3.12**.

By assessing the variation of CH_4 and N_2 concentrations with ^{20}Ne and the crust-derived radiogenic isotopes we can investigate migration pathways and the constraints these may place on sources for ^{4}He and the other radiogenically sourced gases.

Plots for the crustal-sourced noble gases and ^{20}Ne normalised to N_2 show that most data points fall along up to two mixing lines which are within error of the origin (**Figure 3.14**). There are different endmembers for $^{20}Ne/^{4}He$, $^{20}Ne/^{21}Ne^*$ and $^{20}Ne/^{40}Ar^*$ which are indicators of differing degrees of groundwater contact associated with sample subsets. These can vary for a number of reasons including migration distance (greater contact time with groundwater), differing rates of accumulation or of different migration routes in the crust. Mixing between the dominant trends is also observed with the most scatter occurring in the graph associated with ^{4}He and the least in the graph associated with $^{40}Ar^*$.

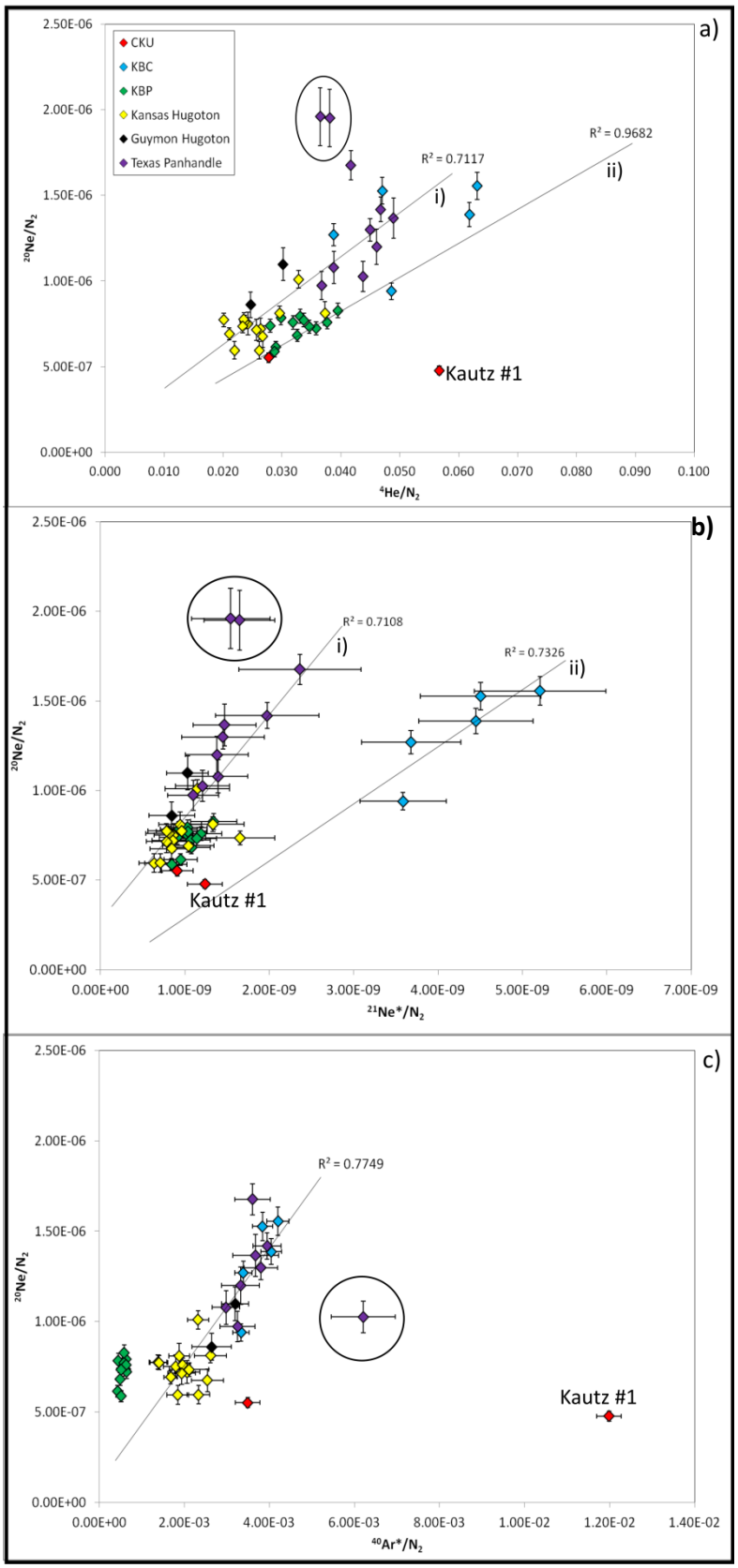

Figure 3.14: Plots showing groundwater-derived ^{20}Ne vs the radiogenic isotopes (^{4}He, $^{21}Ne^{*}$ and $^{40}Ar^{*}$) where both variables are normalised to N_2 a) Plot of $^{20}Ne/N_2$ vs. $^{4}He/N_2$ i) Original trend from Ballentine and Sherwood-Lollar, (2002) (Hugoton-Panhandle without the Sarah Claybaugh and Donelson, et al. outliers), ii) Southern

KBP samples, b) Plot of $^{20}Ne/N_2$ vs. $^{21}Ne^*/N_2$ i) Hugoton-Panhandle without Sarah Claybaugh and Donelson et al., outliers ii) KBC samples. c) Plot of $^{20}Ne/N_2$ vs. $^{40}Ar^*/N_2$ which shows only one trendline involving the Hugoton-Panhandle dataset (without Witherbee) and the KBC samples. The intersection of all lines of best fit are within error of the origin.

The graphs associated with the ^4He and $^{21}Ne^*$ isotopes show two dominant positive trends which indicate that three endmembers can be assigned to the datasets. One of these endmembers is a shared nitrogen endmember for both mixing lines and is associated with low to no ^4He, $^{21}Ne^*$ or ^{20}Ne. This potentially confirms the existence of the same non-^4He associated, $\delta^{15}N$ enriched nitrogen endmember observed in **Figure 3.12** which is thought to be associated with the overmature production of hydrocarbons.

The two nitrogen endmembers enriched in ^4He and ^{20}Ne are also consistent with the $\delta^{15}N$ depleted nitrogen endmembers observed in **Figure 3.12** which indicates that not only are these nitrogen endmembers associated with crust-sourced N_2 and high ^4He but that these crustal-derived endmembers are also associated with groundwater. This implies that for the majority of samples ^4He and crustal-N_2 were mixed in groundwater before degassing occurred since only then would there be an association between all three components. This is consistent with observations reached in Ballentine and Sherwood-Lollar, (2002) and shows that the mixing of crust derived components with groundwater has happened on not just a field scale but on a regional scale.

Unlike the ^4He and $^{21}Ne^*$ graphs the $^{40}Ar^*$ graph shows a single mixing line which passes within error of the origin and encompasses only the KBC and Hugoton-Panhandle datasets. The graph consists of two endmembers both of which are similar to those described above for ^4He and $^{21}Ne^*$: 1) a nitrogen endmember which is associated with low $^{40}Ar^*$ or ^{20}Ne and 2) a nitrogen endmember associated

with high $^{40}Ar^*$ and ^{20}Ne. These nitrogen endmembers are also associated with: 1) an enriched $\delta^{15}N$ endmember which is similar to that seen in **Figure 3.12** and is likely associated with the overmature production of hydrocarbons, and 2) a depleted $\delta^{15}N$ endmember which is associated with a crustal source (graph not included).

This singular mixing line could indicate a shared source for both the crustal-sourced N_2 and the radiogenically sourced $^{40}Ar^*$. This commonality between the Hugoton-Panhandle and the KBC subsets is reflected by the similar $^4He/^{40}Ar^*$ shown in **Figure 3.13**.

Assuming that the significant $^{40}Ar^*$ concentrations associated with samples show the introduction of a source to the systems which has close to crustal production $^4He/^{40}Ar^*$ ratios (~ 5.0) then the above average $^4He/^{40}Ar^*$ ratios associated with the Hugoton-Panhandle and KBC systems could be the result of the overprinting of this signal by ^4He produced from shallower crust which also accumulated in the groundwater.

In the CH_4 graphs, all subsets apart from the Kautz #1 well in the CKU exhibit three component mixing (**Figure 3.15**). Since all trend lines pass within error of the origin one of the endmembers uniformly shows an input of CH_4 which is not necessarily associated with any of the radiogenic isotopes or ^{20}Ne. This also does not indicate that this CH_4 endmember is associated with the low-^4He associated N_2 endmember observed in **Figure 3.14**.

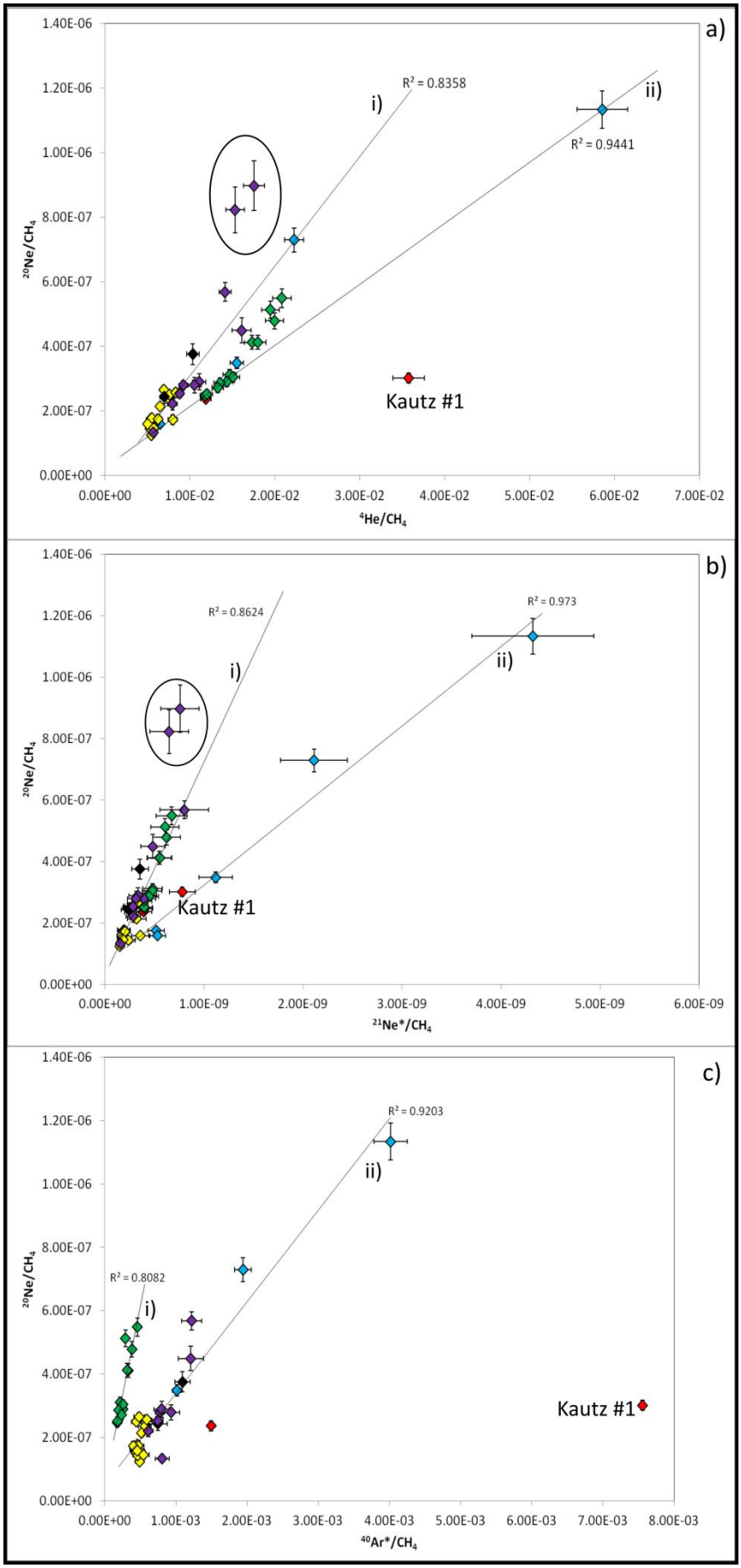
a)
1.40E-06
1.20E-06
1.00E-06
8.00E-07
6.00E-07
4.00E-07
2.00E-07
0.00E+00
$^{20}Ne/CH_4$
0.00E+00
1.00E-02
2.00E-02
3.00E-02
4.00E-02
5.00E-02
6.00E-02
7.00E-02
$^{4}He/CH_4$
$R^2 = 0.8358$
i)
ii)
$R^2 = 0.9441$
Kautz #1
b)
$R^2 = 0.8624$
$R^2 = 0.973$
i)
ii)
Kautz #1
0.00E+00
1.00E-09
2.00E-09
3.00E-09
4.00E-09
5.00E-09
6.00E-09
$^{21}Ne^*/CH_4$
c)
$R^2 = 0.9203$
ii)
$R^2 = 0.8082$
i)
Kautz #1
0.00E+00
1.00E-03
2.00E-03
3.00E-03
4.00E-03
5.00E-03
6.00E-03
7.00E-03
8.00E-03
$^{40}Ar^*/CH_4$

Figure 3.15.: Plots showing groundwater-derived ^{20}Ne vs the radiogenic isotopes (^{4}He, $^{21}Ne^*$ and $^{40}Ar^*$) where both variables are normalised to CH_4. a) Plot of $^{20}Ne/CH_4$ vs. $^{4}He/CH_4$. All lines pass within error of the origin. The north and south groups within the KBP appear to have different gradients however this could be due to CH_4 dilution. i) trend line for the Hugoton-Panhandle dataset excluding the Sarah Claybaugh and Donelson et al., wells, ii) southern KBP samples. b) Plot of $^{20}Ne/CH_4$ vs. $^{21}Ne^*/CH_4$. All lines pass within error of the origin. i) trend line for the Hugoton-Panhandle and KBP dataset excluding the Sarah Claybaugh and Donelson et al., wells, ii) KBC samples. c) Plot of $^{20}Ne/CH_4$ vs. $^{40}Ar^*/CH_4$. All lines pass within error of the origin. i) KBP samples and ii) KBC and Hugoton-Panhandle samples. All excluded samples are circled.

When we consider the isotopic ratios for N_2 and CH_4, given the large variation in $\delta^{15}N$ values (+1.45‰ to +9.40‰) compared to the very narrow range of $\delta^{13}C$ values observed for the Hugoton-Panhandle in Ballentine and Sherwood-Lollar, 2002 (-41.8‰ to -45.1‰) it shows that unlike the variable $\delta^{15}N$ values for N_2 there is no direct relationship between the $\delta^{13}C$ values, or CH_4 concentrations and the noble gas concentrations and ratios.

CH_4 isotopic values indicate that the gas source was a moderately mature, oil-producing, marine rock in contrast to the low-radiogenic associated N_2 endmember which instead indicates a post-mature sedimentary source (Ballentine and Sherwood-Lollar, 2002).

The most probable explanation for this phenomenon is that although these gases may have been sourced from the same region (the Anadarko Basin) they were produced under different thermal regimes. This shows that either they were sourced at different times during the formation of hydrocarbons or that they were sourced from separate strata.

The other endmembers are associated with high radiogenic content and high ^{20}Ne relative to CH_4 indicating that groundwater contact is the primary determining factor for the mixing line gradients whereas CH_4 acts as a dilutant for both radiogenic and groundwater-derived isotopes.

In summary, in all samples it appears that the degree of groundwater contact primarily determines both radiogenic content and, in the case of N_2, the ^{4}He-associated N_2 content. There are also two low-radiogenic endmember gases (CH_4 and N_2) which most likely originate from the Anadarko Basin and act as variable dilutants to the subsets.

Further support for the prior mixing of crust-sourced radiogenic components and crust-sourced ^{4}He-associated N_2 can be derived from the previously observed mixing relationship between crust-sourced ^{4}He-associated N_2 with groundwater-sourced ^{20}Ne prior to degassing into trapping structures. By using the known ^{20}Ne concentration of modern ASW we can compare an estimate of the ^{4}He-associated N_2 concentration in groundwater with the saturation threshold of N_2 in the same groundwater. This can help us to determine whether the crust-sourced ^{4}He-associated N_2 could have been present as a free gas phase therefore facilitating the degassing of the radiogenic isotopes from groundwater or if CH_4 (the dominant hydrocarbon gas phase in fields) needed to be present before degassing could occur.

If we make the assumption that all crust-derived N_2 is associated with high ^{4}He and therefore also with total concentrations of ^{20}Ne we can correct N_2 concentrations for low-^{4}He associated N_2 using either of the δ^{15}N values assigned to the two high ^{4}He-associated N_2 endmembers (-3.00‰ or +1.00‰). As an example, correcting for the δ^{15}N endmember of -3.00‰ gives average $N_2/^{20}$Ne ratios of: 5.08 x 10^5 for the Hugoton-Panhandle, 8.86 x 10^5 for the KBP, 5.4 x 10^5 for the KBC, 1.44 x 10^6 for Kautz #1 and 1.15 x 10^6 for McCune 1-A (**Table 3.10**).

Next we need to calculate the N_2 concentrations required in ASW in order to source the total concentration of high ^{4}He-associated N_2 measured in reservoirs. This

is then compared to the calculated saturation threshold for N_2 in ASW under present reservoir conditions which are outlined in **Table 3.10**.

Modern groundwater equilibrated at 1000 m altitude at 10°C with a 10% excess air Ne addition contains 1.8 x 10^{-7} $cm^3STP(^{20}Ne)/cm^3$. Using this, the groundwater which degassed the total ^{4}He-associated N_2 in the Hugoton-Panhandle would have a N_2 concentration of 0.09 $cm^3STP(N_2)/cm^3$. By taking into account the current reservoir conditions in the study areas e.g.: for the Hugoton-Panhandle (where temperature = 310 K, pressure = 30 bar and salinity = 4 M NaCl) we can calculate that the same groundwater would become saturated in N_2 at a concentration of 0.24 $cm^3STP(N_2)/cm^3$ (Pierce et al., 1964; Battino,1983; Ballentine and Sherwood-Lollar, 2002).

Therefore, in the Hugoton-Panhandle, under present reservoir conditions, there would not be enough high ^{4}He-associated N_2 in the source groundwater to form a free gas phase by itself. In the past, the pressure would have had to be 2.0-2.7 times lower for a N_2 gas phase to form, making it unlikely that a free N_2 gas phase existed before the introduction of a hydrocarbon gas phase given the geological history of the field.

The Hugoton-Panhandle was subject to an extended period of burial starting from the Cambrian until a period of uplift began shortly after the early Tertiary culminating in modern day pressures (Sorenson, 2005). Therefore, since modern day pressures are the lowest the field has experienced since its inception, CH_4 and low ^{4}He-associated N_2 needed to be present in traps before high ^{4}He-associated N_2, ^{4}He, ^{3}He and ^{20}Ne could exsolve from groundwater.

It is interesting that the Hugoton-Panhandle and the KBC contain similar high ^{4}He-associated N_2 concentrations in groundwater. The KBC and Hugoton-

Panhandle also lie along the same mixing line with regard to radiogenic content (**Figure 3.13**). This could indicate a regional groundwater source which encompasses both the Hugoton-Panhandle and KBC study areas.

In the KBP, conversely, under current reservoir temperatures and pressures groundwater becomes saturated in N_2 at 0.08 $cm^3STP(N_2)/cm^3$. Therefore the current high ^4He associated N_2 concentration in the groundwater is 2-2.5 times higher than the saturation threshold indicating that concentrations of high ^4He-associated N_2 are high enough in the groundwater to form a free gas phase. This means that there was either an external influx of high ^4He-associated N_2 into the system or that the system either underwent significant uplift or the removal of overburden during the Late Tertiary facilitated the lowering of pressure (Sorenson, 2005). More importantly it indicates that the degassing of groundwater associated with the KBP is not dependent on the presence of CH_4 in traps compared to the Hugoton-Panhandle and KBC systems; both of which are below the N_2 saturation threshold.

The CKU samples are similar to the KBP samples; they also show high ^4He-associated N_2 concentrations which are significantly above the saturation threshold indicating that they are not dependent on a CH_4 gas phase to facilitate groundwater degassing. The Kautz #1 well is also the most oversaturated in high ^4He-associated N_2 with concentrations 4.3-5.5 times greater than the N_2 saturation threshold. This, alongside the $^4He/^{40}Ar^*$ of the gas, most likely indicates the input of some of the high ^4He-associated N_2 as a free gas phase from depth however we have limited information on the field geology to comment on whether this was facilitated by a fault or by proximity to basement outcrops.

Study Area	Average corrected $N_2/^{20}Ne$ (with endmembers -3.00‰ to +14.60‰)	^{4}He-associated N_2 concentration in groundwater ($cm^3STP(N_2)/cm^3$) (with endmembers -3.00‰ to +14.60‰)	Average corrected $N_2/^{20}Ne$ (with endmembers +1.00‰ to +14.60‰)	^{4}He-associated N_2 concentration in groundwater ($cm^3STP(N_2)/cm^3$) (with endmembers +1.00‰ to +14.60‰)	N_2 concentration saturation point in groundwater under current reservoir conditions ($cm^3STP(N_2)/cm^3$)	Modern reservoir conditions (temperature (K)/pressure (bar)/salinity (M)
Hugoton-Panhandle	5.08×10^5	0.09	6.57×10^5	0.12	0.24	310/30/4
KBP	8.86×10^5	0.16	1.15×10^6	0.20	0.08	313/91/4
KBC	4.82×10^5	0.09	6.24×10^5	0.11	0.13	326/174/4
Kautz (CKU)	1.44×10^6	0.26	1.87×10^6	0.33	0.06	308/22/4
McCune 1-A (CKU)	1.15×10^6	0.20	1.48×10^6	0.26	0.08	314/97/4

Table 3.10.: Comparisons of N_2 saturation in groundwater compared to modern reservoir conditions.

We can also check the saturation threshold for ^{4}He in these systems by following a similar methodology and assuming that all of the ^{4}He in reservoirs is associated with the ^{20}Ne (**Table 3.11**).

Study Area	**Average $^{4}He/^{20}Ne$**	**^{4}He concentration in groundwater ($cm^3STP(^4He)/cm^3$)**	**^{4}He concentration saturation point in groundwater under current reservoir conditions ($cm^3STP(^4He)/cm^3$)**
Hugoton-Panhandle	3.33×10^4	0.006	0.10
KBP	4.51×10^4	0.008	0.03
KBC	3.96×10^4	0.007	0.06
Kautz (CKU)	1.19×10^5	0.02	0.01
McCune 1-A (CKU)	5.01×10^4	0.009	0.04

Table 3.11.: Comparisons of ^{4}He saturation in groundwater compared to modern reservoir conditions.

For all subsets except Kautz #1 from the CKU subset, ^{4}He concentrations in groundwater are lower than the ^{4}He saturation point in groundwater, meaning that there would have to be other gases present in the reservoir before ^{4}He would exsolve from solution; in this case low ^{4}He-associated N_2 and CH_4. However, unusually, in the case of Kautz #1, concentrations of ^{4}He are locally high enough in the groundwater to be forming a free gas phase which is most likely directly related to the oversaturation observed for ^{4}He-associated N_2 (**Table 3.10**).

In summary it is observed that the Hugoton-Panhandle and KBC reservoirs, which are undersaturated in ^{4}He-associated N_2 relative to modern day reservoir conditions, in the past required a CH_4 gas phase to already be present in order for crustal N_2 and the ^{4}He associated with it to exsolve from the groundwater. However, in the case of the CKU and the KBP samples, under current reservoir temperatures and pressures ^{4}He-associated N_2 is oversaturated in groundwater and is therefore

capable of exsolving to form a free gas phase and causing related ^{4}He exsolution from the groundwater and into the gas phase. In the Kautz #1 well there may also be an input of deep crustal free gas (^{4}He-associated N_2, ^{4}He, $^{21}Ne^*$ and $^{40}Ar^*$) which causes the amplified oversaturation observed in the reservoir.

Following on from Ballentine and Sherwood-Lollar, (2002) we can use a simple mass balance to assess the volumes of groundwater involved in the degassing of ^{4}He in each subset. The $^{20}Ne/^{36}Ar$ ratios observed in samples vary between each subset which implies different degassing processes affecting each study region however the coupling between ^{4}He and ^{20}Ne is observed across all samples (**Figure 3.8**). We assume that despite the differences in the degassing process which produced the varying ^{20}Ne and ^{36}Ar concentrations in the subsets that the process is efficient thereby enabling us to determine a minimum volume of groundwater which has interacted with ^{4}He from the ^{20}Ne concentrations (Ballentine et al., 1991; Ballentine and Sherwood-Lollar, 2002).

For these calculations we use the same derived ^{20}Ne concentration in groundwater as for the N_2 saturation calculations (1.8×10^{-7} $cm^3STP(^{20}Ne)/cm^3$). Using the individual $^{4}He/^{20}Ne$ ratios of the Hugoton-Panhandle samples relative to the ^{4}He concentrations gives an average ^{20}Ne concentration of 1.85×10^{-7} $cm^3STP(^{20}Ne)/cm^3$) across the field. Therefore, for an estimated OGIP volume (and therefore reservoir gas volume) of 1.85×10^{12} m^3STP in the Hugoton-Panhandle, this gives a total volume of ^{20}Ne of 3.41×10^{5} $m^3STP(^{20}Ne)$ for the field. Assuming the total degassing of ^{20}Ne this is the equivalent of 1913 km^3 of groundwater.

In a reservoir of 15% porosity (from Ballentine and Sherwood-Lollar, 2002) the above volume of groundwater would occupy a rock volume of 12,756 km^3 (**Table 3.12**). To place this in perspective, this is equivalent to the static volume of

water in an arbitrarily 100 m-thick 15% porosity aquifer covering an area of 127,560 km^2.

All subsets apart from the KBC are assigned a 100 m thick aquifer. For the KBC the assumption is made that the aquifer is the 30 m thick Mississippian aquifer (Nissen et al., 2004).

Study Area	Average ^{20}Ne concentration (cm^3 STP(^{20}Ne)/cm^3)	Estimated reservoir gas volume (m^3)	Groundwater volume involved (km^3)	Aquifer volume with 15% porosity (km^3)	Aquifer area (km^2)
Hugoton-Panhandle	1.85×10^{-7}	2.30×10^{12}	1913	12,756	127,560
KBP	2.32×10^{-7}	5.90×10^{9}	8	51	512
KBC	2.96×10^{-7}	5.80×10^{7}	0.1	0.6	21
CKU	1.75×10^{-7}	7.03×10^{7}	0.07	0.5	5

Table 3.12: Workthrough of hypothetical aquifer volumes associated with study areas.

From the minimum aquifer volumes calculated the Hugoton-Panhandle requires an aquifer over 6 times its own area whereas the KBP, KBC and CKU study areas require areas 2.5, 2.1 and 0.6 times their own area. This demonstrates that the hypothetical aquifer for each study area except for the CKU is potentially large enough to act as an overlying regional focus for ^4He produced from the crust both within and outside of the study areas enabling the mixing of components from both the deep and shallow crust before they are focused into trapping structures. This fits with the ^4He mass balance calculations which also support an external source of ^4He which has: 1) been focused into the reservoirs, 2) is not necessarily confined to the field areas and 3) would compensate for less than 100% release and trapping efficiency.

The CKU is unusual in that not only do groundwater volumes appear to support localised production but both well samples also record relatively little groundwater interaction when $^{4}He/^{20}Ne$ ratios are examined. This could indicate that groundwater is not the only pathway which has brought high ^{4}He concentrations into these shallow reservoirs. Another pathway could have been migration from depth of a free gas phase containing ^{4}He which was also proposed as a pathway for one of the sources of crustal N_2 for the CKU system.

In summary, groundwater generally plays a critical role in both mixing and focusing crustal N_2 and ^{4}He into pre-existing traps. In the CKU and KBP, the presence of gas phase CH_4 in reservoirs is not required to degas N_2 and therefore ^{4}He from the groundwater whereas in the Hugoton-Panhandle and KBC crustal N_2 concentrations are undersaturated in groundwater indicating that a CH_4 gas phase needed to be in place before isotopic partitioning between gas and groundwater.

3.5.4. The interaction between ^{4}He, crustal N_2, organic N_2 and CH_4

From the previous sections it has been observed that externally produced radiogenic ^{4}He and high ^{4}He-associated N_2 from both the deep and shallow crust encounters laterally moving groundwater. The deep and shallow components were then pre-mixed in the groundwater before degassing into pre-existing traps which, depending on the study area, either contained a hydrocarbon gas phase or was already degassing due to oversaturation by high ^{4}He-associated N_2 before encountering a hydrocarbon phase.

The hydrocarbon gas phase and low ^{4}He-associated N_2 gas do not appear to be co-genetic or related to the groundwater system indicating movement as a

separate free gas phase into traps (**Figure 3.14**). The presence of low concentrations of ^{4}He, ^{20}Ne, $^{21}Ne^{*}$ and $^{40}Ar^{*}$ in these hydrocarbon gases are likely due to the stripping of groundwater as the hydrocarbons migrated southwards into the Texas Panhandle and northwards up the Anadarko shelf and up the Central Kansas Uplift.

When considering the ^{4}He system in these study regions we need to consider the interactions between at least four components as a minimum. High ^{4}He-associated N_2 and ^{4}He are coupled by both source and groundwater whereas the low ^{4}He-associated N_2 and CH_4 are most likely sourced from different strata in the Anadarko Basin.

In the Hugoton-Panhandle gas field the way these components interact may be explained by the following events:

From the late Pennsylvanian onwards hydrocarbons were produced from strata in the Anadarko Basin ranging between Ordovician to Pennsylvanian-age. The most prolific of these strata was the Devonian-Mississippian aged Woodford Shale which is widely thought to be the primary producer of all gas associated with Mid-continental fields. Gases containing CH_4, low ^{4}He-associated N_2 and low concentrations of ^{4}He, $^{21}Ne^{*}$, ^{20}Ne and $^{40}Ar^{*}$ were focused southwards into the Panhandle field which gradually filled until the early Tertiary (Carr et al., 2003; Sorenson, 2005).

In the Mesozoic the lowest Palaeozoic layers in the Anadarko Basin (presumably the Cambrian and Ordovician) entered overmaturity whereas the Woodford Shale would have reached maturity; the products of these layers would have still filled the Panhandle until the Early Tertiary making it conceivable that the mature CH_4 and overmature low ^{4}He-associated N_2 were both sourced from the Anadarko Basin but were generated under different thermal conditions and added to

the field together. Until the early Tertiary the Texas Panhandle contained most of the Permian reservoir gas observed in the Mid-continent (Sorenson, 2005).

The introduction of CH_4 into the Panhandle could have caused static undegassed groundwater which already contained ^4He and its related isotopes ^3He, ^{20}Ne and high ^4He-associated N_2 to begin degassing throughout the field. Alternatively, later external groundwater moving through the system degassed into capped reservoirs when it contacted CH_4 and low ^4He-associated N_2 already in place.

Groundwater flow in the Panhandle section of the Hugoton-Panhandle is observed to be dynamically SW to NE and started during the Early Tertiary. In the adjoining Palo Duro Basin flow is from west to east with sources in New Mexico (Larson, 1971; Gosselin et al., 1992; Ballentine and Sherwood-Lollar, 2002; Sorenson, 2005). In the Hugoton section of the field groundwater contact is lower and more irregular than in the Panhandle section potentially due to varying distance from the main groundwater contact for the field (**Figure 3.8**). There is evidence of the encroachment of the regional Cedar Hills aquifer into the south of Kansas (Morton and Stevens counties) which shows salt dissolution from west to east however the timing and extent of this event is uncertain since it appears to be fairly localised (Sorenson, 1996; Young et al., 2005).

Determining the gas-water contact in the Hugoton part of the field is complicated by faults acting as flow barriers and log interpretation difficulties caused by water saturation in some areas but not others, loss of reservoir quality due to thin, heterogenous strata and the compartmentalisation of strata generally below the Chase Group in the Fort Riley formation due to faulting (Olson et al., 1997; Sorenson, 2005). However, palaeoflow in this region is generally thought to be from

west to east and the current groundwater contact is thought to be updip to the west and flattens out towards the east of the field (Larson, 1971; Sorenson, 2005).

Across the Hugoton-Panhandle $N_2/^{20}Ne$ ratios which have been corrected for low ^4He-associated N_2 display uniform ratios (on average: $N_2/^{20}Ne = 6.57 \pm (1.57) \times 10^5$). This could be caused by either: 1) high ^4He-associated N_2, ^4He and associated gases degassed from a static body of water which was contacted by varying concentrations of CH_4 and low ^4He-associated N_2 across the field during filling or 2) groundwater rich in high ^4He-associated N_2, ^4He and associated gases contacted the Panhandle section of the field flowing from SW to NE. Scenario 2 would have delivered the highest concentrations of crustal and magmatic gases to the Panhandle versus the Hugoton part of the field which is seen with regard to the distribution of ^4He, crustal N_2, ^{20}Ne, $\delta^{15}N$ values and R_a values. Subsequent mixing with the more 'sedimentary influenced' Hugoton section of the field could then have produced the trends seen within the dataset.

During the late Tertiary post-Laramide erosion and evaporite dissolution of outcrops to the east of Kansas removed 700-1700 m of Cretaceous to Permian overburden. Sorenson proposes that this led to a drop in the overall pressure of the region as the interconnected hydraulic head exceeded the outcrop elevations and discharged eastwards having been previously controlled by burial depth (Schmoker, 1989; Carter et al., 1998; Sorenson, 2005).

This loss of pressure in the region caused hydrocarbon gases which were filling the Panhandle to spill northwards into the Hugoton section of the field, which due to the eastward tilt generated by the Laramide Orogeny filled up westward and northward first which is mirrored by the N_2 isotope data from the region (**Figure 3.9**). The initial pressure decrease in the Hugoton section of the field would not have

been enough to bring the current concentrations of crustal N_2 into the gas phase, however the introduction of CH_4 and organic N_2 from the south most likely started the degassing of crustal N_2, ^4He and the other noble gases out of solution in the Hugoton section of the field.

If we examine the Hugoton field, we notice that there is a general trend towards increasing ^4He-associated N_2 input to well gases which are situated in the 'low BTU rim' area which partially occupies the east of the field. However there are only three wells which potentially occupy this position (Baughman H-2, Mills C-1 and Parsley A-1) and have had nitrogen isotope analysis conducted on them but it would be interesting to see if this trend for increasing amounts of high ^4He-associated N_2 is also observed in the low BTU gases encountered in the Bradshaw and Byerly fields to the north of the Hugoton field. This would imply that as groundwater derived high ^4He-associated N_2 and ^4He degassed it migrated north and east in response to both the drop in reservoir pressure and the introduction of CH_4 and low ^4He-associated N_2 filling the Hugoton (Sorenson, 2005).

Due to the lack of magmatism in the region since the Cambrian local sourcing of the magmatic components in the gas seems unlikely so we are more inclined to support their transport by groundwater. The Hugoton-Panhandle may exhibit higher $^3He/^4He$ ratios (R_a) than the other study areas due to it being the first point of contact for groundwater bearing a latter addition of magmatic gases (Cenozoic to Quaternary) either from the vicinity of the Sierra Grande Uplift (W to E) or from further SW in New Mexico into the Texas Panhandle portion of the field (Staudacher, 1987; Ballentine and Sherwood-Lollar, 2002). It is likely that crustal gases are still migrating into the Panhandle region given the observations made in Pierce et al., (1964) of elevated helium concentrations along the south-west

boundary of the Panhandle field. This also serves to potentially pinpoint the area of entry of enriched crustal gases into the field which implies that a substantial area including the Palo Duro Basin and parts of New Mexico could be involved in the sourcing of the helium in the study areas.

A detailed geological history of the Kansas Basin and Central Kansas Uplift is unavailable at this time and any information on these study areas pales in comparison to the number of studies on the Hugoton-Panhandle. We will assume that the Kansas Basin, like the Hugoton-Panhandle, experienced downwarping until the early Tertiary whereas the Central Kansas Uplift experienced uplift until the Permian (Merriam, 1963; Sorenson, 2005).

When compared to the Hugoton part of the Hugoton-Panhandle the CKU, KBP and KBC areas all contain significantly higher amounts of high ^{4}He-associated N_2 (46-75% of the N_2 concentration in well gases compared to 39-53% for the Hugoton (Kansas and Guymon)) however they have similar amounts of high ^{4}He associated N_2 to the Texas Panhandle (53-68% of the N_2 concentration in well gases) when using the δ^{15}N value -3.00‰.

The KBP and CKU areas have groundwater associated with them that is oversaturated in N_2 given current reservoir conditions. While it is possible that reservoirs were at higher pressures in the past thereby increasing the saturation threshold it is more likely that high ^{4}He-associated N_2 and ^{4}He was exsolving into traps in these regions before the introduction of low ^{4}He- associated N_2 and CH_4 from the south.

If pressures were initially keeping gases in solution it would take a pressure increase of at least ~2 times that of modern day conditions in the KBP to raise the saturation point of N_2 in the groundwater system. This is a narrower tipping point

than that associated with the CKU samples which range between 2.5 and 5.5 times greater than the N_2 saturation threshold depending on the high ^{4}He-associated N_2 endmember value used. This discrepancy can be explained in two ways: firstly the CKU was an area of continued uplift from the Precambrian to the Permian relative to the Hugoton Embayment which in counterpoint was downwarped. Temperatures and pressures in the Hugoton Embayment relative to the CKU would have been higher overall due to burial thereby raising the saturation threshold for gases in that region. Secondly, Sorenson, (2005) refers to a period in the late Tertiary when erosion and evaporite dissolution of outcrops to the east of Kansas removed Cretaceous to Permian overburden. This may have affected the Central Kansas Uplift by lowering pressures and therefore decreasing the N_2 saturation threshold in the region causing high ^{4}He-associated N_2 to exsolve out of groundwater.

In summary, in the KBP and CKU ^{4}He and high ^{4}He-associated N_2 which was exsolving out of solution due to low pressures and possibly a depressurisation event (the CKU may have already been exsolving high ^{4}He-associated N_2 and ^{4}He before this due to lower pressures) interacted with northward moving CH_4 and low ^{4}He-associated N_2 sourced from the Anadarko Basin.

We cannot identify at which stage of thermal maturity the CH_4 and N_2 were sourced in either the KBP or CKU due to lack of $\delta^{13}C$ values for samples however since low ^{4}He-associated N_2 is present in the hydrocarbon gas it is likely that the gases found in these fields were sourced during the Mesozoic and the less enriched $\delta^{15}N$ values associated with the fields represents the dilution of an in place gas phase by migrating hydrocarbons.

During the beginning of the Mesozoic the Hugoton Embayment was tilted westwards by the Western Interior Seaway which might explain why the wells which

would have been updip of this tilt (the eastern-most wells of the KBP) generally have the highest $\delta^{15}N$ values in the study area (+3.45‰ to +4.70‰) (Sorenson, 2005).

It is difficult to determine what has affected each individual field in terms of its $\delta^{15}N$ value which does not appear to fit any specific pattern. The variation may be due to local effects which we do not currently have the geological information to comment on. Gases in these fields are a mixture of low ^4He-associated N_2 which has migrated northwards from the Anadarko Basin and high ^4He-associated gases which exhibit a predominantly shallow crustal radiogenic signature with $^4He/N_2$ ratios similar to the Hugoton part of the Hugoton-Panhandle field. This could indicate that both the KBP and Hugoton field are dominated by a shallow sedimentary component relative to a groundwater-driven basement/deep-sourced helium and nitrogen input.

In the CKU there either appears to be a general dilution of pre-existing gas from south to north due to the addition of hydrocarbons from the Anadarko Basin or there has also been an addition of ^4He and ^4He-associated gases to local reservoirs either due to advection up faults or proximity to basement outcrops on the uplift. These reservoir gases show predominantly basement-derived radiogenic ratios and high $^4He/N_2$ ratios relative to any sedimentary component.

The KBC samples which lie to the south of the study region and are close to the Anadarko Basin show the same dependence as the Hugoton-Panhandle on CH_4 to start ^4He and ^4He-associated N_2 exsolution. The KBC may also have experienced the same depressurisation as the overlying layers due to there being evidence of communication between the Carboniferous and Permian layers in the study areas however it was not enough to bring ^4He-associated N_2 out of solution until CH_4 migration out of the Anadarko Basin given current pressures and temperatures.

The margin for reaching the saturation threshold in the KBC requires the pressure to be lowered to only 1.2-1.4 times that of modern day pressures before exsolution occurs therefore if any of the wells experienced a pressure fluctuation then ^{4}He-associated N_2 would have exsolved without the need for CH_4. Since only one of the wells in the KBC, Maverick #1, shows $\delta^{15}N$ values similar to that in the Hugoton-Panhandle and a correspondingly lower high ^{4}He-associated N_2 component, the other wells may either have experienced degassing at some point in their history which would have generated the low $\delta^{15}N$ values and high ^{4}He and ^{4}He-associated N_2 components.

The KBC also displays mixing with the Hugoton-Panhandle gas field (**Figure 3.8, Figure 3.13, Table 3.9**) which is probably due to both areas sharing a groundwater source. The well furthest to the east of the Hugoton field, Baughman H-2, appears to show a decrease in $N_2/^{20}Ne$ indicating an increase in ^{20}Ne and therefore groundwater contact. However, this is only one well and may be a local effect. There does not appear to be any significant groundwater interaction with the eastern edge of the Hugoton field showing that the system is potentially isolated from the regional groundwater sourcing the Panhandle and KBC areas.

The KBP may also be within the same groundwater catchment however there appears to be at least two episodes of degassing and re-solution associated with the gas which is beyond the scope of this work.

3.6. Summary

The gases associated with reservoirs in the Hugoton-Panhandle, Kansas Basin and Central Kansas Uplift areas are all composed of four main components:

^{4}He, CH_4, organic N_2 and ^{4}He-associated N_2 which are derived from a combination of three possible sources.

The CH_4 and low ^{4}He-associated N_2 components in all study areas are sourced from the Anadarko Basin however they were not generated within the same strata and they show low groundwater interaction; potentially indicating that the ^{20}Ne associated with these components was stripped from porewater during migration. By using a combination of $\delta^{15}N$ values and noble gas isotopes we established that the low ^{4}He-associated N_2 endmember is shared by all samples and is characterised by $\delta^{15}N$ = +14.60‰ which falls within the range of overmature sediments.

The bulk of the ^{4}He and high ^{4}He-associated N_2 components show strong associations with groundwater and there are two crustal N_2 endmembers which can either be characterised by: 1) $\delta^{15}N$ = -3.00‰, $^{4}He/N_2$ = 0.043 and 2) $\delta^{15}N$ = -3.00‰, $^{4}He/N_2$ = 0.089 or 3) $\delta^{15}N$ = +1.00‰, $^{4}He/N_2$ = 0.036 and 4) $\delta^{15}N$ = +1.00‰, $^{4}He/N_2$ = 0.072. Despite the differences in $^{4}He/N_2$, the $\delta^{15}N$ values calculated fall within a narrow range and are consistent with two types of crust; either a low grade metamorphic release from the basement or the release of ammonia from clays.

The most likely scenario is that endmember 2) is the N_2 endmember for the basement in the region and endmember 3) is the N_2 endmember for the sediments (release of ammonia from clays). Samples show variable mixing between all three of these endmembers.

Similar $N_2/^{20}Ne$ ratios and the same radiogenic mixing line indicates a common groundwater source for both the Texas Panhandle and KBC areas. The CKU wells indicate very little groundwater contact and gas in these reservoirs is thought to have a significant portion added from depth by advection up faults.

In the Hugoton-Panhandle and the KBC, groundwater is undersaturated in high ^{4}He associated N_2 indicating the need for CH_4 and organic N_2 to already be in place in order for the dissolved isotopes to partition into the reservoir as a gas phase. The KBP and CKU on the other hand are oversaturated in high ^{4}He-associated N_2 therefore isotopes dissolved in the groundwater were already exsolving into the gas phase in reservoirs before CH_4 and N_2 migrated into the reservoirs.

The ^{4}He mass balances for the different study areas indicate that only up to 17% of the ^{4}He found in reservoirs could have been sourced in situ, indicating that the area involved with the sourcing of the ^{4}He is not confined to the boundaries of the study areas and most likely covers a significant portions of Texas and New Mexico.

Chapter Four: The Geochemical Characteristics of the ^4He-N_2 source in Helium Systems

4.1 Introduction

Since the first discovery of natural gas containing 1.84% helium in Dexter, Kansas in 1903 the USA has been the world's largest producer, consumer and exporter of helium. Total helium reserves and resources (including measured, probable, possible and speculative) in the USA are estimated to be 20.6 x 10^9 m^3 which is roughly 40% of the world's total estimated helium reserves (USGS, 2017).

Commercially viable helium reservoirs are classified as those containing over 0.3% helium by volume of gas. The USA contains over 100 identified high helium fields (defined as containing 0.3% by gas volume helium) however 92% of its measured helium reserves are contained in three fields: Riley Ridge (Wyoming), the Hugoton-Panhandle giant gas field (Oklahoma, Kansas and Texas) and the Cliffside Federal Reserve situated in Bush Dome (which contains enriched helium gas from the Hugoton-Panhandle).

Large scale, high volume production of liquified natural gas (LNG) in Qatar and Algeria has enabled separation of helium as a by-product of the cryogenic process involved. For such LNG plants the economic limit for concentration of helium in the original natural gas is lower at <0.1%. The helium reserve associated with Qatar's North Dome Field (the world's largest gas field) is estimated to be 10.1 x 10^9 m^3 despite helium concentrations in the field of around 0.04%. The helium reserves estimated for this field is the equivalent of approximately 20% of the total estimated world helium reserves (USGS, 2017).

Producing helium fields predominantly fall into three categories as defined by the primary gas component: N_2-rich (Pinta Dome, Harley Dome), CH_4-rich (Hugoton-Panhandle, North Dome/South Pars) and CO_2-rich (LaBarge/Riley Ridge,

Doe Canyon). To date, most geochemical studies have been conducted on CH_4-rich high helium systems e.g.: the Hugoton-Panhandle and smaller fields in the Kansas Basin and Central Kansas Uplift, and on CO_2-rich high helium systems e.g.: LaBarge/Riley Ridge and Doe Canyon (Ballentine and Sherwood-Lollar, 2002; Gilfillan et al., 2008; Merrill et al., 2014; Chapter 3, this thesis). In this study we present new data on N_2-rich high helium systems from three wells in Utah, Montana and Saskatchewan, Canada.

Following on from previous studies on the Hugoton-Panhandle, Kansas Basin and Central Kansas Uplift systems we attempt to constrain the communal crustal N_2 isotopic endmember linked with high ^4He concentrations in these regional systems (Ballentine and Sherwood-Lollar, 2002; Chapter 3).

By using data from these new N_2-rich wells which contain minimal CH_4 and therefore N_2 linked to the production of hydrocarbons we can potentially determine the N_2 isotope endmember associated with the crust for these systems and whether it is related to the endmember in the previous studies.

4.2 Geological context of the N_2-^4He rich wells

All N_2-^4He rich wells discussed in the sections below differ from the Hugoton-Panhandle, Kansas Basin and Central Kansas Uplift samples discussed in the previous chapter in that they are all orders of magnitude smaller and are N_2-rich ^4He systems rather than CH_4-rich ^4He systems **(Figure 4.1**).

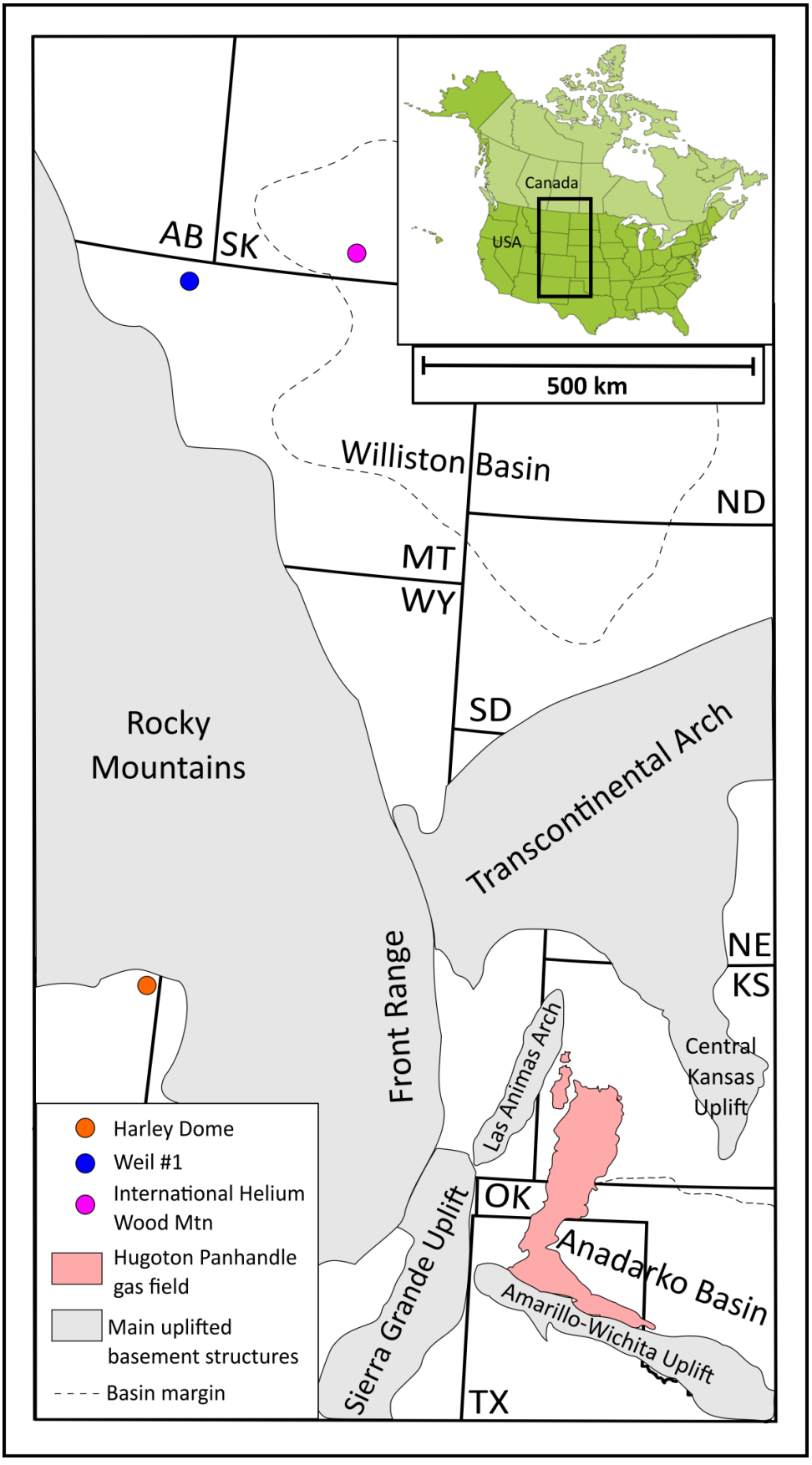

Figure 4.1: Locations of all N_2-^4He rich wells relative to regional structures and the Hugoton-Panhandle gas field.

4.2.1 Harley Dome, Grand Co, Utah, USA

The Harley Dome field is a NW plunging faulted anticline which lies on the Uncompahgre Uplift; a 100 mile long NW-SE trending reactivated basement fault spanning Colorado and Utah which has a maximum displacement of 500 ft (Keebler, 1956; Young, 1983). Harley Dome has 90 ft of structural closure (Dobbin, 1935) (**Figure 4.2**).

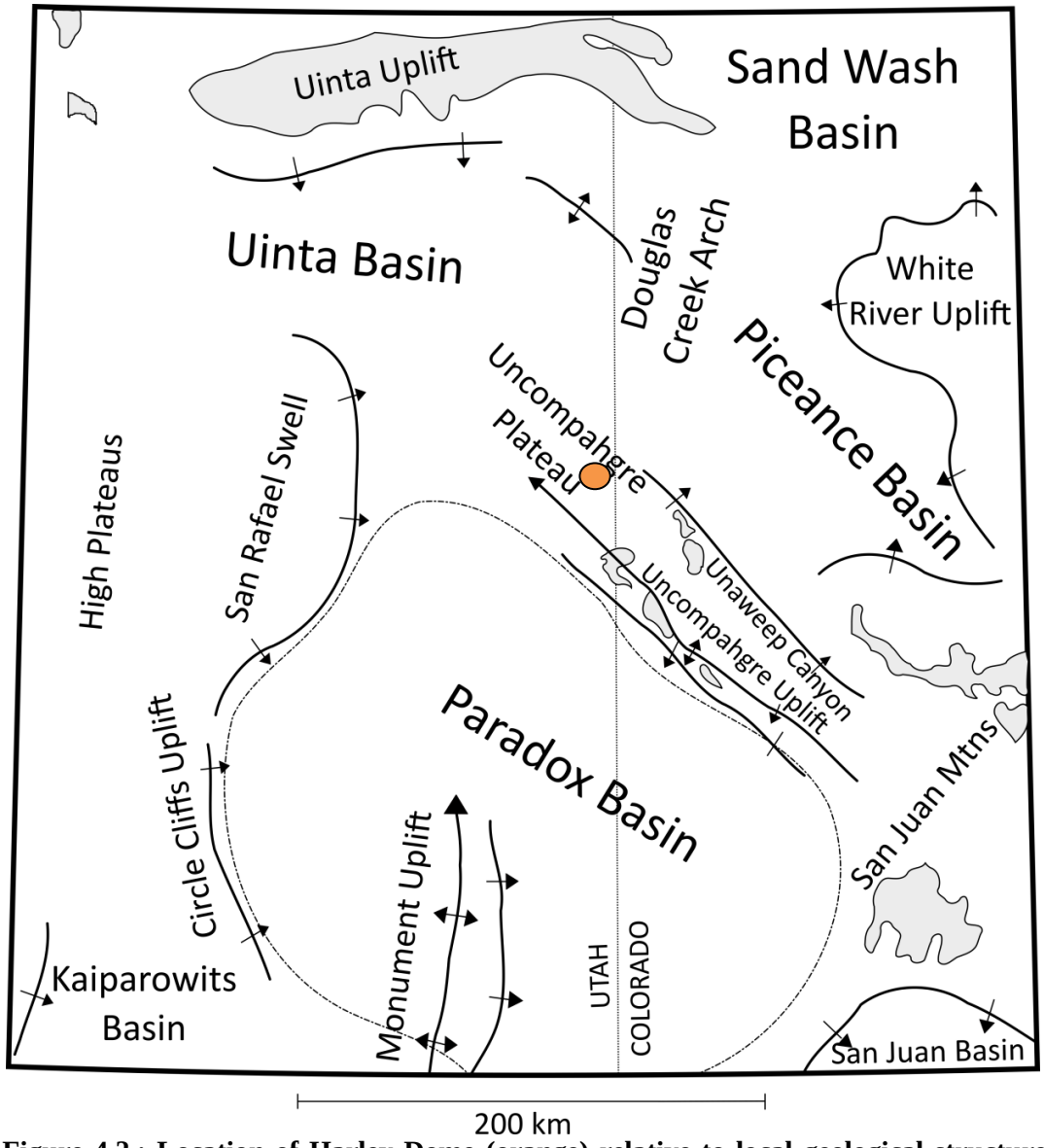

Figure 4.2.: Location of Harley Dome (orange) relative to local geological structures. Redrawn and modified from Case, 1966.

Helium-rich gas was discovered in the Entrada Sandstone (Jurassic) and also the Salt Wash member of the Morrison Formation (Jurassic) (Dobbin, 1935; Otto and Picard, 1976; Young, 1983). Documented percentages of helium record around 7% in the Entrada Sandstone and 2% in the Morrison Formation (Dobbin, 1935; Winchester, 1935; Burchell, 1964). Readings from the Cretaceous-aged Dakota Formation show 0.2% helium with an 84.2% methane content (Stowe, 1972; Young 1983). The Entrada Sandstone reservoir at Harley Dome is only 300 m above the Precambrian-aged basement (1.05-1.81 Ma) due to the uplifted and eroded basement core beneath (Osmond, 1964; Morgan and Chidsey Jr, 1991) (**Figure 4.3**).

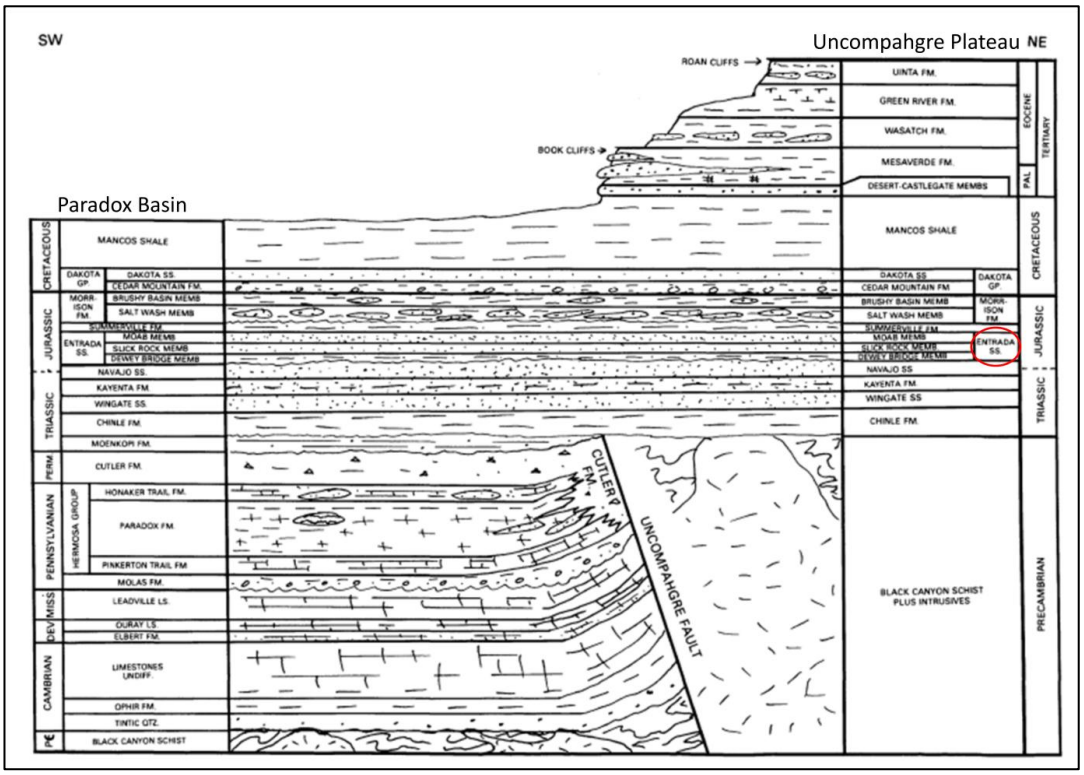

Figure 4.3.: Generalised cross section from the Paradox Basin to the Uncompahgre Plateau where Harley Dome is located. Modified from Young, (1983). The producing reservoir for the Harley Dome field is circled in red on the diagram.

The Uncompahgre Uplift is a reactivated fault block of the Ancestral Rocky Mountains; an amagmatic, intraplate, crustal-scale system of uplifts and basins

which occurred in the Carboniferous (Kluth et al., 1998; Kluth and DuChene, 2009). It separates the Piceance Basin in Colorado from the Paradox Basin in Utah and acts as the eastern boundary of the Colorado Plateau. The NW trending fault forms an upwarp up to 100 miles long across the Colorado Plateau. The region shows evidence of multiple reactivations of Precambrian basement faults culminating in the formation of the current geological structures during the Laramide orogeny (Case, 1966).

The start of the Uncompahgre Uplift began in the SE of Utah during the Pennsylvanian and moved NW into the Permian displaying vertical displacement of several thousand feet (Baars and Stevenson, 1981). This pattern of activation was due to pre-existing lines of weakness in the underlying Precambrian rocks which were established as long ago as 1.7 Ga (Baars and Stevenson, 1981; Heyman, 1983). During the Laramide Orogeny the Uncomphagre Uplift potentially acted as an immovable basement fault block, deflecting thrusting from the event to maintain the Colorado Plateau (Stokes, 1976; Baars and Stevenson, 1981). Movement along the Uncompahgre fault ceased by the middle of the Triassic (Elston and Shoemaker, 1960).

The basement complex of the Uncompahgre Uplift and Plateau is composed of a combination of gneiss and granite. Samples collected from the top of the basement in the Uncompahgre Plateau in Rønnevik et al., (2017) show ages ranging from 1.8-1.6 Ga (indicating either the age of the original Yavapai-Mazatzal province or the age of granitic plutons in the region) from zircons to 63.5±4.0 Ma from apatites. This lowered age indicates that temperatures in the region rose above ~70°C (the apatite closure temperature) but did not reach the temperatures necessary to cause the reset of zircon fission track ages (180-200°C) (Lippolt et al., 1994; Wolf et

al., 1996; Farley, 2000; Farley, 2002; Reiners, 2005; Shuster et al., 2006; Reich et al., 2007; Cherniak et al., 2009; Hunt et al., 2012).

Subsequent modelling of the thermal history of the plateau suggests that maximum burial occurred around 80 Ma. Temperatures at the top of the basement are thought to have reached at least 90°C which corresponds to a burial depth of ~3 km (given a surface temperature of 11°C and a thermal of 25-30°C). This was followed by uplift, exhumation and cooling during the Laramide Orogeny (65-60 Ma). It has also been suggested that a minor reheating event (50-80°C) occurred during the early Oligocene which may be related to either elevated thermal gradients or magmatism in the region (Rønnevik et al., 2017).

4.2.2 Rudyard field, Hill Co, Montana, USA

The Rudyard field is located on the Rudyard anticline; a minor structural feature on the flank of the larger Sweetgrass Arch. The Sweetgrass Arch is a broad, NW trending, structural upwarp which spans over 51,800 km^2 in northern Montana. The arch was initially created in the Precambrian/Cambrian with further epeirogenic movement in the Jurassic however the current arch configuration is due to deformation during the late stages of the Laramide orogeny (Peterson, 1957; Nordquist and Leskela, 1968; Shepard and Bartow, 1968).

The east flank of the Sweetgrass Arch, where the Rudyard field is situated, dips homoclinally until interrupted by two major areas of Tertiary igneous activity: the Sweetgrass Hills (consisting of laccoliths) and the Highwood Mountains (consisting of dikes, sills, laccoliths and extrusive rocks) (**Figure 4.4**).

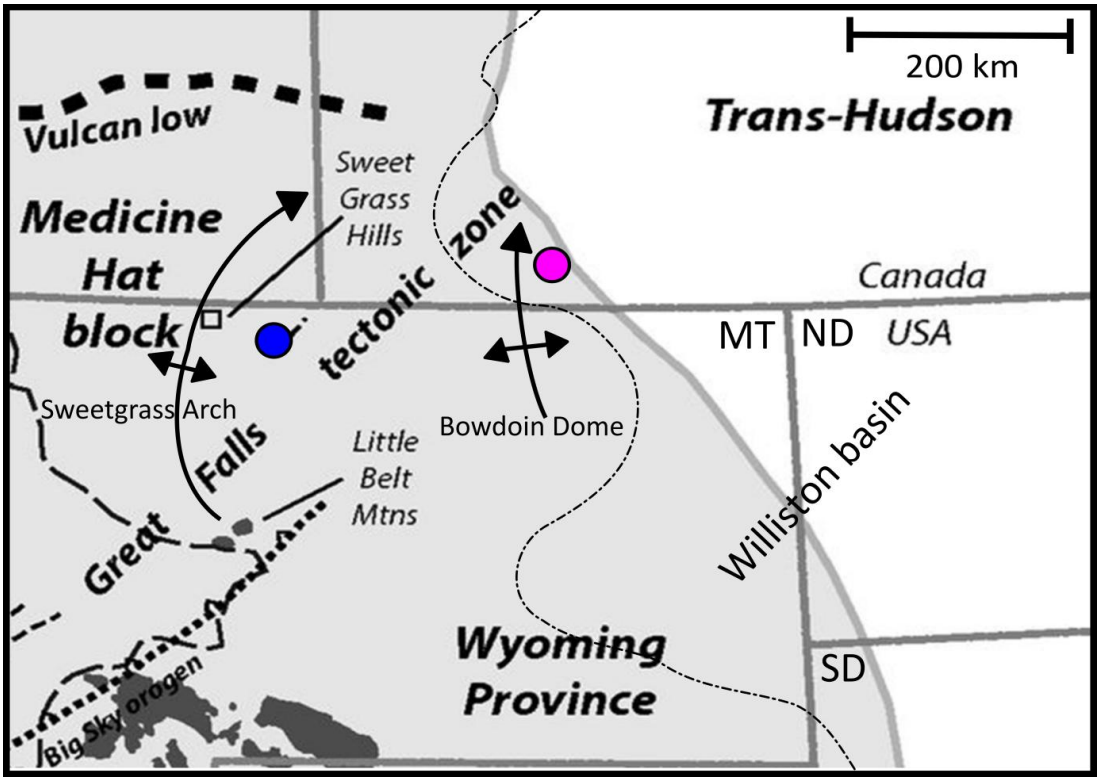

Figure 4.4.: Locations of the Weil #1 well (blue) and International Helium Wood Mtn well (pink) relative to local and regional geological structures and cratonic provinces. The grey area denotes basement of < 2.5 Ga which includes the Wyoming craton and Medicine Hat block. Modified from Vervoort et al., (2016).

The Rudyard field lies within the Western Canadian Sedimentary Basin (WCSB). The Rudyard Anticline is a laccolith which intruded into the Cambrian layer from the Precambrian below. Several of these laccoliths have been drilled and documented in the region and are aligned along a NE trend which mirrors underlying basement faults in the region (Connolly, 2012).

The underlying Precambrian rocks in the region are designated as part of the Great Falls Tectonic Zone (GFTZ); a zone of NE-trending lineaments and high angle faults which coincides with a zone of Tertiary-age magmatism. This zone stretches from the Snake River Plain in SE Idaho to Saskatchewan (Armstrong, 1974; O'Neill and Lopez, 1985; Dudás, 1991; Mueller et al., 2002). There are currently opposing hypotheses as to how the GFTZ formed. Both Mueller et al., (2002) and Holm and Schneider, (2002)'s geochronological and geochemical studies favour the

explanation that the GFTZ is a Palaeoproterozoic suture zone which developed due to the subduction of a segment of oceanic crust and associated depleted mantle which separated the Wyoming block from the Hearne-Medicine Hat block during the formation of southern Laurentia whereas Boerner et al., (1998) found minimal evidence to support this in their geophysical study and instead favoured the explanation that the GFTZ is an Archean-aged reactivated intracontinental shear zone. Recent work by Gifford, (2013) concludes that the GFTZ formed along the margin of the Medicine Hat Block where it was subsequently reworked by collision with the Wyoming Craton sometime after 1.8 Ga supporting the conclusions made by both Mueller et al., (2002) and Holm and Schneider, (2002).

On a continental scale, the GFTZ is taken as the marker for the NW boundary of the Wyoming craton (Condie, 1976; O'Neill and Lopez, 1985; Mueller et al., 2002).

During the Tertiary (Eocene), the GFTZ Precambrian faults served as conduits for potassic extrusives during a pulse of magmatic activity (O'Brien et al., 1991; Lopez, 2000; Connelly, 2012). Occurring around 50 Ma this short-lived pulse of activity started in what is now Idaho and moved northwards through Montana into what is now Canada (Connelly, 2012). Geochemical and mineralogical analyses of extrusives and intrusives from the region point to the interaction of a partially melting asthenospheric mantle wedge (most likely the subducted Farallon plate) with the Wyoming craton (O'Brien et al., 1991; O'Brien et al., 1995).

Basement outcrop exposures in the GFTZ at localities such as the Little Belt Mountains show Palaeoproterozoic dioritic orthogneisses and migmatites which have been intruded by mafic (amphibolites) dikes, pegmatites and post-tectonic

leucogranites. U-Pb and Ar-Ar ages from the location range from between 1.77-1.88 Ga (Gifford et al., 2014).

Despite evidence for basement faults acting as conduits the region has been very stable over the course of geologic time with no evidence of significant movement along the faults beneath the Rudyard field since the Precambrian (Connelly, 2012).

Producing helium zones of interest in the Rudyard field are the Ordovician-age Red River Formation and the Devonian-age Souris River Formation.

The Red River Formation, which contains a highly porous and permeable dolomite gas pay zone, is divided into an Upper Member which is present in all wells in the region and a Lower Member which is absent in the Weil #1 well. An anhydrite bed known as the 'Last Anhydrite' forms an effective seal on top of the Upper Red River Member in the Weil #1 well (Connelly, 2012). Reports show that gases from this layer are predominantly high N_2, high helium and the Lower Red River Member is thought to be a stratigraphic trap leading to the hypothesis that the gas found in the Upper Red River Member at Weil #1 is remigrated gas from the Lower Red River Member however this has yet to be confirmed.

The Souris River Formation, which unconformably overlies the Red River Formation, consists of a series of anhydrite-dolomite-limestone cycles and is thought to be a structural trap. Gas shows have been recorded in dolomite beds underlying an anhydrite layer. Reports of gas shows from this layer show considerable diversity with records of N_2, CH_4, He and CO_2. This has been interpreted as lack of communication between the Devonian and Ordovician reservoirs which is also suggested from differing pressure data from the two reservoirs (Connelly, 2012).

Pinch-out stratigraphic traps in the Sweetgrass Arch region have reportedly been in place for around 500 Ma and the timing of the laccolith formation beneath Rudyard is approximately 50 Ma (Connelly, 2012).

4.2.3 International Helium Wood Mountain, Saskatchewan, Canada

International Helium Wood Mountain is a single well located approximately 270 km NE of the Rudyard Anticline. It is situated on the east flank of the Bowdoin Dome (Thompson, 1964). The Bowdoin Dome is a large structural uplift of approximately 1550 km^2 on the west flank of the intracratonic Williston Basin. It plunges northwards from central Montana into Canada (Schroth, 1953; Rice et al., 1990) (**Figure 4.4**). The basement beneath the Bowdoin Dome is highly fractured and these fractures extend into southern Saskatchewan (Dyck and Dunn, 1986; Shurr et al., 1993).

The helium reservoir at the Wood Mountain site is the Cambrian Deadwood Formation. Despite the thickening of Cambrian-age sediments towards the Williston Basin centre, for the most part, the sediment patterns for the Deadwood formation show no evidence of basinal control on sedimentation (Kent, 1987).

The basement beneath the Wood Mountain field is most likely made up of a significant Archean crustal component from either the Wyoming Craton or the Medicine Hat Block. There is evidence from Sm-Nd dating in Collerson et al., (1990) that the south Saskatchewan region shows differential reworking of Archean-aged crust by the Trans-Hudsonian orogeny due to the spread in ages (3.04-2.25 Ga). Basement cores from southern Saskatchewan are composed of meta-igneous and

metasedimentary rocks which range from amphibolite facies to granulite facies metamorphism.

In the Swift Current area, to the NW of the Wood Mtn well, the basement consists of mafic tonalitic gneiss, massive orthoquartzite, granites, felsic volcanics and high-level porphyry intrusions. Granitoids were extruded into Archean-aged gneisses around 1.76 Ga (Collerson et al., 1990). The occurance of these granitoids in the SW of Saskatchewan was broadly interpreted to be a potential continuation of the NE-trending Great Falls Tectonic Zone termed the Swift Current Anorogenic Province.

4.3 Sample collection and analytical techniques

Samples were collected in the field directly from the wellhead by connecting a high pressure regulator with a 3/4" NPT adaptor to the wellhead. The regulator was then attached to a 70 cm length of internally polished, refrigeration grade copper tubing with a diameter of 3/8” via a length of high pressure hose. Well gas was then flushed through the collection apparatus at pressures around 1 bar (atmospheric) for approximately 10 minutes so as to decrease the possibility of air contamination before the copper tube was cold welded at both ends by closing a pair of stainless steel clamps. This follows the same procedures as Ballentine and Sherwood-Lollar, (2002), Zhou, (2004) and Gilfillan, (2006).

Splits of each sample were taken in the lab not only for the purpose of determining noble gas isotopic composition and concentration but also for the analysis of nitrogen concentration and isotopes by University of Toronto. Noble gas analyses were carried out at the Noble Lab at University of Oxford.

Stable helium isotopes ^{3}He and ^{4}He were specifically measured on the Helix SFT mass spectrometer which has a split flight tube. This gives it the ability to simultaneously measure both isotopes thereby decreasing the error on the measurement.

All stable isotopes of the other noble gases (Ne, Ar, Kr and Xe) were measured on the Argus VI mass spectrometer (see Methods Chapter).

All data errors are quoted at the 1σ level of confidence and include the analytical, blank and standard errors. In the case of concentration errors the expansion volume, pressure and relative prep volume errors are also included. All error corrections on noble gas analyses were made during data reduction.

Due to the radiogenic nature of the majority of the samples, errors were 1.1% to 2.3% for helium ratios however this does not affect sample reproducibility. Ratios were the most affected in this respect due to the statistical counting error on the very low ^{3}He signal which at that early a stage in the laboratory setup was not yet optimally adjusted.

During analyses mass peaks $^{40}Ar^{++}$ and $^{44}CO_2^{++}$ which could cause major interference to ^{20}Ne and ^{22}Ne signals respectively were monitored. Across all samples it was determined that the ^{22}Ne signal of the sample was high enough that the $^{44}CO_2^{++}$ contribution was below 1% and therefore negligible. Corrections were made accordingly to the ^{20}Ne signal of samples for $^{40}Ar^{++}$ interference during data reduction which varied between 10.6% to 11.7% $^{40}Ar^{++}$ contribution following the methods of Niedermann et al. (1993). Uncertainties in $^{40}Ar^{++}$ contribution were propagated through to the final calculated error.

Nitrogen isotope analysis for all samples was undertaken at University of Toronto using procedures detailed in Ballentine and Sherwood Lollar (2002) and

Sherwood Lollar et al., (1997). Individual errors on the $\delta^{15}N$ (‰) results range between ±0.06 to 0.46‰.

4.4. Results

A total of 3 samples were collected from across North America for this part of the study. These were collected from N_2-^{4}He rich wells at: Harley Dome in Utah, Rudyard field in Montana and Wood Mountain in Saskatchewan, Canada.

Results discussed in the following sections pertain to the N_2-^{4}He rich wells sampled only. For information on the Hugoton-Panhandle, CKU and Kansas Basin samples please see Chapter 3.

In all samples $^{4}He/^{20}Ne$ ratios are significantly higher than that of air (0.032) and range between 18,616 and 219,090 (Kipfer et al., 2002). This indicates that there is a negligible air contribution to ^{4}He in samples and that increases to $^{3}He/^{4}He$ ratios are likely due to resolvable mantle contributions.

Sample well and geological province	Location Lat/Long	Producing Formation	Geological age of formation	$^{3}He/^{4}He$ (R_a)	$^{20}Ne/^{22}Ne$	$^{21}Ne/^{22}Ne$	$^{40}Ar/^{36}Ar$	$^{38}Ar/^{36}Ar$
Colorado Plateau								
Harley Dome #1	39°11'13.32"N, 109° 8'52.95"W	Entrada Sandstone	Jurassic	0.10 (0.001)	9.00 (0.029)	0.083 (0.0009)	4452 (10)	0.190 (0.002)
Harley Dome #1				0.11 (0.001)	9.03 (0.029)	0.083 (0.0009)	4448 (10)	
Great Falls Tectonic Zone								
Weil #1	48°40'24.75"N, 110°33'44.44"W	Red River	Ordovician	0.74 (0.01)	10.21 (0.037)	0.067 (0.0007)	8839 (50)	0.185 (0.003)
Weil #1				0.73 (0.01)	10.21 (0.034)	0.067 (0.0007)		
International Helium Wood Mountain	49°22'21.15"N, 107° 0'45.76"W	Deadwood Formation	Cambrian	0.18 (0.004)	9.78 (0.036)	0.071 (0.0008)	7118 (33)	0.188 (0.004)

Table 4.1.: Noble gas ratios from N_2-^{4}He rich wells in this study. 1σ errors for samples are shown in brackets.

Sample well and geological province	^{4}He concentration (x 10^{-2}) (cm^3 STP)	^{20}Ne concentration (x 10^{-7}) (cm^3 STP)	^{40}Ar concentration (x 10^{-4}) (cm^3 STP)	^{84}Kr concentration (x 10^{-8}) (cm^3 STP)	^{130}Xe concentration (x 10^{-10}) (cm^3 STP)	N_2 concentration (±5%) (cm^3 STP)	$\delta^{15}N(N_2)$
Colorado Plateau							
Harley Dome #1	7.18 (0.10)	3.27 (0.031)	36.11 (0.34)	2.90 (0.09)	2.81 (0.03)	0.844	1.00 (0.06)
Harley Dome #1	7.03 (0.10)	3.24 (0.031)	35.83 (0.33)				
Great Falls Tectonic Zone							
Weil #1	0.98 (0.01)	1.01 (0.010)	22.75 (0.23)	0.66 (0.02)	0.56 (0.01)	0.955	2.40 (0.20)
Weil #1	1.00 (0.01)	1.02 (0.010)					
International Helium Wood Mountain	1.06 (0.02)	0.84 (0.086)	19.92 (0.20)	0.70 (0.03)	0.79 (0.01)	0.960	1.40 (0.46)

Table 4.2.: Noble gas concentrations, N_2 concentrations and N_2 isotope values from this study. Nitrogen concentrations for the samples are taken from IACX well tests and are deemed to be within acceptable limits due to ^{4}He concentrations from this study being within 1σ error of previously recorded helium concentrations from wells. 1σ errors for samples appear in column headers as % or in brackets if variable.

4.4.1 Noble gases

4.4.1.1 Helium

The R_a values of the N_2-^4He rich samples (where 1 R_a is relative to the atmospheric $^3He/^4He$ ratio of 1.4 x 10^{-6}) vary dependent on location. The Harley Dome well has a R_a value of 0.10, Weil #1 has a R_a value of 0.70 and International Helium Wood Mountain has a R_a value of 0.17. The R_a values for these wells are comparable to the R_a values from the Hugoton-Panhandle which range between 0.14 to 0.25 R_a. Out of the N_2-^4He rich samples only International Helium Wood Mountain falls within the range of the Hugoton-Panhandle samples.

Magmatic contributions to the ^4He concentration in samples are: 1.0% in the Harley Dome sample, 8.6% in the Weil #1 sample and 1.8% in the International Helium Wood Mtn sample, assuming a crustal endmember of 0.02 R_a and a MORB mantle endmember of 8.0 R_a.

Concentrations of ^4He in samples range from: 9.8 x 10^{-3} $cm^3STP(^4He)/cm^3$ in the Weil #1 well, to 1.06 x 10^{-2} $cm^3STP(^4He)/cm^3$ in the International Helium Wood Mtn sample, to 7.18 x 10^{-2} $cm^3STP(^4He)/cm^3$ in the Harley Dome well. Corresponding ^3He concentrations for each sample are: 9.64 x 10^{-9} $cm^3STP(^3He)/cm^3$ for Weil #1, 2.46 x 10^{-9} $cm^3STP(^3He)/cm^3$ for International Helium Wood Mtn, and 1.00 x 10^{-8} $cm^3STP(^3He)$ for Harley Dome. Once again only International Helium Wood Mtn falls into the range of a CH_4-rich ^4He system such as the Hugoton-Panhandle gas field which has ^3He concentrations between 6.8 x 10^{-10} to 3.3 x 10^{-9} $cm^3STP(^3He)/cm^3$ (Ballentine and Sherwood, 2002; this study Chapter 3).

4.4.1.2. Neon

^{20}Ne concentrations in the N_2-^{4}He rich well gases varies between samples from: 0.84 x 10^{-7} $cm^3STP(^{20}Ne)/cm^3$ in the International Helium Wood Mtn well to 1.01 x 10^{-7} $cm^3STP(^{20}Ne)/cm^3$ in the Weil #1 well to 5.03 x 10^{-7} $cm^3STP(^{20}Ne)/cm^3$. These concentrations all fall within range of the ^{20}Ne concentrations recorded in the Hugoton-Panhandle sample set which vary between 0.86 x 10^{-7} to 5.0 x 10^{-7} $cm^3STP(^{20}Ne)/cm^3$ (Ballentine and Sherwood-Lollar, 2002; this thesis Chapter 3).

$^{20}Ne/^{22}Ne$ ratios across the N_2-^{4}He rich wells varies between: 10.21 for the Weil #1 well, 9.78 for the International Helium Wood Mtn sample and 9.00 for the Harley Dome sample when compared with the air value of 9.80. Out of the N_2-^{4}He rich wells International Helium Wood Mtn is again the only sample which falls into the same range as the Hugoton-Panhandle samples of between 9.59 to 9.91.

The $^{21}Ne/^{22}Ne$ ratios are: 0.067 for Weil #1, 0.071 for International Helium Wood Mtn and 0.083 for Harley Dome compared with the air value of 0.029. All N_2-^{4}He rich samples show ratios which are significantly higher than the air ratio indicating significant resolvable excesses of ^{21}Ne ($^{21}Ne^*$). In these samples this excess varies from 57.0%-65.4% of the ^{21}Ne concentration of the gas. All N_2-^{4}He rich samples are significantly more enriched in $^{21}Ne^*$ than samples from the Hugoton-Panhandle dataset which exhibit ^{21}Ne concentrations ranging between 0.037-0.051.

The air, crust and mantle endmembers of $^{20}Ne/^{22}Ne$ and $^{21}Ne/^{22}Ne$ are well defined and can be affected by both mass fractionation and mixing between endmember groups. From the three neon isotopic graph it can be seen that the N_2-^{4}He rich wells show potential mixing between different endmembers (**Figure 4.5**).

The Harley Dome sample can be interpreted as mass fractionation and/or a mantle component addition has affected the sample which should fall along the air-modern crust mixing line but is still close to it. It is notable that the CKU and KBC samples from the Kansas sample set fall along the same air-crust mixing line which could indicate that the CKU, KBC and Harley Dome share the same source rock.

Samples Weil #1 and International Helium Wood Mtn appear to be related to the air-Archean crust mixing line identified by Lippmann-Pipke et al., (2011). This could indicate a significant basement input to both these samples from crust which is older than that associated with the CKU, KBC and Harley Dome samples.

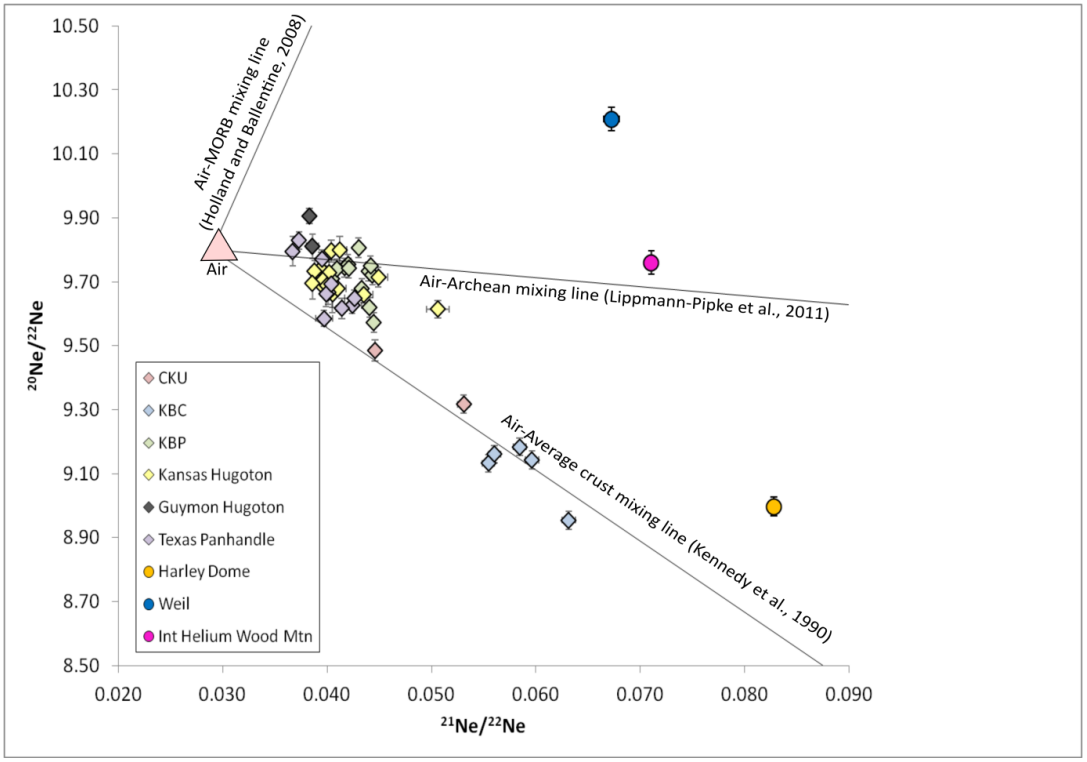

Figure 4.5.: Three neon isotope graph showing isotopic ratios in samples relative to predefined mixing lines for air-crust and air-mantle mixtures. All samples show significant excesses of $^{21}Ne/^{22}Ne$.

The mantle and crustal contributions to the $^{21}Ne^*$ concentration can be calculated from $^{20}Ne/^{21}Ne/^{22}Ne$ using methods outlined in Ballentine and O'Nions, (1992) and Ballentine, (1997) assuming no mass fractionation of the samples. In all

N_2-^{4}He rich wells crustal $^{21}Ne^*$ dominates $^{21}Ne^*$ concentrations. The $^{21}Ne^*$ concentration at the Harley Dome well is 99% sourced from modern crust with a maximum resolvable MORB mantle component of 1%. The other N_2-^{4}He rich wells have a maximum resolvable MORB mantle component of 2% for International Helium Wood Mtn and 18% for Weil #1 when the source is assumed to be the Archean aged endmember.

4.4.1.3 Argon

The $^{40}Ar/^{36}Ar$ ratios between the N_2-^{4}He rich samples vary from: 4452 in the Harley Dome well, 7118 at International Helium Wood Mtn and 8839 at the Weil #1 well. All ratios are significantly higher than air which has a $^{40}Ar/^{36}Ar$ ratio of 295.5 indicating that there is a resolvable excess of radiogenic ^{40}Ar ($^{40}Ar^*$). The $^{40}Ar^*$ concentration contributes between 93.4 to 96.7% of the total ^{40}Ar concentration (**Table 4.3**).

It is not possible to separate out crust from mantle contributions with regard to $^{40}Ar^*$ in the N_2-^{4}He rich samples however it can be assumed that the dominant contribution is from the crust with a potential mantle contribution to the Weil #1 well.

The ratios of atmospherically derived $^{38}Ar/^{36}Ar$ for samples Weil #1 and International Helium Wood Mtn are within 1σ error of air values (where $^{38}Ar/^{36}Ar$ of air = 0.188) (**Table 4.1**). The $^{38}Ar/^{36}Ar$ value for the Harley Dome sample is within 2σ of air.

4.4.1.4. Krypton and xenon

In the N_2-^{4}He rich wells ^{84}Kr concentrations range from: 6.58 x 10^{-9} $cm^3STP(^{84}Kr)/cm^3$ in the Weil #1 well, 7.05 x 10^{-9} $cm^3STP(^{84}Kr)/cm^3$ in the International Helium Wood Mtn well and 2.90 x 10^{-8} $cm^3STP(^{84}Kr)/cm^3$ in the Harley Dome well. The Weil #1 and International Helium Wood Mtn wells have ^{84}Kr concentrations in samples which are within 1σ error of each other whereas the Harley Dome well has approximately 4 times more ^{84}Kr than those wells (**Table 4.2**).

The wells show ^{130}Xe concentrations from: 5.59 x 10^{-11} $cm^3STP(^{130}Xe)/cm^3$ in the Weil #1 well, 7.88 x 10^{-11} $cm^3STP(^{130}Xe)/cm^3$ for the International Helium Wood Mtn well and 2.81 x 10^{-10} $cm^3STP(^{130}Xe)/cm^3$ in the Harley Dome well. Unlike for ^{84}Kr concentrations, Weil #1 and International Helium Wood Mtn are not within 1σ error of each other and Harley Dome has up to 5 times more ^{130}Xe than both these wells.

4.4.1.5. Crust-derived noble gases

The $^{4}He/^{21}Ne^*$ ratios for samples from this study are presented in **Table 4.3**. All ratios for the N_2-^{4}He rich wells are significantly higher than the average observed $^{4}He/^{21}Ne^*$ value of 1.71±(0.09) x 10^7 and fall within range of values from the Hugoton-Panhandle field (2.85±(0.62) x 10^7) (Ballentine and Burnard, 2002; Ballentine and Sherwood-Lollar, 2002). However, both the Weil #1 and International Helium Wood Mtn samples fall within error of theoretical values for crustal $^{4}He/^{21}Ne^*$ (2.33±(0.44) x 10^7). For the Harley Dome and International Helium Wood Mtn wells the correction of both ^{4}He and $^{21}Ne^*$ isotopes for magmatic contributions

does not significantly affect $^{4}He/^{21}Ne^{*}$ ratios however correction increases the $^{4}He/^{21}Ne^{*}$ ratio associated with the Weil #1 well gas.

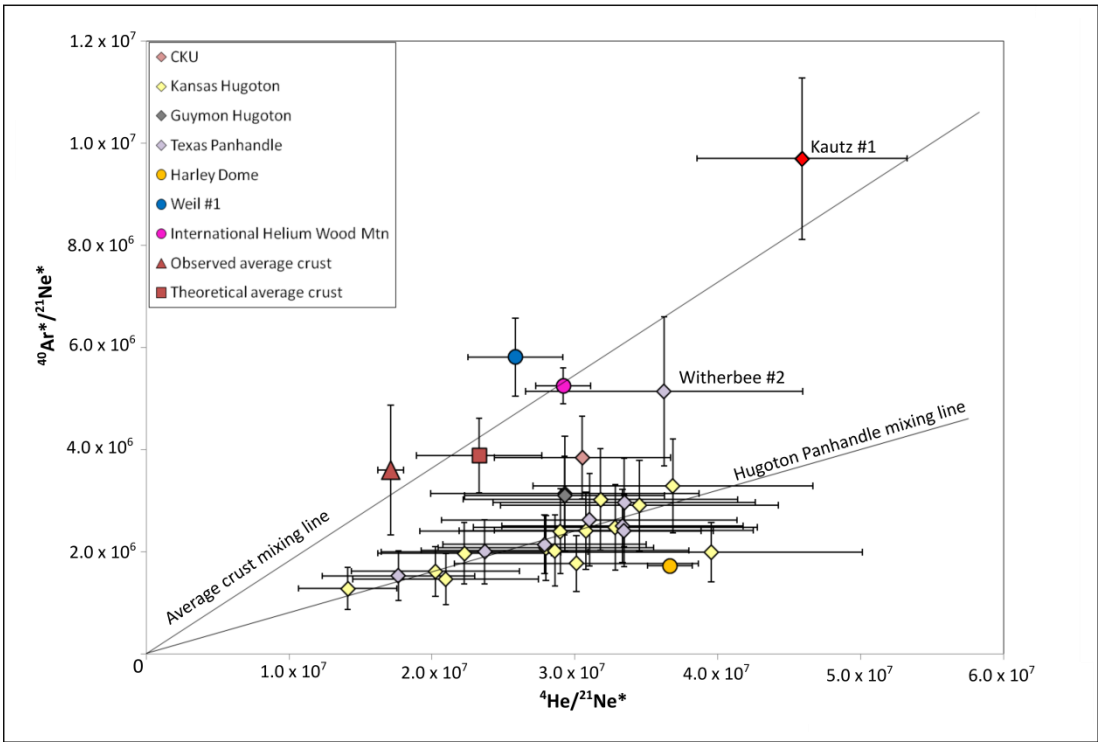

Figure 4.6.: Plot showing the relationship between radiogenic ^{4}He and $^{40}Ar^{*}$ normalised to nucleogenic $^{21}Ne^{*}$.

Well name/geological province	$^{4}He/^{40}Ar^{*}$	$^{4}He/^{21}Ne^{*}$	$^{40}Ar^{*}/^{21}Ne^{*}$	$^{21}Ne^{*}$ (%)	$^{40}Ar^{*}$ (%)
Harley Dome	21.29 ± 0.50	3.66 ± (0.16) x 10^{7}	1.72 ± (0.78) x 10^{6}	64.3	93.4
Weil	4.45 ± 0.14	3.09 ± (0.40) x 10^{7}	6.95 ± (0.92) x 10^{6}	57.0	96.7
International Helium Wood Mtn	5.56 ± 0.15	2.45 ± (0.16) x 10^{7}	4.39 ± (0.30) x 10^{6}	58.2	95.8
Average upper crust (theoretical) (Ballentine and Burnard, 2002)	6.0	2.33 ± (0.44) x 10^{7}	3.88 ± (0.73) x 10^{6}		
Average upper crust (observed) (Ballentine and Burnard, 2002)	5.0±1.0	1.71 ± (0.09) x 10^{7}	3.60 ± (1.27) x 10^{6}		

Table 4.3.: Concentrations and ratios of the radiogenically produced isotopes in samples. Errors are to 1σ.

The northern-most N_2-^{4}He rich wells Weil #1 (Montana) and International Helium Wood Mtn (Saskatchewan) show $^{4}He/^{40}Ar^{*}$ ratios which are within error of average observed crustal production values (5.0 ±1.0). The Harley Dome well shows $^{4}He/^{40}Ar^{*}$ ratios which are higher than both the average crustal $^{4}He/^{40}Ar^{*}$ ratio and $^{4}He/^{40}Ar^{*}$ ratios measured in the Hugoton-Panhandle system (12.46±2.48) (**Figure 4.6**).

The $^{40}Ar^{*}/^{21}Ne^{*}$ ratios for the Weil #1 and International Helium Wood Mtn wells fall close to and within error of the observed $^{40}Ar^{*}/^{21}Ne^{*}$ ratios for the average crust as well as each other (6.95×10^{6} and 4.39×10^{6} compared with $3.60 \pm (1.27) \times 10^{6}$). The $^{40}Ar^{*}/^{21}Ne^{*}$ ratio for the Harley Dome well is significantly lower than average crustal ratio (1.72×10^{6} compared with $3.60 \pm (1.27) \times 10^{6}$).

Only the Harley Dome well directly compares to $^{40}Ar^{*}/^{21}Ne^{*}$ ratios from the Hugoton-Panhandle field ($2.43 \pm (0.81) \times 10^{6}$) despite the Hugoton-Panhandle, Weil #1 and International Helium Wood Mtn falling within the range of average $^{40}Ar^{*}/^{21}Ne^{*}$ crustal values. When ratios are corrected for magmatic contributions to the $^{21}Ne^{*}$ concentrations discrepancies from the average crustal $^{40}Ar^{*}/^{21}Ne^{*}$ increase significantly for the Weil #1 well and less significantly for Harley Dome and International Helium Wood Mtn.

In summary the Weil #1 and International Helium Wood Mtn wells show $^{4}He/^{21}Ne^{*}$ ratios, $^{40}Ar^{*}/^{21}Ne^{*}$ ratios and $^{4}He/^{40}Ar^{*}$ ratios which are within error of average crustal values whereas the Harley Dome well shows preferential enrichment in ^{4}He relative to $^{21}Ne^{*}$ and $^{40}Ar^{*}$.

4.4.1.6. Relationships between ^{20}Ne and the crust-derived isotopes

Correlations between atmosphere-sourced ^{20}Ne and radiogenically-sourced ^{4}He have been noted in studies on the Hugoton-Panhandle and also in Chapter 3 of this thesis with regards to the Kansas Basin and Central Kansas Uplift (Ballentine and Sherwood-Lollar, 2002). Strong positive correlations between these two separately generated isotopes is thought to show mixing of the isotopes prior to their degassing into reservoirs which is an indicator of varying degrees of groundwater contact with the radioisotopes.

Since the N_2-^{4}He wells are all single wells with no spatial connection we assume that groundwater does play a role in their individual sourcing such that without the influence of groundwater there are no radioisotopes in the reservoir gas; however this may not necessarily be the case (**Figure 4.7**).

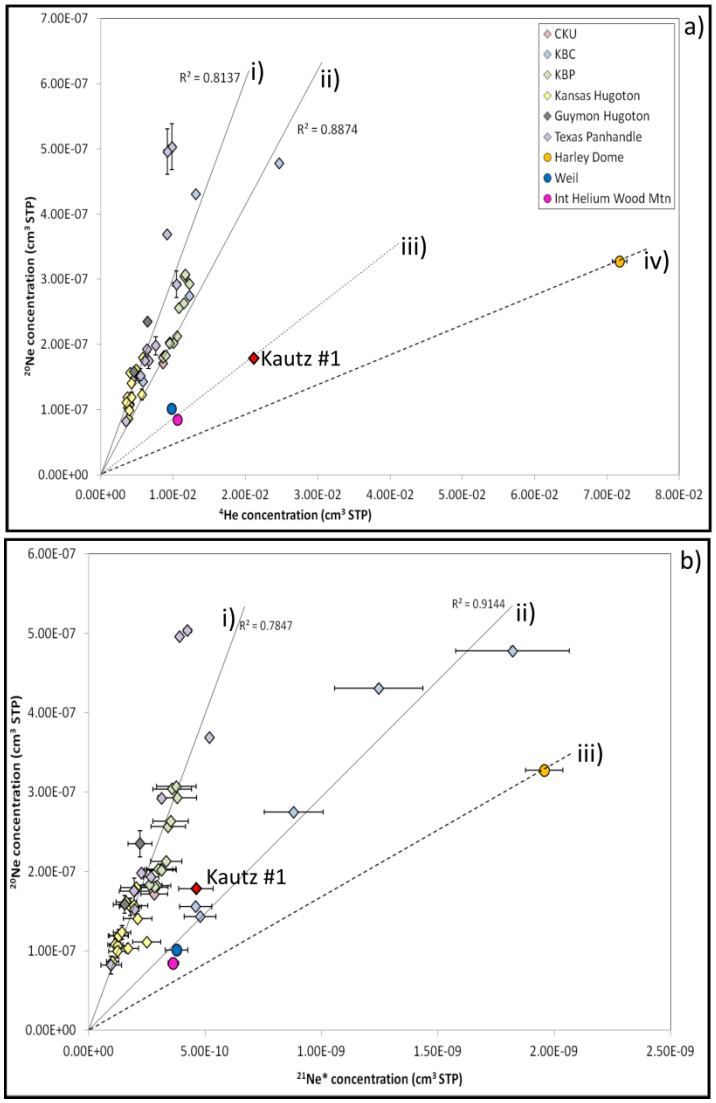

Figure 4.7.: Plots showing positive correlations between radiogenically and nucleogenically derived components a) ^{4}He, b) $^{21}Ne^{*}$, c) $^{40}Ar^{*}$ and groundwater-derived ^{20}Ne. All lines and hypothetical lines (dashed) fall within error of the origin. Mixing lines i) and ii) are trends observed in the previous chapter. Separate trends are observed for the Weil #1 and International Helium Wood Mtn wells and the Harley Dome well with the assumption that the radiogenic and nucleogenic isotopes in each well have been degassed from groundwater.

It can be seen from the graphs that Weil #1 and International Helium Wood Mtn appear to have very similar $^{4}He/^{20}Ne$ ratios and $^{21}Ne^{*}/^{20}Ne$ ratios. These radioisotopes have also experienced a greater degree of groundwater contact than the ^{4}He and $^{21}Ne^{*}$ concentrations associated with the sample from Harley Dome.

However, the reverse to the above observations is seen in the graph for ^{20}Ne vs $^{40}Ar^{*}$ which appears to show mixing between the samples from Weil #1 and International Helium Wood Mtn. These samples also show a lesser degree of groundwater contact for $^{40}Ar^{*}$ concentrations in the Weil #1 and International Helium Wood Mtn samples compared with the Harley Dome sample. This shows the fractionation of $^{40}Ar^{*}$ relative to ^{4}He and $^{21}Ne^{*}$ in the Harley Dome well which is mirrored in the radiogenic ratios associated with the well (**Figure 4.3**). This fractionation could have been caused by the inefficient release of $^{40}Ar^{*}$ from minerals compared with ^{4}He and $^{21}Ne^{*}$ which is caused by the low thermal regime of the region (Ballentine et al., 1994; Ballentine and Sherwood-Lollar, 2002).

4.4.2. Other Major Gases

4.4.2.1. Methane, ethane, propane and CO_2

Methane is also present in the N_2-^{4}He wells with concentrations ranging from: 2.5% in the Weil #1 well, 2.9% in the International Helium Wood Mountain well and 7.5% in the Harley Dome well. Ethane and propane are also present in Harley Dome and Weil #1 wells (0.23% and 0.02% in the Harley Dome well and 0.13% and 0.10% in the Weil #1). Due to the lack of data for International Helium Wood Mtn we are unable to comment on any other associated gases. There is no

mention in previous literature as to the source of the methane or higher homologues measured in reservoirs.

Carbon dioxide is present in gases from the Harley Dome and Weil #1 wells (1.13% and 0.42%) of unknown origin.

4.4.2.2. Nitrogen

Nitrogen concentrations in the N_2-^{4}He rich wells are: 95.5% in the Weil #1 well, 96.0% in the International Helium Wood Mtn and 84.4% in the Harley Dome well. Isotopic $\delta^{15}N$ values span a very narrow range for the N_2-^{4}He rich wells and are: +2.40‰ in the Weil #1 well, +1.40‰ in the International Helium Wood Mtn well and +1.00‰ in the Harley Dome well.

Due to the higher than air ratios associated with $N_2/^{40}Ar$ associated with all N_2-^{4}He wells (233.8 to 482.0 compared with the air $N_2/^{40}Ar$ value of 84.0) we can assume that there have been negligible additions of air-derived N_2 to the samples or air saturated water which has a $N_2/^{40}Ar$ ratio of 44.0.

This leaves three other possibilities as to the origin of the nitrogen in samples: the crust, the mantle or the thermal cracking of over-mature hydrocarbons. If we assume a $N_2/^{3}He$ ratio for a Mid-Oceanic Ridge Basalt (MORB) mantle of 6×10^{6} we can calculate the proportions of mantle-derived N_2 associated with the samples (Ballentine and Sherwood-Lollar, 2002). This gives mantle-derived N_2 contributions to the N_2 concentrations of samples of: 6.1% for the Weil #1 well, 1.5% for the International Helium Wood Mtn well and 7.1% for the Harley Dome well.

Less than 8% of the total nitrogen in wells is associated with a mantle source therefore the majority of the N_2 concentrations measured in wells must be sourced by a combination of crust and hydrocarbons. However, because CH_4 concentrations measured in wells are less than 8% of the total gas concentration it is more likely that the majority of the N_2 was sourced from crustal rocks.

4.4.3. Relationships between N_2 and the crust-derived noble gases

In general high N_2 concentrations are positively correlated with high ^4He concentrations although in the case of the Weil #1 and International Helium Wood Mtn wells this is not necessarily the case when compared with the Harley Dome well (**Figure 4.8**). In the Weil #1 and International Wood Mtn wells $^4He/N_2$ ratios are the same at 0.010 whereas in the Harley Dome well the $^4He/N_2$ ratio is 0.085. While the ^4He concentrations in the Weil #1 and International Wood Mtn wells are not the lowest sampled in the entire dataset (**Appendix B**), their N_2 concentrations are the highest in the wells sampled. This combination of factors places them outside the 'lower limit' for $^4He/N_2$ ratios associated with helium producing fields of between 0.02 and 0.20 into which the Harley Dome sample still fits.

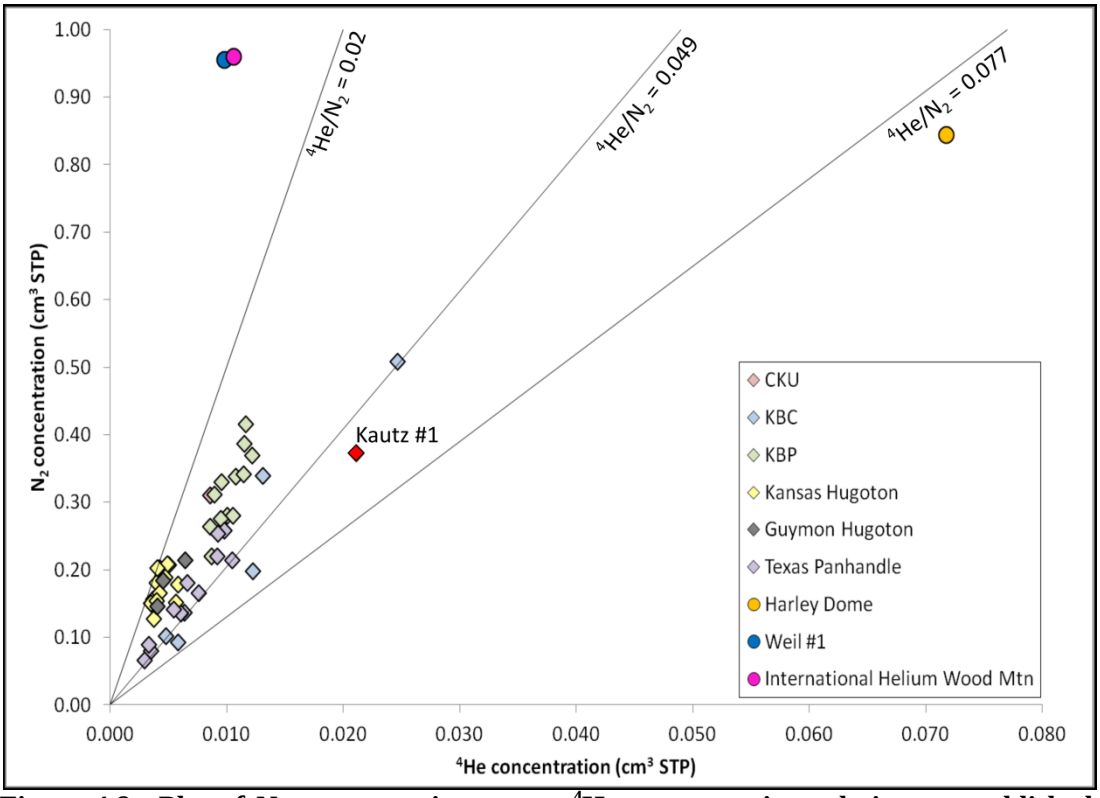

Figure 4.8.: Plot of N_2 concentration versus ^4He concentration relative to established $^4He/N_2$ ratios from the Hugoton-Panhandle, Kansas Basin and Central Kansas Uplift.

4.5. Discussion

Nitrogen is the most abundant non-hydrocarbon gas found within petroleum systems. The process of uncovering the dominant source and the processes responsible for the focusing and enrichment of N_2 within these systems is not only complicated but also not well understood. This is mainly due to the multiple sources of nitrogen in the subsurface which includes: nitrogen released from sedimentary organic matter, nitrogen released from sediments and the basement during metamorphism, atmosphere-derived nitrogen which has been dissolved in groundwater and mantle nitrogen inputs within areas of recent magmatic activity (Stahl et al., 1977; Kreulen et al., 1982; Haendel, 1986; Coveney, 1987; Gold and Held, 1987; Jenden et al., 1988; Bebout and Fogel, 1992; Boyd et al., 1993; Krooss et al., 1993; Littke et al., 1995; Gerling et al., 1998; Bebout et al., 1999; Hutcheon,

1999; Weinlich et al., 1999; Zhu et al., 2000; Boyd, 2001; Ballentine and Sherwood-Lollar, 2002).

This problem with identifying the nitrogen endmembers associated with gases is complicated further; not only by the overlapping ranges quoted for the nitrogen isotopic values of the nitrogen endmembers but also by the uncertainty in the isotopic range of the endmembers (Zhu et al., 2000; Boyd, 2001).

It has been noted in previous literature that occasionally high N_2 concentrations are associated with high ^4He concentrations in gas fields (Cady and McFarland, 1906; Cady and McFarland, 1907a; Dobbin, 1935; Zartman and Wasserburg, 1961; Pierce et al., 1964; Poreda et al., 1986; Gold and Held, 1987; Jenden et al., 1988b; Jenden and Kaplan, 1989; Stilwell, 1989; Hiyagon and Kennedy, 1992; Hutcheon, 1999; Ballentine and Sherwood-Lollar, 2002; Gilfillan, 2006). Fields which produce ^4He-rich gases (where ^4He makes up 0.1%≤ of the gas volume) almost always contains high N_2 concentrations; usually within a $^4He/N_2$ range of 0.02 to 0.20. However, the inverse is not true; we do not always find high ^4He concentrations in conjunction with high N_2 concentrations which shows the variation of N_2 sources within natural gas fields.

The close association of N_2 with crustal-radiogenic sourced ^4He has been used to support a metasedimentary or crystalline origin for the associated nitrogen. This was also proposed as the source of the N_2 endmember associated with ^4He in the previous chapter which expanded on the study conducted on the Hugoton-Panhandle by Ballentine and Sherwood-Lollar (Jenden et al., 1988b; Ballentine and Sherwood-Lollar, 2002).

In this section we discuss the possible origins and characteristics of the ^4He-associated N_2 endmember as characterised by the 3 sampled N_2-^4He-rich wells and

whether this component is related to groundwater in the regions in a similar way to the CH_4-^4He rich Hugoton-Panhandle, Kansas Basin, or Central Kansas Uplift study areas outlined in the previous chapter. We then apply these characteristics to literature values from CO_2-^4He fields: McCallum, McElmo Dome, St John's Dome and Doe Canyon to observe whether we can determine the local/regional controls on the ^4He source to all wells (Gilfillan et al., 2008).

4.5.1. The N_2 isotopic endmember for ^4He

In the previous chapter we expanded on the study conducted by Ballentine and Sherwood-Lollar in 2002 on the CH_4-^4He rich Hugoton-Panhandle gas system and identified that most samples from the Hugoton-Panhandle, Kansas Basin and Central Kansas Uplift could be adequately explained by the three component mixing of two ^4He associated N_2 endmembers of varying $^4He/N_2$ endmember composition (0.089 for the upper mixing line and a hypothetical lower mixing line with an endmember at least twice as low) and a common N_2 endmember which was not associated with ^4He and had an enriched $\delta^{15}N$ isotopic value of approximately +14.60‰ (**Figure 4.9**).

It is difficult to determine the cause of the low $^4He/N_2$ ratios below the lower limit mixing line however it is either due to mixing between a lower $^4He/N_2$ endmember which is unique to those samples and the rest of the dataset or that the gases in those reservoirs have experienced greater dilution by the migration of CH_4 from the prolifically hydrocarbon-producing Anadarko Basin located to the south of the study areas.

Interestingly the ^4He-associated N_2 endmembers appeared to fall within a very narrow $\delta^{15}N$ range and were in agreement with the $\delta^{15}N$ value of -3.00‰ calculated in the previous study by Ballentine and Sherwood-Lollar, (2002). This alongside evidence from the associated radiogenic ratios of the gases and the helium mass balance calculated for the system led us to the conclusion that both these ^4He-associated N_2 endmembers were dominantly sourced from the low temperature metamorphism of the crust (Zhu et al., 2000).

Despite the agreement between both studies of the potential source for the ^4He associated N_2 endmember none of the CH_4-rich wells sampled were within range of the endmember nitrogen isotopic value to confirm this extrapolation. To better constrain these endmember characteristics, we sampled 3 N_2-rich ^4He wells for which there was a lack of publically available noble gas analyses until this study.

In the graph below we present the first evidence which may confirm the consistently low $\delta^{15}N$ characteristic of the N_2 endmember predominantly associated with the source of ^4He in North American high ^4He well gases.

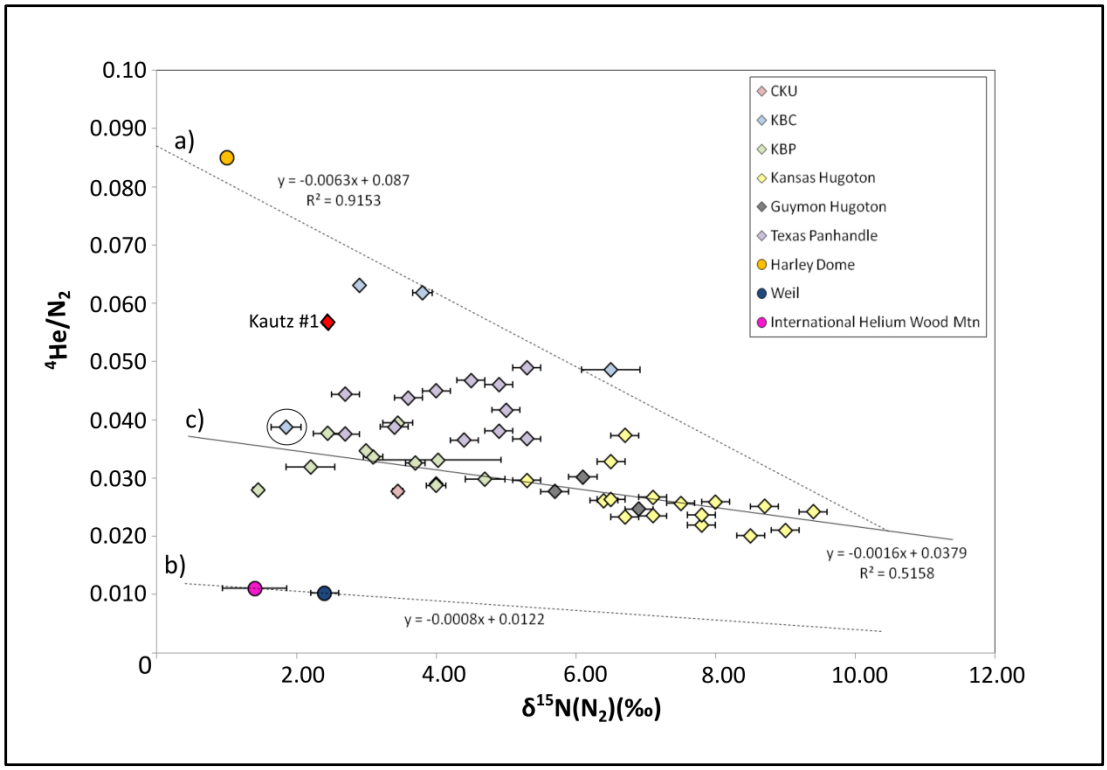

Figure 4.9.: Plot of $^4He/N_2$ vs. $\delta^{15}N(N_2)$. Mixing lines shown are a) the KBC samples excluding the anomalously low #1 Blew well (circled), b) International Helium Wood Mtn and Weil #1 wells and, c) the KBP and Kansas Hugoton samples.

From Figure 4.9 it can be observed that there is a commonality between the Harley Dome sample and the KBC wells which make up the upper mixing limit of the Mid-Continent dataset from the previous chapter. This is particularly of interest since these wells are seemingly unrelated; they have significantly different geological histories and are over 800 km apart, however, they share nearly the same enriched $^4He/N_2$ endmember and potentially the same $\delta^{15}N$ isotopic endmember. This is most likely either due to common process or a common source rock for ^4He and N_2.

As a single well it is difficult to determine whether the $\delta^{15}N$ value of the Harley Dome sample is the product of mixing between multiple N_2 endmembers or is the representation of just one N_2 endmember.

From the composition of the noble gas isotopes outlined in the results section the radiogenic and nucleogenic content of the gas is not purely crust-derived which gives a potential mantle-sourced contribution to the Harley Dome system of approximately 7%. This concentration of N_2 is not significant to the total N_2 concentration and therefore mixing would most likely not affect the $\delta^{15}N$ value indicating that the dominant source of N_2 and ^{4}He to the reservoir is either from the release of ammonium from clay-rich sediments (+1‰ to +4‰) or from the low temperature metamorphism of the crust (-5‰ to +4‰) (Zhu et al., 2000).

Another interpretation of the Harley Dome sample is that it experienced an input from an enriched N_2 endmember which has been sourced from devolatilised crust that has degassed most of its ^{4}He and has become progressively enriched in ^{15}N over time (Haendel et al., 1986; Boyd, 2001). However, the Harley Dome sample radiogenic isotopes show high $^{4}He/^{21}Ne^{*}$ concentrations and low $^{40}Ar^{*}/^{21}Ne^{*}$ ratios therefore it is unlikely that high heat and pressure has facilitated the release of ^{4}He in this region otherwise radiogenic ratios would exhibit close to average crust radiogenic ratios instead of radiogenic ratios which indicate a low temperature, relatively shallow thermal environment.

The International Helium Wood Mtn and Weil #1 wells also indicate a commonality between their $^{4}He/N_2$ endmember ratio which is around 6 times lower than the Harley Dome $^{4}He/N_2$ endmember ratio. These wells show similar $^{4}He/N_2$ ratios, radiogenic ratios and fall within a very narrow range of N_2 isotopic values (+1.45‰ to +2.45‰). These wells either share a regional source rock or a similar production and mixing mechanism is at work in both locations.

Despite the narrow range of N_2 isotopic values shared by the high N_2-^{4}He wells there is a wide range of $^{4}He/N_2$ values associated with these wells. These

differences in ratio could be caused by: differing accumulation times before release, variations in the N_2 content of the source rock, differences in uranium content relative to N_2 in the source rock or dilution of the $^4He/N_2$ by CH_4 due to prior degassing of N_2 and ^4He before the introduction of a hydrocarbon gas phase such as in the KBP fields (Chapter 3, this thesis).

The common characteristics between these wells appear to be dependent on region but represent the regional release of ^4He and ^4He-associated N_2 with distinct $^4He/N_2$ endmember ratios. Since these are regional trends the systems still need a focusing mechanism which, like in the Hugoton-Panhandle system, could be provided by groundwater.

4.5.2. Groundwater (^{20}Ne) relationships with ^4He and N_2

In the previous chapter it was determine that groundwater (examined via the proxy of the ^{20}Ne isotope) played a major role in transporting and focusing ^4He and ^4He-associated N_2 in the Hugoton-Panhandle, Kansas Basin and Central Kansas Uplift systems. Three main interactions were seen in well gases based on mixing trends and the saturation threshold calculated for each study area: 1) groundwater was under-saturated relative to depth and pressure controlled saturation threshold leading to ^4He-associated N_2 degassing in the presence of CH_4, 2) groundwater was oversaturated in ^4He-associated N_2 relative to depth and pressure controlled saturation threshold leading to ^4He-associated N_2 degassing without the need for CH_4 to be present as a gas phase and 3) groundwater was heavily oversaturated in ^4He-associated N_2 relative to depth and pressure controlled saturation threshold leading to

the conclusion that a significant portion of the gas present was transported into the reservoir as a free gas phase from depth.

In this section we perform similar calculations to those in Chapter 3 Section 3.4.1.7. to not only calculate whether the groundwater at the time of field discovery would have been oversaturated or undersaturated in ^4He-associated N_2 but also, if the reservoir is oversaturated, to determine at what depth the saturation threshold starts.

In the following calculations presented in Table 4.4, all N_2 in the N_2-^4He rich wells is assumed to be sourced from the groundwater.

Study Area	**$N_2/^{20}Ne$ (x 10^6)**	**^4He-associated N_2 concentration in groundwater ($cm^3STP(N_2)/cm^3$)**	**N_2 concentration saturation point in groundwater under reservoir conditions ($cm^3STP(N_2)/cm^3$)**	**Reservoir conditions: pressure (atm)/ salinity (M)NaCl/ depth (m)**	**Depth at which saturation threshold is reached under reservoir conditions (m)**
Harley Dome	2.58	0.46	0.18	10.5/0.17/288	1050
Weil #1	9.46	1.69	0.89	129.3/4/1676	3130
International Helium Wood Mtn	11.37	2.03	1.28	190.5/4/2499	3570

Table 4.4.: Comparisons of N_2 saturation in groundwater compared to modern reservoir conditions. Reservoir conditions for the Harley Dome well sourced from Dobbin, (1935) and Downs, (2009); reservoir conditions for the Weil #1 well sourced from Connelly, (2012); reservoir conditions for the International Helium Wood Mtn well sourced from Thompson, (1964).

From the calculations of ^4He-associated N_2 observed in the fields it can be seen that all three N_2-^4He rich wells contain groundwater oversaturated in ^4He-associated N_2. The Harley Dome well is the most oversaturated of these wells at approximately 2.6 times higher than the N_2 saturation threshold. Notably the International Helium Wood Mtn and Weil #1 wells are 1.6-1.9 times higher than the N_2 saturation threshold. The oversaturation of these wells indicates that a pre-

existing gas cap was not required for ^4He-associated N_2 to begin degassing and that the ^4He and N_2 in these systems is almost entirely sourced from groundwater.

In all wells the depth of the limit of the N_2 saturation threshold appears to start within the underlying basement, indicating the potential for the mobilisation and degassing of fluids containing ^4He-associated N_2 and ^4He from depths up to 3.5 km below the producing reservoir in the case of the International Helium Wood Mtn.

The shallow depth (~1 km) associated with the Harley Dome field N_2 saturation threshold supports the radiogenic ratios exhibited (**Figure 4.6**) which indicate a low temperature, shallow crustal source. The same can be observed of the deeper crustal saturation threshold associated with the Weil #1 and International Helium Wood Mtn wells which show radiogenic ratios similar to average crustal values (**Figure 4.10**).

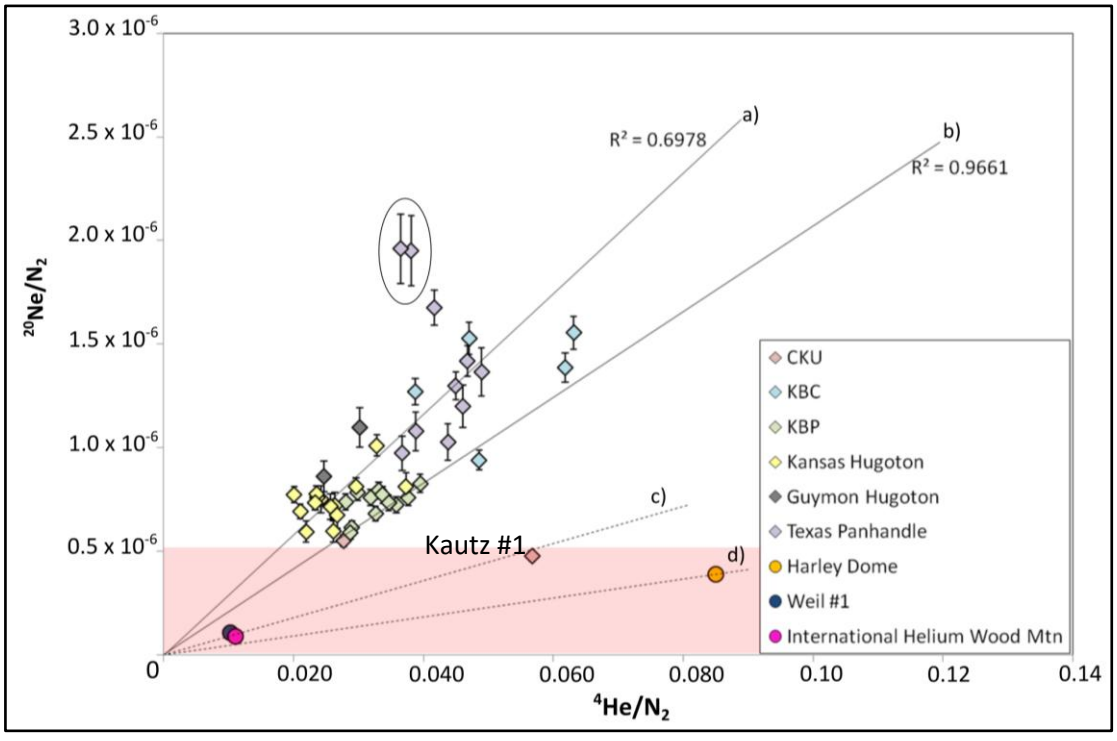

Figure 4.10.: Plot showing groundwater-derived ^{20}Ne vs radiogenic-sourced ^4He where both variables are normalised to N_2. Mixing lines a) and b) are from the previous dataset (Chapter 3, this thesis). Hypothetical mixing lines (dashed): c) includes only the International Helium Wood Mtn and Weil #1 wells and d) includes only the Harley Dome sample. The area highlighted red denotes a potential zone of low groundwater

contact with gases which may indicate that sample gases were exsolved into traps shortly after mixing with groundwater.

From Figure 4.10 the N_2-^4He-rich wells have all experienced significantly less groundwater contact than the CH_4-rich Hugoton-Panhandle and Kansas Basin systems except for the Kautz #1 well from the CKU samples which falls along mixing line c) associated with the International Helium Wood Mtn and Weil #1 wells. The International Helium Wood Mtn and Weil #1 wells have $^4He/N_2$ and $^{20}Ne/N_2$ ratios which are within error of each other which potentially indicates both a similar source and amount of groundwater contact.

The N_2-^4He rich wells and the Kautz #1 well all fall within a lower groundwater contact region (designated on Figure 4.10. as a highlighted red zone) which could indicate the degassing of a significant portion of the ^4He-associated N_2 and ^4He as a free gas phase; a condition which is stipulated for explaining the highly oversaturated Kautz #1 well (Chapter 3, this thesis). However, we do not observe the extent of oversaturation seen in the Kautz #1 well in any of the N_2-^4He wells; in fact the extent of oversaturation in these wells is similar to that seen in the KBP and McCune 1-A wells from the Kansas Basin and Central Kansas Uplift datasets.

We propose that this similarity could still be due to the introduction of a free gas phase contacting groundwater before degassing into reservoirs so reservoirs which show an oversaturation of ^4He-associated N_2 greater than ~2x the saturation limit may indicate the interaction of a free gas phase with groundwater; the higher the degree of oversaturation, the less contact the free gas phase has had with local groundwater.

4.5.3. Characterising the groundwater component of ^4He-rich fields

By looking at other wells and calculating saturation thresholds for literature data we may be able to begin to characterise the groundwater relationship between ^4He-rich fields (<0.1% ^4He). The ^4He-rich fields for which N_2 saturation is calculated below are all CO_2-^4He rich fields from Gilfillan et al., (2008) due to the scarcity of noble gas datasets for ^4He-rich fields. The assumption is made that all N_2 in these fields is sourced from the crust and therefore associated with the ^4He.

Study Area	**Average $N_2/^{20}Ne$ (x 10^7)**	**Range of ^4He-associated N_2 concentration in groundwater ($cm^3STP(N_2)/cm^3$)**	**Range of N_2 concentration saturation points in groundwater under reservoir conditions ($cm^3STP(N_2)/cm^3$)**	**Depth range (m)**	**Depth at which max saturation threshold is reached under reservoir conditions (m)**
McCallum Field, Colorado, USA	1.57	1.39-5.19	1.06-1.29	1500-1900	4890
McElmo Dome, Colorado, USA	0.65	0.61-2.52	1.45-2.09	1800-2600	3010
Doe Canyon, Colorado, USA	0.24	0.43	0.35	2550	3050
St John's Dome, Arizona, USA	0.05	0.08-0.09	0.39	200-700	

Table 4.5.: Comparisons of N_2 saturation in groundwater compared to modern reservoir conditions for CO_2-rich helium reservoirs. For McCallum and St John's Dome a hydrostatic gradient (1 atm/m) and a salinity of 4M is assumed due to lack of data on these aspects of reservoir conditions. Reservoir depths are sourced from Gilfillan, (2006) except for: 1) the Doe Canyon well which has instead derived the depth of the reservoir from the USGS, 1995 and the reservoir pressure of 51.0 atm from Back et al., (2012) and 2) McElmo Dome which was calculated with a pressure of 175.6 atm at 2107.7 m depth and salinity of 0.86M NaCl from Gerling, (1983). The temperature gradient at locations is assumed to be 30°C/km.

Unlike the N_2-^4He rich wells there are variations within the different CO_2-rich fields. In the McCallum Field all wells sampled by Gilfillan et al., (2008) are oversaturated with regard to the N_2 saturation threshold at that depth whereas St John's Dome is undersaturated with N_2 concentrations approximately 4 times lower than the saturation threshold. From the previous study this indicates to us that the ^4He associated N_2 gas in St John's Dome required an in-place gas phase before groundwater degassing of N_2 and ^4He took place. In this case the in place gas phase was most likely CO_2 instead of CH_4. This is the opposite of the McCallum field which, due to N_2 oversaturation of the groundwater, did not require an in place gas phase to begin degassing N_2 and presumably associated ^4He into pre-existing traps. This was then most likely diluted by the introduction of CO_2 into the reservoir.

Despite the low ^{20}Ne associated with the field, the McElmo Dome shows under-saturation of N_2 in groundwater relative to the N_2 saturation threshold except in one well, HD-2, which is oversaturated in N_2. There is no clear geological reason as to why this well would be unique however the $N_2/^{20}Ne$ ratio from that well is within 1σ error of other wells which are below the saturation threshold, therefore given the large uncertainty associated with the reservoir parameters too it is likely that all wells at McElmo Dome are under-saturated in N_2. Interestingly the Doe Canyon reservoir, which is oversaturated in N_2, is only 5 km away from McElmo Dome but is apparently from a separate, structurally isolated field (Gilfillan, 2006).

Gilfillan et al., (2008) postulated that there were active groundwater flow regimes associated with the McElmo Dome, St John's Dome and McCallum field which was causing the re-dissolution of CO_2 into the groundwater phase due to an influx of undersaturated freshwater. This influx of freshwater potentially containing ^4He-associated N_2 and associated radiogenic gases (^4He, $^{21}Ne^*$ and $^{40}Ar^*$) may have

contacted the resident CO_2 gas phase which lead to the degassing of ^{4}He-associated N_2 and associated gases into these reservoirs while at the same time CO_2 was being dissolved into solution; a similar mechanism to that associated with the CH_4-rich Hugoton-Panhandle and KBC datasets. Data from the St John's Dome also shows that ^{4}He and N_2 are positively correlated to closer proximity and depth to the gas-water contact in the fields (Gilfillan, 2006).

The McCallum field may not have as straightforward a mechanism as St John's Dome and McElmo Dome since it also seems to have a significant CH_4 component associated with reservoir gases; the source of which has not been determined and the groundwater-derived noble gases from the field indicate that closed system batch equilibration (either dissolution into or degassing of noble gases from groundwater) may have occurred across the field.

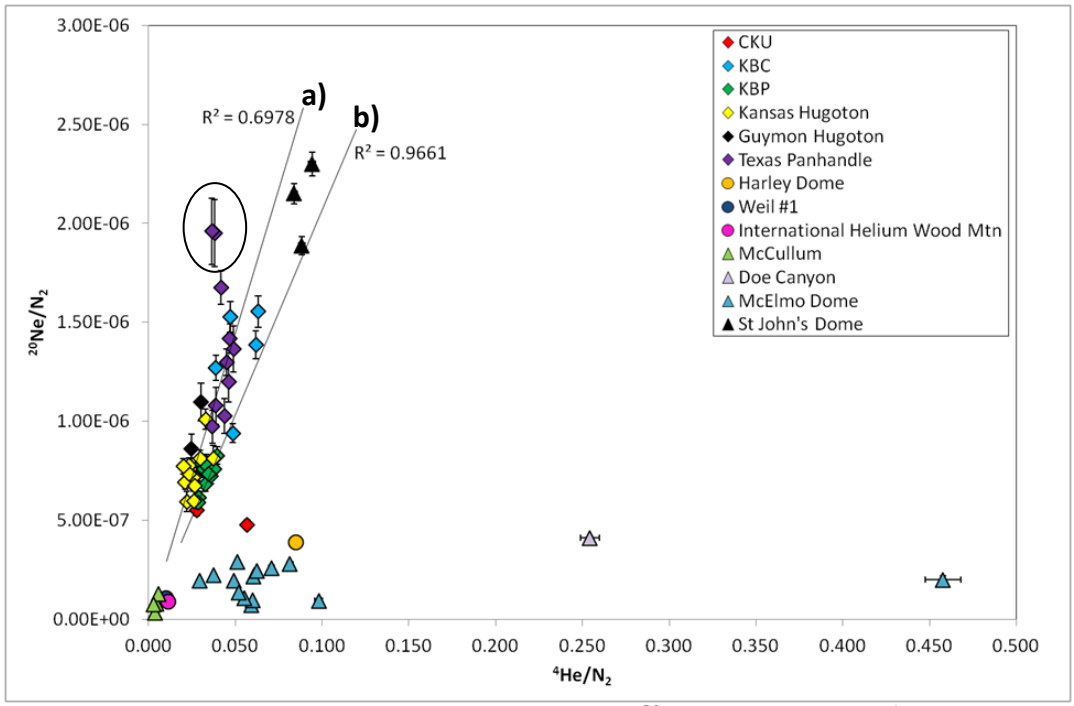

Figure 4.11.: Plots showing groundwater-derived ^{20}Ne vs radiogenic ^{4}He where both variables are normalised to N_2. a) Original trend from Ballentine and Sherwood-Lollar, (2002) (Hugoton-Panhandle without the Sarah Claybaugh and Donelson, et al. samples), b) Southern KBP samples. The intersection of all lines of best-fit are within error of the origin.

Despite the lack of N_2 isotopic data from these fields if we apply the same assumptions to CO_2-rich fields as with N_2-rich and CH_4-rich fields then the ^4He in these fields should be associated with a crust-sourced N_2 component which are both positively correlated with groundwater (^{20}Ne). However we do not have enough data at this time to definitively confirm this for these fields.

4.6. Summary

Spatially unrelated N_2-^4He rich wells from both the south and north of North America show a relatively narrow range of N_2 isotopes which are preferentially depleted in ^{15}N (+1.00‰ to +2.45‰) indicating a source which is most likely low temperature metamorphosed crust. In the northern wells (International Helium Wood Mtn and Weil #1) radiogenic ratios are within error of average crustal ratios and this combined with the depth of wells to basement most likely indicates that the source is from the underlying basement, however, for the Harley Dome well, the source is considerably shallower (< 1km) and could be either basement or sediment derived.

Despite the narrow range of $\delta^{15}N$ values, these wells have a wide range of $^4He/N_2$ endmembers which are remarkably consistent within each locality (0.010 to 0.011 in the north and 0.085 to 0.089 in the south). This polarisation of the $^4He/N_2$ endmembers may either be related to the chemical composition of the underlying source rocks in the regions or the accumulation time within the source rocks before the release of ^4He-associated N_2 and associated radiogenic isotopes.

All N_2-^4He rich wells show consistently less groundwater contact than in the Hugoton-Panhandle-Kansas Basin dataset and lie in the range of the Kautz #1 well

from the Central Kansas Uplift samples which may indicate contact between a free gas phase and groundwater before degassing into reservoirs. CO_2-rich wells in the south record $^4He/N_2$ ratios of up to 0.254 in the Doe Canyon field showing enrichment in ^4He which could be explained by a longer accumulation time in the crust before release.

In all fields the mechanism for ^4He and associated N_2 degassing into reservoirs appears to be related to the groundwater and the saturation threshold of ^4He associated N_2. In cases where the groundwater is oversaturated in ^4He-associated N_2, groundwater degassing will occur without the need for a primary gas cap such as CH_4 or CO_2 to be present in the reservoir, occasionally allowing the formation of N_2-rich ^4He field unless it is diluted by another gas. Conversely, in cases where the groundwater is undersaturated in N_2, contacting a primary gas cap is needed in order for the exsolution of ^4He-associated N_2 to occur and with it ^4He and other associated noble gas isotopes.

Chapter Five: High helium systems in Tanzania

5.1. Introduction

Following on from previous chapters the key geological features which an area must have in order to be considered potentially helium-rich are: 1) an area of stable crust which has been quiescent for a significant period of geological time, 2) the area has then been disturbed by a more recent tectonic event such as orogeny or rifting and 3) there are trapping structures in place for the released crust-derived gases from the tectonic event.

An area which potentially fits all three of these key features is Tanzania which contains: 1) the Archean-aged Tanzanian Craton and surrounding mobile belts which have been stable since at most 2.7 Ga, 2) rifting and associated volcanism occurred around the craton and mobile belts from approximately 25 Ma onwards and 3) trapping structures have been reported in this region for the rift basins in the Western Rift Arm such as the Rukwa Basin and the Albert Basin (**Figure 5.1**). The Rukwa Basin is of particular interest for helium exploration due to recent developments in the region by the exploration company Helium One.

The region surrounding the Tanzanian Craton offers a unique opportunity for a first look at a 'play fairway' analysis for helium exploration which could potentially be used to further narrow down basin areas that could contain helium-rich reservoirs. The following sections detail the stages involved in the 'play fairway' analysis of the Tanzania region and culminate in a 'play fairway' analysis of the areas surrounding the craton.

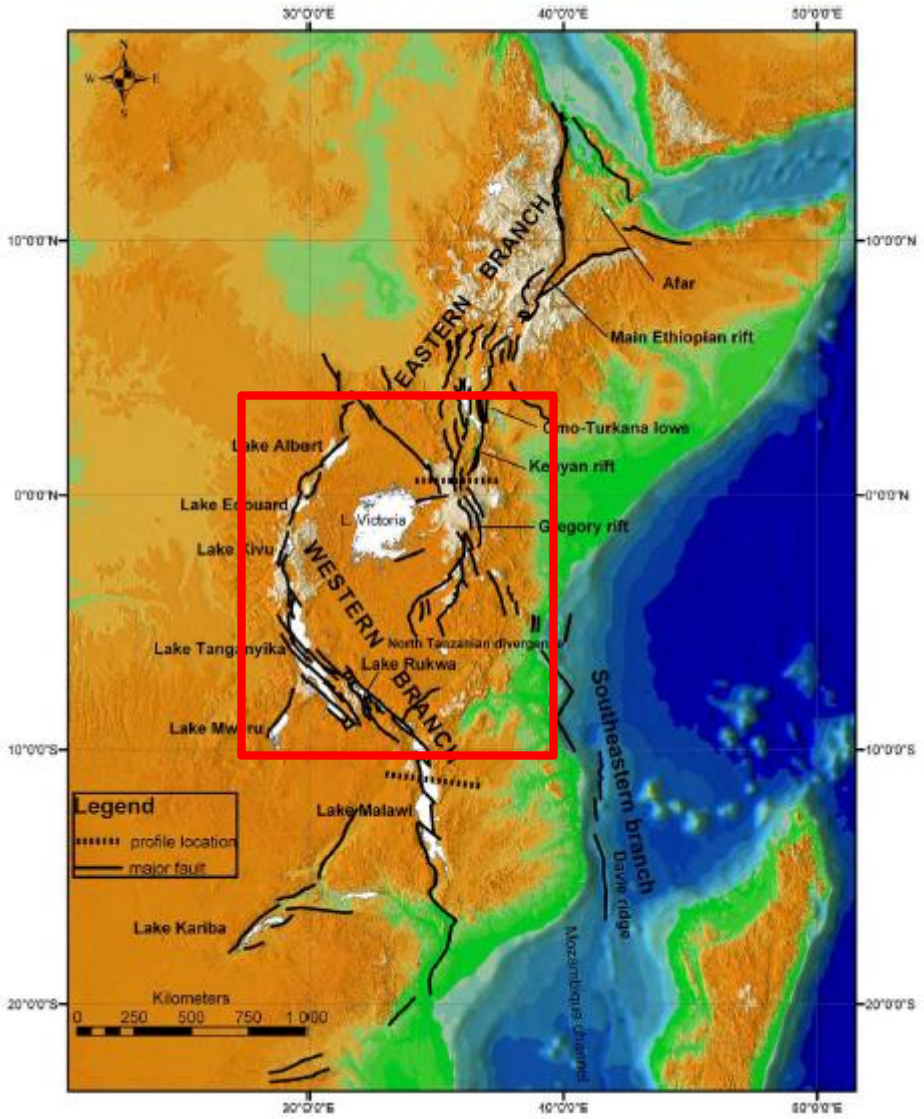

Figure 5.1.: Modified from Chorowicz, (2005). The position of the full study region in relation to the rest of Africa (red box).

5.2. The geological history of Tanzania

The Archean-aged Tanzanian Craton, which has been radiometrically dated as between 2.5-1.8 Ga, lies in the centre of Tanzania within the East African Plateau in-between two branches of the East African Rift System (EARS) (**Figure 5.2**). It is approximately 350,000 km^2 and has an average elevation of 1.3 km (Weeraratne et al., 2003). The craton was emplaced around approximately 2.7 Ga and is primarily composed of granite-greenstone terranes with ages upward of 2.4 Ga (Pinna et al., 1994; Dawson, 2008). Greenstone belts within the craton typically show greenschist to amphibolites facies metamorphic grade however granulite facies metamorphism is present within the Dodoman gneiss belts to the south. This shift in metamorphic grade from north to south has been speculated to be due to domains within the craton being produced from different depths of the crust (Borg and Shackleton, 1997).

The Tanzanian Craton has experienced several collisional events in the early stages of its geological history resulting in the mobile belts surrounding its perimeter. The Usagara (2.0-1.8 Ga) and Ubendian (2.1-1.8 Ga) mobile belts formed via subduction-related accretion against the craton in the early Proterozoic to the southeast and southwest (Quennell et al., 1956; Dawson, 2008; Boniface et al., 2012).

Metamorphism within the Usagaran Belt has been determined as predominantly high-grade granulite and eclogite facies with a low-grade overprint from reworking by the Pan-African Orogeny (Lenoir et al., 1994; Möller et al., 1995). The Ubendian Belt has a similar composition to the Usagaran and displays the same degree of medium to high-grade granulite facies metamorphism with terranes within the belt consisting of gneiss and granite. Localised eclogite facies in

the region point to maximum temperatures of 17 kbar and 900°C. Close to the Rungwe Volcanic Province (RVP) in the south, the Mbozi terrane contains syenite and granulite (Lenoir et al., 1994).

The eastern Mozambique Belt was formed by a younger, late Proterozoic oblique collisional event (<1.3 Ga) thought to be between east and west Gondwana and was subsequently reworked by the multistage Pan African Orogeny (950-550 Ma) (Muhongo and Lenoir, 1994; Lenoir et al., 1994; Mruma, 1995; Fritz et al., 2005; Vogt et al., 2006; Dawson, 2008; Macheyeki et al., 2008). Within the belt, estimated values for peak granulite facies metamorphism are 12–13 kbar and 750–800°C. Post this stage retrogression to amphibolites facies occurred (Sommer et al., 2003).

The Cenozoic-aged East African Rift System (EARS) is one of the few modern examples of a currently active intracontinental rift zone. The EARS consists of two main branches: the younger, less volcanically active Western rift valley and the older, volcanic Eastern (Gregory) rift valley. The Eastern Branch of the EARS is approximately 2200 km long and runs from the Afar Triangle in the north to terminate against the Tanzanian Craton at the North Tanzanian Divergence whereas the Western Branch is approximately 2100 km long running from Lake Albert to Lake Malawi.

In Tanzania the initiation of the first stage of rifting for the south propagating Western branch is determined to be around 12 Ma whereas most of the Eastern branch of the EARS had been established by approximately 20 Ma (Delvaux, 1991; Wescott et al., 1991; Burke, 1996; Morley et al., 1999; Nyblade and Brazier, 2002). More recently the Western Branch has been determined to have been initiated earlier than previously measured at around 25 Ma (Roberts et al., 2012).

The pattern of EARS rifting around the Tanzanian Craton, most likely caused by the displacement of melt from a shallow plume beneath the craton, has been preferentially channelled by the mobile belts which have thinner, weaker lithosphere beneath them than the craton and therefore presented areas of weakness susceptible to fault reactivation and volcanism (Ebinger et al., 1997; Weeraratne et al., 2003) (**Figure 5.2**). This ensures that faulting caused by the rift arms is confined to the edges of the craton which has left the majority of the cratonic interior untouched.

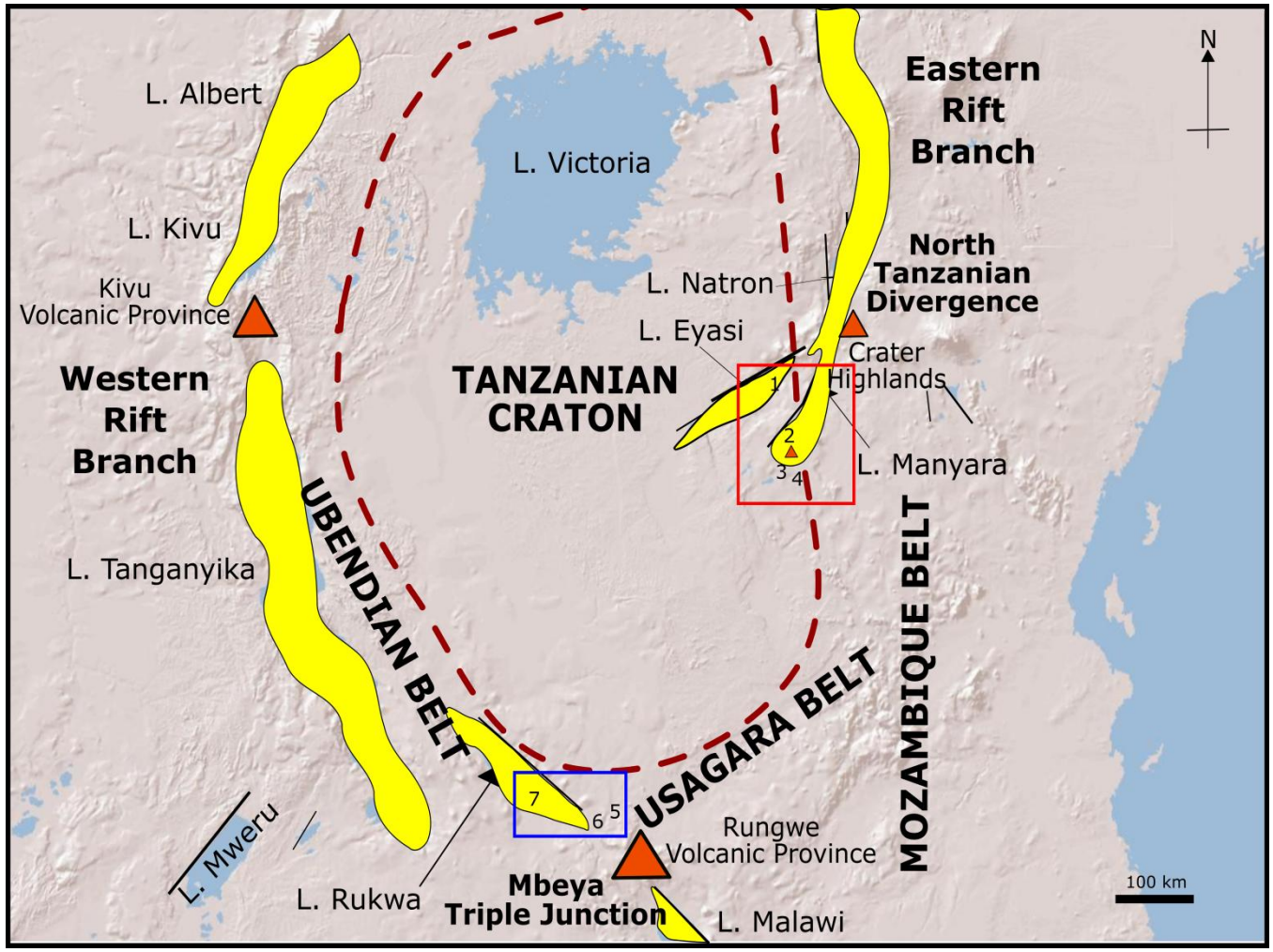

Figure 5.2: Map showing rift sediments (yellow) and volcanoes (orange triangles) in relation to the Tanzanian Craton (red dashed line), surrounding mobile belts, and the study areas (North Tanzanian Divergence (red box) and the Mbeya area (blue box).

Within the EARS rift arms are half graben rift basins. The infilling sediments in these basins are usually from Permian to Pliocene in age and show evidence of the more recent local tectonic events which shaped the region (Delvaux et al., 1991; Roberts et al., 2004; Roberts et al., 2012). In the Western rift branch these sedimentary sequences can be up to 11 km thick in some basins including the Rukwa Basin (the site of one of the samples from the Mbeya study area) (Wheeler and Karson, 1994).

5.3. Prior precedent for ^{4}He release in Tanzania

From the previous section we have established the presence of three components in Tanzania which would aid in producing viable helium-rich reservoirs: 1) a stable craton and surrounding mobile belts which have been tectonically quiescent for at up to 2.5 Ga, 2) a younger tectonic event (25-20 Ma) which is causing heating and faulting of the previously stable crust and 3) localised sedimentary basins near the tectonic event which may contain trapping structures. From previous literature and this study we also have evidence that thermal springs in the region are actively producing high N_2 and ^{4}He gases; another indication that this region may contain viable helium reservoirs.

Thermal springs, both high temperature and low temperature are common but unevenly distributed features within the EARS and have attracted interest in the past due to their potential for commercial salt deposits, noble gases and geothermal energy (Nzaro, 1970; Omenda, 2005; Macheyeki et al., 2008; Delvaux et al., 2010; Kalberkamp et al., 2010; Kraml et al., 2010; Kraml et al., 2014; Harðarson, 2014; Kandie, 2014).

Thermal spring systems clearly follow parallel to the fault systems providing further evidence that these faults are open and active and linked to an underground geothermal system which has been of interest in the past (Hochstein, 2000; Mnjokava, 2007).

Gas samples for this study were taken from thermal springs at 7 locations: Eyasi, Balangida, Gonga, Mponde, Ivuna (Rukwa Basin), Idindiro and Rukwa in 2 main areas on both the Eastern and Western rift branches: 1) on the Eastern Branch the study area (red box) is within the Northern Tanzanian Divergence and 2) on the Western Branch the study area (blue box) is the Rukwa Basin and Rungwe Volcanic Province (**Figure 5.2**).

Previous literature measuring the gas composition of the thermal springs in our first sample study area the North Tanzanian Divergence (NTD) was recorded by James (1967a) who found that the gas emanating from the thermal springs at the locations was predominantly N_2 and ^{4}He-rich (**Figure 5.3a**).

James (1967b) determined that in general the thermal springs in the Northern Tanzanian Divergence area were situated within basement rocks in basins or areas with little to no overlying sediments. It was also observed that the thermal springs were relatively far from centres of volcanic activity such as the Crater Highlands and that most springs in that region were connected with major faults which were most likely basement-linked faults (Macheyeki et al., 2008).

James (1967b) proposed a mixed mantle-meteoric source for the origin of gases from the thermal springs however, until this study, no isotopic analyses were conducted on the gases to either confirm or reject this hypothesis.

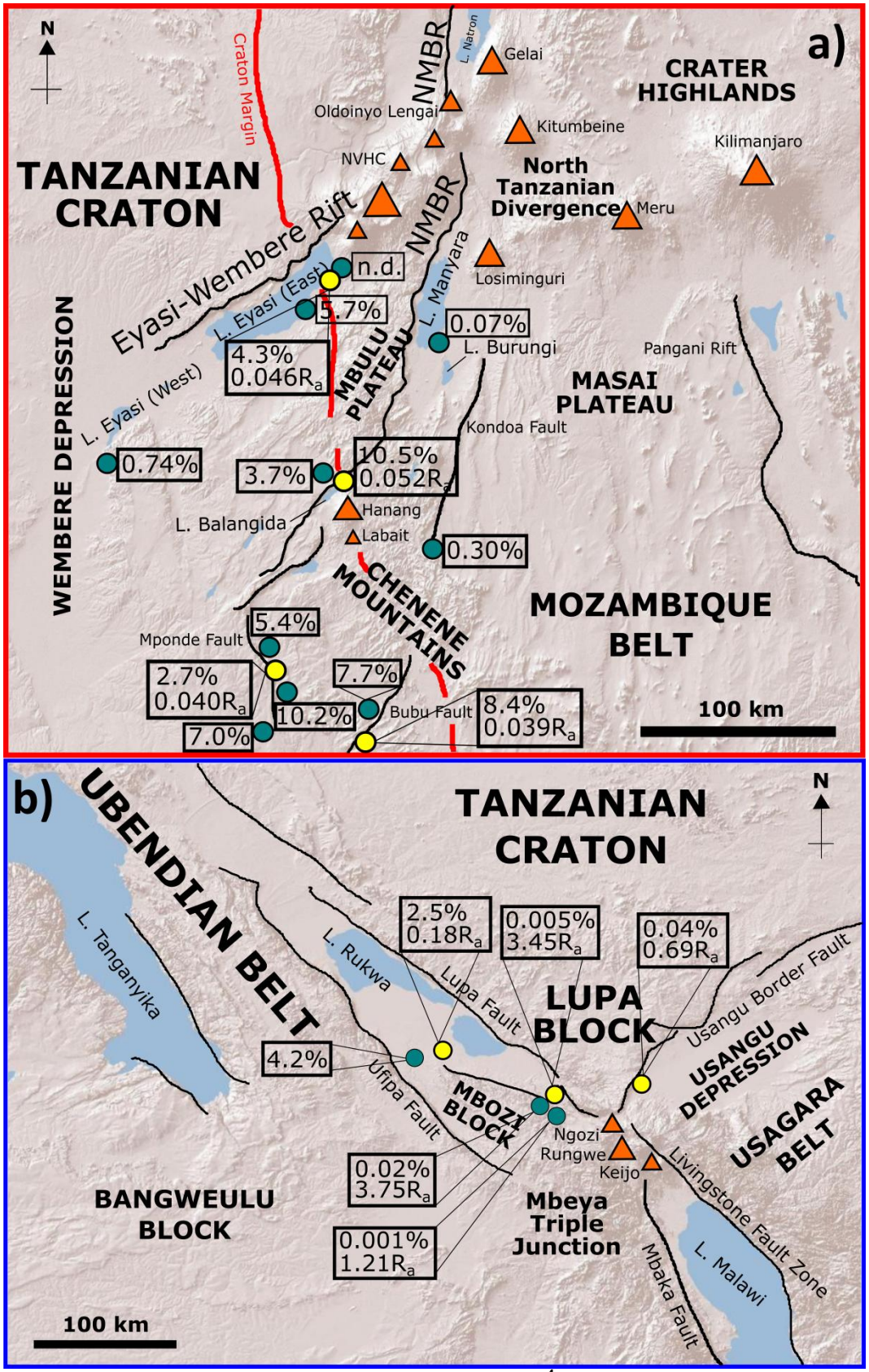

Figure 5.3.: Maps showing the positioning of previous ^{4}He concentrations (blue circles) in comparison with new ^{4}He concentration data and R_a values in the NTD and Mbeya study areas (yellow circles). a) NTD study area; old data is from James (1967) and is in relation to the craton margin (red line), volcanoes (orange triangles) and main faults (black lines). NMBR stands for (Natron-Manyara-Balangida Rift). b) Mbeya study

area; old data is from James, (1967a) and Barry et al., (2013) and is in relation to volcanoes (orange triangles) and main faults (black lines).

Literature values can be found in both James, (1967a) and Barry et al., 2013 on our second study area in the Western branch of the EARS (**Figure 5.3b**).

Barry et al., (2013) measured low ^4He concentrations and high CO_2 concentrations in sampled thermal springs from the Ngozi-Songwe hydrothermal system and the Rungwe Volcanic Province (RVP) consisting of the Ngozi, Rungwe and Keijo volcanoes. They concluded from gas and water analyses that the amount of crustal contamination seen in their samples was controlled by: 1) the proximity of the sample areas to the RVP, 2) the extent of the gas interaction with the hydrothermal system and 3) the extent of rifting in the region which controls the release and therefore input of crustal ^4He.

In contrast, James, (1967a) recorded high concentrations of ^4He within the Rukwa Basin of around 4.2% and high N_2 with it which potentially substantiates the observations made by Barry et al of increasing crustal signal distal from volcanoes in the region.

5.3.1. Determining the ^4He potential of Tanzania

Now that we have identified Tanzania as an area which fulfils two of the criteria for our helium exploration methology: 1) it has an area/areas of crust which have been stable for a long period of geological time enabling them to accumulate high ^4He concentrations (the Tanzanian Craton and surrounding mobile belts from at most 2.7 Ga) and 2) these areas of crust have been disturbed by a relatively recent tectonic event (the EARS from 25-20 Ma depending on the rift branch) plus an extra

point 3) active degassing of N_2-^{4}He rich gases from thermal springs, we can perform a simple ^{4}He mass balance calculation to estimate the maximum volume of ^{4}He which can potentially be produced within the Tanzanian system and compare this to estimates from the under investigation Rukwa Basin.

Within the Tanzanian helium system we can identify 4 distinct producing areas of interest which are related to the sample study areas outlined in the previous section. These areas are: 1) the Tanzanian Craton (350**,**000 km^2), 2) the Ubendian Belt (75,000 km^2), 3) the Usagara Belt (57,600 km^2), 4) the North Tanzanian Divergence (NTD) which consists of parts of the reworked Usagaran Belt, Mozambique Belt and the Tanzanian Craton however for the purposes of the calculation is confined to the Gregory (Eastern) rift arm (42,500 km^2), and on a local scale 5) the Rukwa Basin within the Ubendian Belt (12,800 km^2) (**Figure 5.4**).

For each crustal production area it is assumed due to the information available on the underlying basement that: 1) the crust to a depth of 10 km is a potential source of ^{4}He, 2) the bulk homogenous crust has an average U and Th content (2.8 ppm and 10.7 ppm respectively) despite measurements regarding the Musoma-Mara greenstone belt (Tanzanian Craton) of < 18.70 ppm U and < 52.1 ppm Th (Manya et al., 2007; Mshiu and Maboko, 2012), 3) the basement has an average crustal density of 2.7 cm^3/g and 4) the basement is primarily granitic and has an average porosity of 0.64% (Chaki et al., 2008).

Differing metamorphic grades within lithologies can be responsible for the redistribution of uranium and thorium in the crust. It has been shown in studies that a degree of U depletion and redistribution occurs when rocks pass from pyroxene facies to granulite facies during high grade metamorphism which can be as severe as < 75% (Moorbath et al., 1969; Rosholt et al., 1973). Whether this has occurred

within the study areas is uncertain since no whole rock analyses for U-Th-Pb have been conducted on either the Ubendian or Usagaran Belts. However, in the Mozambique Belt overprinting by several thermal events can be deduced from U-Pb dating of zircons from the region; indicating U and Pb loss as the zircons were reset by each event (Coolen et al., 1982). In an attempt to constrain this factor the youngest zircon ages recorded in each region are taken to be the last time the system was reset by a major thermotectonic event and that since the event average U concentrations have been generating ^{4}He volumes.

For the Rukwa Basin two scenarios are considered: 1) time since the underlying basement was last disturbed by a tectono-thermal event and 2) time since the first deposition of sediments in the basin (the Karoo Supergroup). For the calculations the thickness of sediments in the Rukwa Basin is averaged to be 7.5 km (Delvaux et al., 1998) and the porosity is averaged to be 16.5% (Baiyegunhi et al., 2014) (**Table 5.1**).

Region and age of last major thermotectonic zircon reset event prior to rifting	**Reset event**	**Helium volume produced (m^3)**	**Source area (km^2)**	**References**
Tanzanian Craton (2.4 Ga)	Last phase of metamorphism	1.7×10^{13}	350,000	Pinna et al., 1994; Weeraratne et al., 2003
Ubendian Belt (570 Ma)	Reworking during the Pan-African Orogeny	7.4×10^{11}	75,000	Boniface et al., 2012; Boniface and Schenk, 2012
Southern Usagaran Belt (570 Ma)	Reworking during the Pan-African Orogeny	5.7×10^{11}	57,600	Reddy et al., 2004; Boniface et al., 2012
North Tanzanian Divergence (2.0 Ga)	Accretion onto the Tanzanian craton	1.6×10^{12}	42,500	Ebinger et al., 1997; Dawson, 2008

Rukwa Basin (basement) (570 Ma)	Reworking during the Pan-African Orogeny	1.3×10^{11}	12,800	Wescott et al., 1991; Boniface et al., 2012
Rukwa Basin (sediments) (260 Ma)	Deposition of the Karoo Supergroup	3.3×10^{10}	12,800	Wescott et al., 1991; Delvaux et al., 1998; Baiyegunhi et al., 2014

Table 5.1.: Helium volume produced from different parts of the Tanzanian system.

When the ^{4}He volumes calculated above are compared to the probable ^{4}He reserves calculated for the Rukwa Basin of 1.5×10^9 m^3 it is observed that the basement beneath the Rukwa Basin could supply the entire reserve by releasing only 1.2% of its produced ^{4}He volume when efficient migration and trapping in the region are assumed.

The Tanzanian Craton and the surrounding mobile belts have the capability of producing vast ^{4}He volumes totalling at least 2.0×10^{13} m^3 (STP) since the last period of crust stability before rifting. From the above helium mass balance calculations it is apparent that generating a reserve on the potential scale of the Rukwa Basin does not require the efficient release of gases from source in this region and that the release of helium-rich gases is still occurring during modern times which could indicate that newer traps are being filled in the Tanzania region. The potential reserves estimated for the Rukwa Basin are the equivalent of the supply for approximately 14 years worth of global helium demand.

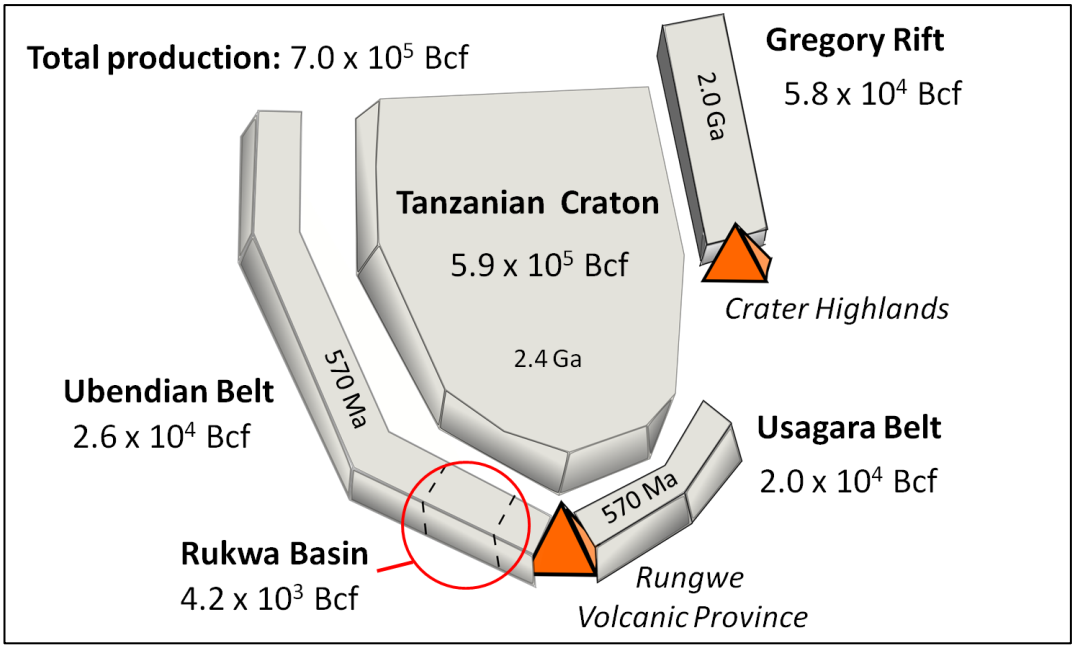

Figure 5.4.: Helium production from different areas of the Tanzanian system from the time since their last tectonic event (before the EARS).

5.4. The geology of the study locations

5.4.1. Study area 1: The North Tanzanian Divergence

The North Tanzanian Divergence (NTD) is situated within the Eastern arm of the EARS. The main rift segment associated with the sample areas contains the Eyasi-Wembere, Natron-Manyara-Balangida (NMBR), Mponde and Bubu fault systems. These diverging rift structures are underlain by the Precambrian-aged basement rocks of the Mozambique Belt and the Archean-aged Tanzanian craton (Le Gall et al, 2008).

All faults related to the sample locations in the NTD were formed during the second stage of rifting in the region (approximately 1.2 Ma) and are linked together through a zig-zag string of rifting. Rift patterns at the surface mirror basement faulting at depth which indicates the reactivation of these basement faults (Ebinger et al., 1997; Nyblade and Brazier, 2002).

Fault-bounded half-graben basins up to 3 km deep are only documented along the Eyasi and Manyara parts of the rift (Ebinger et al., 1997).

The rift structures in the NTD do not represent the termination of the Eastern rift system; EARS related extension still exists approximately 600 km south of the region where it may link into the Western branch of the EARS around the Mbeya Triple Junction (Le Gall et al., 2004; Le Gall et al., 2008).

5.4.1.1. Eyasi

The Eyasi Basin is a half-graben split into two sub-basins. The sub-basins are thought to either be separated by a section of uplifted basement beneath the main basin) or by a transfer fault (Ebinger et al., 1997; Foster et al., 1997). The eastern part of the basin is strongly bounded by the Eyasi fault (100 km long) to the NW. On the opposite side of the basin the faults are smaller in length (<10 km) and probably represent faulting of the central basement upwarp that splits the main basin in two. The Eyasi Basin is relatively shallow (1-2 km) (Ebinger et al., 1997; Dawson, 2008).

Volcanic units at Eyasi are only exposed at the northern-most margin of the basin which is the nearest to the Crater Highlands. These volcanics are derived from the nearby Crater Highlands; specifically from eruptions of the Lemagrut and Oldeani volcanoes around approximately 5.5 Ma.

The last movement along the Eyasi-Wembere Fault has been dated to after 3.1 Ma ± 0.3 Ma which postdates the formation of the Crater Highlands.

5.4.1.2. Balangida

The thermal spring is situated in the half-graben Balangida Basin which lies along the Balangida fault. The Balangida Basin is separated from the Manyara Basin

by uplifted metamorphic rocks (Dawson, 2008). Nearby volcanoes are Hanang (1.5-0.9 Ma) and Labait; with Hanang occupying the eastern end of the Balangida Basin. There is a potential high temperature thermal anomaly around the southern end of the east propagating rift near Labait which may indicate that this rift arm is still propagating (Foster et al., 1997; Dawson, 2008).

Archean-aged basement rocks of the Tanzanian craton are exposed throughout the area indicating very little cumulative extension and subsidence took place. The depth of the Balangida Basin is believed to be very shallow compared with other rift basins in the same region and has been estimated to have a depth of < 1 km (Ebinger et al., 1997; Dawson, 2008).

Balangida and Eyasi are thought to be linked by rifting in the area via two branches of the Eastern Rift (the Natron-Manyara-Balangida and the Eyasi-Wembere). These two rifts are known to transect the boundary between Archean and Proterozoic aged crust (Foster et al., 1997).

5.4.1.3. Gonga

The Gonga thermal spring is situated on a segment of the Bubu fault; a seismically active normal fault. Evidence of oldest event along the Bubu fault was carbon dated to a maximum of 8536 years indicating that it is a very recent fault which is prone to cyclic earthquake events (Macheyeki et al., 2012). Predicted earthquakes for some of the fault segments are up to magnitude 7.8 indicating the fault is potentially deep and the throw on most of the fault segments are on a km scale.

The Bubu fault crosses the Chenene Mountains which was uplifted by a thrust fault between the Mozambique Belt and the Tanzanian Craton (Macheyeki et al., 2008; Msabi, 2010).

5.4.1.4. Mponde

The Mponde thermal spring is situated on the Mponde fault which is a seismically active normal fault within the Tanzanian craton (Macheyeki et al., 2008; Macheyeki et al., 2012). There is not much background literature around this area aside from previous gas component measurements of the thermal springs (James, 1967a; Walker, 1969).

5.4.2. Study area 2: The Mbeya Triple Junction

The Mbeya Triple Junction is thought to be an accommodation or transfer zone between the Rukwa, Livingstone and Usangu rift segments (Ebinger et al., 1989; Morley et al., 1990; Delvaux and Hanon, 1991; Delvaux, 2001). The Mbeya Triple Junction acts as the confluence for the Eastern and Western rift branches with the RVP in the middle of all three rift segments (Delvaux and Hanon, 1991; Mnjokava, 2007; Fontijn et al., 2010; Barry et al., 2013).

The Rukwa-Livingstone rift segment developed during the Permian-Triassic and was rejuvenated during the Mesozoic. The Usangu Basin developed in the Cenozoic which coincided with the second reactivation of the Rukwa-Livingstone rift segment and the onset of volcanism in the RVP (Ebinger et al., 1989; Delvaux and Hanon, 1991; Delvaux et al., 1992).

The Rukwa Basin, a NW trending half-graben, is bordered by the SW dipping Lupa fault which runs approximately NW-SE towards the RVP and the Livingstone rift segment. The orientation of the basin is thought to have been determined by the fabric of the pre-existing Precambrian Ubendian belt and Permian-aged rift alignment beneath the basin. The basin lies between the Tanganika and Malawi rifts (Delvaux and Hanon, 1991; Morley et al., 1992; Delvaux, 2001; Roberts et al., 2012).

The Rukwa Basin contains up to 11 km thick sediments and is currently under investigation for its viability as a high helium reservoir by the helium exploration company Helium One.

5.5. New results from Tanzania

In this section we present both the gas composition and noble gas makeup of the thermal spring gases sampled within the two study areas outlined in previous sections. All samples were collected by Dr Pete Barry (University of Oxford) and Thomas Abraham-James (Helium One). All noble gas measurements were conducted at the Noble Lab, University of Oxford and gas compositional analyses were conducted by Dr Thomas Darrah at Mendenhall Laboratory, Ohio (**Tables 5.3 and 5.4**).

In all samples $^{4}He/^{20}Ne$ ratios are significantly higher than that of air (0.032) and range between 330 and 8920. Air corrections to R_a ratios in samples have no significant effect on the R_a value. This indicates that there are negligible air contributions to ^{4}He concentrations in samples which means that $^{3}He/^{4}He$ ratios

which deviate from purely crustal ratios (0.020 R_a) are likely due to resolvable mantle contributions.

Sample name	**$^{3}He/^{4}He$ (Ra)**	**$^{20}Ne/^{22}Ne$**	**$^{21}Ne/^{22}Ne$**	**$^{40}Ar/^{36}Ar$**	**$^{38}Ar/^{36}Ar$**
Study area 1 (NTD)					
Balangida	0.053 (0.001)	9.74 (0.030)	0.031 (0.0003)	544 (1.2)	0.186 (0.0005)
Balangida	0.052 (0.001)	9.73 (0.030)	0.031 (0.0003)	549 (1.0)	0.186 (0.0005)
Gonga	0.039 (0.001)	9.71 (0.030)	0.029 (0.0003)	432 (1.1)	0.183 (0.0006)
Eyasi	0.046 (0.004)	9.72 (0.030)	0.029 (0.0003)	440 (1.5)	0.187 (0.0006)
Mponde	0.040 (0.002)	9.71 (0.030)	0.030 (0.0004)	410 (0.8)	0.184 (0.0005)
Study area 2 (Mbeya)					
Idindiro	0.69 (0.01)	10.04 (0.033)	0.030 (0.0003)	303 (0.2)	0.187 (0.0003)
Rukwa	3.45 (0.005)	10.04 (0.033)	0.030 (0.0003)	331 (0.9)	0.182 (0.001)
Rukwa	3.45 (0.005)	10.04 (0.033)	0.030 (0.0004)	336 (0.6)	0.184 (0.001)
Ivuna	0.18 (0.01)	9.68 (0.029)	0.032 (0.0004)	787 (0.8)	0.185 (0.0003)
Air *(Porcelli et al., 2002)*	**1**	**9.80 (0.080)**	**0.029 (0.0003)**	**295.5 (0.5)**	**0.188 (0.0004)**

Table 5.2.: Noble gas ratios for both study regions. 1σ errors for samples are shown in brackets.

Sample name	^{4}He concentration (cm^{3} STP) (x 10^{-2})	^{20}Ne concentration (cm^{3} STP) (x 10^{-5})	^{40}Ar concentration (cm^{3} STP) (x 10^{-2})	N_2 concentration (cm^{3} STP)
Study area 1 (NTD)				
Balangida	10.6 (0.42)	1.19 (0.015)	1.47 (0.042)	0.90
Balangida	10.4 (0.42)	1.17 (0.016)	1.59 (0.021)	0.90
Gonga	8.4 (0.35)	1.88 (0.033)	1.69 (0.043)	0.95
Eyasi	4.3 (0.29)	1.30 (0.016)	1.21 (0.020)	0.95
Mponde	2.7 (0.11)	1.10 (0.019)	1.11 (0.019)	
Study area 2 (Mbeya)				
Idindiro	0.04 (0.002)	0.028 (0.0004)	0.73 (0.017)	
Rukwa	0.0047 (0.0002)	0.014 (0.0004)	0.029 (0.0008)	
Rukwa	0.0043 (0.0002)	0.012 (0.0003)	0.025 (0.0006)	
Ivuna	2.5 (0.04)	0.22 (0.0011)	0.46 (0.002)	0.96
Air *(Porcelli et al., 2002)*	**0.000524 (0.000006)**	**1.65 (0.0036)**	**0.93 (0.001)**	0.78

Table 5.3.: Noble gas concentrations and N_2 concentrations from this study. 1σ errors for samples appear in brackets except for N_2 where no errors were provided.

5.5.1. Helium

The $^{3}He/^{4}He$ ratio (R_a) varies considerably both between and within study areas. Samples from study area 1 (NTD) have consistently low R_a values which range between 0.039 to 0.053 whereas samples from study area 2 (Mbeya) have a larger range of values between 0.18 to 3.45. From the R_a values alone it can be observed that samples from study area 1 show predominantly crustal R_a values (where 0.020 R_a = crust) whereas study area 2 shows a move towards a more magmatic signature (where 6.10 R_a = Sub-Continental Lithospheric Mantle or SCLM) (Gautheron and Moreira, 2002).

Concentrations of ^{4}He are above air concentrations throughout the samples however there is a significant split in concentration between the NTD samples and the Mbeya samples. Samples from the NTD are consistently high ^{4}He; ranging from 2.7 x 10^{-2} to 10.6 x 10^{-2} $cm^3STP(^{4}He)/cm^3$ whereas the Mbeya study area contains samples which show differences of orders of magnitude in ^{4}He concentrations from 4.3 x 10^{-5} to x 2.5 x 10^{-2} $cm^3STP(^{4}He)/cm^3$ (**Figure 5.3**).

Magmatic contributions to the ^{4}He concentrations in the NTD samples are between 0.3% and 0.5% assuming a crustal endmember of 0.020 R_a and a SCLM endmember of 6.10 R_a and magmatic contributions to ^{4}He concentrations in the Mbeya study area are significantly higher at 2.6% to 56.5%.

5.5.2. Neon

The concentration of ^{20}Ne in both study areas varies depending on the area. In the NTD samples concentrations range from 1.10 x 10^{-5} to 1.88 x 10^{-5}

$cm^3STP(^{20}Ne)/cm^3$ whereas the samples from the Mbeya study area exhibit lower concentrations of ^{20}Ne of between 1.20×10^{-7} to 2.20×10^{-6} $cm^3STP(^{20}Ne)/cm^3$ (**Table 5.3**).

$^{20}Ne/^{22}Ne$ ratios and $^{21}Ne/^{22}Ne$ ratios in the study areas all fall within 1σ error of air values (where the air $^{20}Ne/^{22}Ne$ ratio = 9.80 and $^{21}Ne/^{22}Ne$ ratio = 0.029) (**Table 5.2**).

5.5.3 Argon

The $^{40}Ar/^{36}Ar$ ratios in the Tanzanian study areas show variations within the study areas. In the NTD samples ratios vary between 410 and 549 and within the Mbeya area samples range from 303 to 787 compared with the air ratio of 295.5. Due to all samples being significantly above the air ratio it can be observed that all samples have a resolvable ^{40}Ar excess ($^{40}Ar^*$). $^{40}Ar^*$ contributes 27.9-46.1% of the NTD samples ^{40}Ar concentrations and 2.3-62.4% of ^{40}Ar concentrations in the Mbeya study area.

The ratios of $^{38}Ar/^{36}Ar$ for samples, which determine atmospheric contributions to gases, are all within 2σ of the air ratio (0.188).

5.6. Discussion

5.6.1. The uses of the radiogenic noble gases as a means of locating ^{4}He-rich areas

The Tanzanian study areas present a unique opportunity to explore the uses of the noble gases as a surface tracer for locating potential high ^{4}He reservoirs. This methodology is entirely dependent on gas escape features in the locality such as the thermal springs.

It can be observed from the gas composition of samples that all samples containing ^{4}He concentrations which exceed the economic threshold for viable reservoirs (0.1% <) contain high concentrations of N_2 as well (90% <).

In the Mbeya study area a trend towards high ^{4}He concentrations, associated high N_2 concentrations and low R_a values (indicating a predominantly crustal input) within the southern Rukwa Basin is seen whereas closer to the currently active RVP high CO_2, low N_2, low ^{4}He and high R_a values (consistent with a predominantly mantle input) are observed (Darrah, pers comms, 2016). This trend was also observed within the RVP by Barry et al., (2013).

As noted in Section 5.2.2. similar spatial patterns of ^{3}He/^{4}He (R_a), N_2 concentrations and CO_2 concentrations versus distance from volcanic centres have been observed in other regions and in all cases is thought to indicate binary mixing between a pure crustal endmember and a mantle endmember which is either SCLM or MORB related (Sano et al., 1984; Marty et al., 1989; Hilton et al.,1993; Van Soest et al., 1998; Weinlich et al., 1999; Barry et al., 2013).

If we assume that $^{3}He/^{4}He$ (R_a) values are primarily controlled by the extent of mixing between crust-derived N_2 and associated ^{4}He with concentrations of mantle-derived CO_2 and associated ^{3}He we can construct a simple binary mixing model for SCLM mantle (6.1 R_a) with a crustal endmember of (0.020 R_a) so as to ascertain 1) whether binary mixing applies to our sample areas and 2) the effect of the mixing of ^{4}He associated N_2 on the $^{4}He/^{40}Ar^*$ ratios in the areas.

For the mixing model we assume that the pure crustal endmember concentrations are represented by the Balangida sample from the NTD study area since the sample does not show significant fractionation and contains the highest concentrations of ^{4}He (10.5%). N_2 concentrations for this endmember are determined to be 89.0% with no CO_2 content. The mantle endmember is taken to be SCLM at 6.1 R_a with CO_2 concentrations of 99.9% and no N_2 content (**Figure 5.5**).

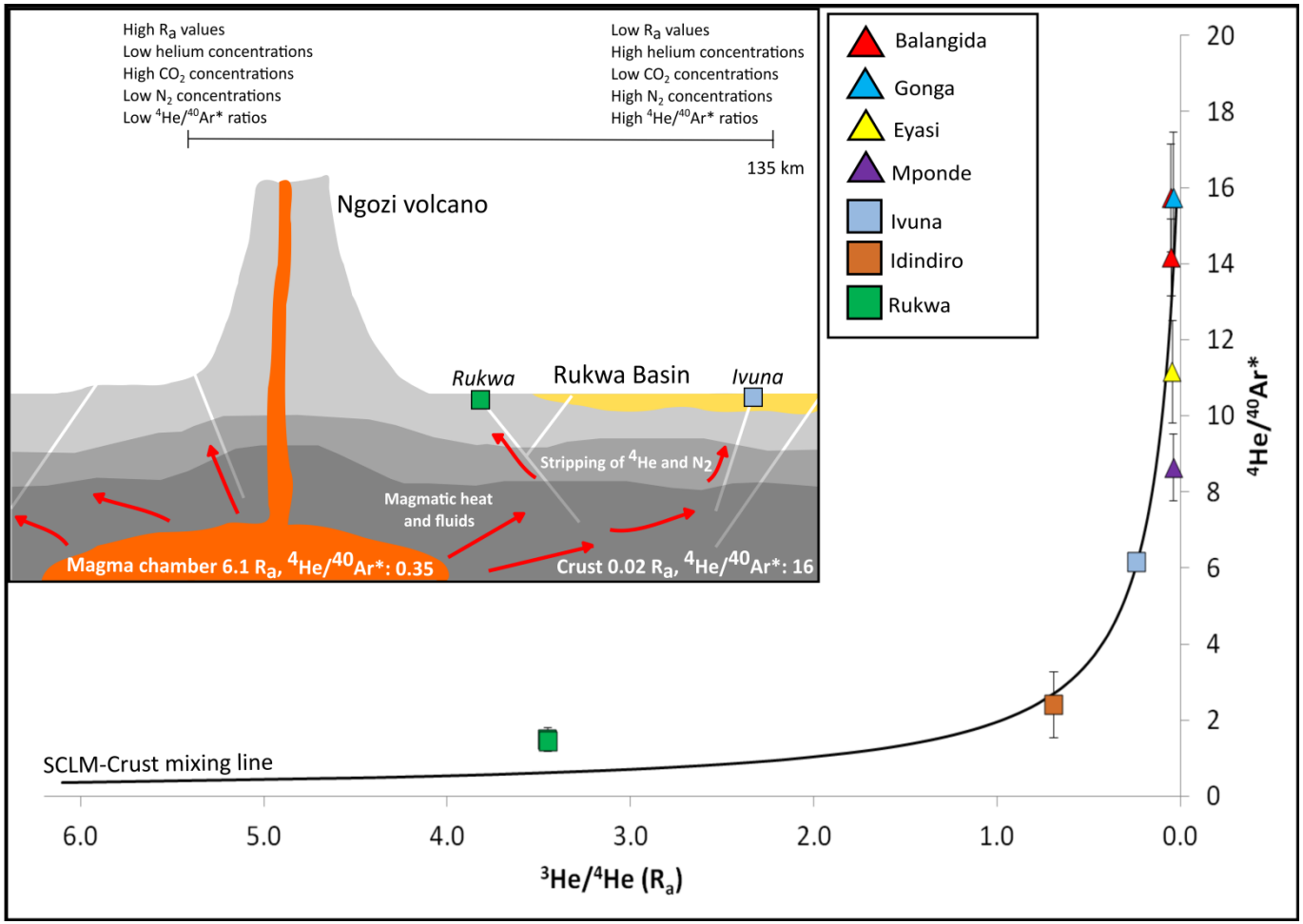

Figure 5.5.: Diagram showing the influence of binary mixing on spatial gas trends within the Mbeya area. Close to volcanic centres CO_2 and R_a values increase whereas N_2, ^4He and $^4He/^{40}Ar^*$ ratios decrease. Further away from the active volcano increases in N_2, ^4He, $^4He/^{40}Ar^*$ ratios and decreases in CO_2 and R_a value are seen.

Samples from both study areas fall along a binary mixing trend between crust-derived gases and mantle-derived gases. Closer to the active volcanic centres in the RVP there appears to be a dilution of magmatic gases produced by volcanism in the region by the older, dominant crust surrounding it which is also releasing accumulated gases due to the ongoing rifting. This binary relationship between crust and mantle gases indicates, in the context of helium exploration, that close to an active volcanic centre, ^{4}He concentrations will be diluted by CO_2 concentration and associated gases whereas 135 km away from the RVP a return to economic ^{4}He concentrations in gases is observed.

This adds another dimension to the process of helium exploration when in areas where active volcanism is occurring and should be taken into account in future studies which establish the boundary around active volcanic provinces where the risk from CO_2 dilution becomes too high to establish a high helium reservoir.

Helium volumes and the nitrogen associated with them in the study areas are being released from the basement and sediments by the heat generated by rifting and volcanism in the region. Helium then either diffuses into the overlying sediments until it is dissolved and transported elsewhere by hydrothermal systems or advects straight into reservoirs if underlying faults and fractures are present (Sano et al., 1988; Kennedy and Van Soest, 2005).

In some areas, such as in the Rukwa Basin, helium can potentially be trapped by stratigraphic traps and overlying salt layers. However, in areas which have high helium seeps, helium and associated gases can advect with nitrogen as a carrier gas up open faults and escape at the surface as a macroseep (Etiope and Martinelli, 2002; Walia et al., 2005). It is probable that these areas also contain active detectable soil

gas microseeps which can aid in the identification of reservoirs (Guerra and Lombardi, 2001).

5.6.2. Compiling a 'play fairway' assessment of Tanzania

From the above sections it has been established that the rocks within the Tanzania Craton and the regions surrounding the central craton have the potential to generate large volumes of helium and that this accumulated helium is currently being released by the heat generated by a potential shallow plume beneath the Tanzanian Craton which also causes associated volcanism (such as the Rungwe Volcanic Province, the Crater Highlands and the Kivu Volcanic Province), geothermal activity and rifting in the region.

The release of accumulated crustal ^{4}He and associated N_2 (< 10.5% ^{4}He) can be seen in the study area locations (Mbeya and the NDT) and has also been recorded in Uvinza (an area approximately 90 km to the east of Lake Tanganiyka) with gases measuring < 2.5% ^{4}He (Pflumio et al., 1994). In this region there are also potential trapping structures in place such as in the Rukwa Rift and the Albertine Graben (which consists of Lake Albert, Lake George, Lake Edward and Lake Kivu) (Abeinomugisha and Kasande, 2012; Abraham-James, pers comms, 2016). The 'play fairway' map showing potential basins which may contain high helium reservoirs in relation to the craton, volcanic centres and known trapping structures has been derived by combining information from Section 5.6.1 and Figure 5.3 (**Figure 5.6**).

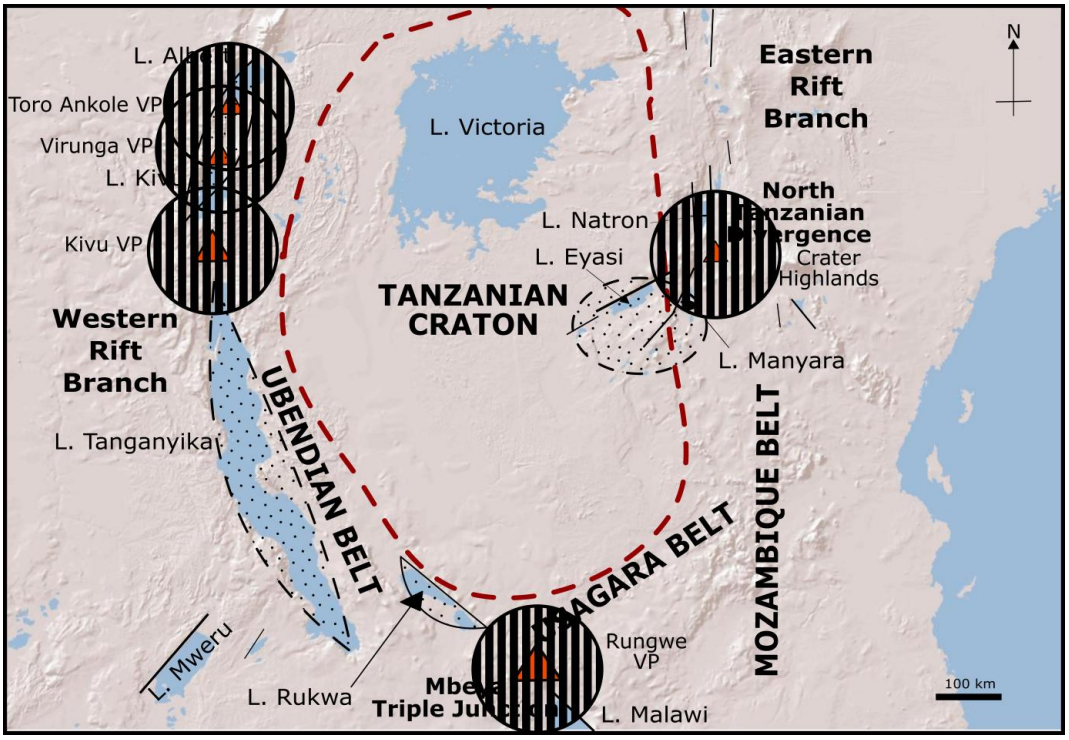

Figure 5.6.: 'Play fairway' map showing potentially helium-rich basins in the region around the Tanzanian Craton. Black striped circles indicate an inferred 100 km radius CO_2 dilution zone around active volcanic provinces in the region, black dashed lines around basins indicate potential helium-rich prospects which are uncertain due to missing information and basins outlined with solid black lines indicate basins with the best helium potential in the region.

The potential dilution effect observed from active volcanic provinces following on from trends seen in the Mbeya region (Section 5.6.1) is now taken into account by assuming a CO_2 dilution zone of approximately 100 km radius around the centre of each province. Although the CO_2 dilution zone is likely to vary for each volcanic province according to factors such as available fluid migration pathways, the rates and volumes of the CO_2 flux from depth, the locations and timing of the activity of volcanoes in the region. However despite this uncertainty as to the precise boundaries of the CO_2 dilution zone an area like the Albertine Graben (to the NW of the map) can be excluded from being potentially helium-rich due to this effect. This is supported further by evidence from this region which shows that Lake Kivu contains high concentrations of CH_4, CO_2 and mantle-derived helium and that seeps around Lake Albert are oil and gas rich with the hydrocarbon gases present in

reservoirs showing CO_2 contamination (Schoell et al., 1988; Tedesco et al., 2010; Abeinomugisha and Kasande, 2012).

Areas which contain basins outlined by dashed lines indicate potential helium-rich locations which may be rendered void by as yet unknown elements. The Lake Tanganyika area appears to be a good prospect due to both its size and the distance from current volcanic activity. There are helium-rich springs to the east of the area in Uvinza which degas gases which are 2.5% ^4He and have an R/R_a value of 0.28 R_a; indicating a preferentially crust-dominated input to gases however gases have not yet been sampled from the hydrothermal vents beneath the lake the helium-rich springs at Uvinza could just be a localised occurrence (Kraml et al., 2016).

At the same time the 'play fairway' map indicates that the north of the Tanganyika rift may be experiencing the introduction of magmatic fluids. Hydrothermal fields at the north end of Lake Tanganyika at Pemba and Cape Banza record fluids which contain predominantly magmatic-origin CO_2 (60% to 90%) and CH_4 with heavier hydrocarbons (Botz and Stoffers, 1993; Tiercelin et al., 1993).

Currently Lake Tanganyika is thought to be an excellent oil prospect which may indicate the presence of viable trapping structure in the rift basin though this remains to be seen as drilling has yet to take place.

Similarly the NDT study area is also ringed as a potentially helium-rich location, however this is hampered by the caveat that the sediments in this region are very shallow compared to those seen in the rift basins in the Western Branch (< 2 km in depth) and that trapping structures in this region are as of yet unknown due to lack of seismic surveying in the region.

The solidly ringed Rukwa Basin contains currently what is considered the best helium prospect in the region due to a combination of all of the points on the

helium exploration method alongside seismic surveys conducted by Helium One in the region which show the presence of potential trapping structures. Once again the results from target reservoirs in the basin remain to be seen, however the P50 estimate for helium reserves in the Rukwa Basin which has been calculated by an independent company from helium measurements in this study currently stands at 98 Bcf or 2.78 x 10^9 m^3.

5.7. Summary

New noble gas data from the West and East branches of the Tanzanian section of the EARS shows ^{4}He concentrations of up to 10.5%. This combined with the potential ^{4}He generated by the Tanzanian Craton and surrounding mobile belts of approximately 7.0 x 10^5 Bcf implies that even with highly inefficient release, migration and trapping there could be many potential high helium reservoirs in the region on the scale of that predicted for the Rukwa Basin (98 Bcf).

In the Mbeya study area (which contains the Rukwa Basin and RVP) crustal helium charge and associated N_2 released by rifting is diluted by CO_2 produced by active volcanoes in the region whereas further away (approximately 135 km) N_2 and high helium dominate (< 2.5% ^{4}He).

This can enable the determination of a ‘goldilocks zone’ for the purposes of helium exploration in areas experiencing active volcanism. The limit of the zone will be close enough to thermal sources (either the thermal aureole from magma chambers or rifting) for helium to be released but without significant CO_2 dilution by nearby volcanoes.

In the Rukwa Basin, which is currently under investigation as a high helium reservoir first estimates derived from our ^{4}He analyses combined with seismic surveys for the basin translates to probable reserves of 98 Bcf which would be enough to supply the current global helium demand for ~ 14 years if current demand remains the same.

Chapter Six: The Principles of Helium Exploration

6.1. The Helium System

It has been established in Chapter 1 that all helium-producing reserves to date have been discovered serendipitously when the target of the exploration was petroleum. In order to ascertain the viability of an area for petroleum exploitation oil and gas companies consider potential source rocks, burial temperatures and depths, migration pathways and regional reservoir/seal combinations also known as 'play fairways' which were explored in Chapter 5 for the Tanzanian system.

These well established hydrocarbon exploration protocols have been adapted to instead make helium the prospecting target. Following this approach similar questions to those put forward by hydrocarbon exploration arise:

1. How and where is helium generated?
2. How physically and thermally stable are these environments to allow helium accumulation?
3. How is accumulated helium released from source rocks (primary migration)?
4. How does helium move significant lateral distances from the source rock into reservoir areas (secondary migration)?
5. How does helium rich gas accumulate and remain in reservoirs (focusing and trapping mechanisms)?
6. How do potentially helium-rich gas accumulations become compromised over geological time periods (trap destruction and/or leakage)?

If we compare the helium system to the hydrocarbon system we begin to see immediate differences at every developmental stage from source to accumulation in

reservoir. The only stage which helium and petroleum seem to have in common is the final stage: trap integrity and longevity (**Table 6.1**). In order to identify potential high helium systems we need to identify the characteristics of the areas which are most likely to facilitate each stage.

Stage	Petroleum System	Helium System
Source	Organic matter	U^{238}, U^{235} and Th^{232} decay in the crust produce alpha particles
Maturation	Burial and consequential heating	Time to accumulate (stable crust) vs volume of stable crust
Primary migration	Pressure driven (phase change from solid kerogen to fluid petroleum results in volume increase)	Heating to above mineral closure temperatures, fracturing of rocks and minerals, mineral dissolution
Secondary migration	Buoyancy driven	Groundwater/buoyancy driven/stripping
Accumulation in reservoir	Beneath caprock, capillary entry pressure seal	Exsolution in presence of existing gas phase beneath caprock/degassing of oversaturated groundwater/direct input into trap of a free gas phase
Trap integrity & longevity	Microseepage, capillary failure, fracture failure, tectonic destruction of trap	Microseepage, capillary failure, fracture failure, tectonic destruction of trap

Table 6.1.: Synthesis of components of the helium exploration system compared to the petroleum system.

6.1.1. Generation and accumulation

The dominant stable isotope of helium, ^{4}He, is radiogenically sourced from the alpha decay of ^{238}U, ^{235}U and ^{232}Th in the crust, whereas petroleum products are predominantly biogenically sourced from the thermal decay of organic matter.

Basement rocks and cratons of Proterozoic and Archean age (0.54 Ga to 3.8 Ga respectively) such as the Canadian Shield or the Yavapai-Mazatzal Province in the southern USA are predominantly metamorphic or granitic in character and contain crustal average or higher concentrations of U and Th ($\leq$ 2.8 ppm and 10.7 ppm respectively). These basement rocks alongside more modern sediments (< 1.8 Ga) of average U and Th content have equal capability of producing ^{4}He however the constraint of time on the system is crucial for the production of significant helium volumes.

6.1.2. Maturation

Concentrations of ^{4}He will naturally increase in the subsurface over time given adequate periods of quiescence with some of the helium remaining in the rocks and some of it being ejected into the fluid within the porosity of the rocks as a consequence of its penetration distance (Reimer, 1976; Bottomley et al., 1984; Zadnik and Jeffrey, 1985; Lippmann-Pipke et al., 2011; Holland et al., 2013).

In past studies it has been shown that continental cratons have acted as closed systems which allowed helium to accumulate over billions of years leading to concentrations of helium in pore water as high as 9.82×10^{-2} $cm^3g^{-1}_{water}$ in the Kaapvaal Craton (Western Australia) and 6.20×10^{-4} $cm^3g^{-1}_{water}$ in the Greenland Craton (Zadnik and Jeffrey, 1985; Lippmann-Pipke et al., 2011).

Additionally, in the Canadian Precambrian Shield, evidence from noble gas ratios shows that pockets of water have been isolated and accumulating radiogenic noble gases since the Precambrian with residence times calculated of 1.1±0.6 Ga (Holland et al., 2013; Warr et al., 2017).

Due to a combination of low helium concentrations across the entire crust (ppm) and the ability of producing minerals such as zircon, apatite and titanite to retain helium below their closure temperatures can hinder the release of helium in the shallow crust. The lowest closure temperatures are associated with apatite and are ~ 70°C; indicating that under a normal crustal temperature gradient of 30°C/km helium would start being released from minerals at around 2 km or deeper given a surface temperature of 10°C. Given that most helium-rich gas reservoirs occur at shallower depths than this and at higher concentrations this indicates that the helium atoms need not only a mechanism for bulk release but also for focusing (**Table 6.2.**).

Field and location	**Producing reservoir**	**Helium concentration (%)**	**Depth of producing reservoir (km)**	**References**
Hugoton-Panhandle, Kansas/Oklahoma/Texas, USA	Chase Group (Permian)/ Council Grove Group (Permian)/Brown Dolomite (Permian)	0.60 (average)	0.90	Ballentine and Sherwood-Lollar, 2002; Gage and Driskill, 2005
Woodside, Utah, USA	Kaibab (Permian)	1.31	0.95	Morgan and Chidsey Jr, 1991; Harris, 1993
Harley Dome, Utah, USA	Entrada (Jurassic)	7.02-7.18	0.26	Dobbin, 1968

Model Dome, Colorado, USA	Entrada (Jurassic)	7.00-8.34	0.31	Dobbin, 1968
Greenwood, Kansas, USA	Topeka (Pennsylvanian) and Wabaunsee (Pennsylvanian)	0.52-0.70	0.94	Wingerter, 1968; Gage and Driskill, 2005
McElmo Dome, Colorado, USA	Leadville (Mississippian)	≤ 0.71	0.50	Gerling, 1983; Gilfillan, 2006; Gilfillan et al., 2008
LaBarge, Wyoming, USA	Madison (Mississippian)	0.50-0.73	4.42-5.03	Hamak, 1989; Stewart and Street, 1992; De Bruin, 1995; Martin et al., 2008; Merrill et al., 2014

Table 6.2.: Average depths of a selection of helium-producing reservoirs in the USA.

6.1.3. Primary migration

The primary migration of helium is a two stage process compared with the hydrocarbon system which involves the pressurised expulsion of liquid and gaseous hydrocarbons from the source rock cause by a time/temperature driven phase change from solid kerogen. Helium primary migration not only involves migration out of the source rock but also the added complication of migration out of the original host minerals.

Radiogenic ^{4}He produced from the alpha decay of ^{238}U, ^{235}U and ^{232}Th usually occurs within 10-20 microns of the parent radioelement which is defined as

the penetration distance of the original alpha particle. As this is usually within the length-scale of the host minerals, helium can become trapped both within the mineral matrix and on mineral grain boundaries depending on the penetration distance.

Diffusion rates for helium out of fine-grained minerals (~0.1 mm) range between $10^{-18}cm^2s^{-1}$ and $10^{-22}cm^2s^{-1}$ for temperatures up to 150°C (Lippolt and Weigel, 1988; Trull et al., 1991; Ballentine and Burnard, 2002). In order for diffusion to occur in the subsurface a concentration gradient must first be established between the producing mineral and the surrounding pore space which is determined by helium concentrations in minerals being higher than the equilibrium concentration of the pore space.

The bulk diffusion of ^4He in the crust is severely limited in terms of length scale. Experiments involving incremental heating alone conducted by Hussain (1997) show diffusion rates of approximately 1×10^{-15} cm^2s^{-1} at 20°C in granite in contrast to the high ^4He diffusivities of between 2×10^{-5} cm^2s^{-1} to 1×10^{-6} cm^2s^{-1} calculated for the Great Artesian Basin (Queensland, Australia) by Torgersen (1989). Such high diffusivities shows that the transport of ^4He in this location was not diffusion and was more likely tied to the movement of fluid (^4He diffusivity in water is 4.2×10^{-5} cm^2s^{-1} from Jähne et al., (1987)). Therefore if most ^4He found in reservoirs is assumed to be from the underlying crust, diffusion rates dictate that this process would be orders of magnitude slower than bulk transport by fluids.

While in general, diffusion from depth can be discounted as a significant contribution to observed reservoir ^4He concentrations (0.1%<) in the case of CH_4-rich fields like the Hugoton-Panhandle the role of diffusion versus advection is less clear and there is a possibility at depths above mineral closure temperatures that

there can be local diffusive contributions to ^{4}He reservoirs due to the rock volumes involved (Chapter 3 this thesis).

The other mechanism which could cause the migration of helium in bulk is advection. However, in order for the advection of helium to occur, two events must occur first: 1) a thermal event which is high enough to overcome the closure temperature associated with the various minerals within which helium is trapped and 2) a fluid e.g.: N_2 or CO_2 to facilitate bulk movement out of the source rock. Both conditions require a significant change in the regional thermal gradient; most likely caused by tectonism such as extensional rifting, orogeny or volcanic activity. Any process which mobilises the carrier fluid involved in the predominantly vertical transport of ^{4}He has the capacity to move it over large distances.

An example of the primary migration of ^{4}He is currently occurring within Yellowstone National Park in the USA. Lowenstern et al., (2015), in their study on the gas geochemistry associated with the supervolcano, calculated that the ^{4}He flux from Yellowstone was tens to hundreds of times higher than the underlying crust could support. From this they speculated that the supervolcano was heating the 2.8 Ga Wyoming craton and releasing the ^{4}He accumulated within this source since at least 2.3 Ga over the course of 2 Ma.

Evidence of a carrier gas involved with the advection of ^{4}He can be seen by the constant presence of N_2 in these high-helium reservoirs ($^4He/N_2$ ratios in natural gas fields typically range between 0.02 to 0.20).

That radiogenically produced helium should be associated with non-radiogenic nitrogen suggests a common source for both gases. It has been found that the $\delta^{15}N$ composition of the N_2 endmember associated with economic ^{4}He deposits falls consistently within a very narrow range (-3.00‰ to +2.45‰) which compares

to the ranges seen from both low temperature metamorphism of the crust (-5.00‰ to +4.00‰) and the release of ammonium from clays (+1‰ to +4‰) (Ballentine and Sherwood-Lollar, 2002; Chapter 3 this thesis; Chapter 4 this thesis).

The link between ^{4}He and N_2 during primary migration can be seen in a study from the Eger Rift by Weinlich et al., 1999 with an added caveat; while this region exemplifies primary migration for the helium system, it is also shows the potential dilution of ^{4}He and N_2-rich gases by the addition of magmatically-sourced CO_2 and associated gases in a tectonically active region.

Gases from the Eger Rift in Central Europe infer a CO_2 dilution trend which correlates with distance from volcanoes in the area (**Figure 6.1**). From this study Weinlich et al., (1999) found that closer to the volcanoes the CO_2 content and R_a values associated with gases increased whereas N_2 concentrations decreased (indicating a greater input of mantle content) whereas further from the volcanic centres the CO_2 of the gas content decreased as did the R_a value whereas N_2 concentrations increased, indicating a return to crustal input.

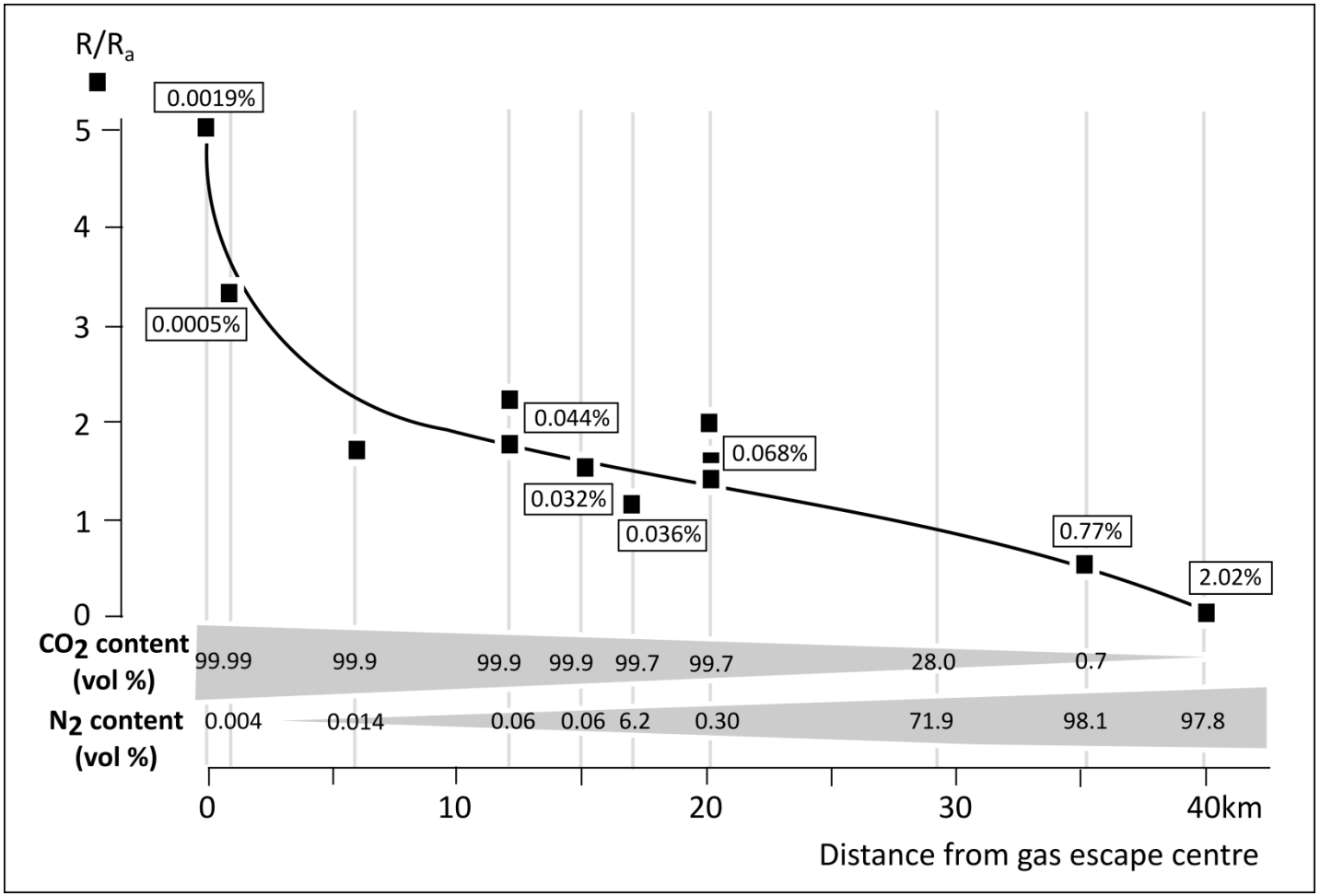

Figure 6.1.: Graph redrawn from Weinlich et al., (1999) showing the relationship between R_a values, He content, CO_2 content, N_2 content and distance from volcanic centres. The numbers in boxes indicate average He volume percentages at sampled sites. Points without numbers recorded trace amounts of helium in the original paper.

Therefore in the right geological setting, the thermal aureole associated with magmatism may provide the heating needed to release helium from its source however if the trap is situated too close to the volcanic centre all that will be found in reservoirs will be predominantly CO_2.

If a trap is already in place when tectonism occurs there is a possibility that the primary migration of ^4He and N_2 as a free gas phase may be all that is needed to generate a helium-rich reservoir, however it would most likely be localised in scale (low volume but high concentration) and probably fault facilitated. This can be evidenced by areas such as Yellowstone and the Eger Rift which show the primary migration stage of gases high in helium but which lack local trapping structures in the case of Yellowstone therefore these large volumes of ^4He are lost to the atmosphere.

However, primary migration alone cannot explain the presence of large volume helium-rich reservoirs in areas which have not experienced any recent tectonic activity such as Kansas. In the case of these reservoirs secondary migration or predominantly lateral migration is required.

6.1.4. Secondary migration

In natural systems ^4He and N_2 are often discovered together with CO_2 or CH_4 which indicates that the same processes and geological structures that control where CO_2 and CH_4 are trapped also apply to these gases. The presence of CO_2 or CH_4 in trapping structures can also play an important role in helium trapping as outlined below.

For the purposes of simplicity the secondary migration of helium is defined as the predominantly lateral movement of helium and other associated gases after primary migration (predominantly vertical movement out of the source rock) has occurred. Secondary migration can occur in several ways: 1) free gas migration, 2) movement of groundwater containing dissolved helium and nitrogen, and 3) the stripping of gases from groundwater by migrating CO_2 or CH_4 (**Table 6.3**).

Secondary migration mechanism	Description
Free gas phase	• The free gas phase from primary migration migrates directly into traps facilitated by fracturing/buoyancy/faults
Groundwater	• The free gas phase from primary migration contacts groundwater where it either degasses due to contact with another gas phase • The free gas phase is dissolved in groundwater and laterally moves picking up crustal gases as it moves until the groundwater is oversaturated/water temperature changes/salinity changes/pressure decreases/it contacts another gas phase whereupon the groundwater degasses
Stripping	• CO_2 and/or CH_4 from a separate, buoyancy driven free gas phase interacts with groundwater containing ^{4}He and associated gases removing them from the groundwater

Table 6.3.: Possible mechanisms of secondary migration for the helium system.

Observed correlations between the air saturated water-derived noble gas isotopes ^{20}Ne and ^{36}Ar and admixtures of ^{4}He and ^{4}He-associated N_2 in fields from Kansas, Oklahoma, Texas and Arizona show strong evidence of varying degrees of groundwater involvement in helium-rich systems (Ballentine and Sherwood-Lollar, 2002; Gilfillan, 2006; Chapter 3 this thesis; Chapter 4 this thesis).

6.1.5. Accumulation in reservoirs

When groundwater that contains dissolved helium and associated N_2 is equilibrated with CO_2 or CH_4 gases, the more insoluble ^4He and N_2 gases will exsolve from the groundwater. In this case a pre-existing gas phase composed of CO_2 or CH_4 is essential for causing the degassing of groundwater containing accumulated ^4He and ^4He-associated N_2 into the trapping structure.

An alternative which has been observed in the Kansas Basin Permian and Central Kansas Uplift wells from Chapter 3 and the N_2-^4He rich wells from Chapter 4 is the possibility of a groundwater which is already oversaturated in ^4He-associated N_2 degassing into reservoirs before the interaction of a separate CH_4 or CO_2 gas phase sourced from a different location.

Once ^4He and ^4He-associated N_2 has migrated into a gas trapping structure the preservation of ^4He in that reservoir is subject to balancing the rate at which ^4He is supplied to the deposit with the efficiency of the seal or trap to contain it. Trap destruction or a leaky seal will result in loss of ^4He and the other gases from the trap.

6.1.6. Trap efficiency, leakage and destruction

Since helium and petroleum gases can occupy the same trap, the main variable which determines whether helium is still present after a significant amount of geological time is the stability of the trapping structure. Most of hypotheses for helium entrapment are based on the same principles as petroleum entrapment, except with greater attention paid to the pore throat radius of sealing rocks due to the small atomic radius of helium due to its potential propensity for microseepage.

One hypothesis is that helium needs a tight sealing caprock such as an evaporite (halite or anhydrite layer) to remain emplaced for large amounts of geological time without significant leakage via diffusion (Broadhead and Gillard, 2004; Broadhead, 2005).

When examining fields where prolific helium discoveries have been made, it can be seen, for the most part, that this hypothesis holds. The Middle East contains some of the world's largest reserves of helium gas, (the South Pars Field, Persian Gulf contains what amounts to a quarter of the world's helium reserve and has made Qatar the second largest producer of helium after the USA), however the concentration of helium contained in the gas is low. At only 0.05% of the gas being helium it is the volume of the reservoir which makes the reserve commercially viable.

Fields in the USA contain reservoirs which are orders of magnitude smaller than those in the Middle East but contain higher concentrations of helium; some as high as 10%. All of these fields are overlain by either a halite or anhydrite layer.

While evaporite deposits always make the best reservoir seals due to their lack of pores and ductility, it may be possible that other caprock types could also suffice since helium is never naturally the primary gas in a reservoir and would therefore be in an admixture with other gases (N_2, CO_2 or CH_4). In a natural system helium would be dependent on the partial pressures of the other gases in the reservoir for mobility since the total pressure in reservoir pores is generally fixed by the overburden pressure. Therefore, hypothetically, as long as the reservoir pressure does not exceed capillary entry pressures in the caprock helium should remain in the trap along with the other gases and would only begin to leak if the trap was breached. Further work is needed to determine the mobility of helium admixtures

under typical helium-rich reservoir conditions (underpressured systems) and by modelling different reservoir sealing rocks which is beyond the scope of this thesis.

Trap leakage occurs when the seal capping a reservoir is breached. It usually occurs in one of two ways; either via capillary failure (the most likely scenario under hydrostatic pressures or moderate overpressures) or via fracture failure which usually only occurs in reservoirs which are highly overpressured and these pressures exceed the minimum stress and tensile strength of the sealing rocks. Adding overpressure to a system can also result in trap leakage depending on the seal capacity for failure which increases with increasing pore throat radius.

Helium-rich reservoirs usually record discovery pressures which are underpressured relative to hydrostatic pressure therefore it is likely that the reservoir pore pressures in viable reservoirs were too low over time to cause seal failure especially in areas sealed by salt deposits which have no pores and are therefore not susceptible to capillary failure.

However, the older the reservoir, the more likely it is that the trap will be disturbed by any active tectonics in the region, causing the loss of the reservoir contents over time. If helium-enriched gas is not supplied on a constant basis, it is likely that disturbed fields which would have been helium-rich are either dry or contain rejuvenated primary gas.

6.2. Summary

Every helium-producing reserve around the globe has been discovered by accident when exploration companies were searching for petroleum gas. This chapter presents the potential framework for a helium exploration methodology which at its

core requires six components: 1) an area of shallow crust, 2) stability for a significant period of geological history to enable helium accumulation in source rocks, 3) a younger tectonic event which aids the release of accumulated helium, 4) secondary migration to trap via gas stripping or groundwater interaction, 5) viable traps to be in place enabling a helium-rich gas reservoir to accumulate and 6) a significant volume of helium to remain in traps until discovery.

This exploration strategy has been successfully tested in the Tanzanian section of the East African Rift System where high-N_2 seeps produce up to 10.5% ^4He and minimal hydrocarbon gases (Chapter 5). This has enabled the quantity of recoverable helium in the Rukwa Basin to be estimated as ~98 Bcf.

Chapter Seven: Conclusions and Further Work

7.1. Conclusions

Global helium reserves to date have originated from chance discoveries made by oil and gas companies while exploring for petroleum. Despite the many and varied uses of helium there has been no impetus to develop an exploration methodology targeting helium-rich gas reservoirs in order to provide and ensure an adequate supply of helium in a similar manner to petroleum products. This thesis synthesises data from both past and current studies of helium-rich reservoirs to provide both a unique insight into the helium system in different regions and the framework for a helium exploration methodology.

In the USA, which contains the highest total of helium-rich ($\geq$0.3% of total) gas discoveries to date, the gases associated with reservoirs in the Hugoton-Panhandle, Kansas Basin and Central Kansas Uplift areas of the central USA are predominantly composed of: ^{4}He, CH_4, N_2 derived from organic matter and ^{4}He-associated N_2. In these reservoirs the CH_4 and low ^{4}He-associated N_2 gases were most likely sourced from the Anadarko Basin to the south of the study regions however they were not generated together and show little to no involvement with groundwater compared with the ^{4}He and high ^{4}He-associated N_2 gases.

By using a combination of $\delta^{15}N$ values and noble gas isotopes it was also established that the low ^{4}He-associated N_2 endmember, which is shared by all sampled reservoirs in that region, is characterised by $\delta^{15}N$ = +14.60‰ which is characteristic of an overmature, hydrocarbon-producing sedimentary source.

The ^{4}He and ^{4}He-associated N_2 components have two distinct high ^{4}He-associated N_2 endmembers which can be characterised by: 1) $\delta^{15}N$ = +1.00‰, $^{4}He/N_2$ = 0.036 and 2) $\delta^{15}N$ = -3.00‰, $^{4}He/N_2$ = 0.089. The endmember $\delta^{15}N$ values

calculated fall within a narrow range and, when combined with ^{4}He mass balance calculations, are consistent with a low grade metamorphic crustal source for the bulk of both ^{4}He and high ^{4}He-associated N_2 which could be derived from variable mixing between sediments and basement rocks in study areas.

$N_2/^{20}Ne$ ratios and the same radiogenic mixing line indicate a common groundwater source for both the Texas Panhandle and KBC areas and potentially the KBP area. In contrast the CKU wells indicate little to no groundwater contact and crust-derived gases in these reservoirs are thought to have had a significant portion added by fault-facilitated advection from depth.

In the Hugoton-Panhandle and the KBC area, groundwater is undersaturated in ^{4}He associated N_2 indicating that a gas phase consisting of CH_4 and organic N_2 needed to already be present in order for the dissolved isotopes to partition into the reservoir gas cap. The KBP and CKU, conversely, are oversaturated in ^{4}He-associated N_2 indicating that isotopes dissolved in the groundwater were already exsolving into the gas phase in reservoirs before CH_4 and N_2 migrated into the reservoirs.

^{4}He mass balances calculated for these study areas indicate that <17% of the ^{4}He volumes in reservoirs could have been produced in situ, which implies that the area involved with sourcing ^{4}He is not confined to the boundaries of the study areas and could cover a significant portion of Kansas, Texas and New Mexico.

On a regional scale, the first noble gas and stable isotope data from N_2-^{4}He rich wells from the south and north of North America (Utah, Montana and Saskatchewan) consistently record a narrow range of $\delta^{15}N$ values (+1.00‰ to +2.45‰) which likely confirms that the source of the ^{4}He and associated N_2 in helium-rich reservoirs is low temperature metamorphosed crust.

In the northern wells (International Helium Wood Mtn, SK and Weil #1, MT) radiogenic noble gas ratios are within error of average crustal production ratios which, when combined with the depth of the reservoir strata, indicates that the source is most likely from the underlying basement, however, for the Harley Dome well, the source is considerably shallower (< 1 km) and is probably also predominantly sourced from the underlying uplifted basement.

Despite the narrow range of $\delta^{15}N$ values, these wells all have a wide range of $^4He/N_2$ end member values which are consistent within each locality (0.010 to 0.011 in the north and 0.085 to 0.089 in the south). The difference in these $^4He/N_2$ end-members may either be related to variations in the chemical composition of the underlying source rocks in the regions or to the accumulation time within the source rocks before the release of high ^{4}He-associated N_2 and ^{4}He.

All of the N_2-^{4}He rich wells show consistently less groundwater contact than in the Hugoton-Panhandle-Kansas Basin dataset and lie in the range of the Kautz #1 well from the Central Kansas Uplift samples which may indicate contact between a free gas phase and groundwater before degassing into reservoirs.

In all fields the mechanism for ^{4}He and associated N_2 degassing into reservoirs appears to be related in some degree to groundwater and the saturation threshold of ^{4}He associated N_2. In cases where the groundwater is oversaturated in ^{4}He-associated N_2, groundwater degassing will occur without the need for a primary gas cap such as CH_4 or CO_2 to be present in the reservoir, occasionally allowing the formation of N_2-rich ^{4}He field unless it is diluted by another gas. Conversely, in cases where the groundwater is undersaturated in N_2, contacting a primary gas cap is needed in order for the exsolution of high ^{4}He-associated N_2 to occur and with it ^{4}He and other associated noble gas isotopes.

New noble gas data from thermal springs in the West and East branches of the Tanzanian section of the EARS show ^{4}He concentrations of up to 10.5% indicating the active release of high helium and high N_2 gases in the region. This combined with the potential ^{4}He volumes generated by the Tanzanian Craton and surrounding mobile belts of approximately 7.0 x 10^5 Bcf implies that even with highly inefficient gas release from source rocks there could be many potential high helium reservoirs in the region on the scale of that predicted for the Rukwa Basin (98 Bcf).

In the Mbeya study area (which contains the Rukwa Basin and the Rungwe Volcanic Province) crustal ^{4}He and associated N_2 which is released by heating and rifting is diluted by CO_2 produced by active volcanoes in the region whereas further from the volcanic province (approximately 135 km) N_2 and high helium dominate (< 2.5% ^{4}He).

In future the seeps in this region could be used to generate models to determine a zone for the CO_2 dilution of the crust-sourced gases. Hypothetically the limit of the zone will be close enough to thermal sources (either the thermal aureole from magma chambers or rifting) for helium to be released but without significant CO_2 dilution by nearby volcanoes.

In the Rukwa Basin, which is currently under investigation as a high helium reservoir, first estimates derived from ^{4}He analyses from Chapter Five combined with seismic surveys for the basin translate to a P50 estimate of probable reserves of 98 Bcf which would be enough to supply the current global helium demand for ~ 14 years if current demand remains the same.

Despite the estimated volume of the helium reserves being low when compared with other fields such as South Pars in Qatar/Iran and Chayandinskoye in

Russia, if a viable helium reserve is discovered in the Rukwa Basin, the implications are huge; firstly because this will have been the first time that a helium reserve has been found on purpose as the target of exploration and secondly it will prove that our helium exploration method is valid (Chapter Five, this thesis).

7.1.1. Expanding the current helium exploration methodology

The framework for a helium exploration methodology requires these components as a starting point: 1) an area of old granitic crust (source) which has been quiescent for a significant period of geological time generating and accumulating dispersed helium, 2) a relatively younger tectonic event which disturbs this area aiding the primary migration of accumulated helium from the source, 3) secondary migration pathways such as groundwater can play a major role in the lateral transport of helium away from sources and 4) viable traps to be in place enabling a helium-rich gas accumulation to form either from the emplacement of a free gas phase or from exsolution from groundwater.

Now that we understand the source of helium and the mechanisms involved in primary migration, secondary migration and accumulation we can use a systematic approach to identifying areas around the globe which are likely to contain commercially attractive helium accumulations.

7.2. Further Work

This thesis represents the first geochemical survey purely conducted for the purposes of characterising helium-rich systems with the end goal of creating a

unifying method for helium exploration which can be applied to new regions in the same way as hydrocarbon exploration and it provides a starting point for other studies on helium-rich systems. Noble gas and stable isotopic analyses have been shown to be very effective tools in characterising the source, migration pathways and potential exsolution mechanisms for helium into trapping structures and should be used in further work pertaining to better identifying elements of the helium system.

Geochemical surveys involving more samples are needed from helium-rich reservoirs especially for N_2-rich wells and CO_2-rich wells to better understand the helium system on a local scale with a view to comparing areas within countries on a regional scale and finally across countries on a global scale. This could aid in the understanding of why fields in areas like Colorado, Utah and Arizona contain helium-rich fields interspersed with CO_2-rich and CH_4-rich fields; an example of this would be the isotopic analysis of carbon isotopes for CO_2 and CH_4 alongside the analyses of N_2 and the noble gases in helium-rich reservoirs as this would aid in better establishing the source and timing of the primary gas phase into the trap and how this has affected the partitioning of helium and other associated gases.

There is also the potential for the exploration of the diversity of the crustal $^4He/N_2$ end member ratios and whether in N_2-rich high helium reservoirs it is related to either the whole rock elemental abundance of the craton which sourced the gases or to the timing of the release of the gases i.e.: the lower the $^4He/N_2$ ratio the earlier in the geological history of the area the release event occurred due to less time accumulating ^4He relative to N_2.

There is more scope for exploring the role of groundwater in high helium systems including identifying the ^4He-associated N_2 groundwater saturation point for each reservoir and how far in excess of this limit is required to classify whether

helium in a reservoir has partitioned from a laterally moving, oversaturated groundwater versus from a free gas phase from primary migration contacting groundwater before locally degassing into reservoirs.

Helium-rich reservoirs which have been geochemically analysed should be compiled in a publically available database similar to global petroleum fields to aid future researchers.

An aspect of the helium system which has not yet been explored is trap integrity over time. The modelling of trap integrity for helium admixtures and for different caprock types could be crucial to understanding how a reservoir retains its helium over long periods of geological time and what factors could affect this leading to a loss of the reservoir contents.

Further modelling work could be done following on from this thesis on risking the dilution of potential high helium reservoirs by CO_2 in volcanically active areas such as the EARS and by CH_4 in/near areas which are hydrocarbon-producing basins.

References

Abeinomugisha, D., and Kasande, R. (2012). Tectonic control on Hydrocarbon Accumulation in the Intra-Continental Albertine Graben of the East African Rift System, *in* D. Gao, ed., *Tectonics and sedimentation: Implications for petroleum systems:* AAPG Memoir 100. pp. 209-228.

Ader, M., Thomazo, C., Sansjofre, P., Busigny, V., Papineau, D., Laffont, R., Cartigny, P., & Halverson, G. P. (2016). Interpretation of the nitrogen isotopic composition of Precambrian sedimentary rocks: Assumptions and perspectives. *Chemical Geology*, *429*, 93-110.

Alkhammali, S. A. (2015). *Geochemical and clay mineralogical characteristics of the Woodford Shale, Payne County, Oklahoma*. Kansas State University. (MS Thesis). pp 82.

American Physical Society, Materials Research Society & American Chemical Society. (2016). *Responding to the U.S. Research Community's Liquid Helium Crisis: An Action Plan to Preserve U.S. Innovation*. Retrieved from: https://www.aps.org/policy/reports/popa-reports/upload/HeliumReport.pdf (Accessed 14 November 2017).

Adams, D. C., & Keller, G. R. (1994). Possible extension of the Midcontinent Rift in west Texas and eastern New Mexico. *Canadian Journal of Earth Sciences*, *31*(4), 709-720.

Adler, F. J., Caplan, W. M., & Carlson, M. P. (1971). Future petroleum provinces of the Mid-Continent, Region 7. *Future petroleum provinces of the United States—Their geology and potential: AAPG Memoir*, *15*, 985-1123.

Allis, R., Chidsey, T., Gwynn, W., Morgan, C., White, S., Adams, M., & Moore, J. (2001, May). Natural CO_2 reservoirs on the Colorado Plateau and southern Rocky Mountains: Candidates for CO_2 sequestration. *In*: Proceedings of the First National Conference on Carbon Sequestration, 14-17.

Anderson, C. C., & Hinson, H. H. (1950). *Helium-bearing natural gases of the United States- analyses and analytical methods*. Bureau of Mines, Washington, DC (USA); Bureau of Mines, Amarillo, Tex.(USA), Bulletin 486, pp. 141.

Armstrong, R. L. (1974). Magmatism, orogenic timing, and orogenic diachronism in the Cordillera from Mexico to Canada. *Nature*, *247*, 348-351.

Baars, D. L., and Stevenson, G. M. (1981). Tectonic evolution of the Paradox basin, Utah and Colorado. *In*: D. L. Wiegand, ed., Geology of the Paradox Basin, Rocky Mountain Association of Geologists, 1981 Field Conference, pp. 23-31.

Back, H. O., Calaprice, F., Condon, C., de Haas, E., Ford, R., Galbiati, C., Goretti, A., Hohman, T., Inanni, A., Loer, B., Montanari, D., Nelson, A., and Pocar, A. (2012). First large scale production of low radioactivity argon from underground sources. pp. 5: https://arxiv.org/pdf/1204.6024.pdf (Accessed 13 December 2017).

Bähr, R., Lippolt, H. J., & Wernicke, R. S. (1994). Temperature-induced ^{4}He degassing of specularite and botryoidal hematite: A ^{4}He retentivity study. *J. Geophys. Res.*, *99*(B9), 17695-17707.

Baiyegunhi, C., Oloniniyi, T. L., & Gwavava, O. (2014). The correlation of dry density and porosity of some rocks from the Karoo Supergroup: A case study of selected rock types

between Grahamstown and Queenstown in the Eastern Cape Province, South Africa. *IOSR Journal of Engineering*, *4*(12), 30-40.

Ballentine, C. J., O'Nions, R. K., Oxburgh, E. R., Horvath, F., & Deak, J. (1991). Rare gas constraints on hydrocarbon accumulation, crustal degassing and groundwater flow in the Pannonian Basin. *Earth and Planetary Science Letters*, *105*(1-3), 229-246.

Ballentine, C. J., & O'Nions, R. K. (1992). The nature of mantle neon contributions to Vienna Basin hydrocarbon reservoirs. *Earth and Planetary Science Letters*, *113*(4), 553-567.

Ballentine, C. J., Mazurek, M., & Gautschi, A. (1994). Thermal constraints on crustal rare gas release and migration: Evidence from Alpine fluid inclusions. *Geochimica et cosmochimica acta*, *58*(20), 4333-4348.

Ballentine, C. J., O'Nions, R. K., & Coleman, M. L. (1996). A Magnus opus: Helium, neon, and argon isotopes in a North Sea oilfield. *Geochimica et Cosmochimica Acta*, *60*(5), 831-849.

Ballentine, C. J. (1997). Resolving the mantle He/Ne and crustal $^{21}Ne/^{22}Ne$ in well gases. *Earth and Planetary Science Letters*, *152*(1), 233-249.

Ballentine, C. J., Schoell, M., Coleman, D., & Cain, B. A. (2000). Magmatic CO_2 in natural gases in the Permian Basin, west Texas: Identifying the regional source and filling history. *Journal of Geochemical Exploration*, *69*, 59-63.

Ballentine, C. J., Schoell, M., Coleman, D., & Cain, B. A. (2001). 300-Myr-old magmatic CO_2 in natural gas reservoirs of the west Texas Permian basin. *Nature*, *409*(6818), 327.

Ballentine, C. J., Burgess, R., & Marty, B. (2002). Tracing fluid origin, transport and interaction in the crust. *Reviews in mineralogy and geochemistry*, *47*(1), 539-614.

Ballentine, C. J., & Burnard, P. G. (2002). Production, release and transport of noble gases in the continental crust. *Reviews in mineralogy and geochemistry*, *47*(1), 481-538.

Ballentine, C. J., & Lollar, B. S. (2002). Regional groundwater focusing of nitrogen and noble gases into the Hugoton-Panhandle giant gas field, USA. *Geochimica et Cosmochimica Acta*, *66*(14), 2483-2497.

Ballentine, C. J., & Holland, G. (2008). What CO_2 well gases tell us about the origin of noble gases in the mantle and their relationship to the atmosphere. *Philosophical Transactions of the Royal Society of London A: Mathematical, Physical and Engineering Sciences*, *366*(1883), 4183-4203.

Banner, J. L., Wasserburg, G. J., Dobson, P. F., Carpenter, A. B., & Moore, C. H. (1989). Isotopic and trace element constraints on the origin and evolution of saline groundwaters from central Missouri. *Geochimica et Cosmochimica Acta*, *53*(2), 383-398.

Barnard, P. C., & Cooper, B. S. (1983). A review of geochemical data related to the northwest European gas province. *Geological Society, London, Special Publications*, *12*(1), 19-33.

Barry, P. H., Hilton, D. R., Fischer, T. P., De Moor, J. M., Mangasini, F., & Ramirez, C. (2013). Helium and carbon isotope systematics of cold "mazuku" CO_2 vents and hydrothermal gases and fluids from Rungwe Volcanic Province, southern Tanzania. *Chemical Geology*, *339*, 141-156.

Battino R. (1983). Nitrogen and air. *In* Solubility Data Series, Vol. 10. International Union of Pure and Applied Chemistry (IUPAC), Pergamon Press, Oxford.

Bebout, G. E., & Carlson, W. D. (1986). Fluid evolution and transport during metamorphism: evidence from the Llano Uplift, Texas. *Contributions to Mineralogy and Petrology*, *92*(4), 518-529.

Bebout, G. E., & Fogel, M. L. (1992). Nitrogen-isotope compositions of metasedimentary rocks in the Catalina Schist, California: implications for metamorphic devolatilization history. *Geochimica et Cosmochimica Acta*, *56*(7), 2839-2849.

Bebout, G. E., Cooper, D. C., Bradley, A. D., & Sadofsky, S. J. (1999). Nitrogen-isotope record of fluid-rock interactions in the Skiddaw Aureole and granite, English Lake District. *American Mineralogist*, *84*(10), 1495-1505.

Bernet, M. (2009). A field-based estimate of the zircon fission-track closure temperature. *Chemical Geology*, *259*(3), 181-189.

Beyerle, U., Aeschbach-Hertig, W., Imboden, D. M., Baur, H., Graf, T., & Kipfer, R. (2000). A mass spectrometric system for the analysis of noble gases and tritium from water samples. *Environmental Science & Technology*, *34*(10), 2042-2050.

Bickford, M. E., Harrower, K. L., Hoppe, W. J., Nelson, B. K., Nusbaum, R. L., & Thomas, J. J. (1981). Rb-Sr and U-Pb geochronology and distribution of rock types in the Precambrian basement of Missouri and Kansas. *Geological Society of America Bulletin*, *92*(6), 323-341.

Boerner, D. E., Craven, J. A., Kurtz, R. D., Ross, G. M., & Jones, F. W. (1998). The Great Falls Tectonic Zone: suture or intracontinental shear zone?. *Canadian Journal of Earth Sciences*, *35*(2), 175-183.

Boniface, N., & Schenk, V. (2012). Neoproterozoic eclogites in the Paleoproterozoic Ubendian Belt of Tanzania: evidence for a Pan-African suture between the Bangweulu Block and the Tanzania Craton. *Precambrian Research*, *208*, 72-89.

Boniface, N., Schenk, V., & Appel, P. (2012). Paleoproterozoic eclogites of MORB-type chemistry and three Proterozoic orogenic cycles in the Ubendian Belt (Tanzania): Evidence from monazite and zircon geochronology, and geochemistry. *Precambrian Research*, *192*, 16-33.

Borg, G., & Shackleton, R. M. (1997). The Tanzania and NE-Zaire Cratons. *Oxford Monographs on Geology and Geophysics*, *35*, 608-619.

Bottomley, D. J., Ross, J. D., & Clarke, W. B. (1984). Helium and neon isotope geochemistry of some ground waters from the Canadian Precambrian Shield. *Geochimica et Cosmochimica Acta*, *48*(10), 1973-1985.

Botz, R. W., & Stoffers, P. (1993). Light hydrocarbon gases in Lake Tanganyika hydrothermal fluids (east-central Africa). *Chemical geology*, *104*(1), 217-224.

Bowen, D. W., & Weimer, P. (2003). Regional sequence stratigraphic setting and reservoir geology of Morrow incised-valley sandstones (lower Pennsylvanian), eastern Colorado and western Kansas. *AAPG bulletin*, *87*(5), 781-815.

Bowring, S. A., & Karlstrom, K. E. (1990). Growth, stabilization, and reactivation of Proterozoic lithosphere in the southwestern United States. *Geology*, *18*(12), 1203-1206.

Boyce, J. W., Hodges, K. V., Olszewski, W. J., & Jercinovic, M. J. (2005). He diffusion in monazite: Implications for (U-Th)/He thermochronometry. *Geochemistry, Geophysics, Geosystems*, *6*(12).

Boyd, S. R., Hall, A., & Pillinger, C. T. (1993). The measurement of δ15N in crustal rocks by static vacuum mass spectrometry: Application to the origin of the ammonium in the Cornubian batholith, southwest England. *Geochimica et Cosmochimica Acta*, *57*(6), 1339-1347.

Boyd, S. R. (2001). Ammonium as a biomarker in Precambrian metasediments. *Precambrian Research*, *108*(1), 159-173.

Broadhead, R. F., & Gillard, L. (2004). Helium in New Mexico: Geologic Distribution and Exploration Possibilities: New Mexico Bureau of Geology and Mineral Resources. *Open File Report 483*, 1-62.

Broadhead, R. F. (2005). Helium in New Mexico—geologic distribution, resource demand, and exploration possibilities. *New Mexico Geology*, *27*(4), 93-101.

Burchell, P. W. (1964). Historical development of oil and gas production in Utah's Uinta Basin. *In*: Guidebook, Thirteenth Annual Field Conference: Intermountain Association of Petroleum Geologists, pp. 184-185.

Burke, K. (1996). Africa's Distinctive Behavior Over the Past 30 Million Years. Houston Geological Society Bulletin, Volume 38, No. 7, March 1996. pp. 10-10.

Burnard, P. G., Hu, R. Z., Turner, G., & Bi, X. W. (1999). Mantle, crustal and atmospheric noble gases in Ailaoshan gold deposits, Yunnan Province, China. *Geochimica et Cosmochimica Acta*, *63*(10), 1595-1604.

Burruss, R. C., and Hatch, J. R. (1989). Geochemistry of oils and hydrocarbon source rocks, Greater Anadarko Basin: Evidence for multiple sources of oils and long-distance oil migration, *in* K. S. Johnson, ed., Anadarko Basin: 1988 Symposium Oklahoma Geological Survey Circular 90, pp 53–64.

Cady, H. P., & McFarland, D. F. (1906). Helium in natural gas. *Science*, *24*(611), 344-344.

Cady, H. P., & McFarland, D. F. (1907a). THE OCCURRENCE OF HELIUM IN NATURAL GAS AND THE COMPOSITION OF NATURAL GAS. *Journal of the American Chemical Society*, *29*(11), 1523-1536.

Cady, H. P., & McFarland, D. F. (1907b). Neon and Argon in Natural Gas. *Transactions of the Kansas Academy of Science (1903-)*, *21*, 64-65.

Caracausi, A., & Paternoster, M. (2015). Radiogenic helium degassing and rock fracturing: A case study of the southern Apennines active tectonic region. *Journal of Geophysical Research: Solid Earth*, *120*(4), 2200-2211.

Cardott, B. J. (1988). Thermal maturation of the Woodford Shale in the Anadarko basin. *In* Anadarko basin symposium, pp. 32-46.

Carr, T. R., Dean K. M., Dubois, M. K., Gerlach, P., Maroney, M. H., Morrison, E., Newell, K. D., Noah, K. E., and Poelchau, H. (2003). Use of information technology for integrated reservoir characterization of Permian gas fields of the Hugoton em-bayment: Kansas Geological Survey Open File Report 2003-29: http://www.kgs.ku.edu/PRS/publication/2003/ofr2003-29/index.html (Accessed 11 November, 2017).

Carter, L. S., Kelley, S. A., Blackwell, D. D., & Naeser, N. D. (1998). Heat flow and thermal history of the Anadarko Basin, Oklahoma. *AAPG bulletin*, *82*(2), 291-316.

Case, J. E. (1966). Geophysical anomalies over Precambrian rocks, northwestern Uncompahgre Plateau, Utah and Colorado. *AAPG Bulletin*, *50*(7), 1423-1443.

Chaki, S., Takarli, M., & Agbodjan, W. P. (2008). Influence of thermal damage on physical properties of a granite rock: porosity, permeability and ultrasonic wave evolutions. *Construction and Building Materials*, *22*(7), 1456-1461.

Chaudhuri, S., Broedel, V., & Clauer, N. (1987). Strontium isotopic evolution of oil-field waters from carbonate reservoir rocks in Bindley field, central Kansas, USA. *Geochimica et Cosmochimica Acta*, *51*(1), 45-53.

Cherniak, D. J., Watson, E. B., & Thomas, J. B. (2009). Diffusion of helium in zircon and apatite. *Chemical Geology*, *268*(1), 155-166.

Chidsey, T. C., Jr., Eby, D. E., and Lorenz, D. M. (1996). Geological and reservoir characterization of small shallow-shelf carbonate fields, southern Paradox Basin, Utah. *In*: A.C. Huffman, Jr., W. R. Lund, and L. H. Godwin, eds., Geology and Resources of the Paradox Basin: Utah Geological Association Guidebook 25, 39-56.

Chorowicz, J. (2005). The east African rift system. *Journal of African Earth Sciences*, *43*(1), 379-410.

Ciotoli, G., Etiope, G., Guerra, M., Lombardi, S., Duddridge, G. A., & Grainger, P. (2005). Migration of gas injected into a fault in low-permeability ground. *Quarterly Journal of Engineering Geology and Hydrogeology*, *38*(3), 305-320.

Clark, S. L. (1987). Seismic stratigraphy of early Pennsylvanian Morrowan sandstones, Minneola complex, Ford and Clark counties, Kansas. *AAPG Bulletin*, *71*(11), 1329-1341.

Clark, M. (1981). Helium in Wyoming. Energy Resources of Wyoming; 32nd Annual Field Conference Guidebook, 1981, Wyoming Geological Association, pp. 119-130.

Clarke, R. H., Nuttall, W. J., & Glowacki, B. A. (2012). Introduction, *in* W. J. Nuttall, R. H. Clarke & B. A. Glowacki, eds., The Future of Helium as a Natural Resource, Abingdon, United Kingdom: Routledge, pp. 1-14.

Clauer, N. (2006). Towards an isotopic modeling of the illitization process based on data of illite-type fundamental particles from mixed-layer illite-smectite. *Clays and Clay Minerals*, *54*(1), 116-127.

Clayton, R. N. (2007). Isotopes: from Earth to the solar system. *Annu. Rev. Earth Planet. Sci.*, *35*, 1-19.

Collerson, K. D., Lewry, J. F., Bickford, M. E., & Van Schmus, W. R. (1990). Crustal evolution of the buried Precambrian of southern Saskatchewan: Implications for diamond

exploration. *In* L. S. Beck, C. T. Harper, Eds., Modern Exploration Techniques, Saskatchewan Geological Society Special Publication Number 10, pp. 150-165.

Condie, K. C. (1976). Trace-element geochemistry of Archean greenstone belts. *Earth-Science Reviews*, *12*(4), 393-417.

Condie, K. C. (1982). Plate-tectonics model for Proterozoic continental accretion in the southwestern United States. *Geology*, *10*(1), 37-42.

Connolly, M., J. (2012). *Summary Report for the Rudyard Field 2012 Deep Drilling Program, Weil #1*. Hill Co., Montana: Brainstorm Energy. pp. 42.

Connor, S. (2013, January 4). A ballooning problem: the great helium shortage. *The Independent*. Retrieved from http://www.independent.co.uk

Coolen, J. J. M. M. M., Priem, H. N. A., Verdurmen, E. T., & Verschure, R. H. (1982). Possible zircon U-Pb evidence for Pan-African granulite-facies metamorphism in the Mozambique belt of southern Tanzania. *Precambrian Research*, *17*(1), 31-40.

Coveney Jr, R. M., Goebel, E. D., Zeller, E. J., Dreschhoff, G. A., & Angino, E. E. (1987). Serpentinization and the origin of hydrogen gas in Kansas. *AAPG Bulletin*, *71*(1), 39-48.

Craig, H., Clarke, W. B., & Beg, M. A. (1975). Excess ^{3}He in deep water on the East Pacific Rise. *Earth and Planetary Science Letters*, *26*(2), 125-132.

Craig, H., & Lupton, J. E. (1976). Primordial neon, helium, and hydrogen in oceanic basalts. *Earth and Planetary Science Letters*, *31*(3), 369-385.

Craig, H., & Lupton, J. E. (1981). 11. HELIUM-3 AND MANTLE VOLATILES IN THE OCEAN AND THE OCEANIC CRUST. *The oceanic lithosphere*, *7*, 391.

Creedy, D. P. (1988). Geological controls on the formation and distribution of gas in British coal measure strata. *International Journal of Coal Geology*, *10*(1), 1-31.

Crovetto, R., Fernández-Prini, R., & Japas, M. L. (1982). Solubilities of inert gases and methane in H_2O and in D_2O in the temperature range of 300 to 600 K. *The Journal of Chemical Physics*, *76*(2), 1077-1086.

Daniels, E. J., Aronson, J. L., Altaner, S. P., & Clauer, N. (1994). Late Permian age of NH_4-bearing illite in anthracite from eastern Pennsylvania: Temporal limits on coalification in the central Appalachians. *Geological Society of America Bulletin*, *106*(6), 760-766.

Dawson, J. B. (2008). The Gregory rift valley and Neogene-recent volcanoes of northern Tanzania. Geological Society of London, London.

Delvaux, D., & Hanon, M. (1991). Neotectonics of the Mbeya area, SW Tanzania. *Annual report of the Royal Museum of Central Africa, Department of Geology and Mineralogy, 1992*, 87-97.

Delvaux, D., Levi, K., Kajara, R., & Sarota, J. (1992). Cenozoic paleostress and kinematic evolution of the Rukwa–North Malawi rift valley (East African Rift System). *Bulletin des Centres de Recherche Exploration-Production ElfAquitaine*, *16*, 383-406.

Delvaux, D., Kervyn, F., Vittori, E., Kajara, R. S. A., & Kilembe, E. (1998). Late Quaternary tectonic activity and lake level change in the Rukwa Rift Basin. *Journal of African Earth Sciences*, *26*(3), 397-421.

Delvaux, D. (2001). Karoo rifting in western Tanzania: Precursor of Gondwana breakup. *Contributions to geology and paleontology of Gondwana in honor of Helmut Wopfner: Cologne, Geological Institute, University of Cologne*, 111-125.

Delvaux, D., Kraml, M., Sierralta, M., Wittenberg, A., Mayalla, J. W., Kabaka, K., Makene, C., & GEOTHERM Working Group. (2010). Surface Exploration of a Viable Geothermal Resource in Mbeya area, SW Tanzania. Part I: Geology of the Ngozi–Songwe Geothermal System. *In*: Proceedings of the World Geothermal Congress, Bali, Indonesia, pp. 25-29.

Dobbin, C. E. (1935). Geology of natural gases rich in helium, nitrogen, carbon dioxide, and hydrogen sulfide. *In:* H. A. Ley, ed., Geology of Natural Gas, Tulsa, Oklahoma. The American Association of Petroleum Geologists Bulletin, pp. 1053–1072.

Dobbin, C. E. (1968). Geology of natural gases rich in helium, nitrogen, carbon dioxide, and hydrogen sulphide. *In:* B. W. Beebe and B. F. Curtis, eds., Natural gases of North America, v. 2: AAPG Memoir 9, pp. 1957 – 1969.

Dong, Z., Holditch, S., McVay, D., & Ayers, W. B. (2012). Global unconventional gas resource assessment. *SPE Economics & Management*, *4*(04), 222-234.

Downey, M. W. (1984). Evaluating seals for hydrocarbon accumulations. *AAPG bulletin*, *68*(11), 1752-1763.

Downs, W. (2009). Influence of Injected Brine Water at Westwater Farms on Spanish Valley Well Water Quality. http://www.riversimulator.org/Resources/farcountry/OilGas/WestwaterFarms/SEC/DownsGeologicReport.pdf (Accessed 10 November 2017).

Dubois, M. K., Byrnes, A. P., Bohling, G. C., and Doveton, J. H. (2006). Multiscale geologic and petrophysical modeling of the giant Hugoton gas field (Permian), Kansas and Oklahoma, U.S.A. *In*: P. M. Harris and L. J. Weber, eds., Giant hydrocarbon reservoirs of the world: From rocks to reservoir characterization and modeling: *AAPG Memoir 88/SEPM Special Publication*, pp. 307-353.

Dubois, M. K. (2007). *Ramp-scale geomodel for reservoir and stratigraphic analysis of the Hugoton field (Wolfcampian, midcontinent USA)* University of Kansas. (PhD Thesis). pp. 320.

Dudás, F. Ö. (1991). Geochemistry of igneous rocks from the Crazy Mountains, Montana, and tectonic models for the Montana alkalic province. *Journal of Geophysical Research: Solid Earth*, *96*(B8), 13261-13277.

Dunai, T. J., & Roselieb, K. (1996). Sorption and diffusion of helium in garnet: implications for volatile tracing and dating. *Earth and planetary science letters*, *139*(3-4), 411-421.

Dunlap, R. E. (1969). *The geology of the Pinta Dome-Navajo Springs helium fields, Apache County, Arizona.* University of Arizona. (MS Thesis). pp. 94.

Duvall, A. R., Clark, M. K., van der Pluijm, B. A., & Li, C. (2011). Direct dating of Eocene reverse faulting in northeastern Tibet using Ar-dating of fault clays and low-temperature thermochronometry. *Earth and Planetary Science Letters*, *304*(3), 520-526.

Dyck, W., & Dunn, C. E. (1986). Helium and methane anomalies in domestic well waters in southwestern Saskatchewan, Canada, and their relationship to other dissolved constituents, oil and gas fields, and tectonic patterns. *Journal of Geophysical Research: Solid Earth*, *91*(B12), 12343-12353.

Ebinger, C. J., Deino, A. L., Drake, R. E., & Tesha, A. L. (1989). Chronology of volcanism and rift basin propagation- Rungwe volcanic province, East Africa. *Journal of Geophysical Research*, *94*(11), 15785-15803.

Ebinger, C., Djomani, Y. P., Mbede, E., Foster, A., & Dawson, J. B. (1997). Rifting Archaean lithosphere: the Eyasi-Manyara-Natron rifts, East Africa. *Journal of the Geological Society*, *154*(6), 947-960.

Eddleman, M. W. (1961). Tectonics and geologic history of the Texas and Oklahoma panhandles. *In*: C. R. Wagner, D. R. Cooley, W. W. Brashear, and M. W. Eddleman, eds., Oil and gas field of the Texas and Oklahoma panhandles: Panhandle Geological Society, pp. 61–68.

Ellis, G.S. (2014). Geochemistry of natural gases of the Anadarko Basin, Chapter 4.
In: D. K. Higley, compiler, Petroleum systems and assessment of undiscovered oil and gas in the Anadarko Basin Province, Colorado, Kansas, Oklahoma, and Texas—USGS Province 58: *U.S. Geological Survey Digital Data Series DDS–69–EE,* pp 31.

Elston, D. P., & Shoemaker, E. M. (1960). Late Paleozoic and early Mesozoic structural history of the Uncompahgre front. *In*: K.G. Smith. ed., Geology of the Paradox Basin Fold and Fault Belt, Third Field Conference, 1960, Four Corners Geological Society. pp. 47-55.

Etiope, G., & Lombardi, S. (1996). Laboratory simulation of geogas microbubble flow. *Environmental Geology*, *27*(3), 226-232.

Etiope, G., & Martinelli, G. (2002). Migration of carrier and trace gases in the geosphere: an overview. *Physics of the earth and planetary interiors*, *129*(3), 185-204.

Farley, K. A. (2000). Helium diffusion from apatite: General behavior as illustrated by Durango fluorapatite. *Journal of Geophysical Research B*, *105*(B2), 2903-2914.

Farley, K. A. (2002). (U-Th)/He dating: Techniques, calibrations, and applications. *Reviews in Mineralogy and Geochemistry*, *47*(1), 819-844.

Flawn, P. T. (1954). Texas basement rocks: a progress report. *AAPG Bulletin*, *38*(5), 900-912.

Flawn, P. T. (1956). Basement rocks of Texas and southeast New Mexico: Bureau of Economic Geology, University of Texas Publications, no. 5605, pp. 261.

Fontijn, K., Delvaux, D., Ernst, G. G., Kervyn, M., Mbede, E., & Jacobs, P. (2010). Tectonic control over active volcanism at a range of scales: Case of the Rungwe Volcanic Province, SW Tanzania; and hazard implications. *Journal of African Earth Sciences*, *58*(5), 764-777.

Foster, A., Ebinger, C., Mbede, E., & Rex, D. (1997). Tectonic development of the northern Tanzanian sector of the East African Rift System. *Journal of the Geological Society*, *154*(4), 689-700.

Fritz, H., Tenczer, V., Hauzenberger, C. A., Wallbrecher, E., Hoinkes, G., Muhongo, S., & Mogessie, A. (2005). Central Tanzanian tectonic map: a step forward to decipher Proterozoic structural events in the East African Orogen. *Tectonics*, *24*(6).

Fu, C. C., Yang, T. F., Walia, V., & Chen, C. H. (2005). Reconnaissance of soil gas composition over the buried fault and fracture zone in southern Taiwan. *Geochemical Journal*, *39*(5), 427-439.

Fu, C. C., Yang, T. F., Du, J., Walia, V., Chen, Y. G., Liu, T. K., & Chen, C. H. (2008). Variations of helium and radon concentrations in soil gases from an active fault zone in southern Taiwan. *Radiation Measurements*, *43*, S348-S352.

Gage, B. D., & Driskill, D. L. (2005). Analyses of Natural Gases, 2002-2004. https://www.blm.gov/nstc/library/pdf/TN418.pdf (Accessed 20 November 2017).

Garven, G., Ge, S., Person, M. A., & Sverjensky, D. A. (1993). Genesis of stratabound ore deposits in the Midcontinent basins of North America; 1, The role of regional groundwater flow. *American Journal of Science*, *293*(6), 497-568.

Garven, G. (1995). Continental-scale groundwater flow and geologic processes. *Annual Review of Earth and Planetary Sciences*, *23*(1), 89-117.

Gautheron, C., & Moreira, M. (2002). Helium signature of the subcontinental lithospheric mantle. *Earth and Planetary Science Letters*, *199*(1), 39-47.

Gerhard, L. C. (2004). A new look at an old petroleum province: Kansas Geological Survey, Current Research in Earth Sciences, Bulletin 250, pt. 1, pp. 27: http://www.kgs.ku.edu/Current/2004/Gerhard/index.html (Accessed 12 December 2017).

Gerling, C. R. (1983). McElmo Dome Leadville carbon dioxide field, Colorado. *In*: Fassett, J.E., ed., Oil and Gas Fields of the Four Corners Area, Volume III: Four Corners Geological Society, pp 735-739.

Gerling, P. (1998). New aspects on the origin of nitrogen in natural gas in Northern Germany. *In* Fuel and Energy Abstracts,Vol. 3, No. 39, pp. 185.

Gerling, P., Geluk, M. C., Kockel, F., Lokhorst, A., Lott, G. K., & Nicholson, R. A. (1999). 'NW European Gas Atlas'–new implications for the Carboniferous gas plays in the western part of the Southern Permian Basin. *In*: Geological Society, London, Petroleum Geology Conference series, Vol. 5, No. 1, pp. 799-808. Geological Society of London.

Gifford, J. N. (2013). *Precambrian crustal evolution of the Great Falls Tectonic Zone*. University of Florida. (PhD Thesis). pp 212.

Gifford, J. N., Mueller, P. A., Foster, D. A., & Mogk, D. W. (2014). Precambrian crustal evolution in the Great Falls tectonic zone: Insights from xenoliths from the Montana Alkali Province. *The Journal of Geology*, *122*(5), 531-548.

Giggenbach, W. F., & Poreda, R. J. (1993). Helium isotopic and chemical composition of gases from volcanic-hydrothermal systems in the Philippines. *Geothermics*, *22*(5-6), 369-380.

Gilfillan, S. M. (2006). *Deep magmatic degassing and the Colorado Plateau uplift*. University of Manchester. (PhD Thesis). pp 141.

Gilfillan, S. M., Ballentine, C. J., Holland, G., Blagburn, D., Lollar, B. S., Stevens, S., Schoell, M., & Cassidy, M. (2008). The noble gas geochemistry of natural CO_2 gas reservoirs from the Colorado Plateau and Rocky Mountain provinces, USA. *Geochimica et Cosmochimica Acta*, *72*(4), 1174-1198.

Gold, T., & Held, M. (1987). HELIUM-NITROGEN-METHANE SYSTEMATICS IN NATURAL GASES OF TEXAS AND KANSAS. *Journal of Petroleum Geology*, *10*(4), 415-424.

Gosselin, D. C., Smith, M. R., Lepel, E. A., & Laul, J. C. (1992). Rare earth elements in chloride-rich groundwater, Palo Duro Basin, Texas, USA. *Geochimica et Cosmochimica Acta*, *56*(4), 1495-1505.

Graupner, T., Niedermann, S., Kempe, U., Klemd, R., & Bechtel, A. (2006). Origin of ore fluids in the Muruntau gold system: constraints from noble gas, carbon isotope and halogen data. *Geochimica et Cosmochimica Acta*, *70*(21), 5356-5370.

Grunau, H. R. (1981). Worldwide Review of Seals for Major Accumulations of Natural Gas: ABSTRACT. *AAPG Bulletin*, *65*(5), 933-933.

Guerra, M., & Lombardi, S. (2001). Soil-gas method for tracing neotectonic faults in clay basins: the Pisticci field (Southern Italy). *Tectonophysics*, *339*(3), 511-522.

Haendel, D., Mühle, K., Nitzsche, H. M., Stiehl, G., & Wand, U. (1986). Isotopic variations of the fixed nitrogen in metamorphic rocks. *Geochimica et cosmochimica Acta*, *50*(5), 749-758.

Halverson, J. R. (1988). Seismic expression of the Upper Morrow sands, western Anadarko Basin. *Geophysics*, *53*(3), 290-303.

Hamak, J. E. (1989). Helium Resources of Wyoming. Gas Resources of Wyoming; 40th Annual Field Conference Guidebook, 1989, Wyoming Geological Association, pp 117-121.

Hamilton, W., & Kroner, A. (1981). Crustal evolution by arc magmatism [and discussion]. *Philosophical Transactions of the Royal Society of London A: Mathematical, Physical and Engineering Sciences*, *301*(1461), 279-291.

Harðarson, B. S. (2014). Structural geology of the western branch of the East African Rift: tectonics, volcanology and geothermal activity. Presented at Short Course IX on Exploration for Geothermal Resources, organized by UNU-GTP, GDC and KenGen, at Lake Bogoria and Lake Naivasha, Kenya, Nov. 2-23, 2014. pp. 14: https://rafhladan.is/bitstream/handle/10802/9124/UNU-GTP-SC-19-0301.pdf (Accessed 13 December 2017).

Harris, J. E. (1993). Woodside: T. 18-20 S., R. 13-14 E., SLPM Emery County, Utah, Oil and Gas Fields of Utah, Utah Geological Association.

Haynes, E. H. (1967). Developments in Eastern and Northwestern Colorado and Western Nebraska in 1966. *AAPG Bulletin*, *51*(6), 1124-1128.

Heaton, T. H. E. (1984). Rates and sources of ^{4}He accumulation in groundwater. *Hydrological sciences journal*, *29*(1), 29-47.

Hemsell, C. C. (1939). Geology of Hugoton gas field of southwestern Kansas. *AAPG Bulletin*, *23*(7), 1054-1067.

Henry, M. E., & Hester, T. C. (1995). Morrow Sandstone Gas and Oil Stratigraphic Play *in* Kansas Geological Survey, Digital Petroleum Atlas http://www.kgs.ku.edu/DPA/frontEnd/Anadarko/Morrow/provSum.html

Heyman, O. G. (1983). Distribution and structural geometry of faults and folds along the northwestern Uncompahgre uplift, western Colorado and eastern Utah. Northern Paradox Basin - Uncompahgre Uplift, 1983, Grand Junction Geological Society. pp. 45-57.

Higley, D. K. (1995). Cambridge Arch/Central Kansas Uplift Province: Kansas Geological Survey, Digital Petroleum Atlas: http://www.kgs.ku.edu/DPA/NMC/Prov/cambridge.html (Accessed 12 December 2017).

Hilton, D. R., Hammerschmidt, K., Teufel, S., & Friedrichsen, H. (1993). Helium isotope characteristics of Andean geothermal fluids and lavas. *Earth and Planetary Science Letters*, *120*(3-4), 265-282.

Hilton, D. R., Fischer, T. P., & Marty, B. (2002). Noble gases in subduction zones and volatile recycling. *Rev Mineral Geochem*, *47*, 319-370.

Hiyagon, H., & Kennedy, B. M. (1992). Noble gases in CH_4-rich gas fields, Alberta, Canada. *Geochimica et Cosmochimica Acta*, *56*(4), 1569-1589.

Hochstein, M. P., Temu, E. P., & Moshy, C. M. A. (2000). Geothermal resources of Tanzania. *In:* Proceedings World Geothermal Congress 2000, May 28-June 10, Kyushu-Tohoku, Japan, pp. 1233-1237.

Holland, G., Lollar, B. S., Li, L., Lacrampe-Couloume, G., Slater, G. F., & Ballentine, C. J. (2013). Deep fracture fluids isolated in the crust since the Precambrian era. *Nature*, *497*(7449), 357.

Holm, D., & Schneider, D. (2002). $^{40}Ar/^{39}Ar$ evidence for ca. 1800 Ma tectonothermal activity along the Great Falls tectonic zone, central Montana. *Canadian Journal of Earth Sciences*, *39*(12), 1719-1728.

Holzner, C. P., McGinnis, D. F., Schubert, C. J., Kipfer, R., & Imboden, D. M. (2008). Noble gas anomalies related to high-intensity methane gas seeps in the Black Sea. *Earth and Planetary Science Letters*, *265*(3), 396-409.

Hong, W. L., Yang, T. F., Walia, V., Lin, S. J., Fu, C. C., Chen, Y. G., Sano, Y., Chen, C.H., & Wen, K. L. (2010). Nitrogen as the carrier gas for helium emission along an active fault in NW Taiwan. *Applied Geochemistry*, *25*(4), 593-601.

Huffman, G. G. (1959). Pre-Desmoinesian isopachous and paleogeologic studies in central Mid-Continent region. *AAPG Bulletin*, *43*(11), 2541-2574.

Hunt, J. M. (1996). Petroleum geochemistry and geology, second edition: W .H. Freeman and Company, New York, 743.

Hunt, A. G., Darrah, T. H., & Poreda, R. J. (2012). Determining the source and genetic fingerprint of natural gases using noble gas geochemistry: A northern Appalachian Basin case study. *Aapg Bulletin*, *96*(10), 1785-1811.

Hutcheon, I. (1999). Controls on the distribution of non-hydrocarbon gases in the Alberta Basin. *Bulletin of Canadian Petroleum Geology*, *47*(4), 573-593.

Hussain, N. (1997). Flux of ^{4}He from Carnmenellis granite: modelling of an HDR geothermal reservoir. *Applied geochemistry*, *12*(1), 1-8.

International Union of Pure and Applied Chemistry. (2005). *Nomenclature of Inorganic Chemistry, IUPAC Recommendations 2005* by N. G. Connelly, T. Damhus, R. M. Hartshorn & A. T. Hutton. Retrieved from the IUPAC website: http://old.iupac.org/publications/books/rbook/Red_Book_2005.pdf (Accessed 12 October 2017).

Jähne, B., Heinz, G., & Dietrich, W. (1987). Measurement of the diffusion coefficients of sparingly soluble gases in water. *Journal of Geophysical Research: Oceans*, *92*(C10), 10767-10776.

James, T. C. (1967a). Thermal springs in Tanzania. *Institution of Mining and Metallurgy*, Transactions/Section B (Applied Earth Science) 76, B1–B18 *in* Macheyeki, A. S., Delvaux, D., De Batist, M., & Mruma, A. (2008). Fault kinematics and tectonic stress in the seismically active Manyara–Dodoma Rift segment in Central Tanzania–Implications for the East African Rift. *Journal of African Earth Sciences*, *51*(4), 163-188.

James, T. C. (1967b). Thermal springs in Tanzania – discussions and conclusions. *Institution of Mining and Metallurgy*, Transactions/Section B (Applied Earth Science) 76, B168–B174 *in* Macheyeki, A. S., Delvaux, D., De Batist, M., & Mruma, A. (2008). Fault kinematics and tectonic stress in the seismically active Manyara–Dodoma Rift segment in Central Tanzania–Implications for the East African Rift. *Journal of African Earth Sciences*, *51*(4), 163-188.

Jenden, P. D., Kaplan, I. R., Poreda, R., & Craig, H. (1988a). Origin of nitrogen-rich natural gases in the California Great Valley: evidence from helium, carbon and nitrogen isotope ratios. *Geochimica et Cosmochimica Acta*, *52*(4), 851-861.

Jenden, P. D., Newell, K. D., Kaplan, I. R., & Watney, W. L. (1988b). Composition and stable-isotope geochemistry of natural gases from Kansas, Midcontinent, USA. *Chemical Geology*, *71*(1-3), 117-147.

Jenden, P. D., & Kaplan, I. R. (1989). Origin of natural gas in Sacramento Basin, California. *AAPG Bulletin*, *73*(4), 431-453.

Jewett, J. M. (1951). Geologic structures in Kansas: Kansas Geological Survey, Bulletin 90, pt. 6, pp. 105-172.

Jewett, J. M., & Merriam, D. F. (1959). Geologic framework of Kansas; a review for geophysicists. In *Symposium on geophysics in Kansas: Kansas Geological Survey Bulletin*, Vol. 137, pp. 9-52.

Kalberkamp, U., Schaumann, G., Ndonde, P.B., Chiragwile, S.A., Mwano, J.M., and GEOTHERM working group, 2010. Surface exploration of a viable geothermal resource in Mbeya area, SW Tanzania. Part III: Geophysics. Proceedings, World Geothermal Congress 2010, Bali, Indonesia 25 – 29 April 2010, pp. 6.

Kandie, R. J. (2014). EASTERN RIFT STRUCTURAL GEOLOGY–TECTONICS, VOLCANOLOGY AND GEOTHERMAL. Presented at Short Course IX on Exploration for Geothermal Resources, organized by UNU-GTP, GDC and KenGen, at Lake Bogoria and Lake Naivasha, Kenya, Nov. 2-24, 2014, pp. 6:

https://rafhladan.is/bitstream/handle/10802/9126/UNU-GTP-SC-19-0303.pdf (Accessed 13 December, 2017).

Kansas Geological Survey, Production from Kansas Oil and Gas Leases: http://www.kgs.ku.edu/Magellan/Field/lease.html (Accessed 4 May 2017).

Kansas Geological Survey, Geology of Riley and Geary Counties: http://www.kgs.ku.edu/General/Geology/Riley/strat03c.html (Accessed 4 May 2017).

Keebler, W. E. (1956). Cottonwood-Harley Dome area, Grand County, Utah. Geology and Economic Deposits of East Central Utah, Seventh Annual Field Conference: Utah Geological Association, pp. 190-194.

Kennedy, B. M., Hiyagon, H., & Reynolds, J. H. (1990). Crustal neon: a striking uniformity. *Earth and Planetary Science Letters*, *98*(3-4), 277-286.

Kennedy, B. M., & van Soest, M. C. (2006). A helium isotope perspective on the Dixie Valley, Nevada, hydrothermal system. *Geothermics*, *35*(1), 26-43.

Kent, D. M. (1987). Paleotectonic controls on sedimentation in the northern Williston Basin, Saskatchewan. *In*: J. A. Peterson, D. M. Kent, S. B. Anderson, R. H. Pilatzke and M. W. Longman, eds., Williston Basin: Anatomy of a Cratonic Oil Province, Rocky Mountain Association of Geologists, pp. 45-56.

Kim, D., Philp, R. P., & Sorenson, R. P. (2010). Geochemical characterization of solid bitumen in the Chesterian (Mississippian) sandstone reservoir of the Hitch field, southwest Kansas. *AAPG bulletin*, *94*(7), 1031-1057.

Kipfer, R., Aeschbach-Hertig, W., Peeters, F., & Stute, M. (2002). Noble gases in lakes and ground waters. *Reviews in mineralogy and geochemistry*, *47*(1), 615-700.

Kluth, C. F., Ye, H., Royden, L., Burchfiel, C., & Schuepbach, M. (1998). Late Paleozoic Deformation of Interior North America: The Greater Ancestral Rocky Mountains: Discussion & Reply. *AAPG bulletin*, *82*(12), 2272-2276.

Kluth, C. F., & DuChene, H. R. (2009). Late Pennsylvanian and Early Permian structural geology and tectonic history of the Paradox Basin and Uncompahgre Uplift, Colorado and Utah. *In*: W. S. Houston, L. L. Wray and P. G. Moreland, eds., The Paradox Basin Revisited – New Developments in Petroleum Systems and Basin Analysis, Rocky Mountain Association of Geologists, pp. 178-197.

Koester, E. A. (1935). Geology of central Kansas uplift. *AAPG Bulletin*, *19*(10), 1405-1426.

Kraml, M., Mnjokava, T.T., Mayalla, J.W., Kabaka, K., and GEOTHERM working group. (2010). Surface exploration of a viable geothermal resource in Mbeya area, SW Tanzania - Part II: Geochemistry. Proceedings World Geothermal Congress 2010, Bali, Indonesia, 25 – 29 April 2010, pp. 8.

Kraml, M., Ochmann, N., Leible, D., Klin g, T., Chiragwile, S.A., Jodocy, M., Kreuter, H., and GPT Exploration Team. (2014). *Results of the pre-feasibility study on Ngozi geothermal project in Tanzania*. Proceedings, 5th African Rift Geothermal Conference, 29-31 Oct. 2014, Arusha, Tanzania.

Kraml, M., Kaudse, T., Aeschbach, W., & Tanzanian Exploration Team. (2016). *THE SEARCH FOR VOLCANIC HEAT SOURCES IN TANZANIA: A HELIUM ISOTOPE*

PERSPECTIVE. Proceedings, 6th African Rift Geothermal Conference, 2–4 November 2016, Addis Ababa, Ethiopia.

Kreulen, R., & Schuiling, R. D. (1982). N_2-CH_4z. sbnd; CO_2 fluids during formation of the Dôme de l'Agout, France. *Geochimica et Cosmochimica Acta*, *46*(2), 193-203.

Krooss, B. M., Littke, R., Müller, B., Frielingsdorf, J., Schwochau, K., & Idiz, E. F. (1995). Generation of nitrogen and methane from sedimentary organic matter: implications on the dynamics of natural gas accumulations. *Chemical Geology*, *126*(3), 291-318.

Krystyniak, A. M. (2005). *Outcrop-based gamma ray characterization of the Woodford Shale of south-central Oklahoma*. Oklahoma State University. (MS Thesis). pp 131.

Kyser, T. K., & Rison, W. (1982). Systematics of rare gas isotopes in basic lavas and ultramafic xenoliths. *Journal of Geophysical Research: Solid Earth*, *87*(B7), 5611-5630.

Lam, C. K., & Yarger, H. L. (1989). State gravity map of Kansas. *Kansas Geological Survey. Bulletin*, *226*, 185-196.

Landes, K. K. (1927). A petrographic study of the pre-Cambrian of Kansas. *AAPG Bulletin*, *11*(8), 821-824.

Larson, T. G. (1971). Hydrodynamic Interpretation of Mid-Continent: Region 7 *in* M 15: Future Petroleum Provinces of the United States--Their Geology and Potential, Volume 2, pp. 1043-1046.

Lee, Y., & Deming, D. (1999). Heat flow and thermal history of the Anadarko Basin and the western Oklahoma Platform. *Tectonophysics*, *313*(4), 399-410.

Lee, Y., & Deming, D. (2002). Overpressures in the Anadarko basin, southwestern Oklahoma: Static or dynamic? *AAPG bulletin*, *86*(1), 145-160.

Le Gall, B., Gernigon, L., Rolet, J., Ebinger, C., Gloaguen, R., Nilsen, O., Dypvik, H., Deffontaines, B., & Mruma, A. (2004). Neogene-Holocene rift propagation in central Tanzania: Morphostructural and aeromagnetic evidence from the Kilombero area. *Geological Society of America Bulletin*, *116*(3-4), 490-510.

Le Gall, B., Nonnotte, P., Rolet, J., Benoit, M., Guillou, H., Mousseau-Nonnotte, M., Albaric, J., & Deverchère, J. (2008). Rift propagation at craton margin.: Distribution of faulting and volcanism in the North Tanzanian Divergence (East Africa) during Neogene times. *Tectonophysics*, *448*(1), 1-19.

Lenoir, J. L., Liégeois, J. P., Theunissen, K., & Klerkx, J. (1994). The Palaeoproterozoic Ubendian shear belt in Tanzania: geochronology and structure. *Journal of African Earth Sciences*, *19*(3), 169-184.

Li, L., Lollar, B. S., Li, H., Wortmann, U. G., & Lacrampe-Couloume, G. (2012). Ammonium stability and nitrogen isotope fractionations for–NH_3 (aq)–NH_3 (gas) systems at 20–70° C and pH of 2–13: Applications to habitability and nitrogen cycling in low-temperature hydrothermal systems. *Geochimica et Cosmochimica Acta*, *84*, 280-296.

Lippmann, J., Stute, M., Torgersen, T., Moser, D. P., Hall, J. A., Lin, L., Borcsik, M., & Onstott, T. C. (2003). Dating ultra-deep mine waters with noble gases and ^{36}Cl, Witwatersrand Basin, South Africa. *Geochimica et Cosmochimica Acta*, *67*(23), 4597-4619.

Lippmann-Pipke, J., Lollar, B. S., Niedermann, S., Stroncik, N. A., Naumann, R., van Heerden, E., & Onstott, T. C. (2011). Neon identifies two billion year old fluid component in Kaapvaal Craton. *Chemical Geology*, *283*(3), 287-296.

Lippolt, H. J., & Weigel, E. (1988). ^{4}He diffusion in ^{40}Ar-retentive minerals. *Geochimica et Cosmochimica Acta*, *52*(6), 1449-1458.

Lippolt, H. J., Leitz, M., Wernicke, R. S., & Hagedorn, B. (1994). (Uranium+thorium)/helium dating of apatite: experience with samples from different geochemical environments. *Chemical Geology*, *112*(1-2), 179-191.

Littke, R., Krooss, B., Idiz, E., & Frielingsdorf, J. (1995). Molecular nitrogen in natural gas accumulations: generation from sedimentary organic matter at high temperatures. *AAPG bulletin*, *79*(3), 410-430.

Lopez, D. A. (2000). Geologic Summary of the Sweet Grass Hills, Liberty and Toole Counties, Montana. Montana Geological Society: 50th Anniversary Symposium: Montana/Alberta Thrust Belt and Adjacent Foreland: Volume I, pp. 27-46.

Løseth, H., Wensaas, L., Arntsen, B., & Hovland, M. (2003). Gas and fluid injection triggering shallow mud mobilization in the Hordaland Group, North Sea. *Geological Society, London, Special Publications*, *216*(1), 139-157.

Lowenstern, J. B., Bergfeld, D., Evans, W. C., & Hunt, A. G. (2015). Origins of geothermal gases at Yellowstone. *Journal of Volcanology and Geothermal Research*, *302*, 87-101.

Luczaj, J. A., & Goldstein, R. H. (2000). Diagenesis of the Lower Permian Krider Member, southwest Kansas, USA: fluid-inclusion, U-Pb, and fission-track evidence for reflux dolomitization during latest Permian time. *Journal of Sedimentary Research*, *70*(3).

Lukert, L. H. (1949). Subsurface Cross Sections from Marion County Kansas, to Osage County, Oklahoma. *AAPG Bulletin*, *33*(2), 131-152.

Macheyeki, A. S., Delvaux, D., De Batist, M., & Mruma, A. (2008). Fault kinematics and tectonic stress in the seismically active Manyara–Dodoma Rift segment in Central Tanzania–Implications for the East African Rift. *Journal of African Earth Sciences*, *51*(4), 163-188.

Macheyeki, A. S., Delvaux, D., Batist, M. D., & Mruma, A. (2012). Paleoseismic Investigations along the Bubu Fault, Dodoma-Tanzania. *Tanzania Journal of Science*, *38*(2), 138-154.

Magnani, M. B., Miller, K. C., Levander, A., & Karlstrom, K. (2004). The Yavapai-Mazatzal boundary: A long-lived tectonic element in the lithosphere of southwestern North America. *Geological Society of America Bulletin*, *116*(9-10), 1137-1142.

Maher, J. C., & Collins, J. B. (1949). Pre-Pennsylvanian geology of southwestern Kansas, southeastern Colorado, and the Oklahoma Panhandle. Tulsa Geological Society Digest: Tulsa Geological Society, Vol. 17, pp 43-47.

Maione, S. J. (2004). Helium Exploration–A 21st Century Challenge. *Houston Geological Society Bulletin*, Vol. 46, No. 6, pp. 27-28 and 30.

Mamyrin, B. A., & Tolstikhin, I. N. (1984). Helium isotopes in nature, volume 3 of Developments in Geochemistry (first ed.), Elsevier, Amsterdam, New York, Tokyo.

Manya, S., Maboko, M. A., & Nakamura, E. (2007). The geochemistry of high-Mg andesite and associated adakitic rocks in the Musoma-Mara Greenstone Belt, northern Tanzania: Possible evidence for Neoarchaean ridge subduction?. *Precambrian Research*, *159*(3), 241-259.

Martel, D. J., O'Nions, R. K., Hilton, D. R., & Oxburgh, E. R. (1990). The role of element distribution in production and release of radiogenic helium: The Carnmenellis Granite, southwest England. *Chemical Geology*, *88*(3-4), 207-221.

Martin, T. G., Smith, S. N., & Bondos, J. (2008). Materials and Corrosion History With Labarge Madison Production: A 20 Year Story Of Success. *Paper*, *8634*, 16-20.

Marty, B., Jambon, A., & Sano, Y. (1989). Helium isotopes and CO_2 in volcanic gases of Japan. *Chemical Geology*, *76*(1-2), 25-40.

Marty, B., Torgersen, T., Meynier, V., O'Nions, R. K., & Marsily, G. (1993). Helium isotope fluxes and groundwater ages in the Dogger Aquifer, Paris Basin. *Water resources research*, *29*(4), 1025-1035.

McClellan, H. W. (1930). Subsurface distribution of pre-Mississippian rocks of Kansas and Oklahoma. *AAPG Bulletin*, *14*(12), 1535-1556.

Merriam, D. F., Cole, V. B., & Hambleton, W. W. (1961). Distribution of Precambrian Basement Rock Types in Kansas: GEOLOGICAL NOTES. *AAPG Bulletin*, *45*(12), 2018-2024.

Merriam, D. F. (1963). The Geologic History of Kansas. Kansas Geological Survey, Bulletin 162, pp 317.

Merriam, D. F. (2010). The geology and petroleum resources of Kansas: A review from alpha to omega or from the Pleistocene to the Precambrian. *Natural resources research*, *19*(4), 293-316.

Merrill, M. D., Hunt, A. G., & Lohr, C. D. (2014). Noble gas geochemistry investigation of high CO_2 natural gas at the LaBarge Platform, Wyoming, USA. *Energy Procedia*, *63*, 4186-4190.

Mingram, B., Hoth, P., Lüders, V., & Harlov, D. (2005). The significance of fixed ammonium in Palaeozoic sediments for the generation of nitrogen-rich natural gases in the North German Basin. *International Journal of Earth Sciences*, *94*(5-6), 1010-1022.

Mnjokava, T. T. (2007). Interpretation of Exploration Geochemical Data for Geothermal Fluids from the Geothermal Field of the Rungwe Volcanic Area, SW-Tanzania. *UNU-GTP Reykjavík, Iceland, Reports*, (14), 303-332.

Möller, A., Appel, P., Mezger, K., & Schenk, V. (1995). Evidence for a 2 Ga subduction zone: eclogites in the Usagaran belt of Tanzania. *Geology*, *23*(12), 1067-1070.

Moorbath, S., Welke, H., & Gale, N. H. (1969). The significance of lead isotope studies in ancient, high-grade metamorphic basement complexes, as exemplified by the Lewisian rocks of northwest Scotland. *Earth and Planetary Science Letters*, *6*(4), 245-256.

Morgan, C. D., & Chidsey Jr, T. C. (1991). Gordon creek, Farnham dome, and Woodside fields, carbon and Emery Counties, Utah. *In*: T. C. Chidsey Jr., ed., Geology of East-Central Utah, Utah Geological Association Publication, vol. 19, pp. 301–309.

Morley, C. K., Nelson, R. A., Patton, T. L., & Munn, S. G. (1990). Transfer zones in the East African rift system and their relevance to hydrocarbon exploration in rifts (1). *AAPG Bulletin*, *74*(8), 1234-1253.

Morley, C. K., Cunningham, S. M., Harper, R. M., & Wescott, W. A. (1992). Geology and geophysics of the Rukwa rift, East Africa. *Tectonics*, *11*(1), 69-81.

Morley, C. K., Karanja, F. M., Wescott, W. A., Stone, D. M., Harper, R. M., Wigger, S. T., & Day, R. A. (1999). Geology and geophysics of the Rukwa rift. *In*: C. K. Morley, ed., Geoscience of rift systems—evolution of East Africa: AAPG Studies in Geology 44, p. 91–110.

Mruma, A. H. (1995). Stratigraphy and palaeodepositional environment of the Palaeoproterozoic volcano-sedimentary Konse Group in Tanzania. *Journal of African Earth Sciences*, *21*(2), 281-290.

Msabi, M. M. (2010). *Seismic source zonation for the northern Tanzania divergence*. University of Dar es Salaam, (MS Thesis). pp. 125.

Mshiu, E. E., & Maboko, M. A. (2012). Geochemistry and petrogenesis of the late Archaean high-K granites in the southern Musoma-Mara Greenstone Belt: Their influence in evolution of Archaean Tanzania Craton. *Journal of African Earth Sciences*, *66*, 1-12.

Mueller, P. A., Heatherington, A. L., Kelly, D. M., Wooden, J. L., & Mogk, D. W. (2002). Paleoproterozoic crust within the Great Falls tectonic zone: Implications for the assembly of southern Laurentia. *Geology*, *30*(2), 127-130.

Muhongo, S., & Lenoir, J. L. (1994). Pan-African granulite-facies metamorphism in the Mozambique Belt of Tanzania: U-Pb zircon geochronology. *Journal of the Geological Society*, *151*(2), 343-347.

Newell, K. D., Watney, W. L., Cheng, S. W. L., and Brownrigg, R. L. (1987). Stratigraphic and spatial distribution of oil and gas production in Kansas: Kansas Geological Survey, Subsurface Geology Series 9, pp 86: http://www.kgs.ku.edu/Publications/Bulletins/Sub9/index.html (Accessed 12 December 2017).

Newton, R., & Round, G. F. (1961). The diffusion of helium through sedimentary rocks. *Geochimica et Cosmochimica Acta*, *22*(2), 106-132.

Nicholas, R. L., & Rozendal, R. A. (1975). Subsurface positive elements within Ouachita foldbelt in Texas and their relation to Paleozoic cratonic margin. *AAPG Bulletin*, *59*(2), 193-216.

Niedermann, S., Graf, T., & Marti, K. (1993). Mass spectrometric identification of cosmic-ray-produced neon in terrestrial rocks with multiple neon components. *Earth and Planetary Science Letters*, *118*(1-4), 65-73.

Nier, A. O. (1940). A mass spectrometer for routine isotope abundance measurements. *Review of Scientific Instruments*, *11*(7), 212-216.

Nissen, S. E., Marfurt, K. J., & Carr, T. R. (2004). Identifying subtle fracture trends in the Mississippian saline aquifer unit using new 3-D seismic attributes. Kansas Geological Survey Open File Report 2004-56: http://www.kgs.ku.edu/PRS/publication/2004/2004-56 (Accessed 4 December 2017).

Nordquist, J. W., & Leskela, W. (1968). Natural gas in Sweetgrass Arch area, northwestern Montana. AAPG Memoir 9, vol. 1, pp. 736 -759.

Nyblade, A. A., & Brazier, R. A. (2002). Precambrian lithospheric controls on the development of the East African rift system. *Geology*, *30*(8), 755-758.

Nzaro, M. A. (1970). Geothermal resources of Tanzania. *Geothermics*, *2*, 1039-1043.

O'Brien, H. E., Irving, A. J., & McCallum, I. S. (1991). Eocene potassic magmatism in the Highwood Mountains, Montana: petrology, geochemistry, and tectonic implications. *Journal of Geophysical Research: Solid Earth*, *96*(B8), 13237-13260.

O'Brien, H. E., Irving, A. J., McCallum, I. S., & Thirlwall, M. F. (1995). Strontium, neodymium, and lead isotopic evidence for the interaction of post-subduction asthenospheric potassic mafic magmas of the Highwood Mountains, Montana, USA, with ancient Wyoming craton lithospheric mantle. *Geochimica et Cosmochimica Acta*, *59*(21), 4539-4556.

Olson, T. M., Babcock, J. A., Prasad, K. V. K., Boughton, S. D., Wagner, P. D., Franklin, M. H., & Thompson, K. A. (1997). Reservoir characterization of the giant Hugoton gas field, Kansas. *AAPG bulletin*, *81*(11), 1785-1803.

O'Neill, J. M., & Lopez, D. A. (1985). Character and regional significance of Great Falls tectonic zone, east-central Idaho and west-central Montana. *AAPG Bulletin*, *69*(3), 437-447.

Omenda, P. A. (2005). The geology and geothermal activity of the East African Rift System. *In*: Workshop for Decision Makers on Geothermal Projects and Management. Naivasha, Kenya, pp. 1-10. http://www.os.is/gogn/unu-gtp-sc/UNU-GTP-SC-01-03.pdf (Accessed 7 November 2017).

O'Nions, R. K., & Oxburgh, E. R. (1988). Helium, volatile fluxes and the development of continental crust. *Earth and Planetary Science Letters*, *90*(3), 331-347.

Osmond, J. C. (1964). Tectonic history of the Uinta basin, Utah. *In* E. F. Sabatka, ed., Guidebook to the geology and mineral resources of the Uinta basin: Intermountain Association of Petroleum Geologists 13th Annual Field Conference Guidebook, pp. 47–58.

Otto, E.P. and Picard, M.D. (1976). Petrology of Entrada Sandstone (Jurassic), northeastern Utah. *In*: Symposium on the Geology of the Cordilleran Hingeline, Rocky Mountain Association of Geologists, pp. 231- 245.

Oxburgh, E. R., O'Nions, R. K., & Hill, R. I. (1986). Helium isotopes in sedimentary basins. *Nature*, *324*, 632-635.

Ozima, M. (1994). Noble gas state in the mantle. *Reviews of Geophysics*, *32*(4), 405-426.

Ozima, M., & Podosek, F. A. (2001). *Noble Gas Geochemistry (2nd Edition)*. Cambridge University Press. pp. 302.

Paxton, S. T., Cruse, A. M., & Krystyniak, A. M. (2006). Detailed fingerprints of global sea-level change revealed in Upper Devonian/Mississippian Woodford Shale of south-central Oklahoma. *In*: AAPG Annual Meeting, Search and Discovery Article (Vol. 40211).

Pepin, R. O., & Porcelli, D. (2002). Origin of noble gases in the terrestrial planets. *Reviews in Mineralogy and Geochemistry*, *47*(1), 191-246.

Peterson, J. A. (1957). Marine Jurassic of northern Rocky Mountains and Williston Basin. *AAPG Bulletin*, *41*(3), 399-440.

Pettke, T., Frei, R., Kramers, J. D., & Villa, I. M. (1997). Isotope systematics in vein gold from Brusson, Val d'Ayas (NW Italy) 3.(U+ Th) He and KAr in native Au and its fluid inclusions. *Chemical geology*, *135*(3-4), 173-187.

Pierce A. P., Gott G. B., and Mytton J. W. (1964) Uranium and helium in the Panhandle gas field, Texas, and adjacent areas. *In*: USGS Prof. Pap., Vol. 454-G, pp. 57.

Pinna, P., Calvez, J. Y., Abessolo, A., Angel, J. M., Mekoulou-Mekoulou, T., Mananga, G., & Vernhet, Y. (1994). Neoproterozoic events in the Tcholliré area: Pan-African crustal growth and geodynamics in central-northern Cameroon (Adamawa and North Provinces). *Journal of African Earth Sciences*, *18*(4), 347-353.

Pinti, D. L., & Marty, B. (1995). Noble gases in crude oils from the Paris Basin, France: Implications for the origin of fluids and constraints on oil-water-gas interactions. *Geochimica et Cosmochimica Acta*, *59*(16), 3389-3404.

Pinti, D. L., & Marty, B. (1998). The origin of helium in deep sedimentary aquifers and the problem of dating very old groundwaters. *Geological Society, London, Special Publications*, *144*(1), 53-68.

Pflumio, C., Boulègue, J., & Tiercelin, J. J. (1994). Hydrothermal activity in the northern Tanganyika rift, East Africa. *Chemical Geology*, *116*(1-2), 85-109.

Poreda, R. J., Jenden, P. D., Kaplan, I. R., & Craig, H. (1986). Mantle helium in Sacramento basin natural gas wells. *Geochimica et Cosmochimica Acta*, *50*(12), 2847-2853.

Poreda, R. J., Hunt, A. G., Lyons, W. B., & Welch, K. A. (2004). The helium isotopic chemistry of Lake Bonney, Taylor Valley, Antarctica: Timing of late Holocene climate change in Antarctica. *Aquatic Geochemistry*, *10*(3-4), 353-371.

Prinzhofer, A. (2013). Noble gases in oil and gas accumulations. In *The Noble Gases as Geochemical Tracers* (pp. 225-247). Springer Berlin Heidelberg.

Quennell, A. M. (1956). The Bukoban System of East Africa. In *Report of the International Geological Congress, 20th Session, Mexico*, pp. 281-307.

Rascoe Jr., B. (1962). Regional stratigraphic analysis of Pennsylvanian and Permian rocks in western mid-continent, Colorado, Kansas, Oklahoma, Texas. *AAPG Bulletin*, *46*(8), 1345-1370.

Rascoe Jr., B. (1978). Late Paleozoic structural evolution of the Las Animas Arch, in J. D. Pruit, ed., Energy resources of the Denver basin: Rocky Mountain Association of Geologists, pp. 113–127.

Rascoe Jr., B., and Adler, F. J. (1983). Permo-Carboniferous hydro-carbon accumulations, Mid-continent, U.S.A.: AAPG Bulletin, v. 67, p. 979 – 1001.

Ray, M. C., Hilton, D. R., Muñoz, J., Fischer, T. P., & Shaw, A. M. (2009). The effects of volatile recycling, degassing and crustal contamination on the helium and carbon geochemistry of hydrothermal fluids from the Southern Volcanic Zone of Chile. *Chemical Geology*, *266*(1), 38-49.

Reddy, S. M., Collins, A. S., Buchan, C., & Mruma, A. H. (2004). Heterogeneous excess argon and Neoproterozoic heating in the Usagaran Orogen, Tanzania, revealed by single grain $^{40}Ar/^{39}Ar$ thermochronology. *Journal of African Earth Sciences*, *39*(3), 165-176.

Reich, M., Ewing, R. C., Ehlers, T. A., & Becker, U. (2007). Low-temperature anisotropic diffusion of helium in zircon: implications for zircon (U–Th)/He thermochronometry. *Geochimica et Cosmochimica Acta*, *71*(12), 3119-3130.

Reimer, G. M. (1976). *Helium detection as a guide for uranium exploration*. US Geological Survey. *Open File Report 76-240*, 1-14.

Reiners, P. W., & Farley, K. A. (1999). Helium diffusion and (U–Th)/He thermochronometry of titanite. *Geochimica et Cosmochimica Acta*, *63*(22), 3845-3859.

Reiners, P. W. (2005). Zircon (U-Th)/He thermochronometry. *Reviews in Mineralogy and Geochemistry*, *58*(1), 151-179.

Rice, D. D., Nydegger, G. L., & Brown, C. A. (1990). Bowdoin Field--USA Bowdoin Dome, Williston Basin. *In* E. A. Beaumont and N. H. Foster, eds., Structural traps III, tectonic fold and fault traps: AAPG Treatise of Petroleum Geology, pp. 337–355.

Rich, J. L. (1931). Source and date of accumulation of oil in granite ridge pools of Kansas and Oklahoma. *AAPG Bulletin*, *15*(12), 1431-1452.

Roberts, E. M., O'Connor, P. M., Gottfried, M. D., Stevens, N., Kapalima, S., & Ngasala, S. (2004). Revised stratigraphy and age of the Red Sandstone Group in the Rukwa Rift Basin, Tanzania. *Cretaceous Research*, *25*(5), 749-759.

Roberts, E. M., Stevens, N. J., O'Connor, P. M., Dirks, P. H. G. M., Gottfried, M. D., Clyde, W. C., Armstrong, R. A., Kemp, A. I. S., and Hemming, S. (2012). Initiation of the western branch of the East African Rift coeval with the eastern branch. *Nature Geoscience*, *5*(4), 289-294.

Robertson, J. O., Chilingar, G. V., Khilyuk, L. F., & Endres, B. (2012). Migration of Gas from Oil/Gas Fields. *Energy Sources, Part A: Recovery, Utilization, and Environmental Effects*, *34*(15), 1436-1447.

Rønnevik, C., Ksienzyk, A. K., Fossen, H., & Jacobs, J. (2017). Thermal evolution and exhumation history of the Uncompahgre Plateau (northeastern Colorado Plateau), based on apatite fission track and (U-Th)-He thermochronology and zircon U-Pb dating. *Geosphere*, *13*(2), 518-537.

Rosholt, J. N., Zartman, R. E., & Nkomo, I. T. (1973). Lead isotope systematics and uranium depletion in the Granite Mountains, Wyoming. *Geological Society of America Bulletin*, *84*(3), 989-1002.

Salah, M. G., & Alsharhan, A. S. (1998). The Precambrian basement: a major reservoir in the rifted basin, Gulf of Suez. *Journal of Petroleum Science and Engineering*, *19*(3), 201-222.

Sano, Y., Nakamura, Y., Wakita, H., Urabe, A., & Tominaga, T. (1984). Helium-3 emission related to volcanic activity. *Science*, *224*, 150-152.

Sano, Y., Nakamura, Y., Notsu, K., & Wakita, H. (1988). Influence of volcanic eruptions on helium isotope ratios in hydrothermal systems induced by volcanic eruptions. *Geochimica et Cosmochimica Acta*, *52*(5), 1305-1308.

Sawin, R.S., Franseen, E.K., Watney, W.L., West, R.R., and Ludvigson, G.A. (2009). New Stratigraphic Rank for the Carboniferous, Mississippian, and Pennsylvanian in Kansas; *in*, Current Research in Earth Sciences: Kansas Geological Survey, Bulletin 256, part 1. http://www.kgs.ku.edu/Current/2009/Sawin/index.html (Accessed 5 October 2017).

Sears, B. (2012). A history of the helium industry. *In*: W. J. Nuttall, R. H. Clarke & B. A. Glowacki. eds., *The Future of Helium as a Natural Resource*. Abingdon, United Kingdom: Routledge, pp. 15-47.

Schmoker, J. W. (1989). Thermal maturity of the Anadarko basin, in K. S. Johnson, ed., Anadarko basin symposium: Oklahoma Geological Survey Circular 90, pp 25–31.

Schroth, H. A. (1953). Bowdoin Dome, Montana. *In* Billings Geological Society, Guidebook: Fourth Annual Field Conference, September 10-12, 1953, pp.137-141.

Schoell, M., Tietze, K., & Schoberth, S. M. (1988). Origin of methane in Lake Kivu (east-central Africa). *Chemical geology*, *71*(1-3), 257-265.

Seneshen, D. M., Chidsey Jr, T. C., Morgan, C. D., & Berg, M. D. V. (2009). New techniques for new discoveries–results from the Lisbon Field area, Paradox Basin, Utah.

Shaw, C. A., & Karlstrom, K. E. (1999). The Yavapai-Mazatzal crustal boundary in the southern Rocky Mountains. *Rocky Mountain Geology*, *34*(1), 37-52.

Shepard, W., & Bartow, B. (1986). Tectonic history of the Sweetgrass arch, a key to finding new hydrocarbons, Montana and Alberta. *In*: J. H. Noll and K. M. Doyle, eds., Rocky Mountain oil and gas fields: Wyoming Geological Association 1986 Symposium, pp. 9–19.

Sherwood-Lollar, B., Ballentine, C. J., & Onions, R. K. (1997). The fate of mantle-derived carbon in a continental sedimentary basin: integration of C/He relationships and stable isotope signatures. *Geochimica et Cosmochimica Acta*, *61*(11), 2295-2307.

Shurr, G. W., Wosick, F. D., & Rice, D. D. (1993). Regional Pressure Patterns as Evidence for Fractured Reservoirs in the Bowdoin and Phillips Sandstones on Bowdoin Dome, Montana. *In*: L. D. V. Hunter, ed., Energy and mineral resources of central Montana: Montana Geological Society, pp. 117–127.

Shuster, D. L., Flowers, R. M., & Farley, K. A. (2006). The influence of natural radiation damage on helium diffusion kinetics in apatite. *Earth and Planetary Science Letters*, *249*(3), 148-161.

Smith, D., Goodwin, T., Schillinger, J. (2004). Challenges to the Worldwide Supply of Helium in the Next Decade, *AIP Conference Proceedings*, pp. 119.

Sommer, H., Kröner, A., Hauzenberger, C., Muhongo, S., & Wingate, M. T. D. (2003). Metamorphic petrology and zircon geochronology of high-grade rocks from the central Mozambique Belt of Tanzania: crustal recycling of Archean and Palaeoproterozoic material during the Pan-African orogeny. *Journal of Metamorphic Geology*, *21*(9), 915-934.

Sorenson, R. P. (1996). Dissolution of Stone Corral Salt in the Hugoton Embayment: Tulsa Geological Society, Digest, pp. 322–330.

Sorenson, R. P. (2005). A dynamic model for the Permian Panhandle and Hugoton fields, western Anadarko basin. *AAPG bulletin*, *89*(7), 921-938.

Stahl, W. J. (1977). Carbon and nitrogen isotopes in hydrocarbon research and exploration. *Chemical Geology*, *20*, 121-149.

Staudacher, T. (1987). Upper mantle origin for Harding County well gases. *Nature*, *325*, 605-607.

Stewart, W. W., & Street, B. A. (1992). Labarge Anticline. Wyoming Oil and Gas Fields Symposium, Greater Green River Basin and Overthrust Belt: Wyoming Geological Association, pp. 200-205.

Stilwell D. P. (1989). CO_2 resources of the Moxa Arch and the Madison Reservoir. Wyoming Geological Association Fortieth Field Conference Guidebook - Gas Resources of Wyoming, pp. 105–115.

Stokes, W. L. (1976). What is the Wasatch Line? *In*: J. G. Hill, ed., Geology of the Cordilleran hinge line: Rocky Mountain Geologists Symposium, Denver, Colorado, pp. 11–25.

Stokes, M. (2013, January 4). Our research is on ice due to shortage of helium. *The Independent*. Retrieved from http://www.independent.co.uk

Stowe, C. (1972). Oil and gas production in Utah to 1970, Utah Geological and Mineralogical Survey, Bulletin 94, pp. 108-110.

Stuart, F., Turner, G., & Taylor, R. (1994). He–Ar isotope systematics of fluid inclusions: resolving mantle and crustal contributions to hydrothermal fluids. *Noble Gas Geochemistry and Cosmochemistry*, 261-277.

Stuart, F. M., Burnard, P. G., Taylor, R. E. A., & Turner, G. (1995). Resolving mantle and crustal contributions to ancient hydrothermal fluids: He-Ar isotopes in fluid inclusions from Dae Hwa W-Mo mineralisation, South Korea. *Geochimica et Cosmochimica Acta*, *59*(22), 4663-4673.

Stute, M., Sonntag, C., Déak, J., & Schlosser, P. (1992). Helium in deep circulating groundwater in the Great Hungarian Plain: Flow dynamics and crustal and mantle helium fluxes. *Geochimica et Cosmochimica Acta*, *56*(5), 2051-2067.

Taylor, S. R., and McLennan, S. M. (1985). The Continental Crust: its Composition and Evolution. Blackwell Scientific Publications. pp. 328.

Tedesco, D., Tassi, F., Vaselli, O., Poreda, R. J., Darrah, T., Cuoco, E., & Yalire, M. M. (2010). Gas isotopic signatures (He, C, and Ar) in the Lake Kivu region (western branch of the East African rift system): Geodynamic and volcanological implications. *Journal of Geophysical Research: Solid Earth*, *115*(B1).

Thompson, J. A. (1964). The occurrence of helium in the Cambrian near Swift Current, Saskatchewan. *In*: 3rd International Williston Basin Symposium. pp. 179-184.

Tiercelin, J. J., Pflumio, C., Castrec, M., Boulégue, J., Gente, P., Rolet, J., Coussement, C., Stetter, K.O., Huber, R., Buku, S., & Mifundu, W. (1993). Hydrothermal vents in Lake Tanganyika, East African, Rift system. *Geology*, *21*(6), 499-502.

Tolstikhin, I. N. (1975). Helium isotopes in the Earth's interior and in the atmosphere: a degassing model of the Earth. *Earth and Planetary Science Letters*, *26*(1), 88-96.

Tomonaga, Y., Marzocchi, R., Pera, S., Pfeifer, H. R., Kipfer, R., Decrouy, L., & Vennemann, T. (2017). Using noble-gas and stable-isotope data to determine groundwater origin and flow regimes: Application to the Ceneri Base Tunnel (Switzerland). *Journal of Hydrology*, *545*, 395-409.

Torgersen, T., & Clarke, W. B. (1985). Helium accumulation in groundwater, I: An evaluation of sources and the continental flux of crustal ^{4}He in the Great Artesian Basin, Australia. *Geochimica et Cosmochimica Acta*, *49*(5), 1211-1218.

Torgersen, T., & Ivey, G. N. (1985). Helium accumulation in groundwater. II: A model for the accumulation of the crustal ^{4}He degassing flux. *Geochimica et Cosmochimica Acta*, *49*(11), 2445-2452.

Torgersen, T. (1989). Terrestrial helium degassing fluxes and the atmospheric helium budget: Implications with respect to the degassing processes of continental crust. *Chemical Geology: Isotope Geoscience section*, *79*(1), 1-14.

Torgersen, T., & Kennedy, B. M. (1999). Air-Xe enrichments in Elk Hills oil field gases: role of water in migration and storage. *Earth and Planetary Science Letters*, *167*(3), 239-253.

Trull, T. W., Kurz, M. D., & Jenkins, W. J. (1991). Diffusion of cosmogenic3He in olivine and quartz: implications for surface exposure dating. *Earth and Planetary Science Letters*, *103*(1-4), 241-256.

Ungerer, P., Burrus, J., Doligez, B., Chenet, P. Y., & Bessis, F. (1990). Basin Evaluation by Integrated Two-Dimensional Modeling of Heat Transfer, Fluid Flow, Hydrocarbon Generation, and Migration (1). *AAPG Bulletin*, *74*(3), 309-335.

United States Geological Survey. (2017). *Mineral Commodity Summaries 2017: Helium* by J. E. Hamak. Retrieved from the USGS website: https://minerals.usgs.gov/minerals/pubs/commodity/helium/mcs-2017-heliu.pdf (Accessed 10 October 2017).

Van Soest, M. C., Hilton, D. R., & Kreulen, R. (1998). Tracing crustal and slab contributions to arc magmatism in the Lesser Antilles island arc using helium and carbon relationships in geothermal fluids. *Geochimica et Cosmochimica Acta*, *62*(19), 3323-3335.

Veroda, V. J. (1958). Morrow Rocks of Western Kansas and Panhandle Counties of Oklahoma: ABSTRACT. *AAPG Bulletin*, *42*(1), 214-215.

Vervoort, J. D., Lewis, R. S., Fisher, C., Gaschnig, R. M., Jansen, A. C., & Brewer, R. (2016). Neoarchean and Paleoproterozoic crystalline basement rocks of north-central Idaho:

Constraints on the formation of western Laurentia. *Geological Society of America Bulletin*, *128*(1-2), 94-109.

Vogt, M., Kröner, A., Poller, U., Sommer, H., Muhongo, S., & Wingate, M. T. D. (2006). Archaean and Palaeoproterozoic gneisses reworked during a Neoproterozoic (Pan-African) high-grade event in the Mozambique belt of East Africa: Structural relationships and zircon ages from the Kidatu area, central Tanzania. *Journal of African Earth Sciences*, *45*(2), 139-155.

Walia, V., Yang, T. F., Hong, W. L., Lin, S. J., Fu, C. C., Wen, K. L., & Chen, C. H. (2009). Geochemical variation of soil–gas composition for fault trace and earthquake precursory studies along the Hsincheng fault in NW Taiwan. *Applied Radiation and Isotopes*, *67*(10), 1855-1863.

Walker, B. G. (1969). Springs of deep seated origin in Tanzania. *In*: Proceedings of the XXIII International Geological Congress, Vol. 19, pp. 171-180.

Walters, R. F. (1958). Differential entrapment of oil and gas in Arbuckle dolomite of central Kansas. *AAPG Bulletin*, *42*(9), 2133-2173.

Walther, J. V., & Orville, P. M. (1982). Volatile production and transport in regional metamorphism. *Contributions to Mineralogy and Petrology*, *79*(3), 252-257.

Warr, O. W. P. (2013). *Understanding phase behaviour in the geological storage of carbon dioxide*. University of Manchester. (PhD Thesis). pp. 265.

Warr, O., Lollar, B. S., Fellowes, J., Sutcliffe, C. N., McDermott, J. M., Holland, G., Mabry, J. C., & Ballentine, C. J. (2017). Tracing ancient hydrogeological fracture network age and compartmentalisation using noble gases. *Geochimica et Cosmochimica Acta*.

Weeraratne, D. S., Forsyth, D. W., Fischer, K. M., & Nyblade, A. A. (2003). Evidence for an upper mantle plume beneath the Tanzanian craton from Rayleigh wave tomography. *Journal of Geophysical Research: Solid Earth*, *108*(B9).

Weinlich, F. H., Bräuer, K., Kämpf, H., Strauch, G., Tesař, J., & Weise, S. M. (1999). An active subcontinental mantle volatile system in the western Eger rift, Central Europe: Gas flux, isotopic (He, C, and N) and compositional fingerprints. *Geochimica et Cosmochimica Acta*, *63*(21), 3653-3671.

Wescott, W. A., Krebs, W. N., Engelhardt, D. W., & Cunningham, S. M. (1991). New Biostratigraphic Age Dates from the Lake Rukwa Rift Basin in Western Tanzania: Geologic Note (1). *AAPG Bulletin*, *75*(7), 1255-1263.

Wheeler, W. H., & Karson, J. A. (1994). Extension and subsidence adjacent to a" weak" continental transform: An example from the Rukwa rift, East Africa. *Geology*, *22*(7), 625-628.

Whelan, J. K., Solomon, P. R., Deshpande, G. V., & Carangelo, R. M. (1988). Thermogravimetric Fourier transform infrared spectroscopy (TG-FTIR) of petroleum source rocks. Initial results. *Energy & fuels*, *2*(1), 65-73.

Whittington II, R. A. (2009). *Clay Mineralogy and Illite Crystallinity in the Late Devonian to Early Mississippian Woodford Shale in the Arbuckle Mountains, Oklahoma, USA.* Georgia State University. (MS Thesis). pp. 139.

Williams, L. B., Ferrell, R. E., Hutcheon, I., Bakel, A. J., Walsh, M. M., & Krouse, H. R. (1995). Nitrogen isotope geochemistry of organic matter and minerals during diagenesis and hydrocarbon migration. *Geochimica et Cosmochimica Acta*, *59*(4), 765-779.

Winchester, D. E. (1935). Natural Gas in Colorado, Northern New Mexico and Utah, *in* Geology of natural gas: Am. Assoc. Petroleum Geologists, pp. 363-384.

Winckler, G., Suess, E., Wallmann, K., de Lange, G. J., Westbrook, G. K., & Bayer, R. (1997). Excess helium and argon of radiogenic origin in Mediterranean brine basins. *Earth and planetary science letters*, *151*(3-4), 225-231.

Winckler, G., & Severinghaus, J. P. (2013). Noble Gases in Ice Cores: Indicators of the Earth's Climate History. *In*: The Noble Gases as Geochemical Tracers, pp. 33-53. Springer, Berlin, Heidelberg.

Wingerter, H. R. (1968). B. Greenwood Gas Field, Kansas, Colorado, and Oklahoma: Natural Gas in Kansas. *In* M 9: Natural Gases of North America, Volume Two, AAPG Special Volumes, pp. 1557-1566.

Wolf, R. A., Farley, K. A., & Silver, L. T. (1996). Helium diffusion and low-temperature thermochronometry of apatite. *Geochimica et Cosmochimica Acta*, *60*(21), 4231-4240.

Yang, J. H., Wu, F. Y., & Wilde, S. A. (2003). A review of the geodynamic setting of large-scale Late Mesozoic gold mineralization in the North China Craton: an association with lithospheric thinning. *Ore Geology Reviews*, *23*(3), 125-152.

Yarger, H. L. (1981). Aeromagnetic survey of Kansas. *Eos, Transactions American Geophysical Union*, *62*(17), 169-178.

Yatsevich, I., & Honda, M. (1997). Production of nucleogenic neon in the Earth from natural radioactive decay. *Journal of Geophysical Research: Solid Earth*, *102*(B5), 10291-10298.

Young, R. G. (1983). Petroleum in northeastern Grand County, Utah, *in* W. R. Averett, ed., Northern Paradox Basin – Uncompahgre Uplift: Grand Juction Geological Society Field Trip, October 1-2, 1983, pp. 1-7.

Young, D. P., Macfarlane, P. A., Whittemore, D. O., & Wilson, B. B. (2005). *Hydrogeologic characteristics and hydrologic changes in the Cimarron River basin, southwestern Kansas*. Kansas Geological Survey Open File Report 2005-26: http://www.kgs.ku.edu/Hydro/Publications/2005/OFR05_26/index.html (Accessed 4 December 2017).

Zadnik, M. G., & Jeffery, P. M. (1985). Radiogenic neon in an Archaean anorthosite. *Chemical Geology: Isotope Geoscience section*, *52*(1), 119-125.

Zartman, R. E., Wasserburg, G. J., & Reynolds, J. H. (1961). Helium, argon, and carbon in some natural gases. *Journal of Geophysical Research*, *66*(1), 277-306.

Zhou, Z. (2004). *Development of the noble gas tool to quantify natural gas and groundwater interaction in the subsurface*. ETH Zurich. (PhD Thesis). pp. 167.

Zhou, Z., Ballentine, C. J., Kipfer, R., Schoell, M., & Thibodeaux, S. (2005). Noble gas tracing of groundwater/coalbed methane interaction in the San Juan Basin, USA. *Geochimica et Cosmochimica Acta*, *69*(23), 5413-5428.

Zhou, Z., Ballentine, C. J., Schoell, M., & Stevens, S. H. (2012). Identifying and quantifying natural CO_2 sequestration processes over geological timescales: the Jackson Dome CO_2 Deposit, USA. *Geochimica et Cosmochimica Acta*, *86*, 257-275.

Zhu, Y., Shi, B., & Fang, C. (2000). The isotopic compositions of molecular nitrogen: implications on their origins in natural gas accumulations. *Chemical Geology*, *164*(3), 321-330.

Appendix A- Further information on the Mid-Continent fields (Chapter 3)

Geology of the Kansas Basin Carboniferous samples

Five oil and/or gas production wells were sampled in Ford County and are denoted in the main text as the KBC (Kansas Basin Carboniferous) samples.

The producing layers for helium-rich gases are part of the Carboniferous system and are denoted as the Upper Mississippian (possibly the Chesterian however this is never made clear) and the Morrow sands (Pennsylvanian) in the KGS database literature (KGS, 2017) (**Figure A1**).

The Morrow formation consists of rhythmic alternations of thin crinoidal, glauconitic limestone, glauconitic sandstone and shale beds. Producing layers associated with the Morrow sandstones are lenticular and usually around 15ft thick in Ford County (Veroda, 1958; Rascoe Jr, 1962; Clark, 1987). Reservoir porosities average 13% and the sands are generally fine-grained and well cemented (Henry and Hester, 1995).

The Chesterian series of the Upper Mississippian lies unconformably beneath the Lower Pennsylvanian Morrow and is made up of the Chester shale and Ste. Genevieve limestone (Kim et al., 2010). The Chesterian series is up to 200ft thick in the Hugoton Embayment (Clark, 1987).

Gas compositions for strata in the various fields are recorded in Table B1.

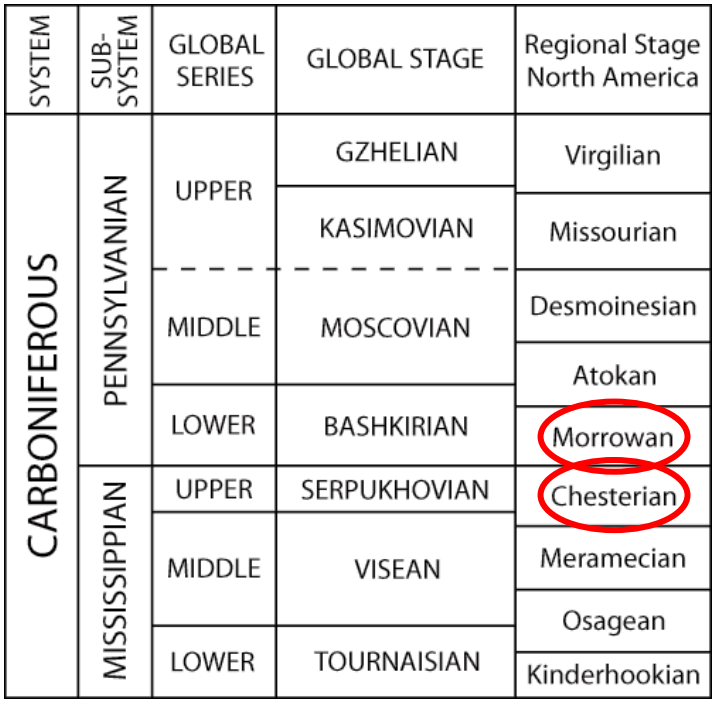

Figure A1: Stratigraphic section from North America compared to the stratigraphy classification of the rest of the world. Red circles indicate the helium-rich producing reservoirs for the KBC samples (modified from Sawin et al., 2009).

Geology of the Kansas Basin Permian samples

Twelve samples were taken from fields in the Hodgeman and Ness counties. In each case the producing reservoir sampled was the Lower Permian (Chase Group) similar to the Hugoton-Panhandle giant gas field (**Figure A2**). The Chase Group consists of a 200 to 400ft thick series of alternating carbonate, shale and siltstone units from the Wreford Limestone (oldest) to the Herrington Limestone Member (youngest) (Lukert, 1949; Jenden et al., 1988b; KGS, 2017). Limestone reservoirs in the Chase Group which produce helium-rich gas are the Florence (33 to 45ft thick), Fort Riley (approximately 35ft thick), Towanda (approximately 15ft thick), Winfield (approximately 95ft thick) and Herrington-Krider (around 20ft thick) (Hemsell, 1939; KGS, 2017) (**Table A1**).

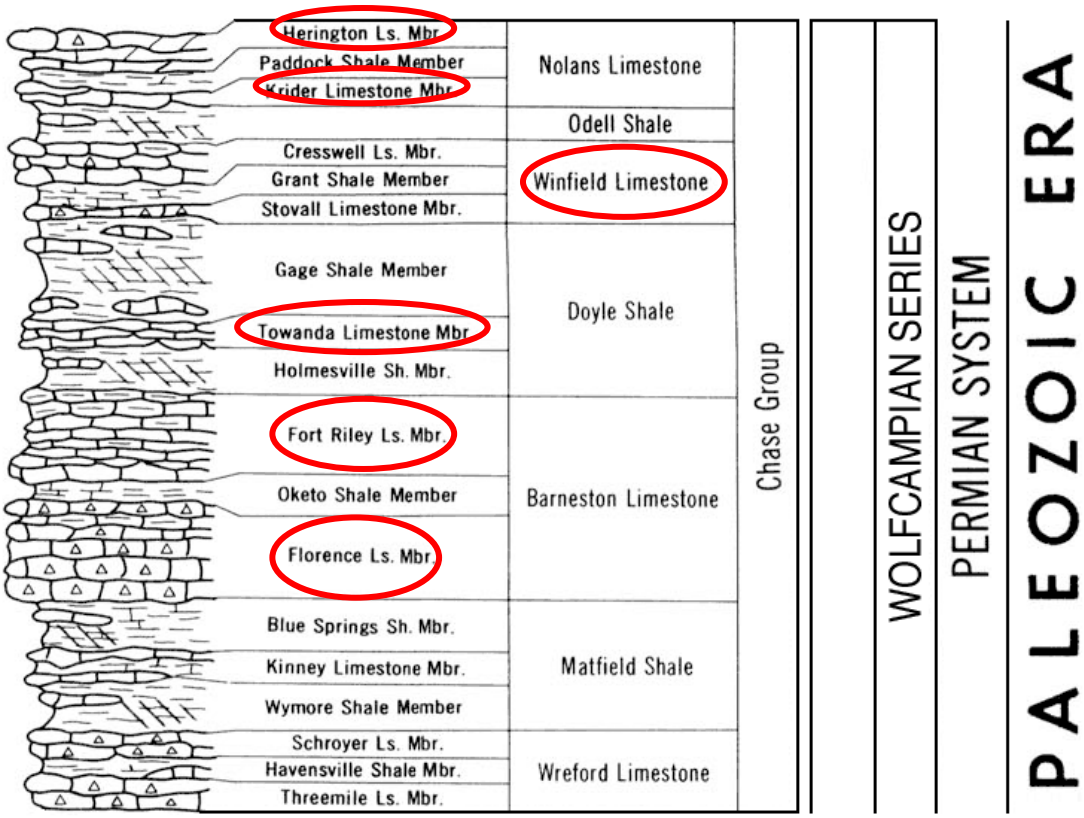

Figure A2: Stratigraphic section from Kansas for the Permian. Red circles indicate the helium-rich producing reservoirs for the KBP samples.

Central Kansas Uplift sample backgrounds

Two fields located on the Central Kansas Uplift (Bahr and Leesburgh) produce helium-rich gas from limestone reservoirs in the Lower Permian Chase group (Winfield and Towanda) and, in the case of the Leesburgh field, from the Lower Permian Council Grove Group (Cottonwood formation; 42ft thick) and from the Upper Pennsylvanian Wabaunsee Group (Bern formation; approximately 78ft thick) (KGS, 2017).

The fields are missing the Mississippian and lower Pennsylvanian layers due to uplift and erosion of the basement complex during the Carboniferous (Merriam, 1963; Chaudhuri et al., 1986).

Field name	Field owner	Field type	Age of producing strata	Producing strata	Depth of producing strata (m)	Initial Bottomhole pressure (Psia)	Gas composition ($CH_4/N_2/CO_2$/He/ other gases) (%)
Carson	Ritchie Exploration Inc	Oil and gas	Mississippian/ Pennsylvanian	Chesterian/Morrow	1493	2318	nr/19.8/0.1/nr/nr
Maverick	Ritchie Exploration Inc	Oil and gas	Pennsylvanian	Morrow	1556	2469	42.2/50.8/0/2.5/4.5
#1 Blew (single well)	Ritchie Exploration Inc	Oil and gas	Pennsylvanian	Morrow	1543	nr	59.1/33.9/0.1/1.2/5.7
Steel	Ritchie Exploration Inc	Oil and gas	Mississippian	Mississippian	1586	2544	nr/9.5-10.2/0.09-0.14/nr/nr
Lamb	Ritchie Exploration Inc	Gas	Mississippian	Mississippian	1799	2744	nr/9.2/0.1/nr/nr
Neho	Becker Oil Corp	Gas	Permian	Krider/Winfield	733	1126	59.8/38.4/0.03/1.1/0.7
Barricklow East	Becker Oil Corp	Gas	Permian	Winfield/Towanda	738	1258	56.8/41.3/0.05/1.1/0.7
Barrick	Becker Oil Corp	Gas	Permian	Krider/Winfield	747	1147	61.9/36.5/0.03/1.1/0.5
Wieland North	Becker Oil Corp	Oil and gas	Permian	Krider/Winfield	756	1290	64.3/33.8/0/1.1/0.8
Wieland	Becker Oil Corp	Oil and gas	Permian	Krider/Winfield	806	1238	64.6/33.5/0/1.1/0.8
Hanston-Oppy	Becker Oil Corp	Oil and gas	Permian	Krider/Winfield	830	1279	64.9/33.0/0.05/1.0/1.1
Groner	Becker Oil Corp	Gas	Permian	Krider/Towanda	782	1294	69.9/28.0/0/0.93/1.2
Sawlog Creek Southeast	Becker Oil Corp	Oil and gas	Permian	Krider/Florence	844	1439	75.8/22.2/0.06/0.90/1.1
Jetport	Becker Oil	Oil and	Permian	Winfield	853	1456	70.8/27.4/0/0.93/0.9

	Corp	gas					
Stella B	Becker Oil Corp	Gas	Permian	Krider	831	1418	71.2/27.0/0.03/0.91/0.9
Don	Becker Oil Corp	Oil and gas	Permian	Krider/Fort Riley/Florence	857	1462	66.7/31.6/0/0.95/0.7
Leesburgh	Becker Oil Corp	Oil and gas	Permian/ Pennsylvanian	Winfield/Towanda/ Cottonwood/Bern	920	1413	72.4/23.7/0.08/0.86/3.0
Bahr	Becker Oil Corp	Oil and gas	Permian	Winfield	579	319	69.5/23.6/1.43/1.3/4.1

Table A1: Synthesis of data from the Kansas Geological Survey, Digital Petroleum Database regarding the sampled fields. Parts marked with (nr) indicate where data was either not recorded or unavailable.

Appendix B: Combined datasets for all North American samples

Well name/geological province	$^{4}He/^{40}Ar^{*}$	$^{4}He/^{21}Ne^{*}$	$^{40}Ar^{*}/^{21}Ne^{*}$
Hugoton-Panhandle (average)	12.46 ± 2.48	2.85 ± (0.62) x 10^{7}	2.43 ± (0.81) x 10^{6}
Kansas Hugoton	13.26 ± 2.46	2.85 ± (0.70) x 10^{7}	2.19 ± (0.59) x 10^{6}
Guymon Hugoton	9.40 ± 0.09	2.93 ± (0.001) x 10^{7}	3.12 ± (0.03) x 10^{6}
Texas Panhandle	11.73 ± 2.10	2.83 ± (0.61) x 10^{7}	2.66 ± (1.09) x 10^{6}
Kansas Basin Carboniferous (average)	13.72 ± 1.75	1.21 ± (0.16) x 10^{7}	8.83 ± (0.53) x 10^{5}
Kansas Basin Permian (average)	59.81 ± 7.63	3.16 ± (0.14) x 10^{7}	5.38 ± (0.83) x 10^{5}
Kautz #1 (CKU)	4.73 ± 0.17	4.59 ± (0.29) x 10^{7}	9.70 ± (1.58) x 10^{6}
McCune 1-A (CKU)	7.94 ± 0.54	3.05 ± (0.33) x 10^{7}	3.84 ± (0.82) x 10^{6}
Harley Dome	21.29 ± 0.50	3.66 ± (0.16) x 10^{7}	1.72 ± (0.78) x 10^{6}
Weil	4.45 ± 0.14	3.09 ± (0.40) x 10^{7}	6.95 ± (0.92) x 10^{6}
International Helium Wood Mtn	5.56 ± 0.15	2.45 ± (0.16) x 10^{7}	4.39 ± (0.30) x 10^{6}
Average upper crust (theoretical) (Ballentine and Burnard, 2002)	6.0	2.33 ± (0.44) x 10^{7}	3.88 ± (0.73) x 10^{6}
Average upper crust (observed) (Ballentine and Burnard, 2002)	5.0±1.0	1.71 ± (0.09) x 10^{7}	3.60 ± (1.27) x 10^{6}

Figure B1: Concentrations and ratios of the radiogenically produced isotopes in samples. Errors are to 1σ.

Sample well and geological province	Location Lat/Long	Producing formation	$^{3}He/^{4}He$ (R_a)	$^{20}Ne/^{22}Ne$	$^{21}Ne/^{22}Ne$	$^{40}Ar/^{36}Ar$	$^{38}Ar/^{36}Ar$
Central Kansas Uplift							
Kautz #1	38°27'4.92"N, 98°57'17.45"W	Chase Group	0.11 (0.008)	9.32 (0.029)	0.053 (0.0006)	1410 (3)	0.189 (0.0005)
			0.12 (0.003)	9.30 (0.029)	0.053 (0.0006)	1409 (3)	0.189 (0.0005)
McCune 1-A	37°53'27.09"N, 98°41'59.37"W	Chase Group	0.08 (0.002)	9.49 (0.033)	0.045 (0.0005)	592 (1)	0.187 (0.0005)
Kansas Basin Carboniferous							
Bonnie Carson #1	37°41'47.10"N, 99°51'36.38"W	Morrow Sands	0.09 (0.003)	9.18 (0.028)	0.058 (0.0006)	1718 (3)	0.183 (0.0006)
Maverick #1	37°41'16.43"N, 99°50'58.85"W	Morrow Sands	0.10 (0.001)	8.95 (0.028)	0.063 (0.0007)	2142 (5)	0.187 (0.0008)
#1 Blew	37°37'35.27"N, 99°48'38.53"W	Morrow Sands	0.09 (0.002)	9.13 (0.028)	0.055 (0.0006)	1642 (3)	0.185 (0.0006)
#1 O Slash-Hill Trust	37°38'31.47"N, 99°47'46.52"W	Mississippian	0.10 (0.001)	9.16 (0.028)	0.056 (0.0006)	1494 (4)	0.184 (0.0009)
Lamb Lance #1	37°37'44.59"N, 99°44'52.86"W	Mississippian	0.09 (0.003)	9.14 (0.028)	0.060 (0.0006)	1635 (4)	0.185 (0.0008)
Kansas Basin Permian							
Barricklow Unit #1	38°15'13.98"N, 99°38'17.73"W	Chase Group	0.10 (0.001)	9.74 (0.030)	0.042 (0.0004)	588 (1)	0.189 (0.0005)
Shank no. 1	38°15'45.71"N, 99°41'48.81"W	Chase Group	0.09 (0.001)	9.71 (0.030)	0.040 (0.0004)	584 (1)	0.189 (0.0005)
McFadden no. 1	38°16'52.86"N, 99°42'56.11"W	Chase Group	0.13 (0.002)	9.74 (0.030)	0.041 (0.0004)	604 (1)	0.189 (0.0005)
Selfridge no. 1-A	38°14'7.62"N, 99°45'21.74"W	Chase Group	0.13 (0.002)	9.75 (0.030)	0.042 (0.0004)	583 (1)	0.189 (0.0005)

Wieland no. 1-A	38°13'19.77"N, 99°44'39.21"W	Chase Group	0.11 (0.001)	9.74 (0.030)	0.042 (0.0004)	591 (2)	0.190 (0.001)
Oppy-Burke no. 1	38° 7'26.40"N, 99°46'37.57"W	Chase Group	0.07 (0.001)	9.73 (0.030)	0.044 (0.0005)	554 (2)	0.189 (0.001)
Lewis Trust #1	38° 5'2.84"N, 99°34'14.74"W	Chase Group	0.10 (0.002)	9.68 (0.030)	0.043 (0.0005)	555 (1)	0.186 (0.0007)
Strecker no. 1	37°59'4.10"N, 99°38'13.99"W	Chase Group	0.06 (0.002)	9.57 (0.030)	0.044 (0.0005)	555 (3)	0.195 (0.004)
			0.06 (0.003)	9.56 (0.032)	0.045 (0.0005)		
Gleason #1	37°59'14.11"N, 99°36'31.71"W	Chase Group	0.06 (0.001)	9.72 (0.030)	0.044 (0.0005)	537 (1)	0.189 (0.0006)
Jetmore-Bradford no. 1	37°58'15.58"N, 99°53'37.79"W	Chase Group	0.06 (0.002)	9.62 (0.030)	0.044 (0.0005)	525 (1)	0.187 (0.0007)
Benish no. 1	37°58'59.37"N, 99°57'47.65"W	Chase Group	0.06 (0.001)	9.75 (0.030)	0.044 (0.0005)	547 (2)	0.191 (0.001)
Poverty Hill no. 1	38°1'30.37"N, 99°55'13.08"W	Chase Group	0.08 (0.001)	9.81 (0.031)	0.043 (0.0004)	569 (1)	0.191 (0.0006)
*__Kansas Hugoton__							
Ratzlaff D ‘A’ #1	38°2'12.2"N, 101°16'43.7"W	Chase Group	0.16 (0.005)	9.70 (0.050)	0.039 (0.0004)	818 (10)	nr
Hefner Gas Unit #1	37°56'5.8"N, 101°23'18.9"W	Chase Group	0.16 (0.005)	9.74 (0.053)	0.039 (0.0005)	851 (11)	nr
Guldner Unit #1	37°43'43.0"N, 101°39'46.9"W	Chase Group	0.14 (0.004)	9.73 (0.041)	0.040 (0.0005)	835 (16)	nr
Guldner Unit #2	37°43'43.0"N, 101°39'46.9"W	Panoma	0.15 (0.004)	9.66 (0.025)	0.044 (0.0009)	889 (5)	nr
Campbell, R.W. #2	37°35'0.8"N, 101°37'35.7"W	Chase Group					nr
Keller, Ernest #2	37°29'47.5"N, 101°16'49.3"W	Chase Group	0.20 (0.006)	9.66 (0.059)	0.041 (0.0005)	1066 (11)	nr
Jarvis Unit #2	37°29'47.5"N, 101°17'54.9"W	Panoma	0.20 (0.006)	9.68 (0.061)	0.041 (0.0006)	1038 (20)	nr
Ball, Clyde H. #2	37°28'3.1"N, 101°27'45.3"W	Panoma		9.61 (0.027)	0.051 (0.0011)	974 (47)	nr
Wright “C” Unit #1	37°24'34.2"N, 101°31'2.1"W	Chase Group	0.18 (0.005)	9.69 (0.018)	0.039 (0.0008)	948 (6)	nr
Baughman H-2	37°14'2.7"N, 100°50'22.7"W	Chase Group		9.69 (0.018)	0.040 (0.0008)	977 (10)	nr
Crayton A-1	37°15'47.6"N, 101°36'3.5"W	Chase Group	0.19 (0.006)	9.70 (0.039)	0.040 (0.0006)	969 (25)	nr

Mills C-1	37°6'10.6"N, 101°9'57.4"W	Chase Group	0.21 (0.006)	9.71 (0.030)	0.045 (0.0009)	1155 (29)	nr
Parsley A-1	37°2'40.7"N, 101°6'41.6"W	Chase Group	0.21 (0.006)	9.80 (0.034)	0.040 (0.0005)	925 (12)	nr
Oberly A-1	37°13'10.2"N, 102°1'4.4"W	Greenwood	0.19 (0.006)	9.73 (0.035)	0.039 (0.0005)	830 (13)	nr
Tucker B-1	37°4'25.7"N, 101°44'45.6"W	Chase Group	0.19 (0.006)	9.80 (0.043)	0.041 (0.0007)	967 (18)	nr
Barnes A-1	37°0'3.4"N, 101°49'6.6"W	Greenwood		9.68 (0.015)	0.041 (0.0008)	913 (18)	nr
*__Guymon Hugoton__							nr
Hill A-1	36°52'15.9"N, 101°42'44.0"W	Chase Group					nr
Buzzard D-1	36°47'56.8"N, 101°44'7.9"W	Chase Group	0.19 (0.006)	9.81 (0.038)	0.039 (0.0006)	938 (26)	nr
Stonebraker A-69	36°38'21.0"N, 101°45'12.5"W	Chase Group	0.21 (0.006)	9.91 (0.023)	0.038 (0.0003)	1113 (7)	nr
*__Texas Panhandle__							nr
Coffee Estate #1	36°3.365'N, 101°43.052'W	Brown Dolomite	0.24 (0.007)	9.63 (0.025)	0.042 (0.0009)	1156 (7)	nr
Blake Trust Estate #2	36° 4.230'N, 101° 40.905'W	Brown Dolomite	0.25 (0.007)	9.77 (0.029)	0.040 (0.0004)	1105 (25)	nr
Mary A Long #1	36° 18.131'N, 101° 45.307'W	Brown Dolomite	0.20 (0.006)	9.67 (0.039)	0.040 (0.0005)	1039 (17)	nr
Donelson et al #1	36° 20.790'N, 101° 59.721'W	Brown Dolomite	0.21 (0.006)	9.83 (0.027)	0.037 (0.0003)	1076 (7)	nr
Sarah Claybaugh #1	36° 22.496'N, 101° 59.681'W	Brown Dolomite	0.18 (0.005)	9.80 (0.046)	0.037 (0.0004)	865 (33)	nr
Cameron Walls #1	36° 16.436'N, 101° 58.614'W	Brown Dolomite		9.66 (0.040)	0.040 (0.0005)	1112 (15)	nr
Horner #1	36° 4.847'N, 102° 6.201'W	Brown Dolomite		9.65 (0.025)	0.043 (0.0009)	1058 (14)	nr
Whitherbee #2	36° 6.224'N, 101° 49.193'W	Brown Dolomite	0.21 (0.006)	9.69 (0.036)	0.040 (0.0005)	983 (11)	nr
Flores 23	36° 2.738'N, 101° 48.120'W	Brown Dolomite		9.59 (0.025)	0.040 (0.0008)	1118 (12)	nr
Nisbett #1	36° 0.146'N, 101° 52.410'W	Brown Dolomite	0.19 (0.006)	9.62 (0.032)	0.041 (0.0005)	1045 (9)	nr
McDade #2 + #5	35° 54.124'N, 102° 2.606'W	Brown Dolomite	0.18 (0.005)				nr
Brumley A #1	35° 57.554'N, 101° 55.098'W	Brown Dolomite					nr
Colorado Plateau							
Harley Dome #1	39°11'13.32"N, 109° 8'52.95"W	Entrada Sandstone	0.10 (0.001)	9.00 (0.029)	0.083 (0.0009)	4452 (10)	0.190 (0.002)
Harley Dome #1			0.11 (0.001)	9.03 (0.029)	0.083 (0.0009)	4448 (10)	
Great Falls Tectonic Zone							
Weil #1	48°40'24.75"N,	Red River	0.74 (0.01)	10.21 (0.037)	0.067 (0.0007)	8839 (50)	0.185 (0.003)

	110°33'44.44"W						
Weil #1 International Helium Wood Mountain	49°22'21.15"N, 107° 0'45.76"W	Deadwood Formation	0.73 (0.01)	10.21 (0.034)	0.067 (0.0007)		
			0.18 (0.004)	9.78 (0.036)	0.071 (0.0008)	7118 (33)	0.188 (0.004)

Figure B2: Noble gas ratios from the Mid-Continent study (Chapter 3), the N_2-rich ^{4}He gas wells study (Chapter 4) and from Ballentine and Sherwood-Lollar, 2002 for the Hugoton-Panhandle (starred sections). 1σ errors for samples are shown in brackets. Nr in the table denotes the $^{38}Ar/^{36}Ar$ values were not recorded.

Sample well and geological province	^{4}He concentration (x 10^{-2}) (cm^3 STP)	^{20}Ne concentration (x 10^{-7}) (cm^3 STP)	^{40}Ar concentration (x 10^{-4}) (cm^3 STP)	^{84}Kr concentration (x 10^{-8}) (cm^3 STP)	^{130}Xe concentration (x 10^{-10}) (cm^3 STP)	N_2 concentration (±5%) (cm^3 STP)	$\delta^{15}N(N_2)$ (±0.2‰)
Central Kansas Uplift							
Kautz #1	2.12 (0.025)	1.78 (0.011)	56.6 (0.57)	1.21 (0.02)	0.31 (0.01)	0.373	2.45 (0.07)
	2.13 (0.025)	1.77 (0.011)	57.0 (0.57)				
McCune 1-A	0.86 (0.011)	1.71 (0.017)	2.16 (0.22)	1.25 (0.02)	0.99 (0.01)	0.237	3.45 (0.07)
Kansas Basin Carboniferous							
Bonnie Carson #1	1.22 (0.013)	2.75 (0.030)	9.67 (0.083)	1.49 (0.05)	3.10 (0.05)	0.198	3.80 (0.14)

Maverick #1	2.47 (0.025)	4.78 (0.051)	19.6 (0.16)	2.43 (0.07)	12.84 (0.12)	0.508	6.50 (0.42)
#1 Blew	1.31 (0.013)	4.31 (0.046)	14.0 (0.12)	2.32 (0.07)	4.42 (0.07)	0.339	1.85 (0.21)
#1 O Slash-Hill Trust	0.48 (0.007)	1.56 (0.017)	4.88 (0.042)	0.63 (0.19)	1.91 (0.03)	0.102	
Lamb Lance #1	0.58 (0.006)	1.43 (0.015)	4.72 (0.041)	0.32 (0.10)	1.52 (0.01)	0.092	2.90 (0.07)
Kansas Basin Permian							
Barricklow Unit #1	1.22 (0.020)	2.93 (0.044)	4.66 (0.071)	1.84 (0.04)	1.27 (0.02)	0.369	4.03 (0.90)
Shank no. 1	1.15 (0.019)	3.04 (0.046)	3.49 (0.053)	1.86 (0.04)	1.28 (0.02)	0.387	4.70 (0.28)
McFadden no. 1	1.16 (0.019)	3.07 (0.047)	5.01 (0.076)	1.92 (0.04)	1.27 (0.02)	0.416	1.45 (0.07)
Selfridge no. 1-A	1.08 (0.018)	2.56 (0.039)	4.17 (0.063)	1.65 (0.03)	1.21 (0.02)	0.338	2.20 (0.35)
Wieland no. 1-A	1.15 (0.019)	2.63 (0.040)	4.00 (0.061)	1.70 (0.03)	1.19 (0.02)	0.341	3.10 (0.14)
Oppy-Burke no. 1	0.96 (0.016)	2.03 (0.031)	3.03 (0.046)	1.45 (0.03)	1.15 (0.02)	0.330	4.00 (0.14)
Lewis Trust #1	1.00 (0.010)	2.03 (0.028)	3.82 (0.034)	1.29 (0.01)	0.96 (0.02)	0.280	
Strecker no. 1	0.87 (0.014)	1.82 (0.028)	2.75 (0.042)	1.35 (0.03)	1.08 (0.02)	0.220	3.45 (0.21)
	0.87 (0.012)	1.77 (0.030)					
Gleason #1	0.86 (0.014)	1.80 (0.027)	2.87 (0.044)	1.40 (0.03)	1.17 (0.02)	0.264	3.70 (0.14)
Jetmore-Bradford no. 1	1.05 (0.011)	2.13 (0.028)	4.03 (0.035)	1.39 (0.01)	1.52 (0.03)	0.280	2.45 (0.21)

Benish no. 1	0.95 (0.016)	2.02 (0.031)	3.03 (0.046)	1.46 (0.03)	1.15 (0.02)	0.275	2.99 (0.01)
Poverty Hill no. 1	0.89 (0.015)	1.83 (0.028)	3.30 (0.050)	1.53 (0.03)	1.18 (0.02)	0.311	4.00 (0.14)
*__Kansas Hugoton__							
Ratzlaff D 'A' #1	0.48 (0.024)		5.53 (0.28)	nm	nm	0.189	8.7
Hefner Gas Unit #1	0.40 (0.020)	1.08 (0.075)	5.12 (0.26)	nm	nm	0.181	7.8
Guldner Unit #1	0.50 (0.025)	1.56 (0.11)	5.75 (0.29)	nm	nm	0.207	9.4
Guldner Unit #2	0.43 (0.004)	1.41 (0.012)	5.10 (0.050)	nm	nm	0.203	9.0
Campbell, R.W. #2	0.40 (0.020)		4.42 (0.22)	nm	nm	0.154	8.0
Keller, Ernest #2	0.38 (0.019)	0.86 (0.060)	4.68 (0.23)	nm	nm	0.145	6.4
Jarvis Unit #2	0.39 (0.020)	1.07 (0.075)	4.27 (0.21)	nm	nm	0.148	6.5
Ball, Clyde H. #2	0.35 (0.004)	1.11 (0.011)	4.58 (0.26)	nm	nm	0.151	
Wright "C" Unit #1	0.37 (0.004)	1.19 (0.012)	4.44 (0.050)	nm	nm	0.156	7.8
Baughman H-2	0.58 (0.006)	1.80 (0.018)	5.92 (0.090)	nm	nm	0.178	6.5
Crayton A-1	0.43 (0.021)	1.19 (0.083)	4.62 (0.23)	nm	nm	0.166	7.5
Mills C-1	0.38 (0.004)	1.03 (0.010)	4.46 (0.16)	nm	nm	0.127	5.3
Parsley A-1	0.57 (0.028)	1.23 (0.086)	4.19 (0.21)	nm	nm	0.152	6.7
Oberly A-1	0.49 (0.025)	1.61 (0.013)	4.46 (0.22)	nm	nm	0.208	7.1

Tucker B-1	0.39 (0.020)	0.99 (0.079)	5.38 (0.27)	nm	nm	0.147	7.1
Barnes A-1	0.41 (0.004)	1.57 (0.016)	4.21 (0.16)	nm	nm	0.203	8.5
***Guymon Hugoton**							
Hill A-1	0.40 (0.020)		5.23 (0.26)	nm	nm	0.146	5.7
Buzzard D-1	0.45 (0.023)	1.58 (0.11)	7.10 (0.36)	nm	nm	0.184	6.9
Stonebraker A-69	0.65 (0.032)	2.35 (0.16)	9.30 (0.47)	nm	nm	0.214	6.1
***Texas Panhandle**							
Coffee Estate #1	0.63 (0.006)	1.93 (0.019)	7.21 (0.080)	nm	nm	0.136	4.5
Blake Trust Estate #2	1.05 (0.052)	2.92 (0.21)	10.73 (0.54)	nm	nm	0.214	5.3
Mary A Long #1	0.76 (0.038)	1.98 (0.14)	7.66 (0.38)	nm	nm	0.165	4.9
Donelson et al #1	0.98 (0.049)	5.03 (0.35)		nm	nm	0.258	4.9
Sarah Claybaugh #1	0.92 (0.046)	4.96 (0.35)		nm	nm	0.253	4.4
Cameron Walls #1	0.66 (0.033)	1.75 (0.12)	7.97 (0.49)	nm	nm	0.180	5.3
Horner #1	0.92 (0.009)	3.69 (0.031)	10.99 (0.24)	nm	nm	0.220	5.0
Whitherbee #2	0.35 (0.018)	0.82 (0.057)	7.10 (0.35)	nm	nm	0.080	3.6
Flores 23	0.61 (0.006)	1.75 (0.018)	6.97 (0.12)	nm	nm	0.135	4.0

Nisbett #1	0.55 (0.027)	1.52 (0.11)	5.86 (0.29)	nm	nm	0.141	3.4
McDade #2 + #5	0.29 (0.015)		2.73 (0.14)	nm	nm	0.066	2.7
Brumley A #1	0.33 (0.017)			nm	nm	0.089	2.7
Colorado Plateau							
Harley Dome #1	7.18 (0.10)	3.27 (0.031)	36.11 (0.34)	2.90 (0.09)	2.81 (0.03)	0.844	1.00 (0.06)
Harley Dome #1	7.03 (0.10)	3.24 (0.031)	35.83 (0.33)				
Great Falls Tectonic Zone							
Weil #1	0.98 (0.01)	1.01 (0.010)	22.75 (0.23)	0.66 (0.02)	0.56 (0.01)	0.955	2.40 (0.20)
Weil #1	1.00 (0.01)	1.02 (0.010)					
International Helium Wood Mountain	1.06 (0.02)	0.84 (0.086)	19.92 (0.20)	0.70 (0.03)	0.79 (0.01)	0.960	1.40 (0.46)

Table B3: Noble gas concentrations from the Mid-Continent study (Chapter 3), the N_2-rich ^{4}He gas wells study (Chapter 4) and the Ballentine and Sherwood-Lollar, (2002) study on the Hugoton-Panhandle (starred sections). Nitrogen concentrations for CKU, KBP and KBC samples are taken from the KGS database and are deemed to be within acceptable limits due to ^{4}He concentrations from the study being within 1σ error of previously recorded helium concentrations from wells. Nitrogen concentrations for the N_2-rich ^{4}He wells are taken from well tests conducted by IACX and Weil Helium and are deemed to be within acceptable limits due to ^{4}He concentrations from the study being within 1σ error of previously recorded helium concentrations from wells. 1σ errors for samples appear in column headers as % or in brackets if variable.